Research and Technology Highlights 1995

Langley Research Center
Technical Memorandum 4765

R&T

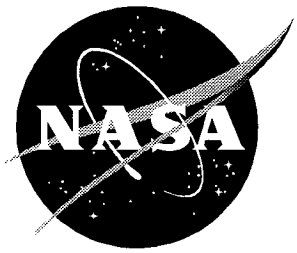

1995

National Aeronautics and Space Administration
Langley Research Center
Hampton, Virginia 23681-0001

NASA Technical Memorandum 4765

FOREWORD

The mission of the NASA Langley Research Center is to increase the knowledge and capability of the United States in a full range of aeronautics disciplines and in selected space disciplines. This mission is accomplished by performing innovative research relevant to national needs and Agency goals, transferring technology to users in a timely manner, and providing development support to other United States Government agencies, industry, other NASA Centers, the educational community, and the local community. This report contains highlights of the major accomplishments and applications that have been made by Langley researchers and by our university and industry colleagues during the past year. The highlights illustrate both the broad range of research and technology (R&T) activities carried out by NASA Langley Research Center and the contributions of this work toward maintaining United States leadership in aeronautics and space research. An electronic version of the report is available at URL http://techreports.larc.nasa.gov/RandT95. This color version allows viewing, retrieving, and printing of the highlights, searching and browsing through the sections, and access to an on-line directory of Langley researchers. For further information concerning the report, contact Dennis M. Bushnell, Senior Scientist, Mail Stop 110, NASA Langley Research Center, Hampton, Virginia 23681-0001, (757) 864-8987.

Dr. Jeremiah F. Creedon
Director

AVAILABILITY INFORMATION

The NASA program office and the corresponding Agency-wide Research and Technology Objectives and Plans (RTOP's) work breakdown structures are listed in the Contents for each research and technology accomplishment. OA designates the Office of Aeronautics; OSMA designates the Office for Safety and Mission Assurance; OLMSA designates the Office for Life and Microgravity Sciences and Applications; OSAT designates the Office for Space Access and Technology; and OMTPE designates the Office for Mission to Planet Earth.

The accomplishments are grouped into 11 categories that are based on NASA's strategic enterprises. These categories include the Aeronautics Enterprise (subdivided into Subsonic Aircraft, High-Speed Civil Transport, High-Performance Aircraft, Hypersonic Technologies, Advanced Concepts—including High-Performance Computing and Communications Technologies—and Critical National Facilities), the Mission to Planet Earth Enterprise, the Human Exploration and Development of Space Enterprise, the Space Science Enterprise, and the Space Technology Enterprise. All important Center facilities are described in detail on the NASA Langley Critical National Facilities World Wide Web Homepage. The URL address is http://techreports.larc.nasa.gov/LaRCfacilities. There is a Technology Transfer and Commercial Development section that summarizes a number of commercially interesting Langley technologies.

For additional information, call the point of contact (POC) that is identified with the highlight. The POC is either a member or leader of the research group that is responsible for the accomplishment or a monitor of the grant or contractual effort. Some of the figures in this report were originally in color; please call the POC for additional information about a particular figure.

Table of Contents

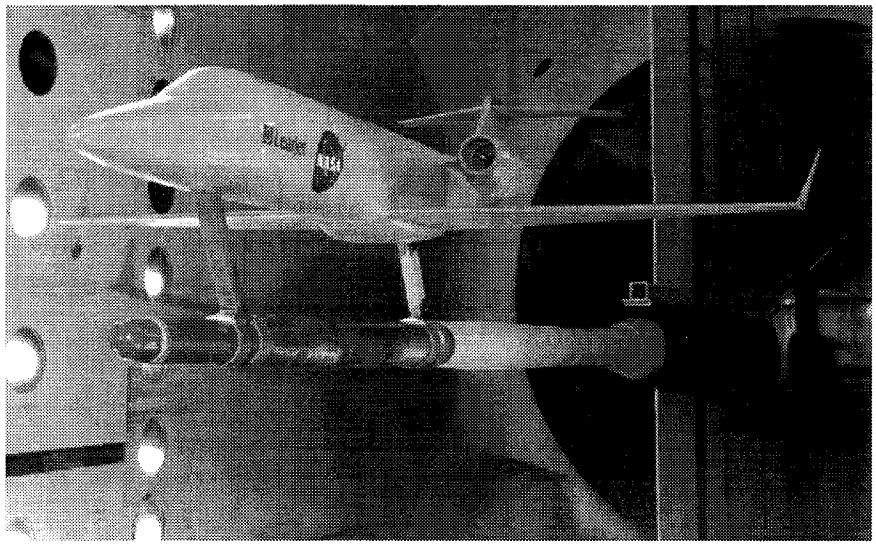

- *Develop high-payoff technologies for a new generation of environmentally compatible, economic U.S. subsonic aircraft and a safe, highly productive global air transportation system.*

Combined Aerodynamic and Aeroelastic Analysis of Subsonic Transport Wing

Testing in the National Transonic Facility supports the investigation of effects of Reynolds number on subsonic transport aircraft. Achieving a wide range of Reynolds number also requires a variation in tunnel dynamic pressure. The resulting variation in wing load and wing deformation yields changes in the airplane aerodynamics, which can be similar in magnitude to those obtained by varying Reynolds number.

An effort to predict the performance of a subsonic transport wind-tunnel model tested across a wide dynamic pressure range has led to the development of a computational wing static aeroelastic deformation method. The method is comprised of two components: an unstructured-mesh Euler flow solver with an interactive strip boundary-layer calculation and an equivalent-plate structural analysis technique. These particular computational methods allow good accuracy to be obtained while requiring a minimum of user preparation time and computer resources.

As illustrated in figure 1, the calculation of wing aeroelastic deformation significantly improves the correlation of calculated and measured wing pressure distributions. The present approximate method has yielded good correlation of wing pressure distributions across the entire range of dynamic pressure and Reynolds number for which wind-tunnel data have been obtained. Very good agreement has also been demonstrated for an aircraft configuration which includes a wing-mounted engine nacelle and pylon. This accurate and efficient method will be applied to additional aircraft geometries to estimate the impact of aeroelastic deformation on aerodynamic trends in advance of wind-tunnel testing. **(J. A. Al-Saadi, 757-864-5164)**

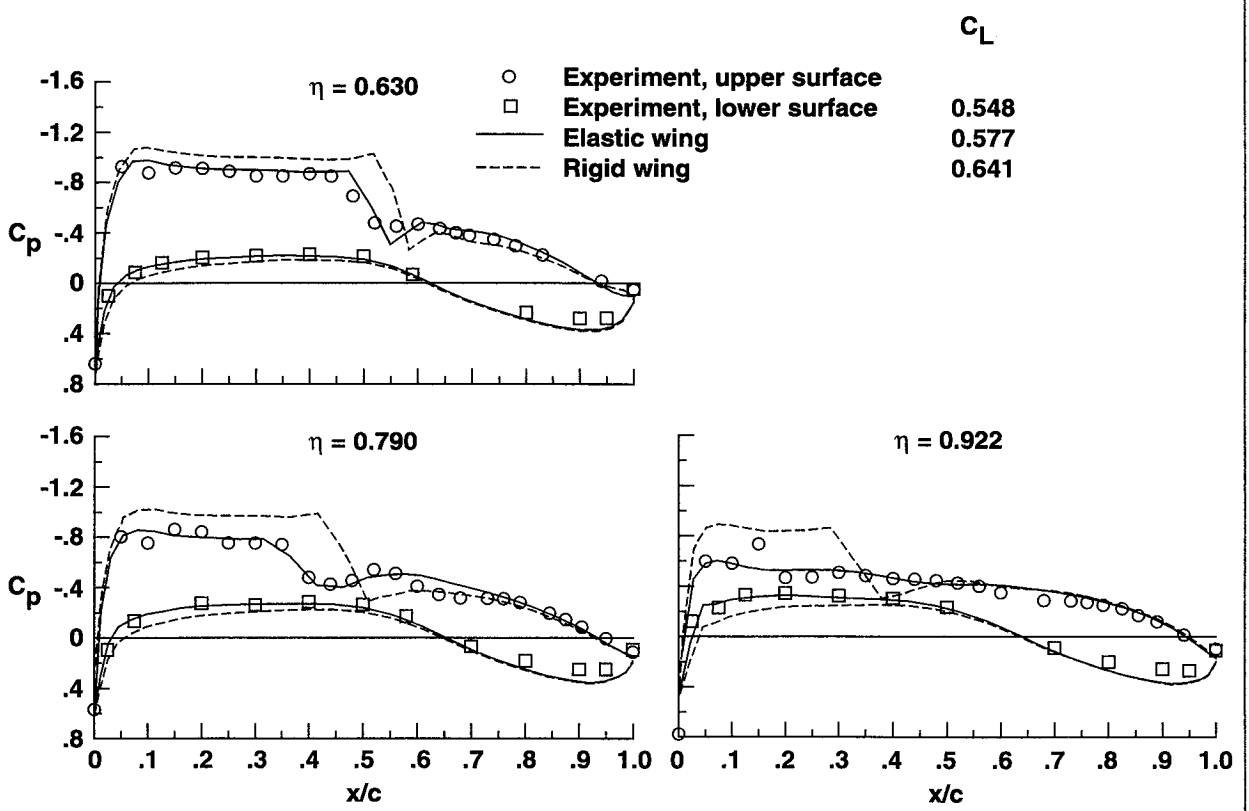

Figure 1. Comparison of calculated rigid and elastic wing pressure distributions with measured values on the outboard portion of the wing at a low dynamic pressure condition.

Cryogenic Validation of Skin Friction Measurement Instrumentation

One of the original goals of the National Transonic Facility (NTF) at the Langley Research Center was to utilize its very high Reynolds number capability to make benchmark measurements. One of these identified goals was to accurately measure smooth wall values of turbulent skin friction to very high values of Reynolds number. These measurements would reduce the amount of uncertainty in extrapolating drag results at moderate values of Reynolds numbers in conventional wind tunnels to flight values of Reynolds numbers.

As a first step toward this goal, Langley Research Center has designed and fabricated a skin friction balance (see fig. 2) a low interference boundary-layer rake, and a number of Preston tubes. These instruments were designed for the thin boundary layers associated with the extremely high unit Reynolds numbers (on the order of 90×10^6 ft^{-1}) that can be seen in the National Transonic Facility.

During a risk reduction program, these instruments were tested on the sidewall turbulent boundary layer of the Langley 0.3-Meter Transonic Cryogenic Tunnel at Mach numbers up to 0.85 and for unit Reynolds numbers up to 100×10^6 ft^{-1}. All instrumentation functioned at the low cryogenic temperatures and a number of hardware improvements were identified that will result in more accurate measurements in the NTF. **(R. M. Hall, 757-864-2883)**

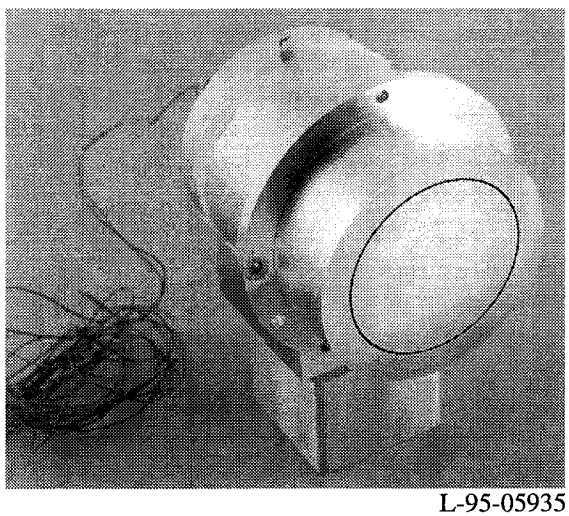

L-95-05935

Figure 2. Skin friction balance which was mounted in the side wall of the Langley 0.3-Meter Transonic Cryogenic Tunnel.

Hybrid Laminar Flow Control Crossflow Transition Experiment

The fuel savings believed possible by implementing laminar flow control (LFC) technology has interested aircraft manufacturers for a number of years. This is especially true when fuel prices are high. Before LFC technology can be implemented, more flow physics information about the behavior of crossflow boundary-layer instabilities at flight Reynolds numbers is needed. To provide this additional flow physics information, a subsonic hybrid laminar flow control (HLFC) crossflow transition experiment was conducted in the Langley 8-Foot Transonic Pressure Tunnel. The experiment was a joint effort between Langley Research Center and Boeing Commercial Airplane Group.

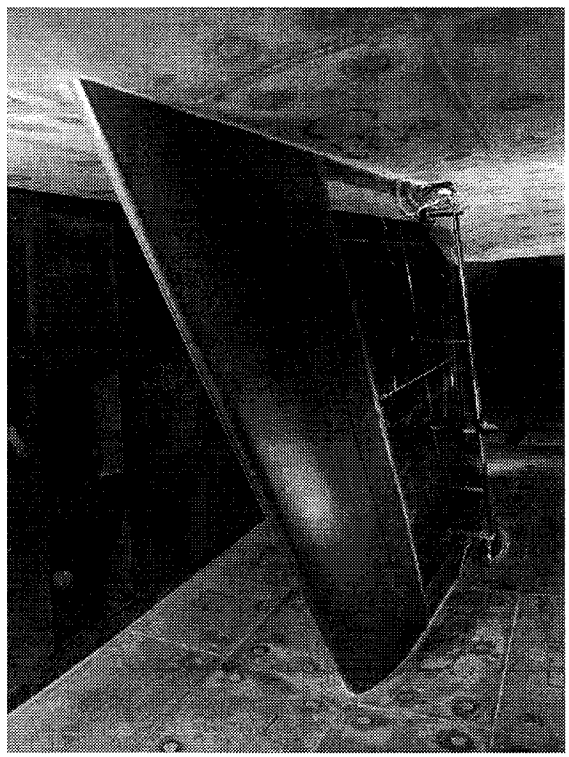

L-95-06919

Figure 3. Swept wing model installed in the Langley 8-Foot Transonic Pressure Tunnel.

The goal of the experiment was to provide flow physics information about the behavior of crossflow boundary-layer instabilities and to provide a database that could be used to guide the development of transition prediction codes. Making extensive use of computational fluid dynamics, a wind-tunnel experiment that would produce a flow field where crossflow instabilities were dominated was designed and executed. A 10-ft chord swept wing model with a porous leading edge was used for the experiment. (See fig. 3.) Innovative use of existing measurement techniques was required to get the data needed on this model.

Detailed hot-wire boundary-layer measurements were made at unit Reynolds numbers ranging from 0.5×10^6 ft^{-1} to 2.5×10^6 ft^{-1} and infrared thermography was used to document the transition front location for multiple suction distributions. Preliminary results from the experiment show that it is possible to get a significant amount of laminar flow at high Reynolds numbers. The database generated during this experiment is critical to understanding how crossflow instabilities on a swept wing grow in the presence of suction.
(L. G. Pack, 757-864-1618)

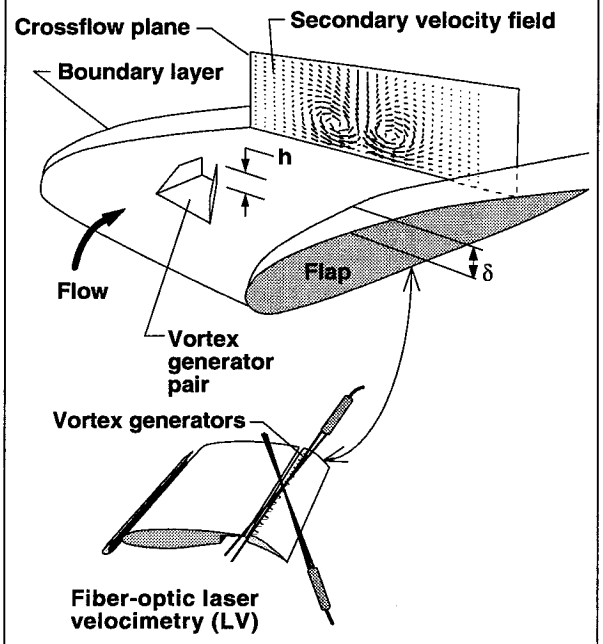

Figure 4. Sketch of experimental setup and measured secondary velocity vectors.

Flow Physics Study of Vortex Generators on Multielement Airfoil

Past research at Langley Research Center had shown that very small vortex generators (VG's) can effectively reduce boundary-layer separation on the flap of a multielement high-lift airfoil. Reduction of flap separation can significantly improve performance of the high-lift system by reducing drag and increasing lift for a given approach angle of attack. A detailed flow physics study of these VG's mounted on the flap of a multielement airfoil has been conducted in a low-speed wind tunnel. The objective of the study was to reduce the VG optimization time and provide data for the development of computer simulation models.

In the present study, counterrotating, trapezoid-wing type vortex generators applied to a high-lift airfoil with 60-percent flap separation caused complete flow reattachment. Vortex/boundary-layer interactions and streamwise vortex decay were investigated using three-component mean velocity and turbulence measurements taken with a laser velocimeter (LV). Figure 4 shows secondary velocities in cross-planes normal to the flap which indicate formation of upflow vortex pairs by the shed vortices. Streamwise vorticity and vortex circulation decayed rapidly downstream of the VG's. The embedded vortices caused large velocity and Reynolds stress disturbances in the confluent boundary layer over the flap. These disturbances remained even after the vortices had diffused. The current data provide detailed turbulence documentation of the flow field affected by the VG's and will be available for code development and advanced turbulence modeling. This research was supported under grant NGT-50984 from NASA Langley Research Center.
(J. C. Lin, 757-864-5556)

Direct Inverse Kinematic Solutions for Wind-Tunnel Model Attitude Control

A computer algorithm that directly solves for the manipulator joint angles required to produce a desired wind-tunnel model attitude has been developed, coded, and tested, using a high-speed civil transport model in the Langley 16-Foot Transonic Tunnel. The solution method accommodates unspecified coordinate system rotations between the manipulator coordinate system and the model coordinate system. The desired wind-tunnel model attitude is defined by the orientation of

the wind-tunnel airflow, expressed in the model coordinate system. The orientation of the wind-tunnel airflow in the model coordinate system is specified by two quantities: the angle of attack, and the angle of sideslip.

Previous methods, whether direct or iterative, required explicit definition of all intermediate coordinate system rotations due to special test jigs, fixtures, or force-measuring devices used to mount the model to the manipulator. Each of these intermediate rotations required the specification of three angles, generally referred to as yaw, pitch, and roll.

The advantages of this method of solution are:

1) All of the intermediate coordinate system rotations between the manipulator and the model coordinate system can be unspecified.

2) The angles of an arbitrary intermediate coordinate system rotation can be solved for given values of angle of attack, angle of sideslip, and manipulator joint angles.

3) All of the effects of the unspecified intermediate coordinate system rotations can be represented by the angles solved for in item 2 above.

4) Manipulator joint angles required for a desired model attitude can be solved for directly, without the need to iteratively search the manipulator's joint space for minima.

5) Direct inverse solutions are provided for both yaw, pitch, and roll (YPR) manipulators and manipulators with only pitch and roll (PR) capability.

(M. A. Motter, 757-864-6978)

Mach Number Disturbance Reduction Using Fuzzy Logic

The National Transonic Facility (NTF) is a fan-driven, closed-circuit, pressurized wind tunnel which operates at test gas temperatures from –250° to 125°F. The test gas may be air or nitrogen. High Reynolds numbers are achieved using nitrogen at cryogenic temperatures. As part of the NTF Productivity Enhancement Project, a fuzzy logic control algorithm has been developed to reduce disturbances in the NTF test section due to changes in test article angle of attack. This control algorithm is called the Mach Number Disturbance Manager (MNDM).

The goal of the MNDM is to reduce the time the test section Mach number is outside an error band of ±0.001 about the desired Mach number for research testing, while the test article angle of attack is changed. The MNDM influences test section Mach number by changing the position of the inlet guide vanes (IGV) for the fan. To achieve its goal, the MNDM uses the Mach error and error rate as well as pitch position and pitch command input for the arc sector in the test article positioning system to calculate an IGV command. Test section Mach number data are used in conjunction with IGV position and arc sector pitch position to create a fuzzy rule-base and to calculate scaling factors, which the MNDM uses to reject disturbances at a particular Mach condition associated with a particular test article.

Figure 5 shows tunnel data collected while testing the MNDM at tunnel conditions of 0.9 Mach and 125°F with air as the test gas. In this case, the MNDM successfully reduces the rms Mach error by 16 percent and the time the Mach number is outside the error band over the duration of the angle-of-attack sequence by 33 percent, when compared with the Mach number response under the current Mach control algorithm used at the NTF. The current Mach control algorithm uses Mach error only, and cannot anticipate Mach number disturbances due to changes in test article angle of attack. Testing of the MNDM at 0.9 Mach and cryogenic temperatures with nitrogen as the test medium indicates the need for scheduling of scaling factors, with respect to temperature and fan speed, to achieve similar results. Future testing will include a variety of test articles as well as other test section conditions.

(D. A. Gwaltney, 757-864-6977)

Design of Three-Axis Dynamic Model Manipulator for Forced Oscillation Testing

The design of a Three-Axis Dynamic Model Manipulator (DMM) for use in forced oscillation testing has been completed. The system is a replacement of an existing single-axis forced oscillation rig (FOR) and is to be used in the Langley 14- by 22-Foot Subsonic Tunnel. Forced oscillation testing is used to measure dynamic derivatives of vehicle configurations. Test vehicles include high performance and general aviation aircraft, reentry spacecraft, submarines, and other fluidic vehicles. The data are used in damping characteristic studies and used in simulation database for control algorithm development and performance analyses.

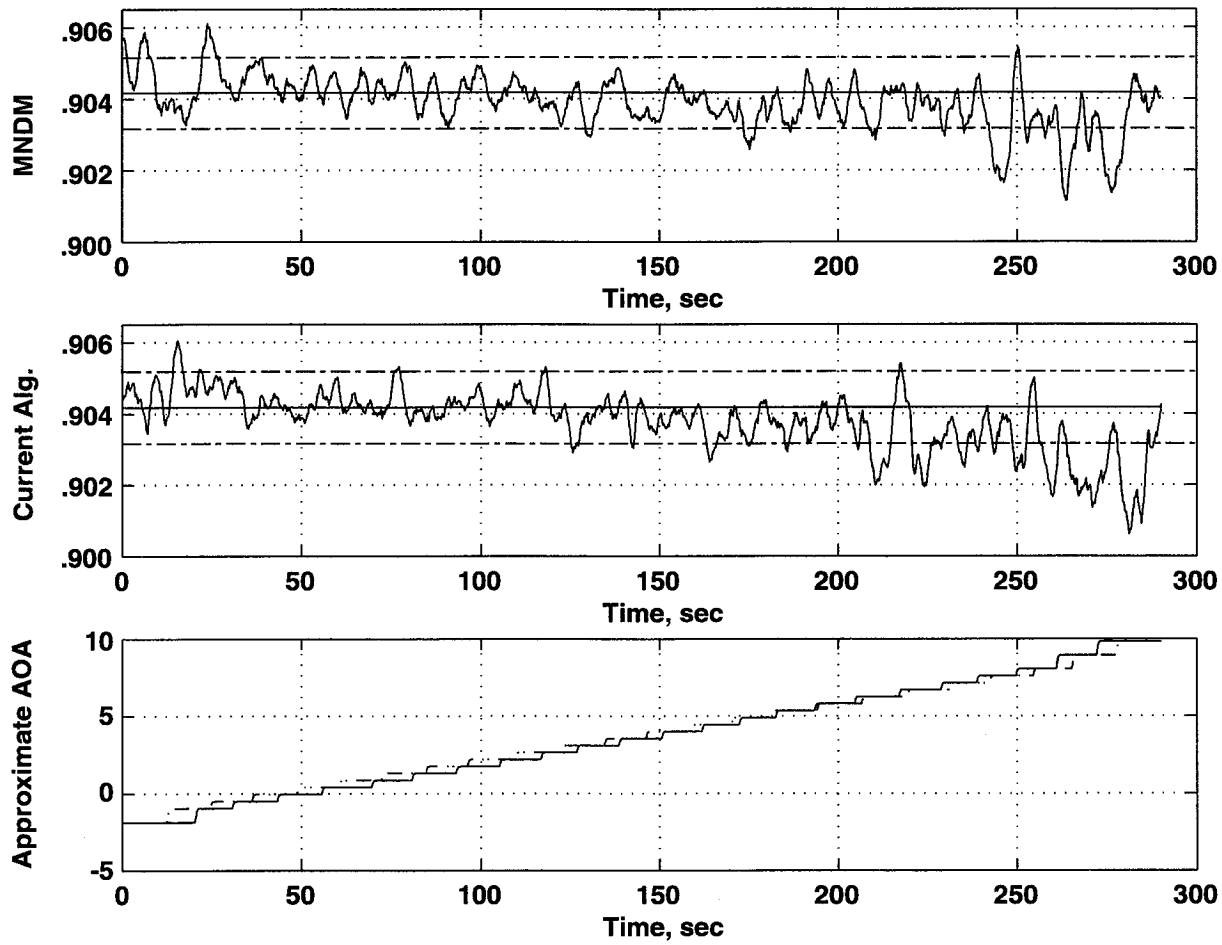

Figure 5. Comparison of NTF Mach number response data for changing angle of attack (AOA).

The Three-Axis DMM will greatly enhance and facilitate forced oscillation testing and thus it significantly increases productivity. The three-axis manipulator allows researchers to test all three model axes (pitch, roll, and yaw) without dismounting the model. It also expands the envelope of testing. The ranges of motion for the axes are as follows: Pitch, ±110°; yaw, 85° to −265°; roll, 90° to −180°. The combined motion completely simulates motion envelopes of an aircraft. Figure 6 shows a comparison of frequency versus amplitude operating envelopes for a 200-lb model in pitch oscillation. The analytical result shows that the new design has the capability to exceed the existing FOR by as much as 70 percent.

The design solution used in the Three-Axis DMM provided potential future capabilities which have never before been realized for forced oscillation testing techniques. Unlike the existing FOR where sinusoidal motion profiles are generating by a mechanical rotating cam, the new design is based on a tracking principle where a desired motion profile is achieved via a fast closed-loop positional controller. The desired oscillatory motion can be changed in the future to a non-sinusoidal profile. Since two of the three axes in DMM are capable of lively oscillatory motion, it is also possible that combined oscillation such as pitch and roll or yaw and roll can be achieved.

The Three-Axis DMM will have a direct impact on forced oscillation testing and thus the design of high-performance aircraft. The productivity gain via the Three-Axis DMM can shorten the testing cycles for control surface and control algorithm development. It

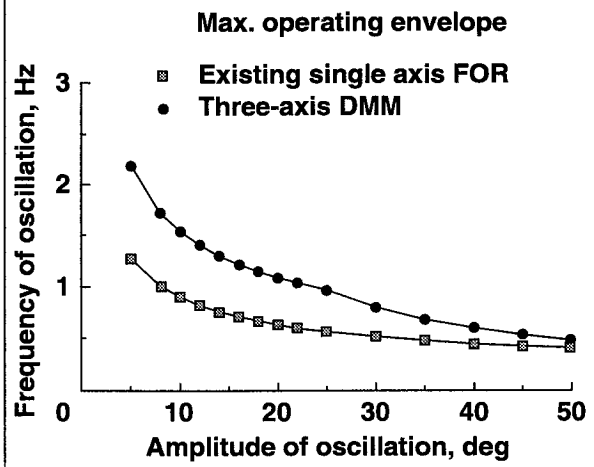

Figure 6. Comparison of frequency versus amplitude operating envelopes for pitch oscillation.

also serves as a testbed for researchers to study and to potentially improve and/or alter future forced oscillation testing techniques. **(B. K. Stewart, 757-864-6902)**

3-D Resin Film Infusion Model for Wing Structures

As part of the NASA Advanced Composites Technology Program (ACT), NASA and McDonnell Douglas are in the final phase of a major program to develop and validate advanced composites wing technology. Damage-tolerant textile material forms and cost-effective manufacturing concepts have been selected for fabrication of the wing structure. Three textile processes, multiaxial warp knitting, triaxial braiding, and through-the-thickness stitching, are being developed for fabrication of certifiable aircraft-quality structures. Fabrication of composite structures from textile preforms requires three steps: (1) fabrication of a near-net shape preform; (2) infusion of the preform with low viscosity resin; and (3) compaction and cure of the composite structure. To minimize costly trial and error manufacturing process development, analytical models of the resin infusion process for the wing structures are required.

Three-dimensional resin film infusion (RFI) process models are being developed under a NASA grant with Virginia Polytechnic Institute to predict resin flow front

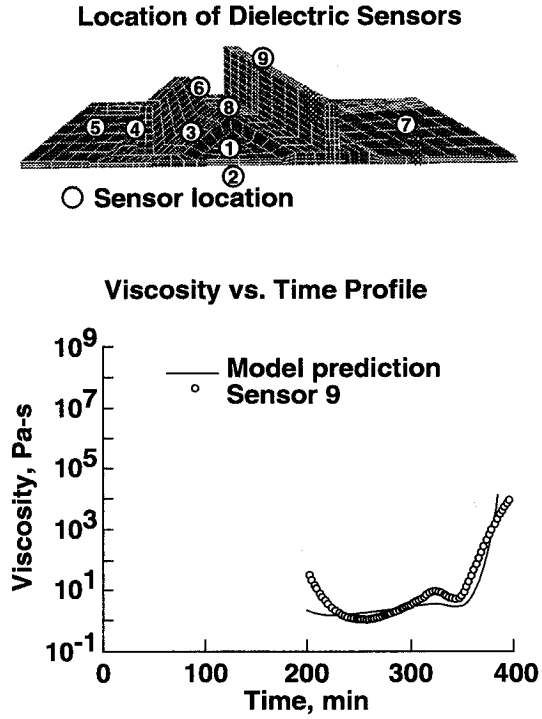

Figure 7. Comparison of predicted and measured viscosity.

position and key resin properties such as viscosity and degree of cure as a function of temperature and time. Resin viscosity is the most important parameter in the cure cycle because the entire textile preform must be infused or wet-out before the resin begins to gel. Since resin viscosity is a function of temperature, the entire thermal mass of the tooling concept must be modeled to accurately model heat transfer. Figure 7 shows a finite-element model of a complex region of a wing cover panel where a stiffener runs out or intersects the spar. The tooling, the resin, and the multiaxial warp knitted/stitched carbon fabric preform were modeled. The flow model is based on Darcy's law for flow through anisotropic porous medium. Empirical relationships for fabric compaction and permeability as a function of pressure and resin kinetics data were provided as input to the finite-element flow simulation model. Transient thermal, viscosity, and flow calculations are performed until the preform is saturated with resin. To establish the accuracy of the 3-D flow model, a series of experiments were conducted with nine dielectric sensors mounted in the tooling at the locations indicated in

figure 7. Through previous laboratory calibrations, the sensors were used to measure resin flow front position, resin viscosity, and degree of cure. The figure shows a comparison between the measured viscosity and the predicted viscosity at sensor location number 9, which is located on top of the stiffener. Sensor number 9 was wet-out with resin after approximately 200 min into the RFI cycle. Results indicate a good correlation between the predicted and measured viscosity as a function of time.

The 3-D RFI flow model is being extended to model large wing panels up to 40 ft long for the NASA/ McDonnell Douglas wing program. Enhancements include development and verification of a residual stress/warpage submodel, refinement in the permeability submodel, and improvements in computational efficiency so the code can be run on workstations. **(H. B. Dexter, 757-864-3094)**

McDonnell Douglas All-Composite Wing Stub Box Successfully Tested to Failure

Advanced structural concepts using lightweight composite materials are being developed for application to transport aircraft wing structures. Structures to be used on commercial transport aircraft must be economical as well as able to meet all structural requirements. One cost-effective structural concept proposed for use on wing structures is based on the Resin Film Infusion manufacturing method. For this manufacturing method, layers of graphite material are stitched together in a desired configuration and the part is placed in an autoclave with a layer of resin film. As the part is heated and pressure is applied, the resin is pulled through the skin and stiffeners. Panels up to 12 ft long have been successfully fabricated in this manner. A wing stub box was designed and fabricated by McDonnell Douglas Aerospace to be representative of a highly-loaded section of a transport wing box.

This wing stub box was tested in the Structures and Materials Laboratory at NASA Langley. (See fig. 8.) The wing stub box was 12 ft long and 8 ft wide at its root. Metal load-introduction structures were attached to the wing stub box, resulting in a 25-ft-long test specimen. A series of structural tests were conducted by loading the wingtip with a hydraulic jack. Tests included loading the structure with no damage, with detectable damage, with nondetectable damage, and with a repair to a damaged area. Strains at 250 locations

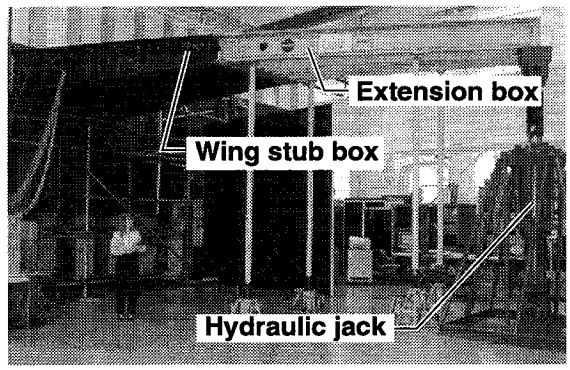

Figure 8. Wing box prior to test.

and displacements at 15 locations on the structure were recorded during each test. For the final test, the structure was loaded until it failed through a nondetectable damage location at 140 percent of design limit load. The tests verified the ability of the wing box structure to satisfy the critical design requirements. Test and analysis results agree very well. **(D. C. Jegley, 757-864-3185)**

Aeroacoustic Prediction of Rotor Blade-Vortex Interactions

Helicopter blade-vortex interactions (BVI) cause one of the most annoying types of helicopter noise that becomes dominant during low-speed descent and maneuvering flight. To alleviate this annoyance, much effort has been focused on developing capabilities to measure, predict, and control BVI and its resulting noise. At Langley a rotor noise prediction capability has been developed to accurately predict the highly impulsive character of BVI. The prediction method consists of several codes: a comprehensive rotorcraft performance analysis, a full potential rotor code, and a rotor acoustic analysis. These prediction capabilities will be used to aid in the design of low-noise rotors as well as low-noise flight operating procedures for commercial applications.

To validate these prediction capabilities, data from the Higher-Harmonic-Control (HHC) Aeroacoustics Rotor Test (HART) were utilized. The HART is the most comprehensive rotor test to date of the aeroacoustics of rotor BVI including its reduction. The test was performed in the Dutch-Nederlandse Windtunnel

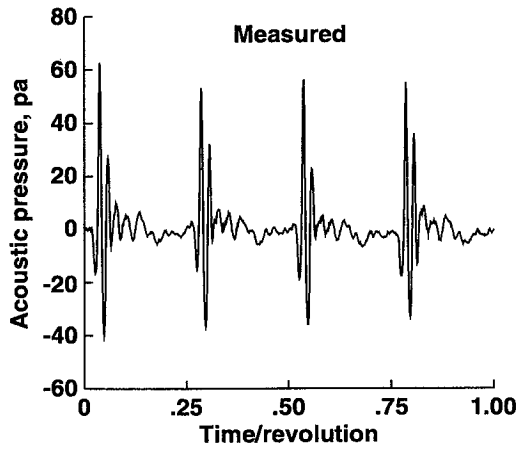

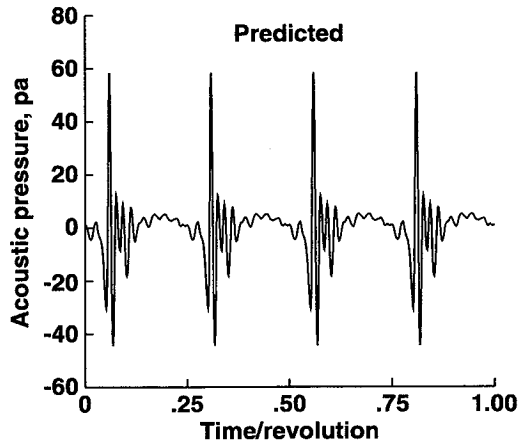

Figure 9. Measured and predicted noise comparison.

(DNW) in 1994 as a cooperative DLR/ONERA/U.S. Army Ames/NASA Langley effort employing German and French hardware. The test provides first-time simultaneous detailed measurements of acoustics, aerodynamics, wake systems, and blade deformations for a rotor.

Figure 9 shows a comparison of predicted acoustics with measurements from the HART test for a non-HHC condition. These posttest predictions, which utilize the measured blade motions and vortex core sizes obtained from the test, clearly demonstrate the high accuracy of these methods. **(C. L. Burley, 757-864-3659)**

UH-60 Growth Rotor Blade Acoustics Flight Test

Acoustics data of a full-scale UH-60 Black Hawk helicopter equipped with growth rotor blades (GRB) were obtained in a joint NASA/U.S. Army/Sikorsky flight test. The GRB were designed to provide improved performance and reduced noise over that of the standard UH-60 rotor blades. The GRB, which are the same length as the standard main rotor blades, feature wider chords and anhedral (angled with respect to true horizontal) tips. (See fig. 10.) The test was performed to acquire an acoustics flight test database for the UH-60 with GRB for comparison with standard main rotor acoustics data collected previously and to provide data for future noise prediction model development for advanced rotor concepts.

Figure 10. Growth main rotor with anhedral tips on UH-60 Black Hawk.

The test was conducted at the Sikorsky Aircraft Acoustics Range in West Palm Beach, Florida, in August 1995 using an Army UH-60L flown by Sikorsky pilots. The aircraft equipped with the GRB flew a matrix of conditions representative of typical terminal area operations over a linear array of 18 ground-based microphones. Data were obtained for level flight, approach (descent), departure (ascent), and turns. Limited acoustic data were also acquired with the standard UH-60 main rotor blades to provide a direct comparison of the two rotor systems at the same test site. Aircraft tracking and guidance were provided by the NASA Ames Research Center using a laser tracking/guidance telemetry system. Aircraft state, weather, and backup Differential Global Positioning System (DGPS) tracking data were also provided by Sikorsky.

GRB acoustic data were collected for 147 flyovers (69 level, 43 approaches, 13 departures, and 18 turns). Data with the standard main rotor were collected for 17 flyovers (10 level and 7 approaches). Following initial processing, the acoustic data, in conjunction with the tracking, weather, and aircraft state data will be compared with the previously obtained standard main rotor data. This data set will also be available to noise prediction model developers for use in code validation. **(O. L. Santa Maria, 757-864-5104)**

Active Flaperon Significantly Reduces Vibratory Loads in Tiltrotor Wing

The fundamental vibration problem in tiltrotor aircraft is caused by blade passage in front of the wing while in high-speed airplane-mode flight. Flow about the wing creates an azimuthally unsymmetric inflow through the rotor system which is the primary contributor to fixed system (pylon, wing, and fuselage) vibrations. The Wing and Rotor Aeroelastic Testing System (WRATS) tiltrotor model is a semispan testbed developed from the former V-22 1/5-scale aeroelastic tiltrotor model, designed and fabricated by Bell Helicopter Textron, Inc. (BHTI). In an effort to control vibrations in the fixed system, BHTI developed the Multipoint Adaptive Vibration Suppression System (MAVSS). The research objective of the current work was to evaluate the ability of the MAVSS system to control vibrations on the WRATS model during a wind-tunnel test in the Langley Transonic Dynamics Tunnel (TDT).

A photograph of the WRATS model mounted in the TDT is shown in figure 11. An active flaperon assembly was installed on the WRATS model and driven by a signal produced by the MAVSS system, with resulting flaperon motion limited to ±6°. The basic test procedure was to choose conditions of high vibration, activate MAVSS, and compare the resulting MAVSS-on and MAVSS-off loads. The bar chart in figure 11 contains results from the wind-tunnel test and illustrates the success of MAVSS in controlling vibratory loads. The pairs of vertical bars at four airspeeds indicate that, compared with the system-off loads, MAVSS significantly reduced (by 84 to 97 percent) three-per-revolution (3P) vibratory wing torsion loads. The flaperon motions (circle symbols) required to accomplish these reductions are within acceptable limits and are proportional to the MAVSS-off loads. This test has

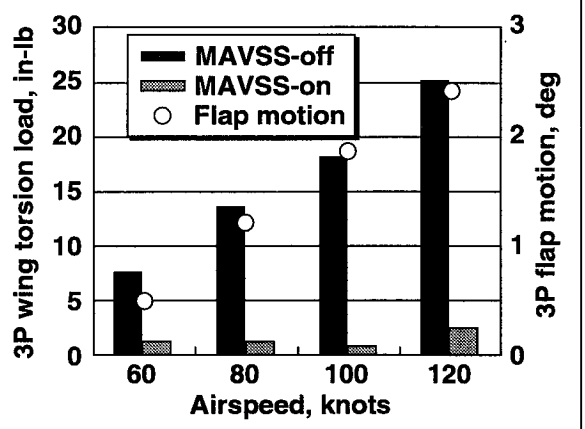

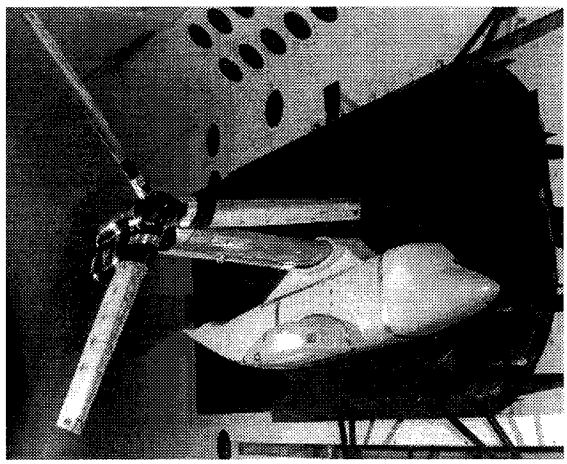

L-95-05100

Figure 11. Effect of MAVSS on loads as a function of airspeed.

confirmed that the MAVSS system is a viable candidate for countering the fundamental vibration problem in tiltrotor aircraft. BHTI will use the data from this test to help design an active elevator for flight testing on the XV-15 tiltrotor aircraft. The test data will also provide a baseline for comparison with future analytical and experimental active controls studies. The next planned active-control test of the WRATS model will have an active swashplate in addition to the active flaperon. **(M. W. Nixon, 757-864-1231)**

Novel High-Performance Piezoelectric Polyimides

A series of novel piezoelectric polyimides have been developed at NASA Langley. The polymers contain pendant polar groups such as trifluoromethyl ($-CF_3$) and cyano (–CN). By applying voltages on the order of 100 MV/m at elevated temperatures, a high degree of orientation of these polar groups is induced resulting in polymer films which exhibit outstanding piezoelectric and pyroelectric properties. Polyvinylidene fluoride (PVDF) is currently the only commercially available piezoelectric polymer; however, its lack of thermal and mechanical durability limits its application in extreme environments. The new polymers boast tremendous improvements over the state of the art in that they have an order of magnitude higher piezoelectric constants at elevated temperatures, are more thermally stable, and may be tailored to exhibit a range of mechanical, thermal, and electromechanical properties. In addition, these polymers are structural materials, polyimides, which means that it may be possible to incorporate them into adaptive structures.

The piezoelectric response for the polyimides is comparable to that of PVDF at room temperature. However, this response dramatically increases with temperature and is an order of magnitude greater than PVDF at elevated temperatures (see fig. 12). The improved piezoelectric voltage output of these polymers is consistent with computational calculations which predict that the dipole moment for a model polyimide moiety, which contains pendant highly polar groups, is an order of magnitude greater than that of PVDF.

The potential applications for this technology are immense. Due to their high sensitivity, flexibility, and high-temperature durability, it may be possible to use these polymers for sensing engine noise and undesired vibrations in aircraft. Other interests include the incorporation of these materials as sensors and microactuators to develop active isolation mounts to align precision instruments collecting data in space or as lightweight, muscle actuators which augment an astronaut's mobility in a spacesuit. **(J. O. Simpson, 757-864-4239)**

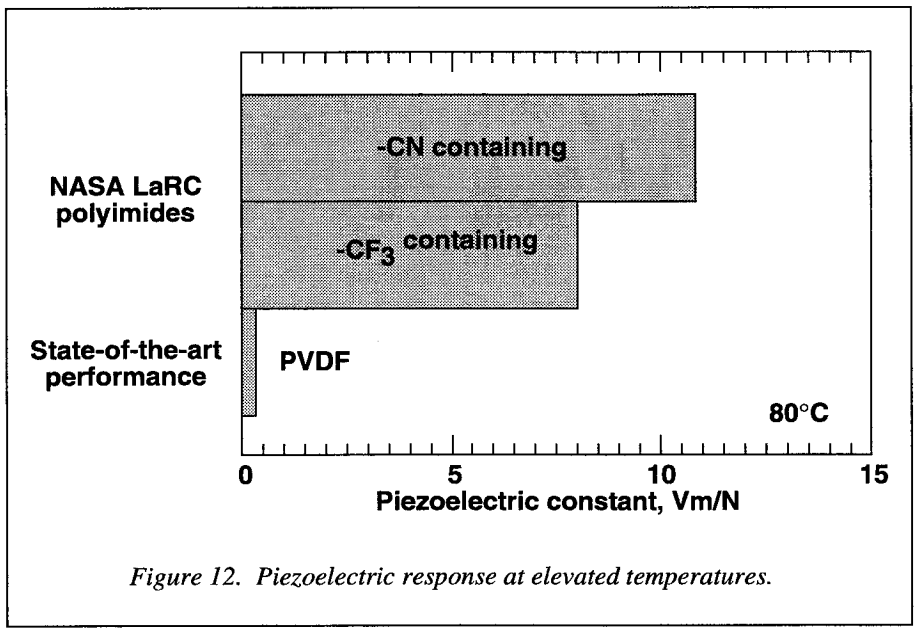

Figure 12. Piezoelectric response at elevated temperatures.

Thermoplastic Composite Fabrication by Automated Robot Heated Head Technology

Selected aircraft structure has been manufactured by automated tape placement of drapable, tacky *thermoset* prepregs such as epoxy and bismaleimide. Once laid up at room temperature by machine, the part has to be bagged and autoclaved in the normal fashion. However, cost models show that *in situ* placement/consolidation of dry boardy *thermoplastic* ribbon/tape by an automated tape placement machine containing a heated head can save up to 25 percent by reducing manufacturing complexity. By using dry material forms, this technique also eliminates solvents normally used in wet fabrication processes.

As part of its polymer composite materials research program, a thermoplastic fiber placement machine was designed and built for NASA Langley Research Center by Automated Dynamics Corporation. During the placement process, up to five individual fully consolidated prepreg ribbons or tape are fed from spools through a delivery system into a head heated with nitrogen gas torches. The head collimates the band of ribbons and applies heat and pressure to melt the thermoplastic tape and laminate them onto a work surface. Figure 13 shows the robot laying ribbon onto a flat heated tool. A spindle for handling closed form tools is shown on the left side of the figure. The tow placement pressure roller contacts the surface of the part and allows for placement in nonnatural paths required for complex parts.

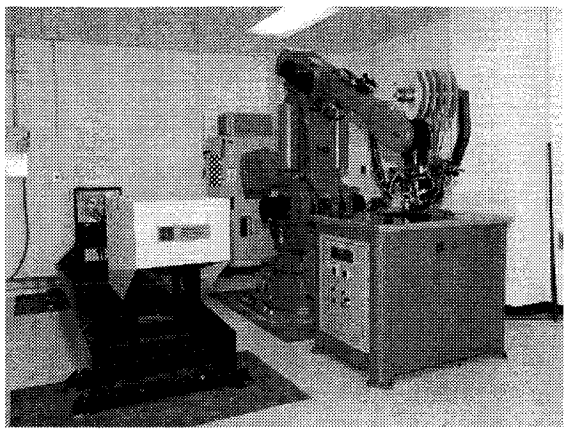

Figure 13. Thermoplastic fiber placement machine.

Current research on this emerging technology emphasizes process issues related to high-temperature materials such as polyimides and polyarylene ethers and machine issues which directly influenced manufacturing costs. Presently, mechanical property data on polyimide composites made by this in situ technique average from 70 to 90 percent of that obtained from autoclave processed composites. Process improvements are expected to increase those percentages.
(N. J. Johnston, 757-864-4260)

Test Methods for Characterizing Composite Skin-Stringer Debonding

Bonding or co-curing of stringers to skins is attractive because of the reduced manufacturing cost compared with mechanically fastened structures. However, out-of-plane loadings such as internal pressure in a fuselage or a postbuckled skin panel may cause debonding failures. A cooperative program has been set up with Boeing Helicopter Company to evaluate simple test configurations for isolating these debonding failure modes in stiffener reinforced structures.

Stringer pull-off subcomponent tests indicated that the bending moment and transverse shear in the skin at the tip of the frame flange drives the failure. Coupon sized specimens consisting of a tapered frame flange bonded onto a skin laminate were manufactured and tested in three and four point bonding to simulate different combinations of moment and transverse shear at the flange tip. Optical micrographs of the specimen edges were obtained to document the damage mechanisms that lead to complete disbonding of the frame from the skin. Two-dimensional plain strain finite-element analyses were performed to identify the stresses responsible for initiating the observed damage.

As shown in figure 14, results indicated that the principal transverse tension stress in the top ply of the laminate skin calculated at the failure load for three different flange and skin combinations labeled QI (quasi-isotropic flange and skin) and AH and BH (braided flange with tow placed skin laminates) fell within the range of the transverse tension strength of the material measured from 90° tension tests.

The simple three and four point bend tests may be very useful in identifying stringer debond failure mechanisms and estimating the bond strength. This research will help provide validated design criteria for skin-stringer bond strength in reinforced composite panels.

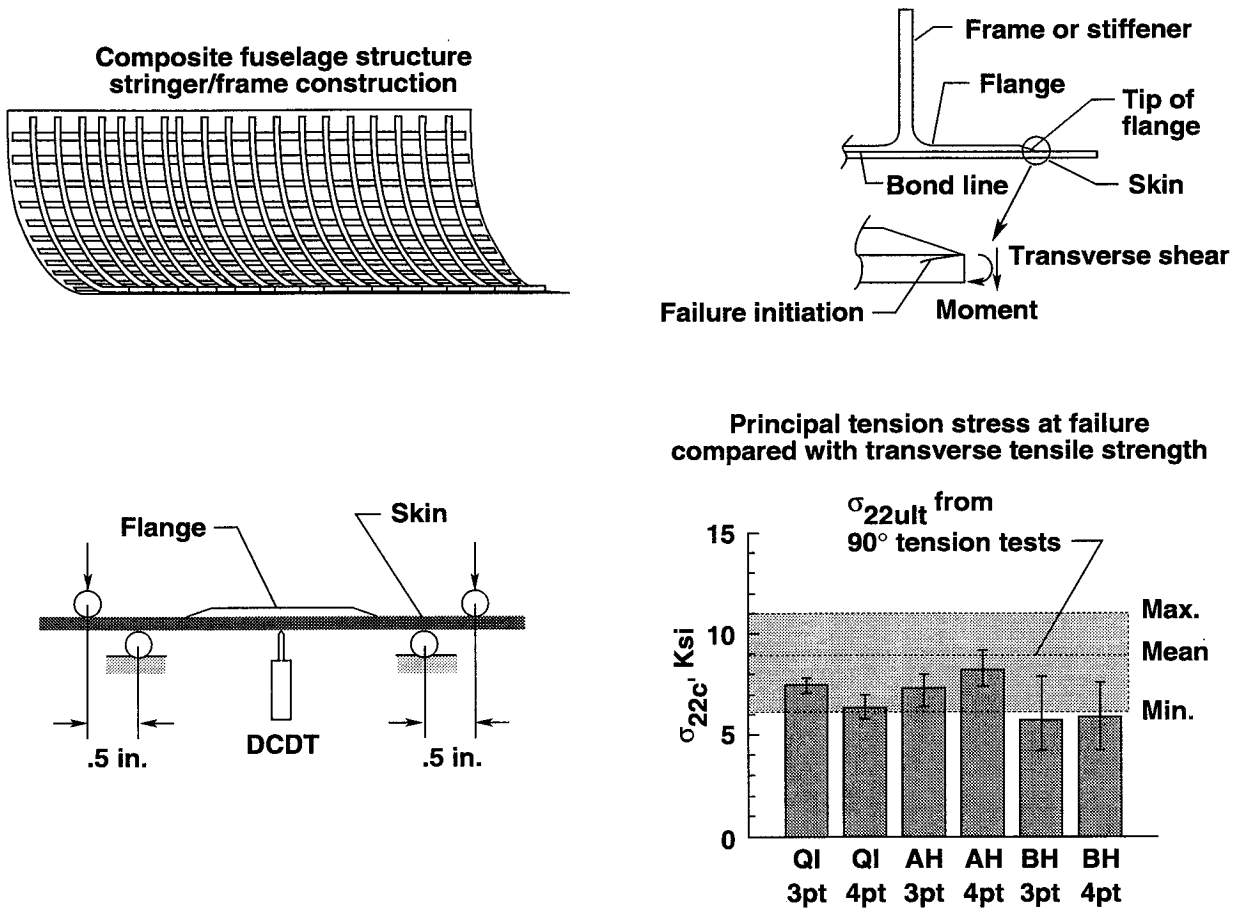

Figure 14. Test methods for characterizing skin stringer debonding.

Parametric tests and analyses will be performed to identify the sensitivity of these results to typical design changes such as frame and skin thickness, layup, material form, etc. **(T. K. O'Brien, 757-864-3465)**

Rapid Superplastic Forming of Aluminum Components

The superplastic forming (SPF) of aluminum aerospace alloys is an emerging technology involving the elevated temperature forming of sheet materials capable of achieving forming strains of 200–1000 percent. The limited room temperature ductility of aluminum aerospace sheet materials has tended to result in costly multistep forming operations and subassemblies to produce a component. The exceptional formability afforded by the SPF process permits the manufacture of complex-shaped parts in a single forming operation. This single-step forming operation makes it possible to fabricate selected aluminum structures which exhibit weight savings of 20–50 percent and cost savings ranging from 30–70 percent compared with components fabricated using conventional metal forming technology. Airframe weight savings have been realized through the use of more structurally efficient designs and reduced part/fastener counts while manufacturing cost savings have been achieved by the reduction in processing steps, tooling, and subassemblies.

A major drawback to the widespread application of SPF technology in the aerospace industry has been the unacceptably long forming times associated with the process cycle. The strain rate at which most aluminum alloys exhibit optimum superplasticity is approximately

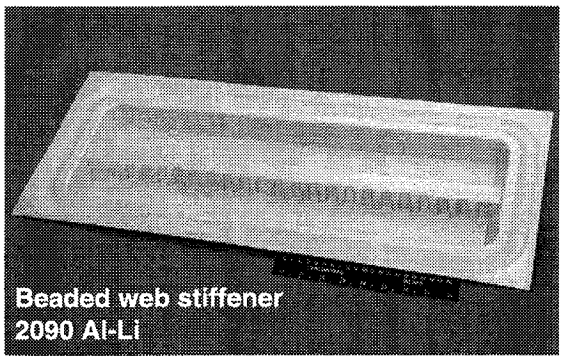

Figure 15. SPF structural subelement.

5×10^{-4} sec^{-1}. This translates into a forming time approaching 40 min for complete formation of the part. Recent studies have shown that a new, innovative pressurization cycle, in combination with superimposed hydrostatic pressure and sheet/die lubrication, reduced the forming time by an order of magnitude. Figure 15 shows a 2090 Al-Li SPF structural subelement which was formed in 4 min. Faster forming will result in higher production rates and lower overall processing costs. **(E. K. Hoffman, 757-864-3127)**

Learjet Model 45 Flutter-Clearance Tests Conducted in Langley Transonic Dynamics Tunnel (TDT)

Business jet aircraft must be designed so flutter will not occur within the aircraft flight envelope with a 20-percent safety margin. This is accomplished using analyses, wind-tunnel testing, and aircraft flight testing. Wind-tunnel flutter testing is often an integral part of a flutter-clearance program, with the results used to provide guidance for flight flutter-clearance testing and to provide flutter data for correlation with flutter prediction codes. The objectives of the present cooperative program with Learjet was to demonstrate that a full-span aeroelastic wind-tunnel model of the Learjet Model 45 aircraft was free of flutter within the scaled flight envelope, which included the required margin of safety, and to provide flutter results at transonic speeds for evaluation of analytical codes.

A 1/6-scale full-span aeroelastic model of the Learjet Model 45 aircraft was tested in the Langley Transonic Dynamics Tunnel (TDT). The model, mounted on a sting in the TDT test section, and a chart showing scaled tunnel conditions achieved as compared with the predicted aircraft flight envelope, is shown in figure 16.

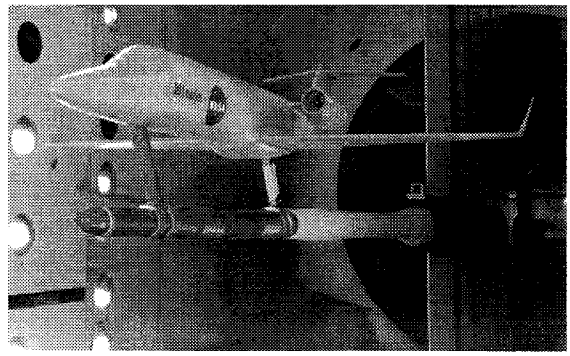

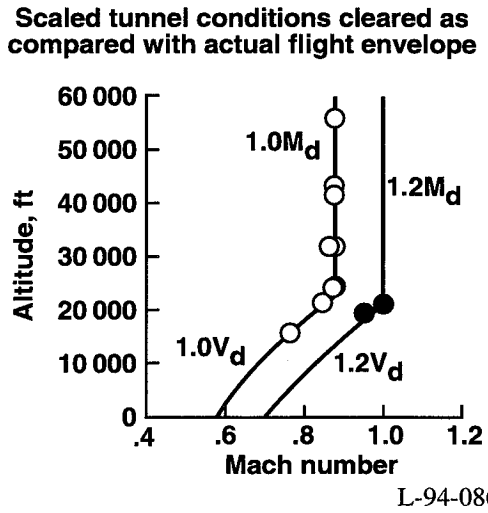

Figure 16. Learjet Model 45 flutter model mounted in the TDT.

Several configurations were tested. The nominal vehicle configuration was tested to $1.2V_d$ and $1.2M_d$. (20 percent beyond the dive speed and dive Mach number) and did not flutter. These data are shown in figure 16 by the shaded circular symbols. Component-failure configurations such as excess control-surface freeplay and control-surface mass balance variations, were flutter cleared up to $1.0V_d$ and $1.0M_d$ (dive speed and dive Mach number). These conditions are shown by the open circular symbols. In addition, transonic flutter was measured for a modified wing configuration (these data are not shown) to evaluate linear flutter prediction codes. Compared with the experiment, the linear flutter predictions were approximately 10-percent conservative.

Tests of this type ensure that flutter problems that may exist for a new design are identified early enough in the design/development cycle so that a solution (fix) can be affected in a timely manner with minimum impact on cost and schedule. In addition, wind-tunnel tests such as those described here reduce the number of more costly flight flutter tests.
(J. A. Rivera, 757-864-1270)

Interface Element Technology Extended to Geometrically Nonlinear Analysis

Reliable, accurate predictions of the impact of design details and modifications on the structural response of critical components are needed in order to understand and predict the failure mechanisms of such components. While linear analyses are quite useful, they often miss important response phenomena. Thus, computational tools that allow detail to be considered early in design in both the linear and nonlinear regimes are needed. Interface technology provides such a tool for treating design details and allowing rapid model modification within the framework of general-purpose finite-element codes. This interface technology, previously developed for linear analysis, has been extended to geometrically nonlinear analysis. Because the method eliminates the need for coincident finite-element model grid points, no transition mesh is required between diversely discretized models. Interface elements, derived from hybrid variational principles of mechanics, are used to connect the independently discretized models. Accurate response and stress predictions are obtained even at the interface of the independent models.

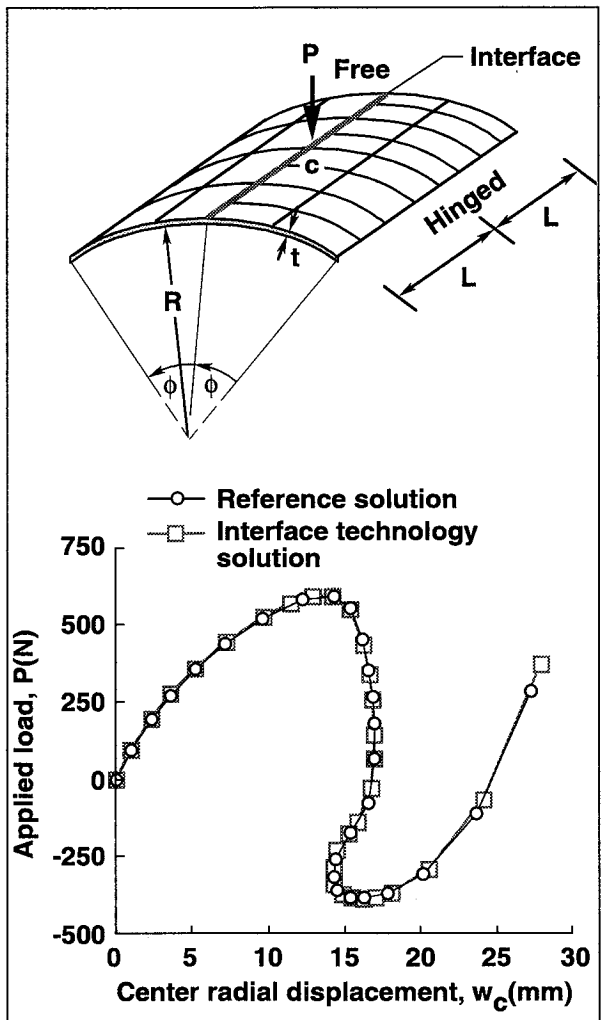

Figure 17. Interface technology used to predict nonlinear response of cylindrical panel.

In figure 17 interface technology is applied to the nonlinear analysis of an isotropic cylindrical panel. The panel is hinged on its two straight edges and free on its curved edges and is subjected to a concentrated load at its center (point *c* in fig. 17). The panel is known to exhibit a snap-through, collapse behavior as well as a snap-back behavior, which are challenging responses for nonlinear solution procedures. The interface element is defined along the straight interface between the two curved shell models having different mesh densities. The panel properties are 3.10275 kN/mm^2 for the Young's modulus and 0.3 for the Poisson's ratio. The panel radius R is 2540 mm, the half length L is 254 mm, the thickness t is 6.35 mm, and the half-opening angle ϕ is 0.1 rad. A reference solution is obtained by extending the mesh of the most refined side of the interface element coupled model over the entire domain. The predicted response using the interface element technology is in excellent agreement with the reference solution. The interface technology has been developed within the COMET (COmputational MEchanics Testbed) research code and has been implemented in the commercially available MSC/NASTRAN finite-element code. **(J. B. Ransom, 757-864-2924)**

Monitoring Functional Integrity in Fault-Tolerant Control Computers for Critical Applications

Future advanced commercial aircraft will require systems for stability augmentation and flutter suppression, as well as guidance and control. Such systems will be designated as flight critical, since the flight of the aircraft will depend on reliable operation of these systems. The problem of verifying the integrity of the control computer in adverse, as well as nominal, operating environments becomes a key issue in the development, certification, and operation of a critical control system. The integrity of critical fault-tolerant control computers can be viewed as the reliable system-level operation of controller functions such as control law calculations, redundancy management decisions, and input/output (I/O) rate and range checks.

A general structure for monitoring the functional integrity of fault-tolerant control computers is under development and consists of three modules (see fig. 18). The fault-tolerant controller is monitored for malfunctions in the control law calculations in module 1; redundancy management logic in module 2; and input/output (I/O) rate and range checks in module 3. Malfunctions in control law calculations result when the basic mathematical operations of the processor are performed incorrectly. An example of a malfunction in the redundancy management logic is the controller deciding that one of the redundant processors is faulty and ignoring its calculations when, in fact, it is operating correctly. Rate and range checks are performed in the input parameter selection process and the output command selection process. Malfunctions in I/O rate and range checks can result in incorrect input parameters being used in calculations or incorrect commands being output from the controller. The decisions for each of these modules are combined in some manner to determine the existence or nonexistence of malfunctions. The design of the Control Law Calculation Malfunction (CLCM) detector, shown in bold lines in figure 18, has been completed and simulated for the longitudinal control laws of a quad-redundant Boeing 737 Autoland controller. The design uses Kalman filters, statistical decision theory, and decision fusion and its performance can be determined analytically. This work was published in a Ph.D. dissertation through Drexel University and in several conference papers. **(C. M. Belcastro, 757-864-6182)**

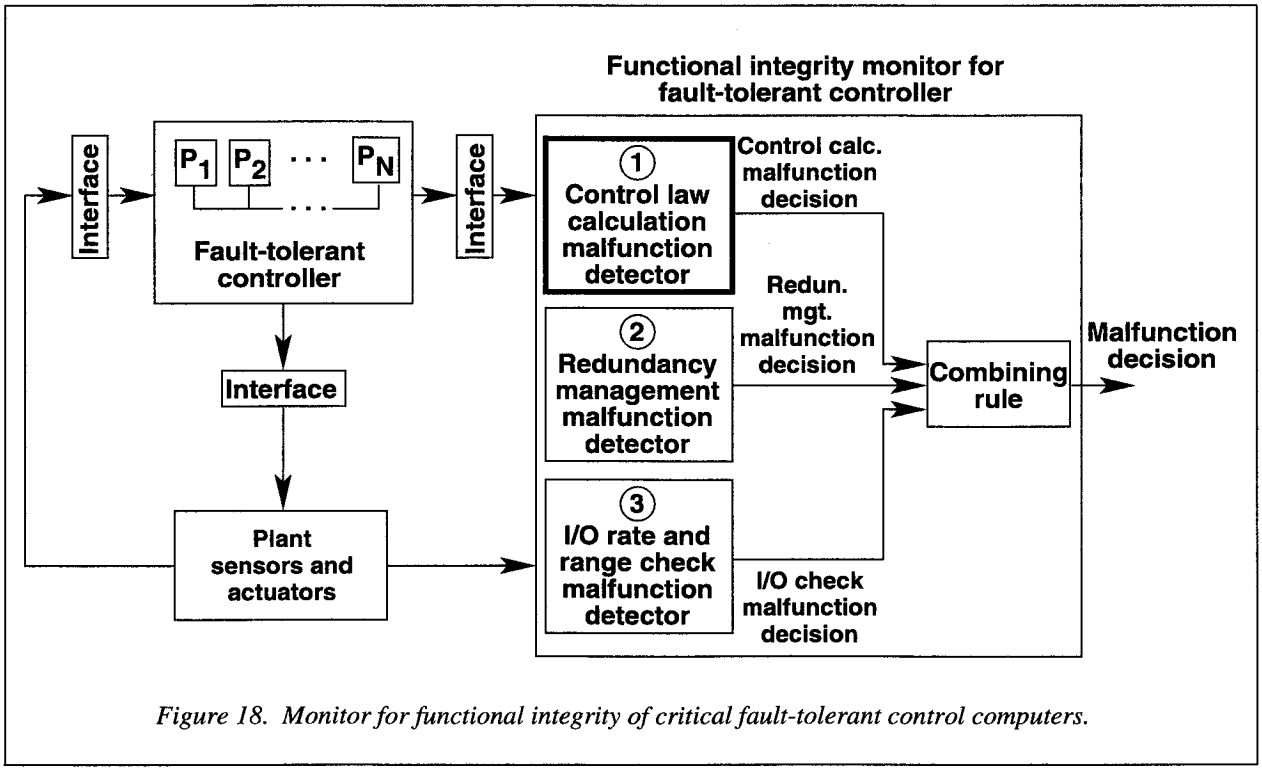

Figure 18. Monitor for functional integrity of critical fault-tolerant control computers.

Formal Methods for Civilian Aircraft

Modern civilian aircraft are undergoing a major revolution in their use of digital computer technology. The Boeing 777, for example, contains 2.6×10^6 lines of code whereas its predecessors, the 757 and 767, contain less than 600000 lines. Consequently, there is a growing realization that the safety of modern aircraft critically depends upon effective and efficient methods for verifying the software and hardware designs used in them. Unfortunately, standard verification and validation techniques, which are based upon process management and extensive testing, are rapidly reaching the point where they are incapable of providing adequate assurance despite consuming over 60 percent of the total development cost.

The formal methods team at Langley is working with industry and other research laboratories to develop methods for verifying the correctness of digital systems, both hardware and software, using the techniques of mathematical logic. Unlike testing, which can never show the absence of design flaws, formal methods exploit techniques from logic such as mathematical induction to show that a design satisfies its specified behavior over all of its input space.

Under NASA funding, Odyssey Research Associates (ORA) has been working with Honeywell Air Transport Systems Division (Phoenix) to develop a tool called TableWise (see fig. 19) that logically analyzes decision tables, a tabular method for representing system requirements. TableWise automatically determines if a particular table is exclusive (for every combination of parameter values, at most one action can be chosen) and exhaustive (for every combination of parameter values, at least one action can be chosen). The tool is also capable of automatically generating documentation and Ada code from a decision table. Rockwell Collins has also obtained a copy of TableWise and is currently assessing its usefulness to them.

Other formal methods projects at Langley include: (1) the formal verification of the Rockwell Collins AAMP-FV microprocessor, (2) the formal analysis of the Honeywell SAFEbus (backplane bus of the Boeing 777 AIMS), and (3) formal analysis of the next-generation train signaling system of Union Switch and Signal. **(R. W. Butler, 757-864-6198)**

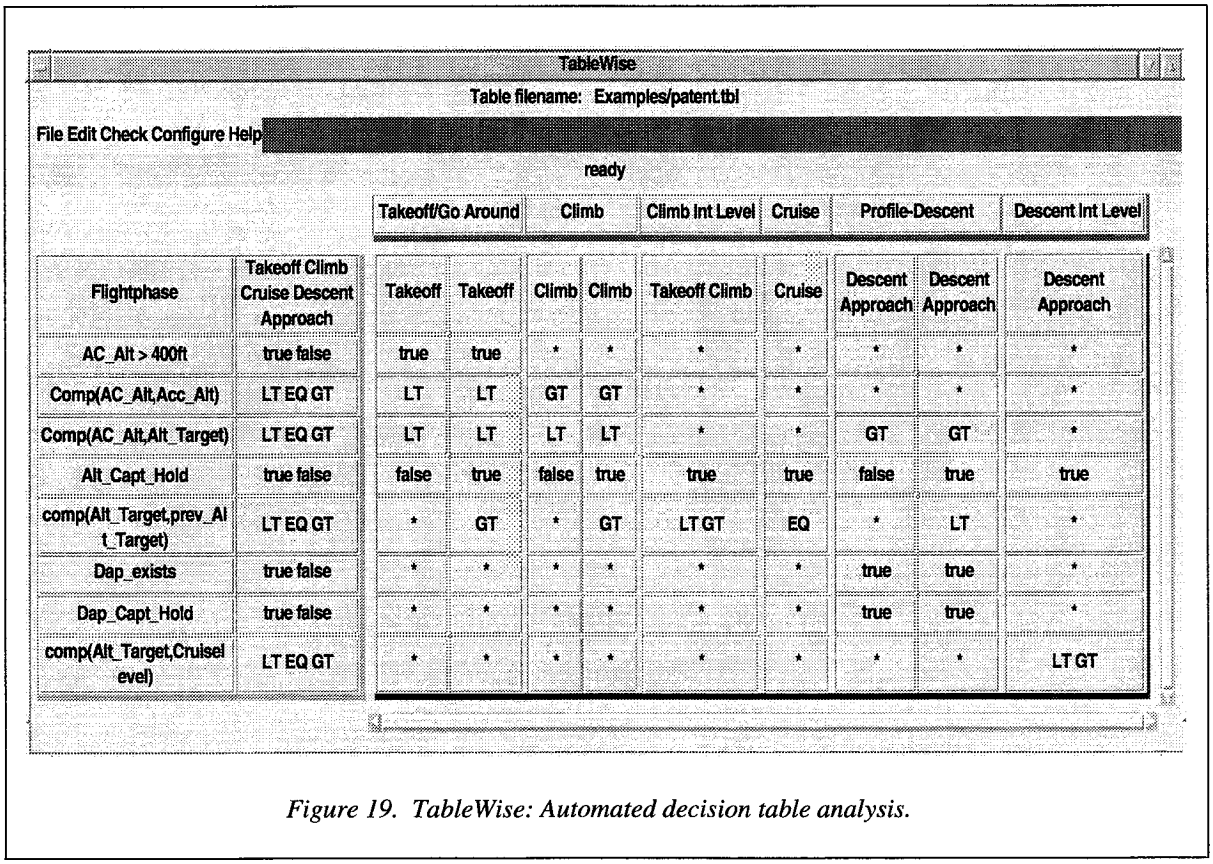

Figure 19. TableWise: Automated decision table analysis.

Assessment Methodology for Critical Control Computers Operating in Harsh Electromagnetic Environments (EME)

The development of a methodology to assess the effects of lightning electromagnetic transients and high intensity radiated fields (HIRF) on digital electronics aboard advanced transport aircraft is critical to the certification of future commercial aircraft. The Federal Aviation Administration (FAA) and Europe have stringent requirements for EME certification and require compliance demonstrations. EME tests involving full-aircraft can be performed on the ground but are extremely costly and do not include dynamic closed-loop system effects over the operating envelope of the equipment.

A low-cost comprehensive approach to assessing EME upset susceptibility (see fig. 20) is under development and consists of four primary elements: EM field modeling and code validation, EM Test Facility, closed-loop test capability, and real-time function monitoring. Costs are reduced by replacing full-aircraft testing with EM field modeling and bench-level testing in an EM test chamber. During these tests, the Equipment Under Test (EUT) is interfaced with a dynamic simulation of the aircraft so that closed-loop dynamics over the operating envelope of the equipment are represented. The functional integrity of the EUT is assessed in real-time during the tests so that the impact of upsets on the operational performance of the closed-loop system can be evaluated. Error margins within which the EUT does not impact performance requirements for the closed-loop system can be determined.

A geometric computer model of the Boeing 757 has been completed for determining the internal EME using EM computer codes. Development of the finite difference time domain EM code is in progress. The design and construction for the EM Test Facility is complete. The facility consists of a GHz Transverse Electromagnetic (GTEM) test cell and three mode-stirred reverberation chambers. Demonstration of the closed-loop test capability on a quad-redundant Boeing 737 Autoland control computer is in progress. A computer simulation of the Boeing 737 aircraft, engines, sensors, and

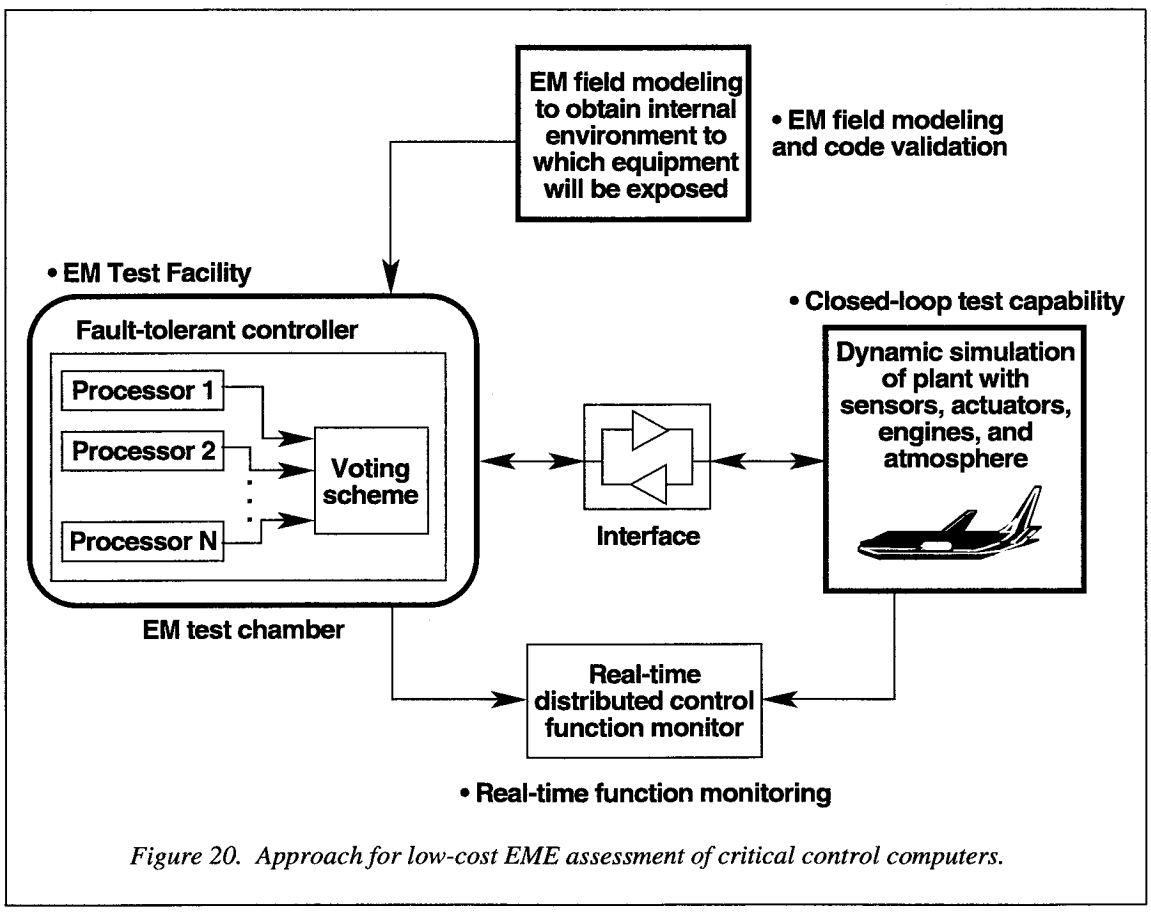

Figure 20. Approach for low-cost EME assessment of critical control computers.

actuators with wind gust and turbulence models is complete. The design of a monitor for detecting malfunctions in the control law calculations of a quad-redundant controller has been completed and simulated for the Boeing 737 Autoland longitudinal control laws.
(C. M. Belcastro, 757-864-6182)

Optical Disk Recorder for Flight Research

An optical disk recording system was developed for application on the NASA OV-10 flight research aircraft. The system is designed to record data from digital data acquisition systems on a variety of transport and high-performance flight research aircraft. The system consists of (1) a data interface printed circuit board containing a serial digital decommutator and serial to parallel data converter, (2) a miniature embedded single board computer with a small computer system interface (SCSI), and (3) a rugged commercial rewritable magneto-optic disk drive which meets military aviation flight environments (see fig. 21). The data interface and computer printed circuit boards are in a 9.0 cm by 9.6 cm form factor utilizing the PC-104 BUS Standard, and are packaged in a small rugged flight enclosure.

Each rewritable optical disk can record 650 megabytes of data on each side. Software was developed for formatting the disks to permit recording of serial digital flight data at bit rates ranging typically from 50 kilobits/sec to 1.0 megabits/sec. These serial data rates provide flight recording time ranging from 30 hr to 1.5 hr, respectively. The minimum and maximum serial data rates are 5 kilobits/sec and 1.5 megabits/sec.

The optical disk recording system operates from 115V 400 Hz single phase AC power and consumes less than 30 W of power. The complete optical disk recording system weighs less than 13 kg. The system is designed to operate from a single pilot's record switch or, on larger transport aircraft, the disk system can be controlled using a laptop computer.
(D. R. Norfolk, 757-864-3820)

General Purpose Research Aircraft Flight Display System

A versatile flight display system was developed as a cost effective tool for performing onboard computations and monitoring data during research flights (see fig. 22). The system consisted of flight hardened commercially available hardware and custom software with experimenter algorithms developed by NASA Langley. A flat-panel VGA display was integrated with a personal computer (PC) into the aft-cockpit of an OV-10A Bronco research aircraft. The system performs engineering unit conversion, computes project specific parameters, and provides a graphical display of the resulting data in real-time. To allow flexibility, the system software is designed to allow data acquisition and display configurations to be easily changed prior to a flight. In addition, the same software, running on ground support equipment (GSE) similar to the flight system, can be utilized on the ground for preflight checkouts and real-time telemetry monitoring.
(N. C. Coffey, 757-864-8486)

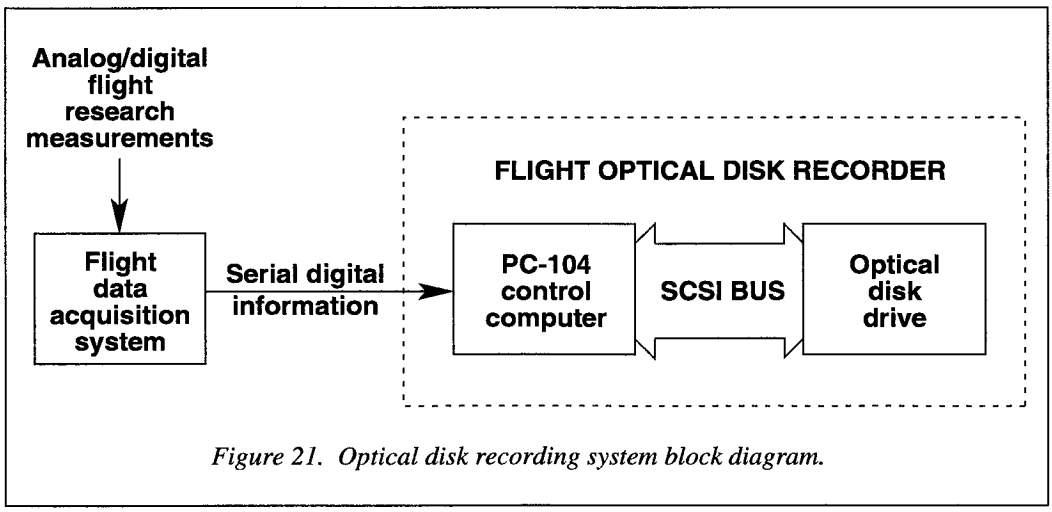

Figure 21. Optical disk recording system block diagram.

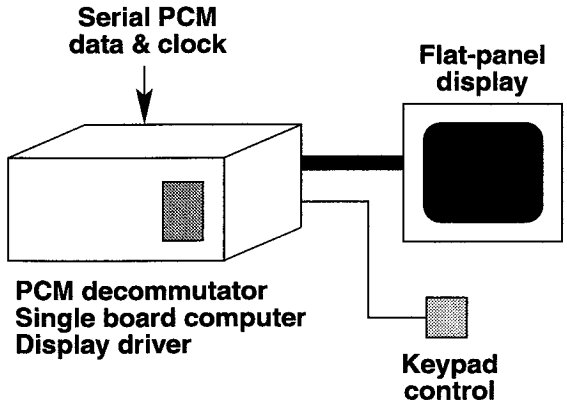

Figure 22. Research aircraft flight display system.

Acceleration of Physical Aging at Elevated Temperatures in Polymeric Composite

New classes of high-temperature polymer matrix composites (PMC's) are being developed for structural materials with applications to both civilian and military aerospace vehicles. For many of these applications, the issue of long-term durability is of overriding concern during materials selection and design. To address the materials selection or screening problem, accelerated test methods and associated analytical models must be developed which provide the means for predicting long-term behavior from short-term test data. For design, long-term exposure (i.e., aging) of PMC's must be accounted for through constitutive models in order to accurately assess the effects of aging on performance. One particular aspect of this aging process, physical aging, is considered in this research.

Physical aging is a thermoreversible process that causes the polymer matrix to become stiffer, more brittle, and the creep and stress relaxation rates to be reduced. To investigate acceleration of physical aging, constant load creep tests and linear viscoelasticity were used along with the concepts of time/temperature-based superposition to shift individual creep compliance curves into material master curves and thereby provide an aging shift rate. It was assumed that temperature may be a primary factor in accelerating creep behavior. Along with exploring aging as a function of temperature, investigations were also made to determine how loading modes and loading directions played a role in accelerating aging behavior.

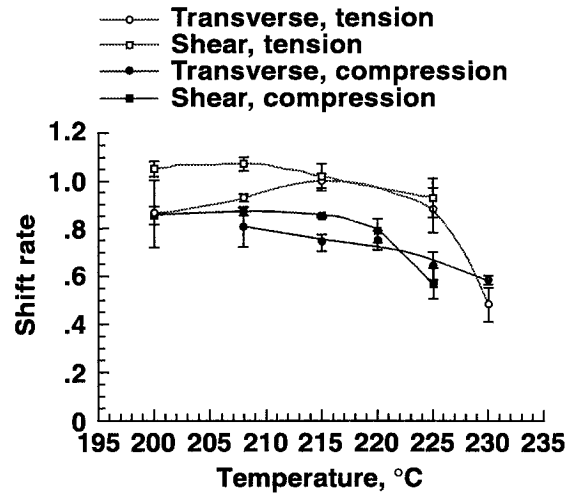

Figure 23. Aging shift rate as a function of temperature, loading mode, and loading direction for the IM7/K3B composite material.

As shown in figure 23, aging shift rate was found for both the transverse and shear loading directions of the graphite/thermoplastic-polyimide composite IM7/K3B. Error bars in this figure indicate the experimental deviation in shift rate. Results of the study indicate that physical aging shift rate may be the most critical parameter in calculating the magnitude of aging's effect on long-term performance. Examination of the trends in shift rate indicate that acceleration of physical aging may be dependent not only on temperature but also on differences between shear and transverse loading modes and differences between tension and compression loading directions.

(T. S. Gates, 757-864-3400)

Compression Tests of Graphite-Epoxy Fuselage Keel Panel With and Without Damage

A graphite-epoxy face-sheet sandwich fuselage keel test panel was fabricated by the Boeing Commercial Airplane Group and is representative of a highly loaded fuselage keel structure. The face sheets of the panel contain 14 terminated or dropped plies along the length of the panel to meet the design goal of maintaining a nearly uniform laminate axial stiffness along the panel

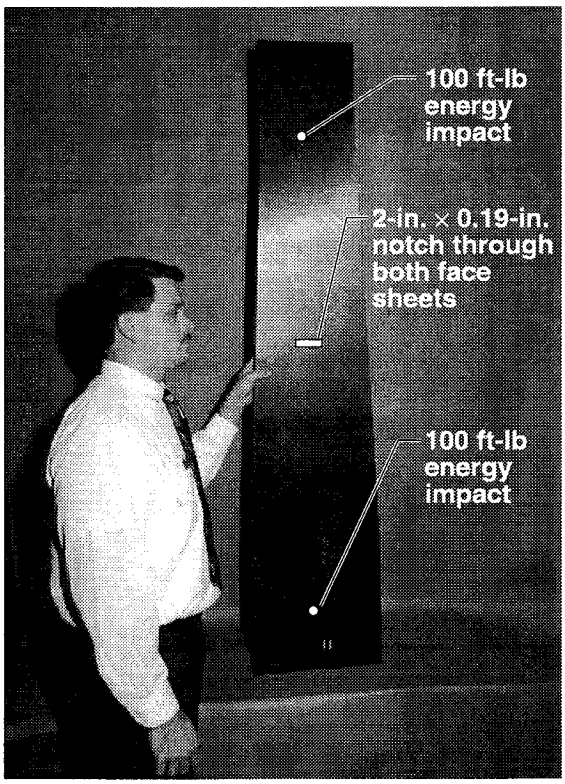

Figure 24. Graphite-epoxy sandwich fuselage keel panel test article.

length. Compression tests of the panel were conducted in the Structures and Materials Laboratory at NASA Langley Research Center with three damage conditions: 1) the undamaged condition, 2) a condition with barely visible impact damage (BVID) in two locations, and 3) a condition with BVID in two locations and a notch through both face sheets. (See fig. 24 for damage locations.) The impact-energy level necessary to inflict BVID on the panel was determined from an impact-damage screening study conducted on another panel of the same design. Finite-element analyses of the undamaged panel and the notched panel were also performed.

The design goal of maintaining a nearly uniform laminate axial stiffness along the length of the panel was verified by testing the undamaged panel. The tests of the impact-damaged and notched panel identified the notch as being the most critical of the three damage sites. Analytical results for strain distributions around the damage sites compare well with the experimental results. The notched panel failed at 202 kips, which is the design ultimate load for the panel. The failure mode was compression failure of the face sheets at the notch location. Since the panel supported design ultimate load with BVID, the design is damage tolerant for nonvisible impact damage.

An important finding from the impact-damage screening study is that significant internal damage occurred at relatively low impact-energy levels and that the corresponding surface damage at the impact sites as measured by the residual dent depth was very small, making it nonvisible to a ground-crew inspection. This internal damage at the impact locations can significantly reduce the residual strength of the panel. These results suggest that the present approach of using residual dent depth as a means of assessing the effect of BVID on the strength degradation of a composite honeycomb-sandwich structure needs to be reevaluated. **(D. M. McGowan, 757-864-4916)**

Progressive Damage Analysis of Laminated Composites Due to Tension Fatigue

The durability and damage tolerance of laminated composites are critical design considerations for airframe composite structures. Therefore, the ability to model damage initiation and growth and predict the life of laminated composites is necessary to achieve efficient and economical structural designs. The damage model developed by Texas A&M and NASA Langley was used successfully to predict the stiffness degradation and residual strength of the IM7/5260-toughened matrix composite material. Experimental verification of the model was established by comparing the stiffness loss of crossply and quasi-isotropic laminates with and without open holes for tension fatigue loadings. Residual strength predictions were also reasonably close to the experimental values as seen in figure 25. The model has predictive capability for intraply matrix cracks and simulation capability, using an empirical relationship, for delaminations. The model successfully predicted both the effects of laminate stacking sequence and loading history on damage growth and stiffness loss. The ability of the model to predict damage growth in the open hole specimens was particularly encouraging. These results suggest that the model is appropriate for spatially varying damage developing in strain gradient fields and not confined to uniform damage that develops in the gage length of an unnotched uniaxial test specimen. The spatial variation in damage is treated through the finite-element discretization because the

damage is assumed to be uniform within an element. The empirical relationship for delamination provided trends in stiffness loss that agreed with the experimental trends. The damage model has been implemented into a general purpose finite-element structural analysis code. Applications of the special processors that compute damage growth and residual strength are documented in NASA TM-4724, *Progressive Damage Analysis of Laminated Composite (PDALC)— A Computational Model Implemented in the NASA COMET Finite Element Code.* Future development activities include implementing failure criteria for compression failure mechanisms. **(C. E. Harris, 757-864-3447)**

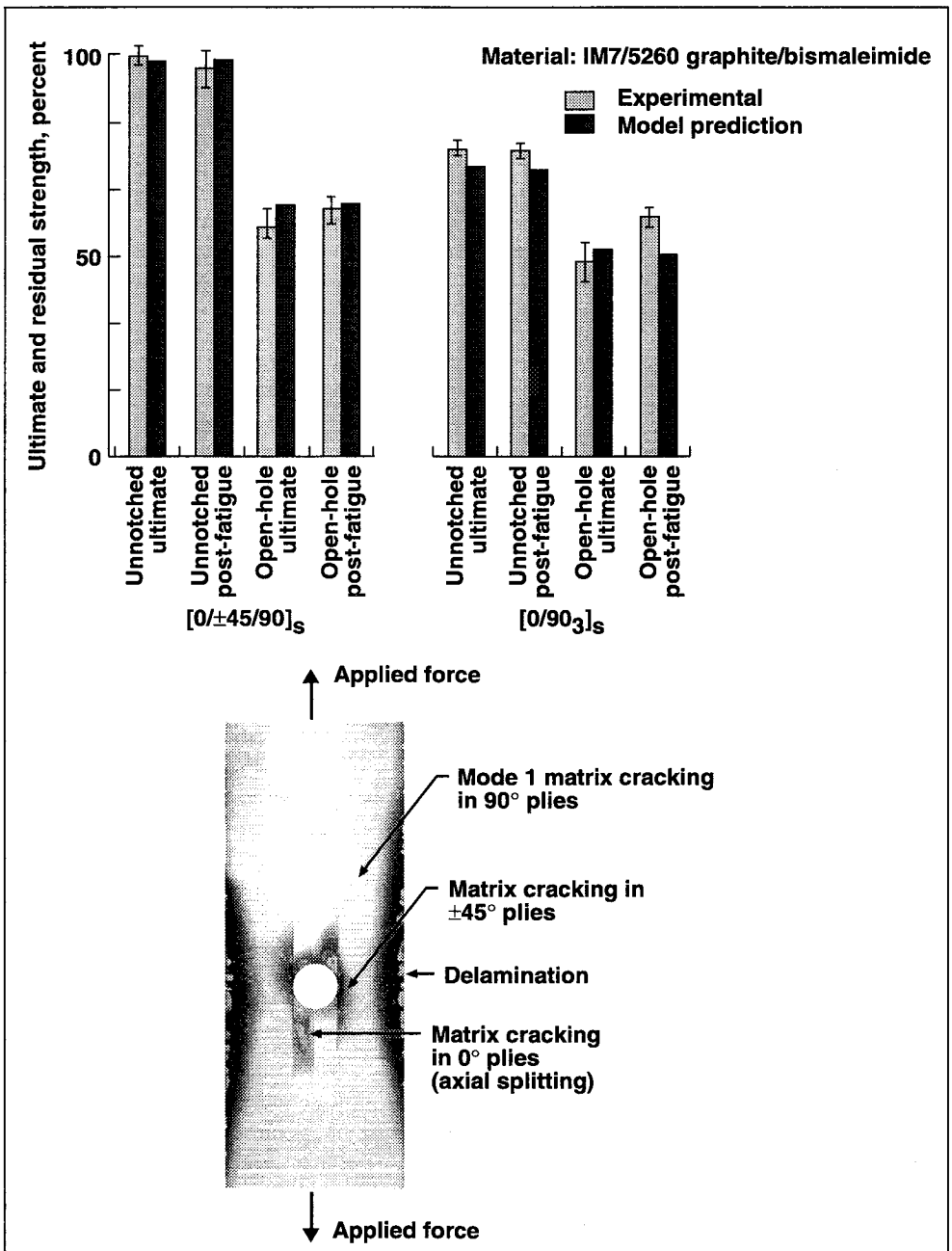

Figure 25. Progressive damage analysis of laminated composites due to tension fatigue.

Fracture Simulation of Cracked Stiffener Panels

Aging of commercial transport fleets around the world increases the possibility of a reduction of structural integrity through fatigue cracking. Widespread fatigue damage (cracks developing at several adjacent locations) is of concern because the residual strength of a damaged stiffened structure (due to fatigue or engine failure) may be greatly reduced by the presence of smaller fatigue cracks at adjacent rivet holes. Whereas a single long crack in a fuselage structure may produce flapping, a process by which a cracked fuselage would peel open in a small local region and lead to safe decompression, a fuselage with a long lead crack and multiple-site or multiple-element damage (MSD and MED) cracking may not flap and may fail at a lower load than the design load. Current fuselage designs must rely upon periodic inspections to assure safe operation. One of the objectives in the NASA Aging Aircraft Research Program is to develop the methodology to predict flapping or failure in damaged fuselage structures in the presence of MSD or MED. The approach is to use a finite-element shell code with global-local, adaptive mesh capabilities and appropriate local fracture criteria to predict progressive failure in complex structures.

To develop the methodology to predict the influence of widespread fatigue cracking on fuselage structures, the behavior of multiple cracks in thin-sheet materials subjected to biaxial loading with various stiffener conditions, typical of fuselage structure, must be tested and analyzed. Recent tests (sponsored by the U.S. Federal Aviation Administration (FAA) Technical Center) on flat unstiffened panels made of 2024-T3 aluminum alloy sheet with a wide variety of MSD crack configurations are showing significant reductions in residual strengths. One of the leading fracture criteria is the crack-tip-opening angle (CTOA). Elastic-plastic finite-element analyses have demonstrated that the CTOA criterion can accurately model the stable tearing behavior of multiple cracks and cracks in specimens subjected to biaxial loading. The critical CTOA for the fuselage material was determined from a test of an unstiffened cracked panel. NASA Langley and the National Research Laboratory of the Netherlands (NLR) conducted fracture tests on 2024-T3 sheet panels with either 2024 or 7075 aluminum alloy stiffeners (intact or broken), as shown in figure 26. Tests results from NLR are shown as symbols in the figure showing applied stress (S_g) against crack length c. The predicted results using a critical angle of 6.5° are shown as the solid curves, which agreed fairly well with the test data. These types of tests form the framework for establishing the creditability of the CTOA fracture criterion for predicting stable tearing and fracture of complex structures. In the future fuselage structures may be designed by analysis and verified by tests to produce flapping or improved crack arresting capability under MSD or MED conditions. **(J. C. Newman, Jr., 757-864-3487)**

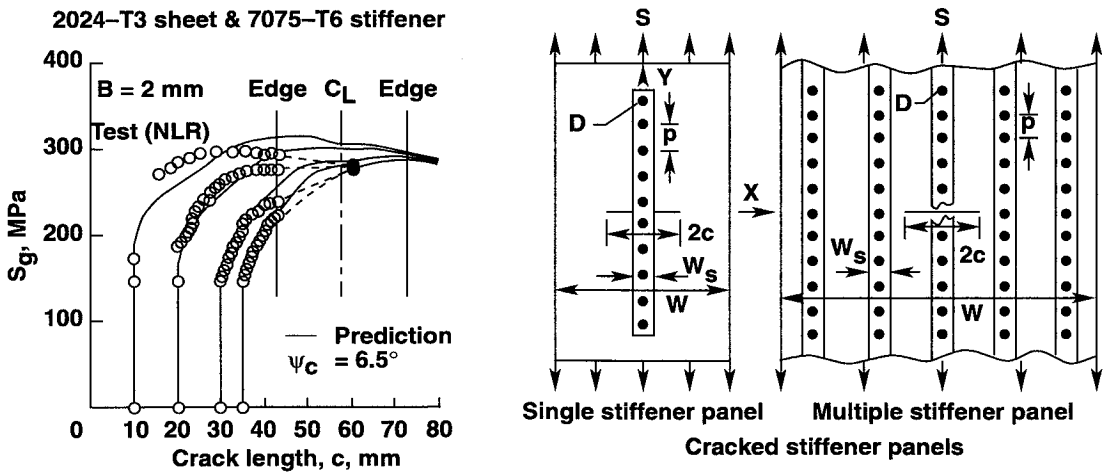

Figure 26. Stable crack growth in multiple stiffener panel.

Detection of Fatigue Cracks Hidden Under Rivet Heads

One of the most recent advancements of self-nulling eddy current sensor technology is the development of a rotating probe system for the detection of fatigue cracks hidden under rivet heads. A hand-held prototype (shown in fig. 27 upper left inset) rotates the probe around a rivet head to record the probe output as a function of angular position. The recorded spectrum is fast-Fourier transformed to filter out the low-frequency components which are due to periodic background noise caused by inevitable misalignment between the centers of the rivet head and the circular path of probe motion, and other artifacts. When the signal is inverse-Fourier transformed, the spectrum contains clear crack signals with their amplitudes nearly proportional to crack lengths and precise positions of the cracks (as shown in fig. 27 lower left inset) for a rivet hole having a single fatigue crack. The capability of the prototype system has been recently evaluated by using the testbed at the Federal Aviation Administration (FAA) Nondestructive Inspection (NDI) Validation Center in Albuquerque, New Mexico. The results of blind tests were used to form a probability of detection (POD) curve, which is shown in figure 27. The POD curve shows that any fatigue cracks longer than 0.84 mm (33 mil) can be detected with a probability higher than 90 percent. Such a detection capability is a considerable improvement over the present leading commercial eddy current instruments.

(M. Namkung, 757-864-4962)

Ultrasonic Phased Array Testbed System for Advancing Nondestructive Evaluation

High-frequency mechanical vibrations, known as ultrasound, are commonly employed to inspect materials and structures for flaws. As the ultrasound propagates through the material, its amplitude and phase vary in response to changes in the material properties. By analyzing these amplitude and phase changes, inspectors can infer something about the condition of the material.

Most commonly utilized materials contain uniform to moderately-variable material properties, and flaws are easily distinguished using conventional ultrasonic probes. In materials which contain more complex internal properties, such as textile-based composites, the ultrasound amplitude and phase changes imposed by the normal material variations may mask the effects due to flaws, leading to errors in interpretation.

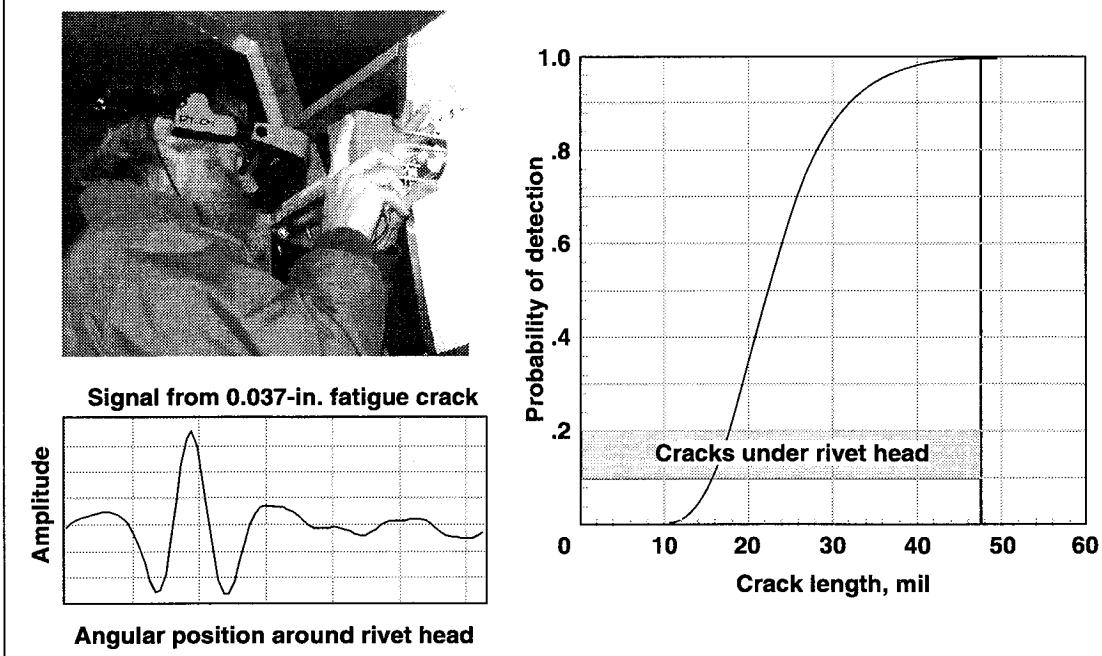

Figure 27. Rotating probe for detection of hidden fatigue cracks.

A standard ultrasound probe is a single-channel device with active area on the order of 2 cm^2. The geometry of the probe largely determines both the characteristics of its conversion of ultrasound to electrical signals and its sensitivity to the ultrasound fluctuations caused by the material. If the single-channel probe is replaced by an array of smaller sensors, each under independent amplitude and phase control, then methods can be employed to interpret the complex variations in the newer materials.

Langley researchers conceived an electronics testbed for exploring the use of phased array methods for materials, which was developed by Southwest Research Institute under contract. The Ultrasonic Phased Array Testbed System (UPATS) provides full control of ultrasound amplitude and phase for transmitting and receiving 100 separate channels. In addition to the 100-element reconfigurable array provided with the testbed, the UPATS can be interfaced with many other array probes. The UPATS enables a three-phase research capability: (1) basic research in measurement of material properties with ultrasound, methods for ultrasound generation and detection, and schemes for array configuration and design; (2) applied research for employing array detectors for improved evaluation of textile composites, layered and honeycomb materials, and other built-up material structures; and (3) system design for inspection of specific complex geometry parts. **(P. H. Johnston, 757-864-4966)**

New Wideband Noise Absorber Made of Grouped Hollow Beads

Under the sponsorship of NASA Langley Research Center, Georgia Tech Research Institute (GTRI) scientists have developed a new wideband noise absorbing

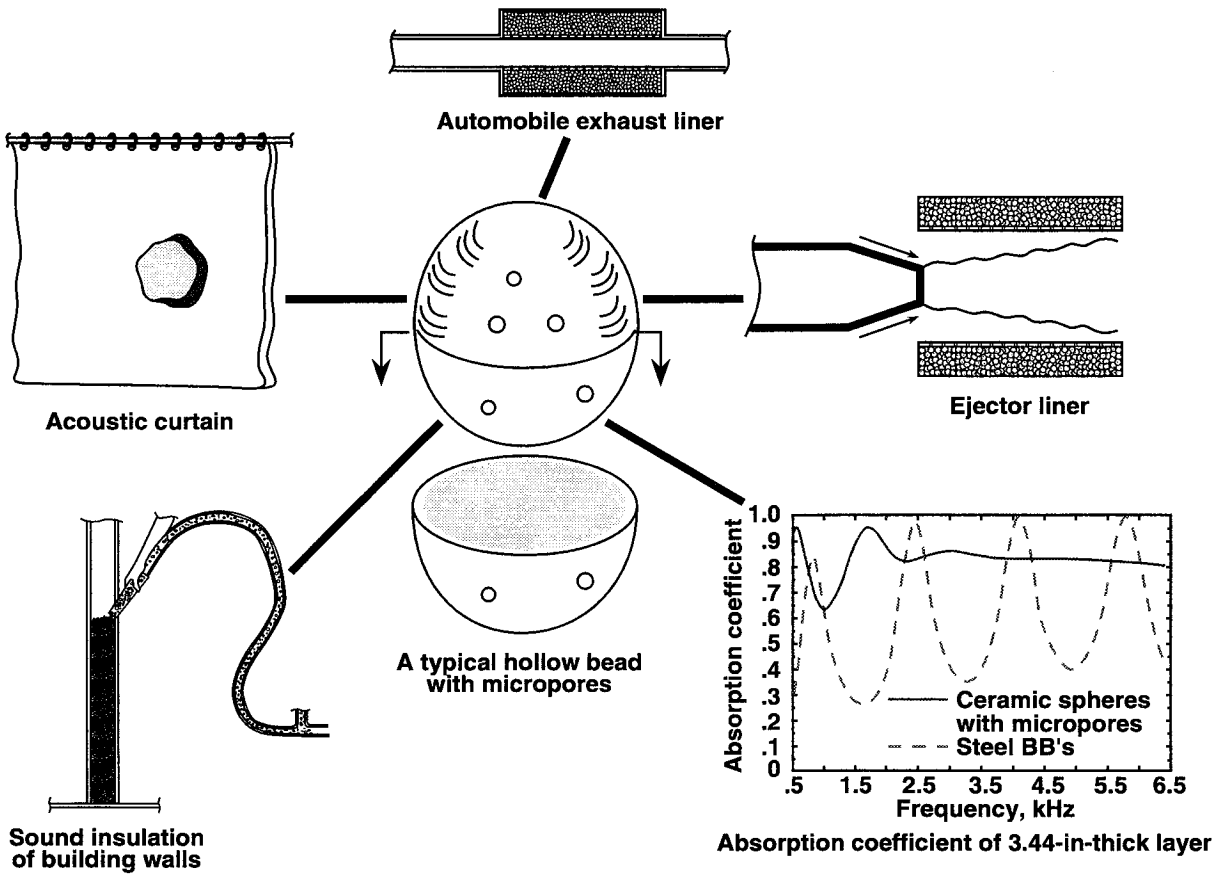

Figure 28. Applications of hollow ceramic, hollow spheres for acoustic noise suppression.

medium. In a given application, it consists of a loose collection of contiguous hollow beads with microporous surfaces. In addition to the familiar viscous loss mechanism for dissipating acoustic energy inside conventional bulk absorbers such as fiberglass, the hollow beads exhibit additional loss mechanisms.

Each individual bead defines an acoustic resonator whose absorption bandwidth is controlled by the bead geometry (see fig. 28). The bead geometry varies with respect to the hollow space, wall thickness, and the number and size of the micropores from bead to bead. This feature broadens the collective absorption bandwidth. Additionally, the micropores assist in converting very low-frequency sound to vorticity as sound passes through the micropores of each hollow bead. Part of the sound is converted into vibrational energy of the collection of beads acting as a wave propagating medium. Typical absorption coefficient spectra are shown in the figure for a 4-in-thick layer of beads with and without micropores (continuous and dashed curves, respectively). The enhanced absorption of the hollow bead absorber is clearly evident. The large excursions of absorption coefficient for the solid beads are characteristic of a conventional bulk material.

The beads can be made from a ceramic material which allows sound absorption at high temperatures in excess of 2500°F. Efforts are underway at GTRI to manufacture lightweight plastic beads for low-temperature applications.

Experiments performed in an impedance tube show that the sound absorption properties of ceramic spheres are comparable with polyurethane foam and other advanced liners. Tests performed with a jet/ejector combination with the ejector lined with ceramic hollow beads displayed excellent noise reduction in the far field.

Some of the applications of this new wideband absorbing medium are ejector liners, automobile exhaust mufflers, construction walls, and acoustic curtains. **(T. L. Parrott, 757-864-5273)**

Effect of Blade Tip Clearance on Noise Radiation From Ducted Fan

Early experiments with the Advanced Ducted Propeller demonstrator showed that blade passage frequency (BPF) tone noise was significantly higher than was expected for this engine design. The demonstrator was designed using procedures common for ducted fan engines in which the fan tone at blade passage frequency does not propagate in the duct. The solid curves on the plots show not only that the blade passage frequency (1 BPF) tone is present, but also that it is higher at all sideline angles than the tone at twice blade passage frequency (2 BPF). (See fig. 29.) Plots of contours of radiated sound measured in a plane below the demonstrator were found not to have the expected azimuthal symmetry. Investigation of the engine showed that the blade tip clearance at the rubstrip was nonuniform both axially and circumferentially.

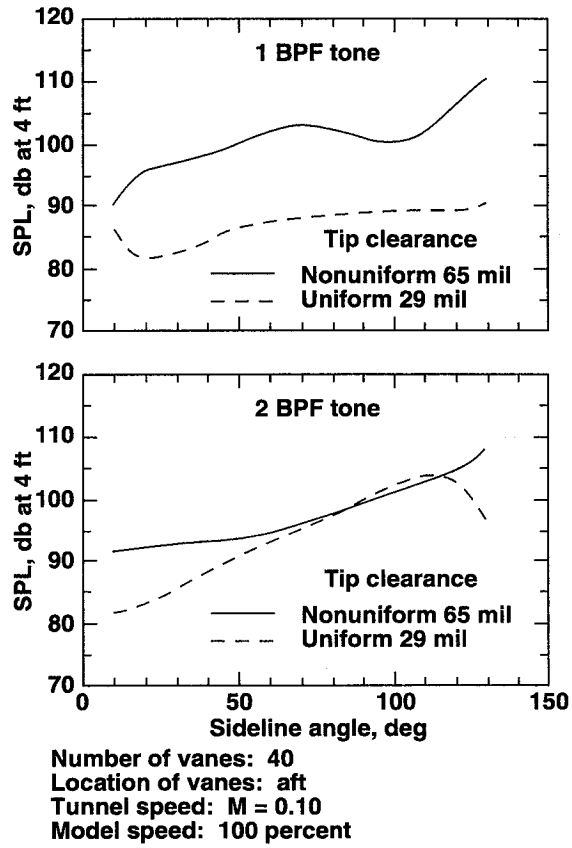

Figure 29. Langley 12-in. ADP fan sideline angle directivity plots.

It was hypothesized that this nonuniformity generates sound at the blade passage frequency in modes that interfere with one another, resulting in high-sound levels and nonsymmetric far field radiation patterns. New rubstrips were manufactured with tightly controlled

clearances. The dashed curves on the plots show that the blade passage frequency tone with the uniform rubstrip is now at or below the twice blade passage frequency tone. Contour plots indicated much greater symmetry of the radiated sound. Tests were made of various other rubstrips to determine the sensitivity of fan noise to the uniformity of tip clearance as well as to the magnitude of the gap. These rubstrip experiments are intended both to demonstrate the importance of design parameters on noise generation and to provide data to quantify the effects.

(C. H. Gerhold, 757-864-5279)

Active Trim Panels for Noise Reduction in Fuselage Model

Actuation of the trim panel of an aircraft for interior noise control is attractive for both new and retrofit applications. It allows a solution that can be designed and fabricated more independently of the airframe and thus may be adapted to a range of vehicles with less engineering development.

An experiment was conducted to evaluate the use of force actuators (piezoceramic) acting on a model aircraft interior trim panel as the control element for active control of interior noise. The trim panel, designed specifically for this study, was constructed in three large axial sections and hard mounted to the ring frames of a composite fuselage model with a floor installed. The intent of this design was to have as nearly a continuous trim panel structure as possible, but which reasonably represented a realistic flight vehicle. A photograph showing the installation of one axial section of the trim panel in the fuselage model is shown in figure 30. These panels have approximately twice the stiffness and weight of standard aircraft interior trim panels. A single acoustic loudspeaker, centered at the axial midpoint, generated the acoustic field to be controlled. Two cross sections of control actuators were symmetrically located on either side of the center cross section.

The results for 210 Hz are shown. For this particular configuration, two actuators and six error microphones were used. The average sound pressure level (SPL) at the center cross section with the controller off is 66.2 dB. Once the controller is turned on, the average cross-section SPL is reduced to 61.5 dB. The average SPL reduction for the entire cylinder was 5.1 dB. Modal decompositions of the data show that the amplitude of the dominant acoustic mode was reduced by 23 dB; however, control was limited by residual modes in the cavity that were not controlled by this actuator and error microphone configuration. Control at other

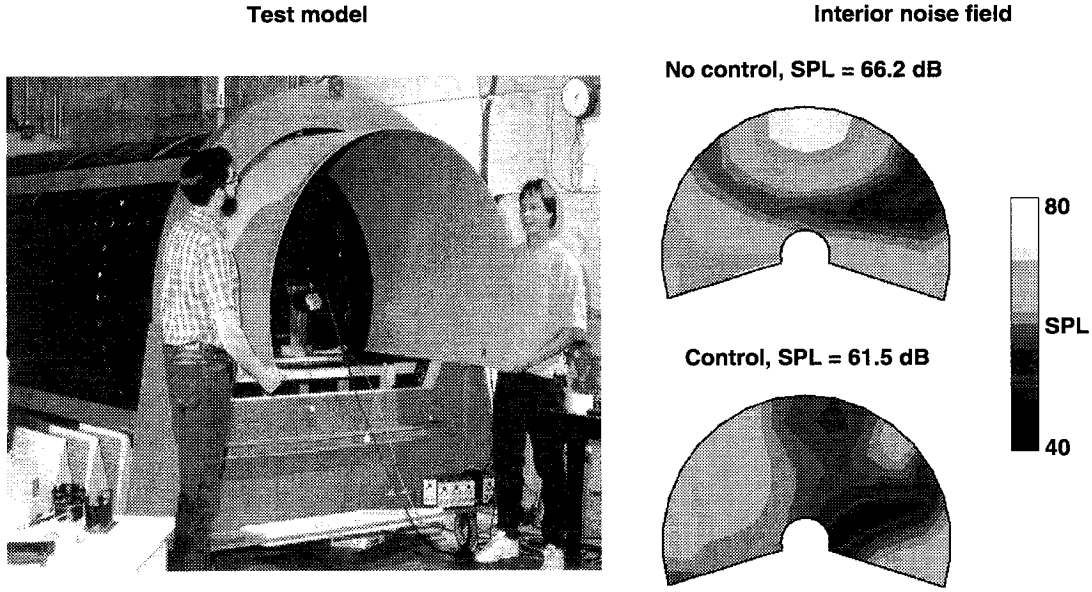

Figure 30. Fuselage model noise reduction with active control.

frequencies was generally not as good. At these frequencies the interior pressure response due to the external acoustic source was dominated by a different acoustic mode than the interior pressure response driven by the piezoceramic actuators. This is attributed to the distributed forcing of the trim panels by the primary structure of the exterior source differing from the localized forcing by the piezoceramic actuators. This difference in modal response is significant and accounts for the very limited performance at most frequencies. These results are in strong contrast to previous results attained for control actuators bonded directly to the primary structure.

Further work is planned to improve the reduction of the interior noise. This will include adding actuators to the remaining trim panels, utilizing control algorithms that will group actuators, and vibration isolating the trim panel from the primary structure. **(K. H. Lyle, 757-864-3588)**

Wake Vortex Lidar Signal Amplification Using Sensitivity Time Control

A Sensitivity Time Control (STC) subsystem was developed for the Wake Vortex Lidar (WVL) project to produce a variable amplification of the lidar return signal (echo) level. The STC adjusts the lidar receiver sensitivity to produce a amplified lidar echo strength which is independent of range. To compensate for the change in lidar echo strength due to differences in range, a control voltage ramp is shaped and applied to a four-quadrant analog multiplier.

The ramp polarity is designed to increase receiver gain proportional to an increase in range. The ramp is shaped to produce receiver power gains directly proportional to the fourth power of time. This process begins when the lidar computer commands a STC amplitude pattern output to be generated as an input to an arbitrary waveform generator (AWG). This STC amplitude pattern output will dictate the ramp polarity and shape from the AWG. The resulting AWG output voltage has a fast response, which is generated over a few microseconds for input to the four-quadrant analog multiplier. (See fig. 31.)

The STC analog multiplier output is a function of the lidar return echo multiplied by the instantaneous values of the compensated control ramp voltage. The STC signal from the multiplier occupies a bandwidth from 45 to 165 MHz, centered at 105 MHz. The gain compensated STC output analog signal is routed to an A/D converter for digitizing, and then to the lidar computer STC feedback control to amplify, or decrease the echo signal level. The data are also recorded in the computer for future data analysis. **(L. J. Cowen, 757-864-8635)**

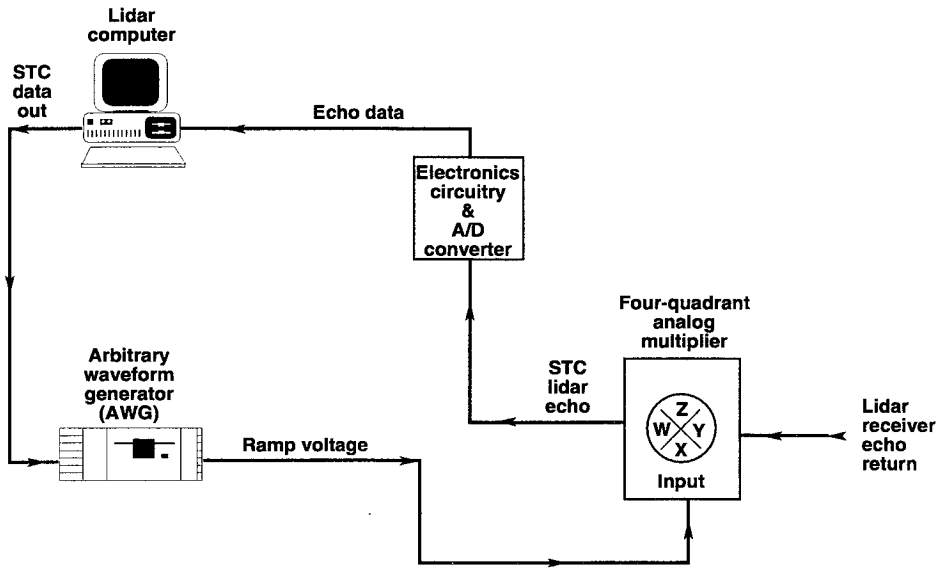

Figure 31. Wake vortex lidar signal amplification sensitivity time control.

Flight Demonstration of Integrated Airport Surface Automation Concepts

The U.S. aviation industry is investing $6 billion over 20 years to increase airport capacity; however, there is a gap between the industry's desired capacity and the ability of the National Airspace System to handle the increased air traffic. Action must be taken to safely increase the capacity of existing airport facilities while reducing controller and pilot workload.

The NASA Terminal Area Productivity (TAP) Program is focused on providing technology and operating procedures for safely achieving clear-weather capacity in instrument-weather conditions. As part of the TAP Low Visibility Landing and Surface Operations (LVLASO) Program, a flight demonstration was conducted in conjunction with industry partners from Westinghouse Norden Systems and ARINC, Inc. The goal was to demonstrate an integrated system that would provide the pilot and controller with enhanced situational awareness information to safely increase the traffic capacity on the airport surface. The demonstration was conducted at the Atlantic City International Airport in June 1995 with the cooperation of the Federal Aviation Administration (FAA) Technical Center.

The demonstration showed an integration of several technologies to government and industry representatives. These technologies consisted of an electronic moving map display, a Differential Global Positioning System (DGPS) receiver, a high-speed data link, an Airport Surface Detection Equipment (ASDE-3) radar, and the Airport Movement Area Safety System (AMASS). (See fig. 32.) Aircraft identification was presented to an air traffic controller on AMASS. The onboard electronic map included the display of taxi routes, hold instructions, and clearances, which were sent to the aircraft via data link by the controller. The map also displayed the positions of other traffic and warning information, which were sent to the aircraft automatically from the ASDE-3/AMASS system.

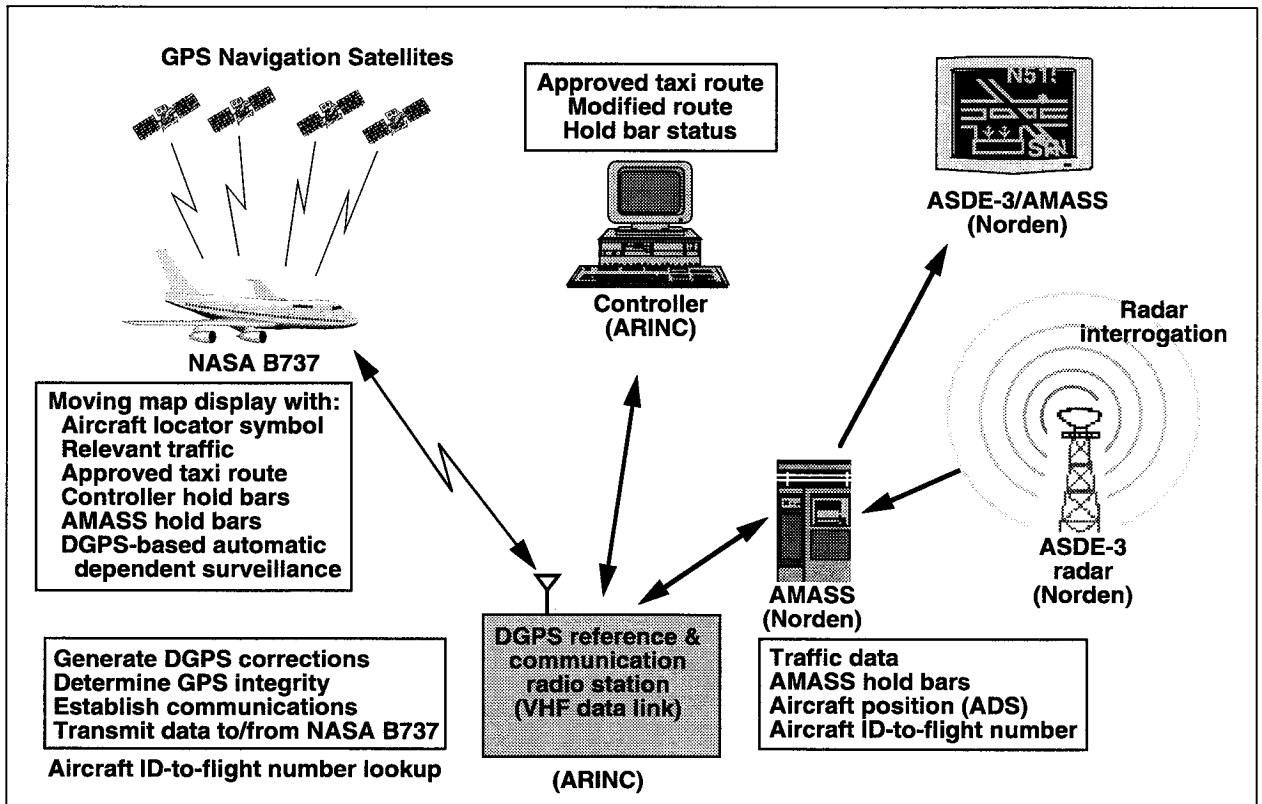

Figure 32. System architecture of airport surface technologies flight demonstration.

The flight trials successfully demonstrated an integration of current airport surface technologies. Preliminary analysis showed that both DGPS (mean position accuracy of ±2 ft) and ASDE-3 (mean position accuracy of ±28 ft) position data were adequate for pilot observation of relative locations of airport traffic; however, DGPS was required for navigation and guidance accuracy. Uplink data delays of traffic position were generally within 5 sec. Further study is required to determine safe delay tolerances. Also, less than 1 percent of uplink messages were observed to be corrupted. The results from this demonstration will be used in subsequent flight testing that will occur over the next several years. **(D. R. Jones, 757-864-2006)**

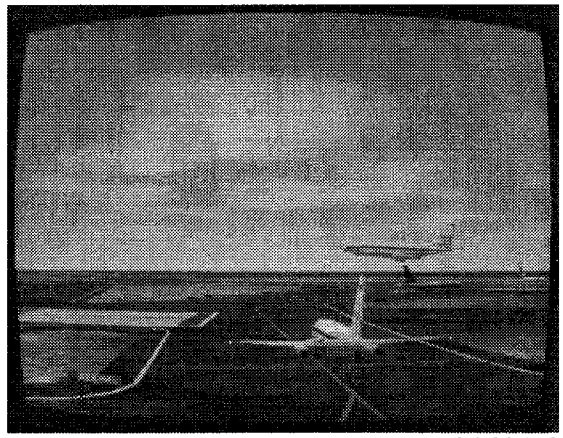

L-95-00576

Figure 33. Flight simulation of the Boston Logan International Airport environment.

Pilot Evaluations of Runway-Status Light System

This work is a coordinated effort by LaRC, the Federal Aviation Administration (FAA), and the Volpe National Transportation Systems Center to develop a flight simulation environment and to use this environment to solicit pilot opinion and input on the Runway-Status Light System (RWSL). The RWSL has been designed to reduce the likelihood of runway incursions by visually alerting pilots when a runway is occupied. Since 1990, more than 100 lives have been lost in accidents caused by runway incursions. Most runway incursions are caused by human error usually brought on by a lack of situational awareness, failure to properly communicate, and navigation errors. RWSL is intended to minimize the effect of human errors by providing an independent source of information for pilots about the state of a runway. Currently, pilots obtain information about the status of the runway from visual scans or from air traffic control.

Functionally, the RWSL is a system of lights automatically controlled using surface radar data. There are two types of lights that make up the RWSL. Takeoff hold lights (THL's) are positioned to warn pilots who are ready to takeoff that the runway is presently not clear or that other aircraft are projected to enter the runway in front of the takeoff. Runway entrance lights (REL's) are designed to inform pilots (or ground vehicle operators) when a runway is unsafe to enter. Both THL's and REL's are bright red when on.

The Transport Systems Research Vehicle (TSRV) simulator consists of a modified Boeing 737 cockpit that contains an "all-glass" instrument panel, dual side-arm controllers, a Boeing 737 throttle quadrant and center aisle stand, and a four-window display configuration that provides crewmembers with a 150° field of view. The TSRV simulates the Boeing 737 flight dynamics during all phases of flight and taxi. The image generator (IG) is capable of rendering day and night scenes with environmental effects such as fog and clouds. The IG generates visual scenes that accurately depict a three-dimensional view of an airport. The lights that make up the RWSL system are also included in the visual scene. Furthermore, other aircraft movements are shown in the field of view.

A pool of pilots from the Airline Pilots Association (ALPA) participated in the evaluation. Average pilot experience was nearly 10000 flight hours. These pilots were asked to operate the aircraft through several scenarios to evaluate the RWSL. The scenarios included taxiing to and from runways under varied weather conditions and traffic patterns. Crews were asked to perform normal operational activities during each scenario. Several of the scenarios placed pilots in potential incursion situations.

Responses reveal that test subjects unanimously support the concept of the RWSL. Further, they feel the status lights will, in fact, reduce the likelihood of runway incursions at airports. Test subjects frequently referred to the independence characteristic as being the most attractive component. By having a passive source of status information to support the information they get from the controller and from their visual scans,

there will be little doubt about the situation with respect to active runways. In addition to obtaining support for the concept, several improvements to the RWSL system have been implemented based on suggestions made by the test pilots. These include adding in-pavement THL's near the runway centerline, adding a third REL on acute angled taxiways, and modifying the timing of the lights to minimize capacity impacts.

A prototype of the RWSL is being installed at the Boston Logan International Airport. This system will be used for extensive trials in order for the RWSL to be fine-tuned at an operational airport. NASA LaRC continues to be involved with this FAA program not only by participating on the development team, but also by implementing a subsequent simulation environment. This environment simulates the Boston Logan International Airport (fig. 33) using an advanced image generator and allows for both the Logan users (controllers, pilots, and operators), and members of the development team, to evaluate the evolving system. **(S. D. Young, 757-864-1709)**

Carbon-Carbon Composite Piston Technology

Carbon-carbon composites are high-temperature materials that are used for thermal protection on the Space Shuttle, for aircraft brakes, and for other aerospace applications that require their unique properties. These unique properties also make them attractive candidates to replace conventional aluminum pistons in internal-combustion engines. Carbon-carbon composites are lighter than aluminum, retain their strength at high temperatures, have virtually zero thermal expansion, and are nongalling. Some of the benefits to be derived from using carbon-carbon pistons include improved engine performance and efficiency, and reduced emissions.

Carbon-carbon pistons are presently being tested in engines ranging in size from Go-Kart engines to a large block V-8 automotive engine. Performance capability has been demonstrated in actual on-the-track races with a Go-Kart. The V-8 automotive engine is successfully operating with these pistons which are 48 percent lighter than aluminum pistons.

Unfortunately, however, the current high cost of carbon-carbon components restricts its application to selected, very-high-performance spark-ignition engines. Therefore, a program has been initiated to develop a process for mass-producing lower cost carbon-carbon components. Pistons, cylinder liners, and cylinder blocks are being evaluated. Valves, exhaust manifolds, and turbocharger scrolls are other components that may become viable as a result of this effort. Prototype pistons produced under a Small Business Innovation Research (SBIR) contract with Materials & Electrochemical Research (MER) Corporation are being tested with very promising results. A piston such as the one shown in figure 34 has driven a 24-kW generator (5-hp engine) for 20 hr at capacity load without degradation. A major research goal is to demonstrate that it is possible to mass produce carbon-carbon pistons for under $20 each. At this cost, it is anticipated that carbon-carbon pistons would become viable alternatives for the automotive industry on a cost-to-benefit basis. **(P. O. Ransone, 757-864-3503)**

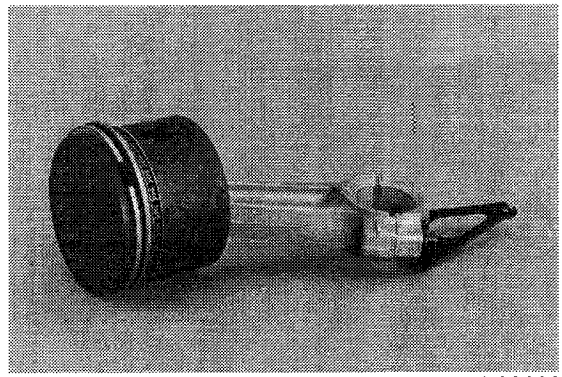

L-95-03033

Figure 34. Net-shape-molded, chopped-fiber carbon-carbon piston.

Aerodynamic Design of Wing-in-Tunnel at Cruise and Buffet-Onset Conditions

As part of the Advanced Subsonic Technology (AST) program, tests will be conducted on a wing in the High Reynolds Number Channel (HRNC) at NASA Ames to obtain data for calibrating and improving turbulence models for Navier-Stokes codes. These codes will be used for analysis and design at multiple flight conditions such as buffet-onset, where there is significant flow separation, as well as attached-flow conditions such as cruise. In order to ensure that the experimental results would be representative of flows over current configurations, the wing was designed to have

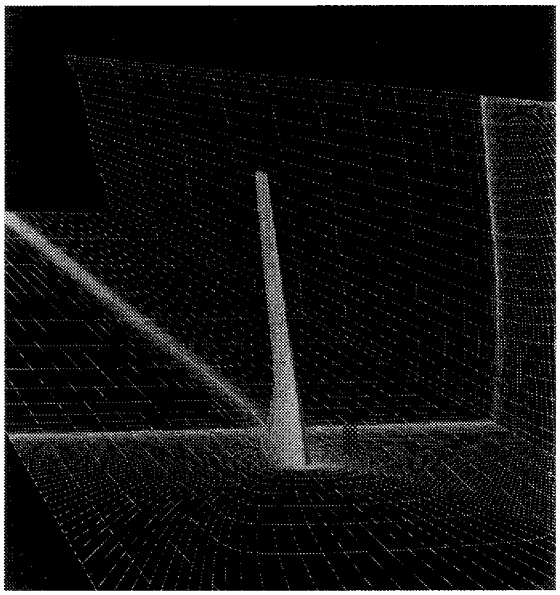

Figure 35. Wing-in-tunnel as modeled in TLNS3DMB code.

separated-flow characteristics similar to an existing advanced-wing configuration at buffet onset while maintaining acceptable cruise performance.

The Constrained Direct-Iterative Surface Curvature (CDISC) design method, coupled with the OVERFLOW and TLNS3DMB Navier-Stokes codes, was used by a joint Ames/Langley team to design the wing. Since the solid walls of the HRNC test section would significantly affect the flow over the wing, it was necessary to model them along with the wing in the Navier-Stokes codes. Figure 35 shows the wing along with the side and bottom wall grids (with every other point removed for clarity) as modeled in the TLNS3DMB code. In addition to the flow-related design objectives, a number of geometry constraints such as wing thickness were imposed from fabrication and safety considerations. Two satisfactory designs were obtained using manual multipoint design approaches and one of these designs was selected for fabrication. The tests will include surface and off-body flow measurements. **(R. L. Campbell, 757-864-2872)**

Wing Design at Conditions Involving Separated Flow

Multipoint design has been identified as a key technology for developing configurations with improved aerodynamic performance while reducing the aerodynamic design cycle time. The multiple design points include not only the usual range of cruise points, but also conditions such as buffet-onset where significant amounts of separated flow are present. In order to accurately model the flow at all of these conditions in the design process, Navier-Stokes codes are required. Because these codes typically require large amounts of computer resources, however, many of the automated design methods currently available become impractical.

One design method that can be used with Navier-Stokes codes in an efficient manner is the Constrained Direct-Iterative Surface Curvature (CDISC) method. It has been coupled with 2-D and 3-D Navier-Stokes codes that use block-structured, overset, and unstructured grid approaches, allowing for viscous design of complex configurations with essentially no increase in computer memory requirements and less than a factor of two in computer time when compared with analysis-only runs. The CDISC method currently has over 30 flow and geometry constraints, and has recently been extended to allow design at conditions involving moderate flow separation. Figure 36 shows an example of design at a buffet-onset condition, where the shock-induced flow separation contour for the baseline wing (left) has been greatly reduced for the new design (right), while maintaining the wing lift coefficient at the buffet condition. Work is underway to automate a multipoint design process using the CDISC method. **(R. L. Campbell, 757-864-2872)**

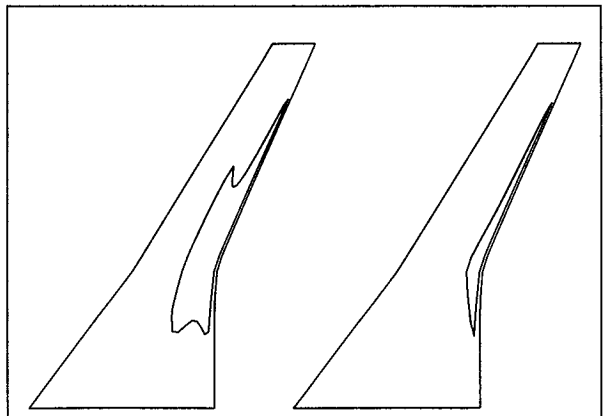

Figure 36. Separated flow contours for baseline (left) and design (right) wings at buffet-onset lift coefficient.

Navier-Stokes Analysis of Wing With Partial-Span Flap

The analysis and design of multielement high-lift systems for advanced subsonic transports is challenging due to the complexity of the geometry (multielement flaps, partial-span flaps) and flow physics (separation, confluent boundary layers) that must be modeled properly. The partial-span-flap aspect of the problem is particularly difficult due to the complexity of the geometry and flow field in the region of the flap and wing cutout.

A computational study was performed to determine the predictive capability of a multiblock structured-grid Navier-Stokes code, CFL3D, for a partial-span-flap configuration. A modification was made to an existing patched-grid preprocessor to account for the spanwise variation in the patched grids without requiring the user to explicitly model the side of the flap and allow for a zero length gap between the deflected flap and wing cutout. This greatly simplifies the grid generation task (which would be significant for a configuration with many partial-span-flap breaks).

The computational study was performed on a wing with an inboard partial-span single-slotted flap. The surface streamline patterns (shown in fig. 37) demonstrate the three-dimensional nature of the surface flow field. Surface pressure distribution comparisons between theory and experiment (not shown) demonstrated very good correlation between the two, even in the region of the deflected flap and wing cutout.
(K. M. Jones, 757-864-5013)

Figure 37. Surface streamlines and pressure contours for a partial-span-flap wing. M = 0.15; α = 12°.

Inverse Design of Installed Nacelle

A nacelle is reshaped "in-place" on an airplane to achieve a specified nacelle (target) pressure distribution. There are no restrictions on the attitude (toe, incidence, and roll) and position of the nacelle. The computational tool used is the Constrained Direct-Iterative Surface Curvature (CDISC) algorithm coupled to the three-dimensional Navier-Stokes code for overset grids (OVERFLOW). The coupling between design and analysis is automated to the point where the design proceeds with minimal user input. The computational cost of the design is of the same order as that of the analysis.

The redesign using OVERFLOW-CDISC to smooth out the pressure distribution on a nacelle installed on a transport airplane operating at a mid-cruise Mach number of 0.85 is shown in figure 38. It can be seen that, for this particular design, the wing has not been adversely affected while the nacelle has been improved. The fuselage-wing, pylon, fan-cowl, core-cowl, and far field are represented by seven overset grids. Analysis proceeds until a user specified criterion is reached. At this point, the CDISC geometry modifier is automatically invoked. The grid is then automatically adjusted to accommodate the geometry change. Next, the interpolation stencils between the relevant grids are recomputed and the analysis then continues until the next design iteration.

OVERFLOW-CDISC is a tool for the inverse design of a component of a complete airplane configuration while it is in the presence and under the influence of the rest of the airplane. Except for the initial grid generation, which will depend on the particular problem of interest, the design process is automated.
(S. E. Krist, 757-864-3046)

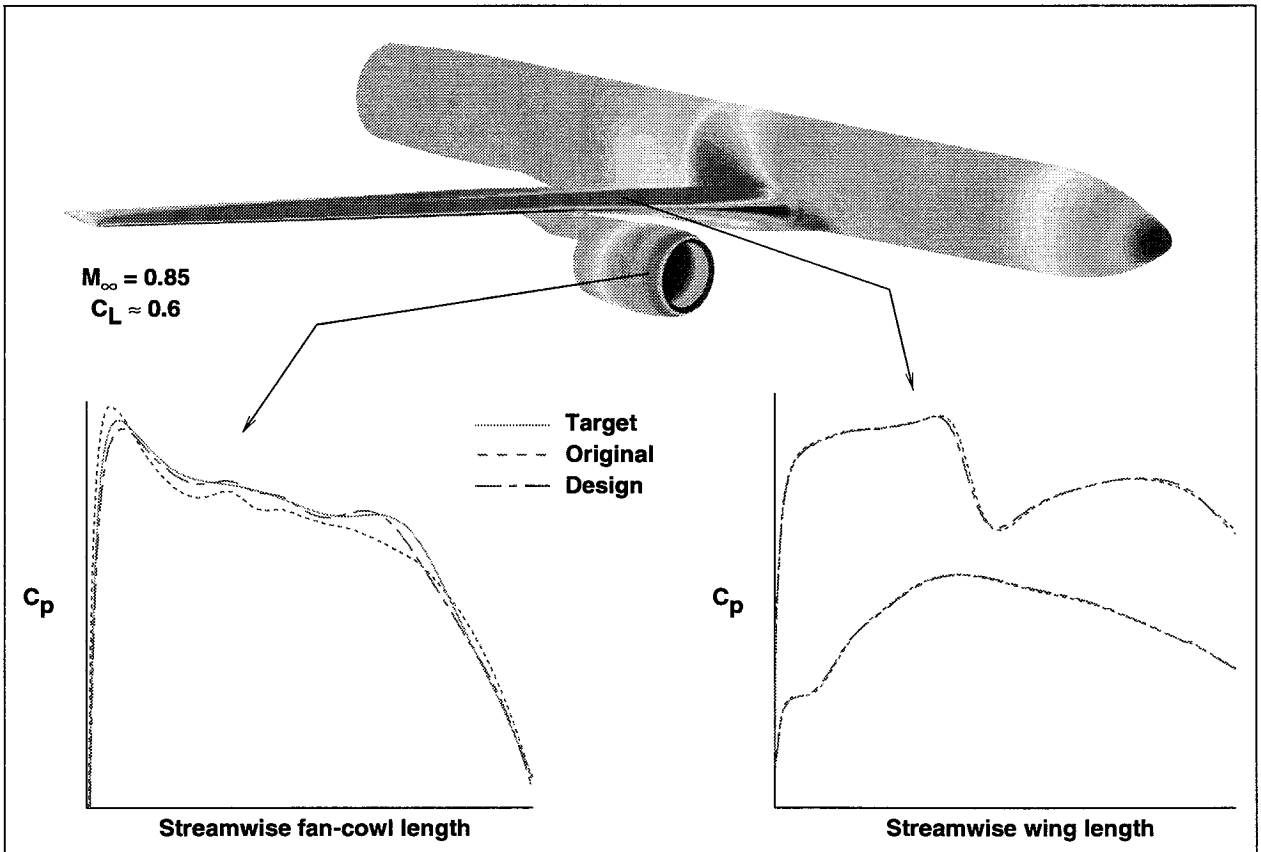

Figure 38. Comparison of pressure distributions for original and inverse designed nacelles.

Advanced Stitching Machine for Composite Wings

Under contract to NASA in the Advanced Composites Technology (ACT) Program, McDonnell Douglas Aerospace is developing composite primary wing structures using a patented stitched/resin film infusion (RFI) process. Results obtained with test panels and a small wing box test article indicate the process produces composite aircraft parts with outstanding damage tolerance. The process has the potential for major reductions in the labor content of manufacturing composite wing primary structures. However, it is critically important to demonstrate a stitching machine with the size and speed required for cost-effective fabrication of full-scale composite wings for commercial transport aircraft.

In the stitched/RFI process, layers of dry carbon fabric are stacked to form the wing structural elements and are stitched with through-the-thickness Kevlar threads. Resin film infusion (RFI) of the preform with epoxy resin followed by autoclave curing completes the process of making an integral wing cover.

Figure 39 shows the features of the computer-controlled machine now in development that will be capable of stitching a contoured wing preform 50 ft long and 8 ft wide. Under its subcontract, Ingersoll Milling Machine Company has completed mechanical fabrication of the unique machine. The stitching heads and bobbins for the machine are being developed by Pathe Technologies, Inc. When completed, the machine will be equipped with four advanced design stitching heads capable of stitching large contoured preforms over 1 in. thick. This prototype machine is expected to demonstrate the potential of the stitched/RFI process as a production manufacturing method for composite primary structures.

Following extensive checkout tests at Ingersoll, the machine will be dismantled, moved, and reassembled at the McDonnell Douglas Aerospace stitching facility in Huntington Beach, California. The machine is expected to be in operation in the fall of 1996. Its first stitching task will be the cover preforms for a test wing with a span of 41 ft and a maximum width of 8 ft. In a later phase of the NASA ACT Program, the machine will be used to stitch the preforms for a full-scale transport wing. **(M. B. Dow, 757-864-3090)**

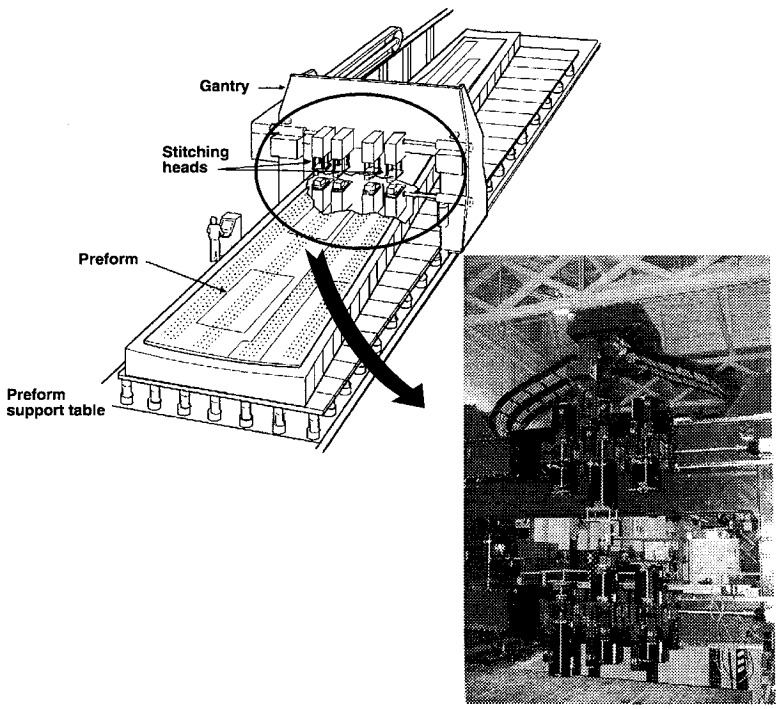

Figure 39. Computer-controlled stitching machine.

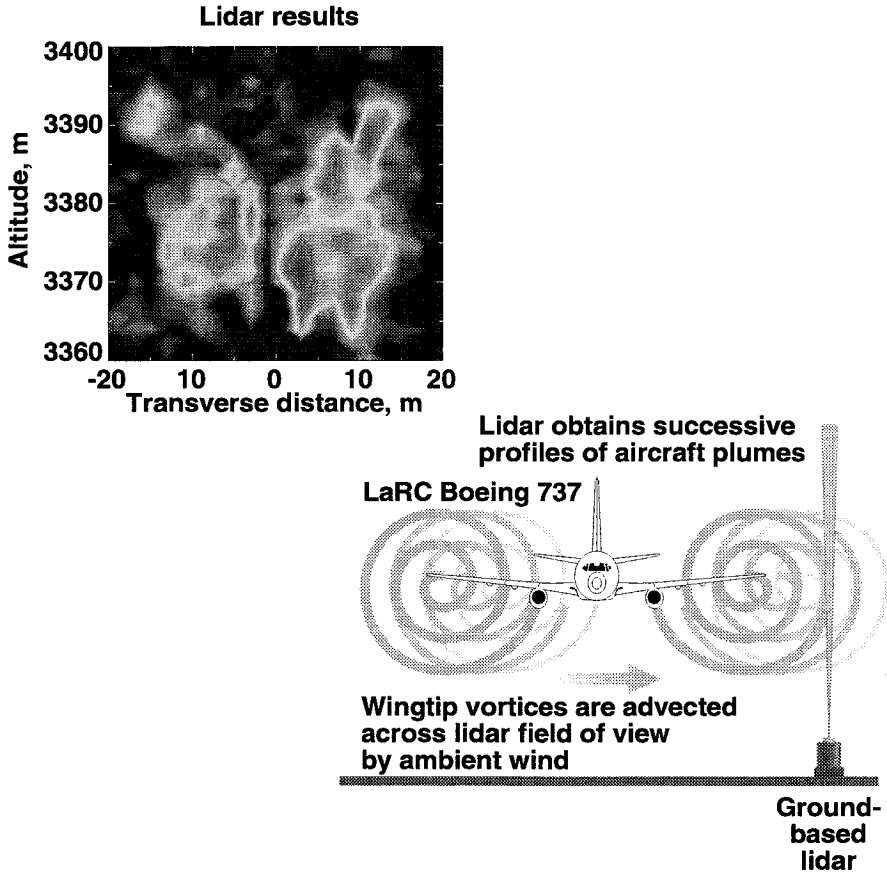

- *Ready the technology base for an economically viable and environmentally friendly high-speed civil transport.*

Turbulence Interactions Research

Numerical simulations with experimental validation were conducted jointly with Wright Laboratories to assess jet noise and laser propagation through the jet plume for an installed powered nacelle. One of the primary goals was to determine if the presence of a wingtip vortex substantially modified the turbulent jet structure to alter jet noise generation mechanisms or influence the beam wander, spread, and scintillation of a propagating laser beam. A powered nacelle with pylon was installed on a NACA 0012 semispan wing using scaled dimensions of an A3 aircraft. The model was mounted at the open throat of the nozzle in the NASA LaRC Low-Speed Aeroacoustic Wind Tunnel on a turret to permit angle-of-attack settings to 15°. The test was conducted with appropriate forward speed, nozzle pressure ratio, and jet temperature consistent with the A3 aircraft.

The experimental tests confirmed all numerical simulations concerning the wingtip vortex roll up and influence of wingtip vortex effects on plume trajectory and turbulence structure. Using the numerical simulations, the effect on laser propagation was predicted and found to compare extremely well with experimental measurements. The turbulence structure was found to contain significant nonazimuthal structure in the principal noise producing region of the jet plume. (See fig. 40.) This finding may explain some of the noise assessment differences between flight tests and ground-based installations with noninstalled engine nacelles. **(J. M. Seiner, 757-864-6276)**

Improved Titanium Alloys for High-Speed Aircraft

Because of their lightweight, high strength, thermal stability, and good fabricability, titanium alloys are of interest for a variety of aerospace applications including subsonic and supersonic airframe structures. However, for some specific emerging aircraft such as the high-speed civil transport (HSCT) to be operationally and economically viable, the performance of materials must be improved significantly over current commercial alloys while minimizing the cost of materials and processes. An integrated national team led by Langley Research Center and including airframe manufacturers, titanium producers, and universities is conducting research to develop titanium alloys and associated fabrication processes that will result in materials with mechanical properties, thermomechanical stability, and suitable fabrication routes sufficient to meet the structural, operational, and economic requirements for

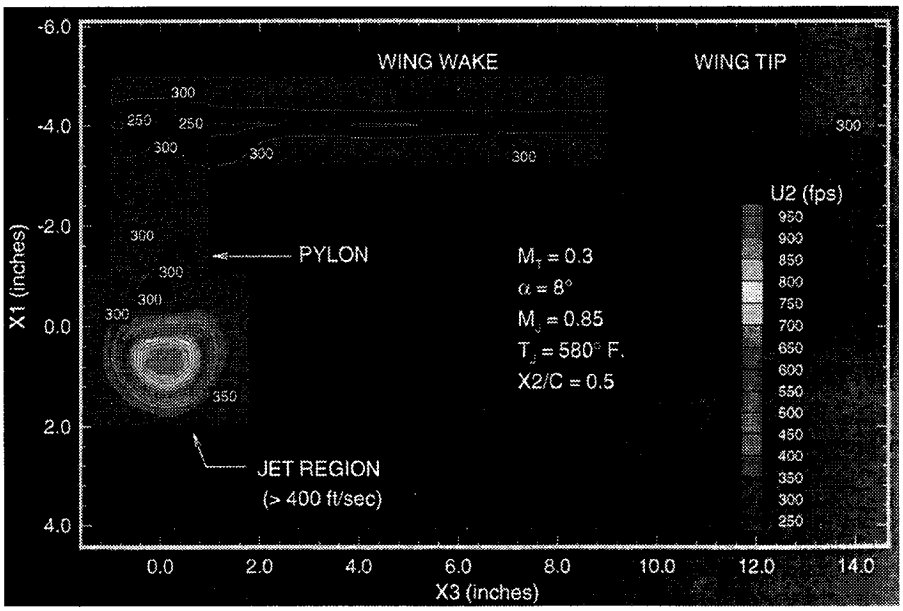

Figure 40. Turbulence interaction research on wing and pylon wake velocity distribution.

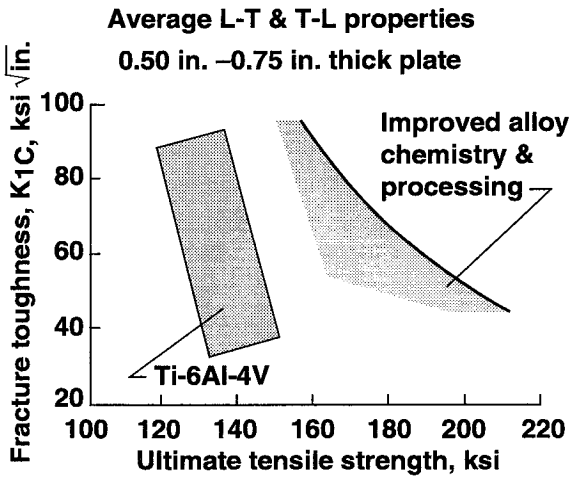

Figure 41. Improved strength/toughness properties of titanium alloys.

a Mach 2.4 high-speed civil transport. This activity includes investigation of a variety of conventional and advanced alloys along with innovative processing routes. Over 75 advanced alloy chemistry and processing variants have been investigated.

Figure 41 shows progress toward improving the strength and fracture toughness of titanium alloys. The shaded area on the left shows the range of properties of Ti-6Al-4V alloy, which is the customary industry standard with which most new alloys are typically compared. The region of the chart labeled "Improved alloy chemistry & processing" contains data developed on some of the alloy variants considered in the HSCT titanium development program. The data are average values for plate products in the longitudinal (L-T) and transverse (T-L) directions and show substantial improvements over the properties of current commercial alloys. Work is continuing to ensure that the thick plate properties shown in the figure translate to other required product forms and that other properties, such as stiffness, ductility, stress-corrosion behavior, resistance to hydraulic fluids, and processibility are maintained at satisfactory levels.

(W. D. Brewer, 757-864-3136)

Solution Coating of High-Speed Research (HSR) Candidate Materials

Since experimental quantities of new resins are initially available in solution, NASA Langley utilizes its custom-built multipurpose prepregger to prepare solution-coated prepreg for composite property determination. Solution prepregging, utilizing polyimides as either fully imidized polymers or as their poly (amide acid) precursors in solvents such as N-methylpyrrolidinone (NMP), is a viable technique for producing unidirectional prepreg tape.

Langley's multipurpose prepregging machine has been used to produce over 16000 linear ft of solution coated prepreg. This corresponds to nearly 500 lb of unidirectional prepreg. These materials were manufactured in-house utilizing the solution dip-tank method shown schematically in figure 42. Eighteen different resin systems and 7 different intermediate modulus carbon fibers have been processed into solution coated prepreg. The majority of this material is newly developed high-speed research (HSR) candidate resin systems. The HSR candidate resin systems processed were not only Langley in-house developed systems like LARC™-PETI-5, but also included industry developed systems such as DuPont Avimid® R1-16. Much of the prepreg produced was shipped to Northrop-Grumman for evaluation as HSR material candidates.

Langley's multipurpose prepreg machine has become a valuable tool for evaluating new resin systems from both NASA and industry. Compared with contracting out experimental resin prepreg production, $1 million has been saved in the HSR program by utilizing Langley's prepregger.

(R. J. Cano, 757-864-3951)

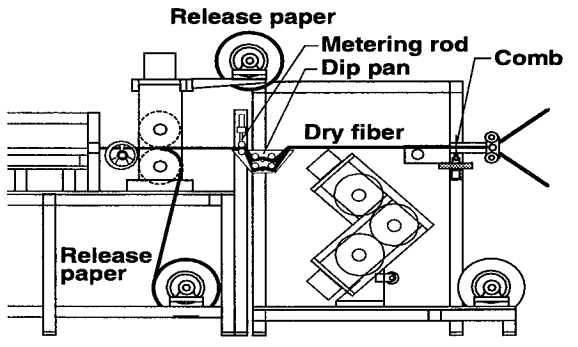

Figure 42. Solution prepregging using the dip-tank method.

High-Speed Civil Transport (HSCT) Structural Adhesives and Composite Resin Matrices

Because no adhesives and composite resin matrices were available with the proper combination of properties (processibility, performance, cost, and worker safety) to meet the demanding requirements of a Mach 2.4 high-speed civil transport (HSCT), work was initiated on pseudothermosetting polyimides called phenylethynyl terminated imide oligomers (PETI's). More than 100 different PETI compositions were prepared and characterized. From these, one material, designated PETI-5, was selected for extensive evaluation. PETI-5 is an imide oligomer prepared from commercially available monomers that is terminated with phenylethynyl groups at a molecular weight of about 5000 g/mol. After in-house work demonstrated potential as an adhesive and a composite resin matrix, the technology was transferred to industry. (See fig. 43.) In 1995, more than 800 ft^2 of adhesive film and more than 1000 lb of IM7 unidirectional tape were produced for evaluation in the High-Speed Research (HSR) Project. Under HSR funding, industry obtained excellent adhesive and composite properties for PETI-5. In an attempt to obtain resins with properties even better than PETI-5, pendent phenylethynyl groups were placed along the polymer backbone to produce PPEI-1. Another approach involved terminal and pendent groups on the same molecule to form PTPEI-1. Although certain resin properties were improved, the overall composite properties of PPEI-1 and PTPEI-1 were no better than PETI-5. This work has provided useful and needed materials to HSR and has also demonstrated that imide oligomers containing phenylethynyl groups can be tailored to provide materials with a wide range of properties. **(P. M. Hergenrother, 757-864-4270)**

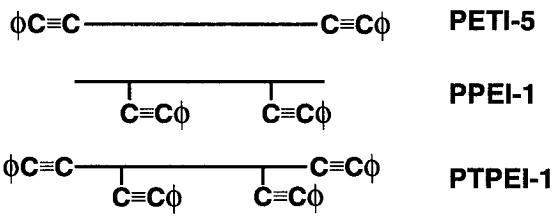

Figure 43. Depiction of chemical structures.

Updated Derivative Method—A Technique Developed To Improve Computational Efficiency for Structural Optimization

Innovative techniques were developed which improve the computational efficiency for structural optimization to allow for optimization using finite-element models with increased fidelity. The approach described here, the updated derivative method, utilizes a newly derived mathematical formula to determine "updated" values for sensitivity derivatives using the results of a single analysis along with a set of previously calculated sensitivity derivatives. Since analysis results are calculated at a fraction of the computational cost of calculating sensitivity derivatives, significant

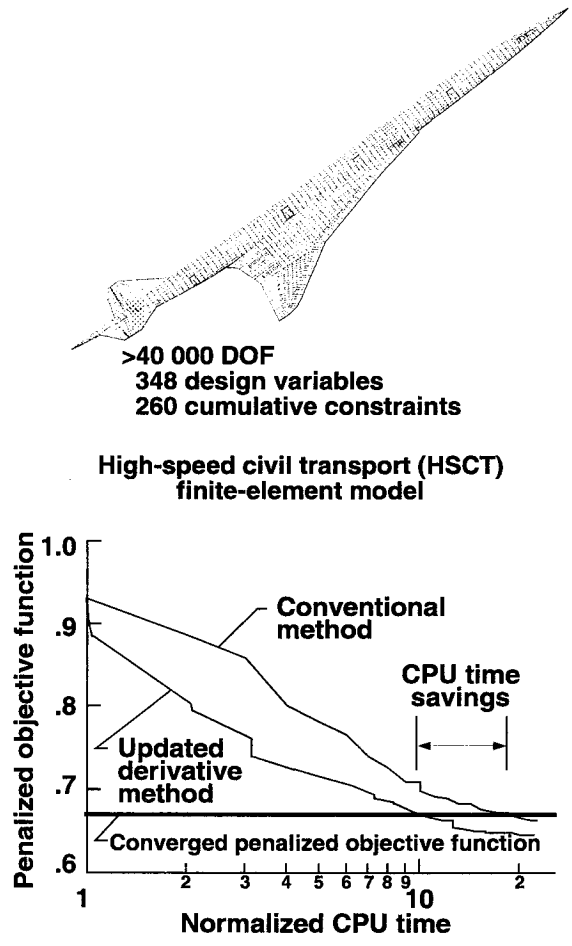

Figure 44. Optimization convergence history for conventional and updated derivative methods.

computational savings are possible using the updated sensitivity derivatives.

A full high-speed civil transport (HSCT) model (>40000 DOF, 348 design variables, and 260 cumulative constraints) was evaluated using the updated derivative method. The HSCT FE model is shown in figure 44. An indication of convergence of the optimization problem for this model is shown by the penalized objective function (which takes into account any violated constraints) in the right of the figure. Results for both a conventional method (sequential linear programming (SLP)) and for the updated derivative method (UDM) are shown in the figure. The conventional approach results are from a sequential linear programming method. The SLP uses the sensitivity derivatives determined at each step to form a linearized optimization problem. The UDM results are from a modification of this conventional approach in which updated sensitivity derivatives are utilized in place of those calculated using a conventional sensitivity analysis. For the HSCT model, a converged result is achieved for the updated derivative method in about half the CPU time required for the conventional method. The improvement in computational efficiency is even larger for smaller optimization problems. A particularly attractive feature of the updated derivative method is that it is relatively easy to incorporate into existing optimization procedures. **(S. J. Scotti, 757-864-5431)**

Ground-Based Lidar Observations of Aircraft Exhaust Particles in Wake Vortex Regime

Ground-based lidar (laser radar) systems at Langley Research Center have been used to obtain high-resolution two-dimensional backscatter measurements of exhaust particles in the wake vortex regime of the Langley Boeing 737 Transport Systems Research Vehicle. Backscatter data from the particles, which act as tracers of air motion, can be used to test and refine computer models of wake vortex fluid dynamics and to study the formation and evolution of new particles in the exhaust plume. Figure 45 shows a sketch of the most common experiment geometry, in which the Boeing 737 flies upwind of the lidar site along a track orthogonal to the local wind. Successive range-resolved profiles of laser backscatter from the exhaust particles entrained in the wingtip vortices are then obtained as the vortex structure is advected over the lidar site. Also in the figure is a contour plot of backscatter data obtained in March 1995 at a distance approximately 1.1 kilometers (equivalent to about 75 aircraft semispans) downstream of the Boeing 737. The vertical and horizontal resolution of the data are about 3 m and 2 m, respectively. The data are qualitatively similar to results obtained from a wake vortex fluid dynamics model, and they clearly show the entrainment of exhaust particles into the two Boeing 737 wingtip vortices. This research has demonstrated the utility of ground-based lidar for studying the wake vortex regime that is virtually inaccessible by other measurement techniques. **(L. R. Poole, 757-864-2689)**

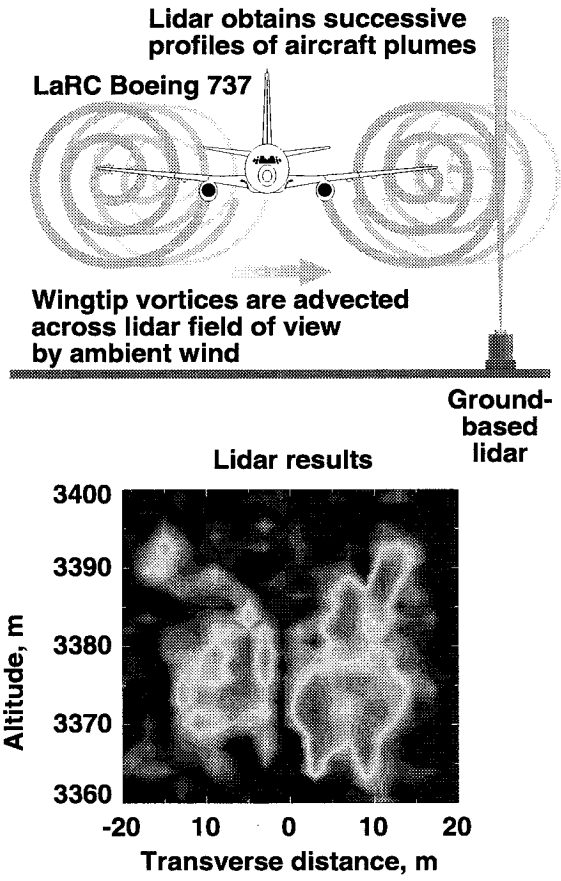

Figure 45. Sketch of experiment geometry and sample ground-based lidar backscatter of exhaust particles from the Langley Boeing 737 aircraft.

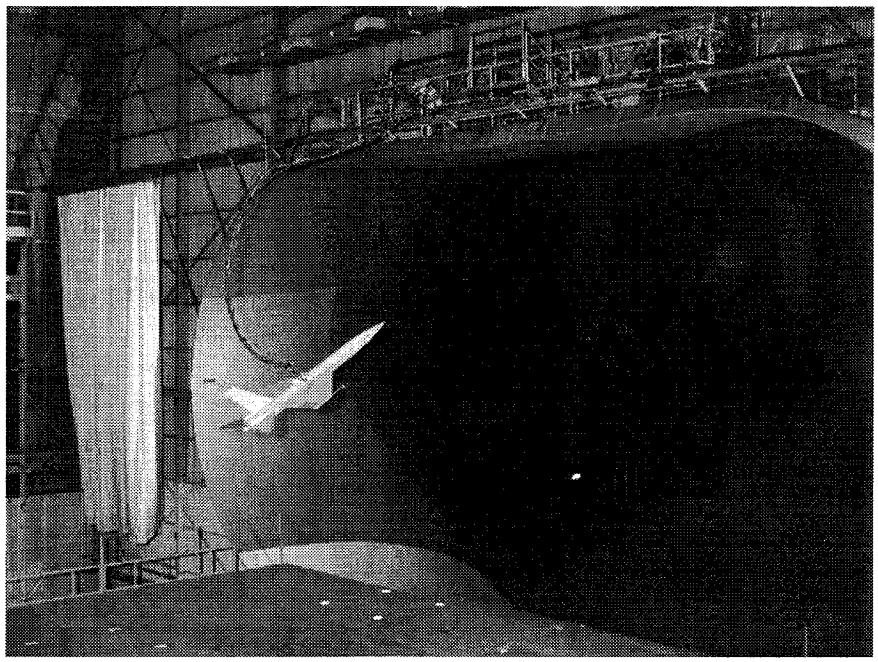

- *Ready the technology options for new capabilities in high-performance aircraft.*

Approach to Data Management, Archive, Protection, and Transmission (ADAPT)

The Approach to Data Management, Archive, Protection, and Transmission (ADAPT) was developed through a collaboration between Langley's Information Systems and Services Division and the Fluid Mechanics and Acoustics Division to meet information system requirements for a wind-tunnel test with Boeing. (See fig. 46.) The test team had a requirement to allow researchers away from the test site to access information about the test immediately after generation. Researchers wanted to exchange multimedia (text, plots, images, etc.), and because the information was proprietary to Boeing, they had to have a secure mechanism for data exchange.

Wind-tunnel tests typically produce large amounts of data that is usually stored on tape or in personal user's file systems. Documentation is limited to the final report and personal notations scattered among the participants. Local storage of this information limits access to local researchers. These conventional techniques would not meet the objectives of the test team.

Prior to the test, a team composed of researchers and information systems experts was assembled to analyze the requirements and design a system that would utilize advanced information technology and data management techniques to provide the desired capabilities. The test schedule would be intense and the team recognized early that, if their efforts were to be successful, the system designed would have to reduce the work of the researchers; it could not add burden. There also would not be time for a large training effort. Modern distributed and networked computer systems provided the means for remote access to data but the sensitive nature of the data added a requirement for security of

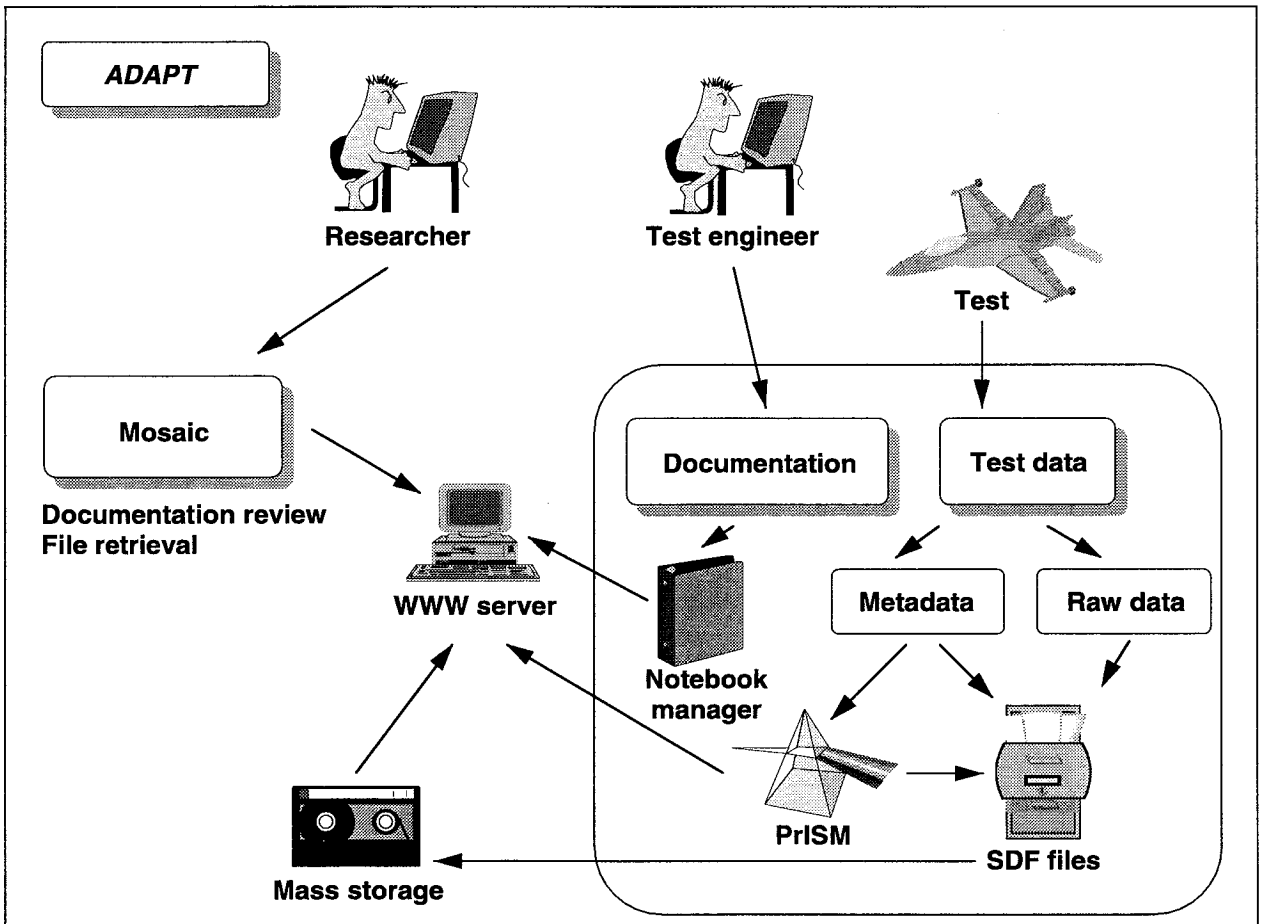

Figure 46. Approach to Data Management, Archive, Protection, and Transmission (ADAPT).

data transfer. Again, the implementation of security could not adversely affect the productivity of the researchers. To achieve these goals, automation had to be maximized.

With these factors in mind, the ADAPT system was designed so that data generated in the tunnel are automatically organized and stored in such a way that it can be easily located and retrieved for analysis; documentation is easily created on-line during tunnel operation and immediately available to remote researchers; remote researchers can retrieve data, perform analysis, and submit their results back to the archive for others to view; the data archive supports multimedia (text, plots, images, etc.); and all data are encrypted before storage and transfer and are automatically decrypted upon retrieval.

ADAPT far exceeded the expectations of the researchers. Some researchers originally expressed reservations about the use of on-line systems for all data creation and review, but early in the test they embraced ADAPT as a significant process improvement over conventional techniques. ADAPT has subsequently been used in two other LaRC tunnels. It is also being adopted by the High-Speed Research program to solve their problems of secure information exchange between NASA and its industrial partners. **(K. H. Jones, 757-864-6720)**

A Translating Throat Nozzle Concept

The objective of this study was to validate a concept designed to improve the off-design performance of single-expansion-ramp nozzles (SERN). In a high-speed configuration, a fixed geometry SERN has a fixed design point where on-design performance levels are acceptable. However, a fixed design point nozzle has substantial penalties in afterbody pressure drag, nozzle thrust, and propulsive efficiency at off-design conditions. The translating throat SERN implements actuated doors to relocate the throat of the nozzle and provide a wide range of expansion ratios. This will improve performance by optimizing flow expansion at various flight conditions. Three design points and two ramp surfaces were investigated at nozzle pressure ratios (NPR's) up to 13 in the Static Test Facility of the Langley 16-Foot Transonic Tunnel. (See fig. 47.) Additionally, a computational study was conducted using the Navier-Stokes code PAB3D with a k-ε turbulence model.

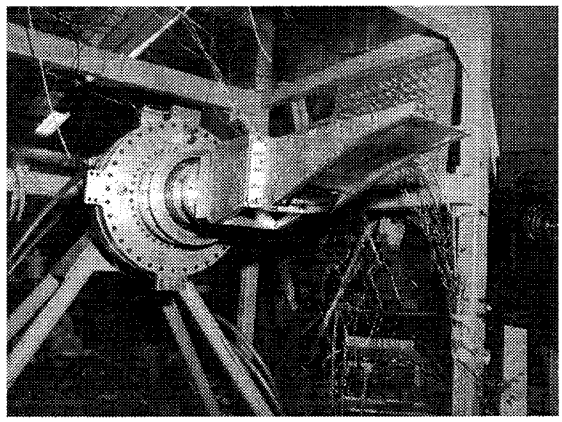

L-95-00094

Figure 47. High-speed configuration mounted on the dual flow propulsion simulation system in the Static Test Facility of the Langley 16-Foot Transonic Tunnel.

A 4-percent improvement in thrust was demonstrated at low NPR's by relocating the throat from the high-speed, high-expansion ratio position to the low-speed, low-expansion ratio position. Results also indicate that resultant thrust vector angle was minimized near the design point. The thrust ratio and thrust vector angle trend of the low-speed configuration was well predicted by two-dimensional computations using PAB3D. **(K. A. Deere, 757-864-8986)**

Twin-Engine Afterbody Analysis

The AGARD Fluid Dynamics Panel sponsored Working Group (WG) #17 for the investigation of the aerodynamics of aircraft afterbodies. The WG #17 selected seven test cases for a computational methods validation study: three from ONERA and four from NASA Langley. All these test cases have well-documented shape definitions, free stream and jet operating conditions, and test data. A NASA twin-engine afterbody test case with various empennage arrangements was selected for the current study and the study results were transmitted to AGARD for inclusion in the final AGARD report. Data for this test case were obtained in the Langley 16-Foot Transonic Tunnel. Configurations with the vertical tails in mid and forward positions were computed (horizontal tail position held constant at the mid position).

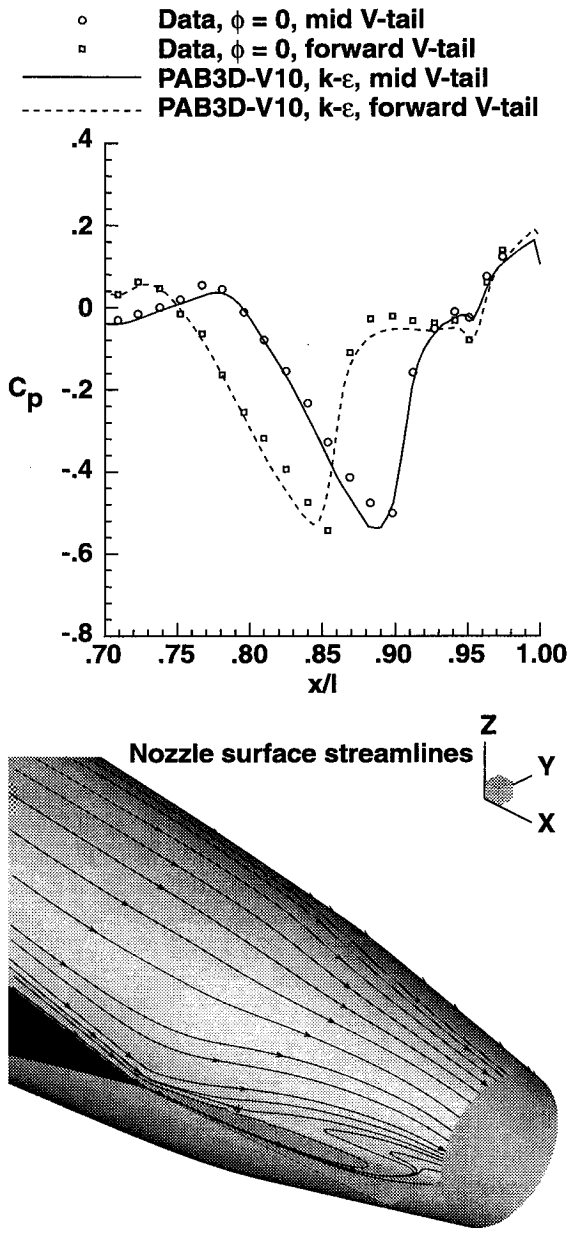

Figure 48. Computed afterbody surface pressure coefficient and particle traces.

The computed and measured pressure coefficients at Mach 0.9 along a row at the top-center position above the left side engine (inboard of the vertical tails) are compared in figure 48. Both the mid and forward vertical tail leading-edge positions are clearly indicated in the pressure coefficient C_p distributions. In the region between the vertical tails, C_p values as low as −0.56 are created by flow expansion for both vertical tail positions. The flow expansion was terminated by a shock ahead of the trailing edge of the vertical tail in both cases. An unusual detail at the $x/l = 0.95$, in the form of a small dip in C_p, was captured in these flow solutions. This feature is thought to be caused by a slope discontinuity between the afterbody and the nozzle. Some detail of the forward vertical tail flow solution on the inboard side of the nozzle is shown by the computed particle traces. Although the measured pressure distribution on the inboard side of the nozzle was similar to that over the top of the nozzle, a mild flow separation has occurred according to the computations. The measured nozzle pressure drag values were predicted well by the computation, but the total aft-end drag values with the tail surfaces included were not well predicted. However, the predicted drag increment between the two computed configurations had excellent agreement with the measured data. **(S. P. Pao, 757-864-3044)**

Missile Alternate Controls Technology Program

The objective of the Alternate Controls Technology (ACT) program is to develop types of missile control, other than purely conventional aerodynamic controls, that will enhance the high-angle-of-attack performance of air-to-air missiles. Propulsive controls, such as reaction jets, may be ideal for this application because they can generally provide control forces which are invariant with angle of attack. In order to study this alternate control concept, an investigation was conducted in the Langley 16-Foot Transonic Tunnel using a 75-percent scale model (jointly funded by NASA and the U.S. Air Force Wright Laboratory) of an advanced missile concept. (See fig. 49.) The model featured independently controlled reaction jets that were located near the nose and tail of the missile model. Aerodynamic control was also provided by four fins located near the tail jet. This investigation was conducted at Mach numbers of 0.35 and 0.60, at angles of attack up to 75°, and at nozzle pressure ratios of up to 96.

Results indicate that substantial jet-induced interference effects on pitching moment occurred from operating the nose jet either on top or on the bottom of the ACT missile model. Operating the nose jet on top

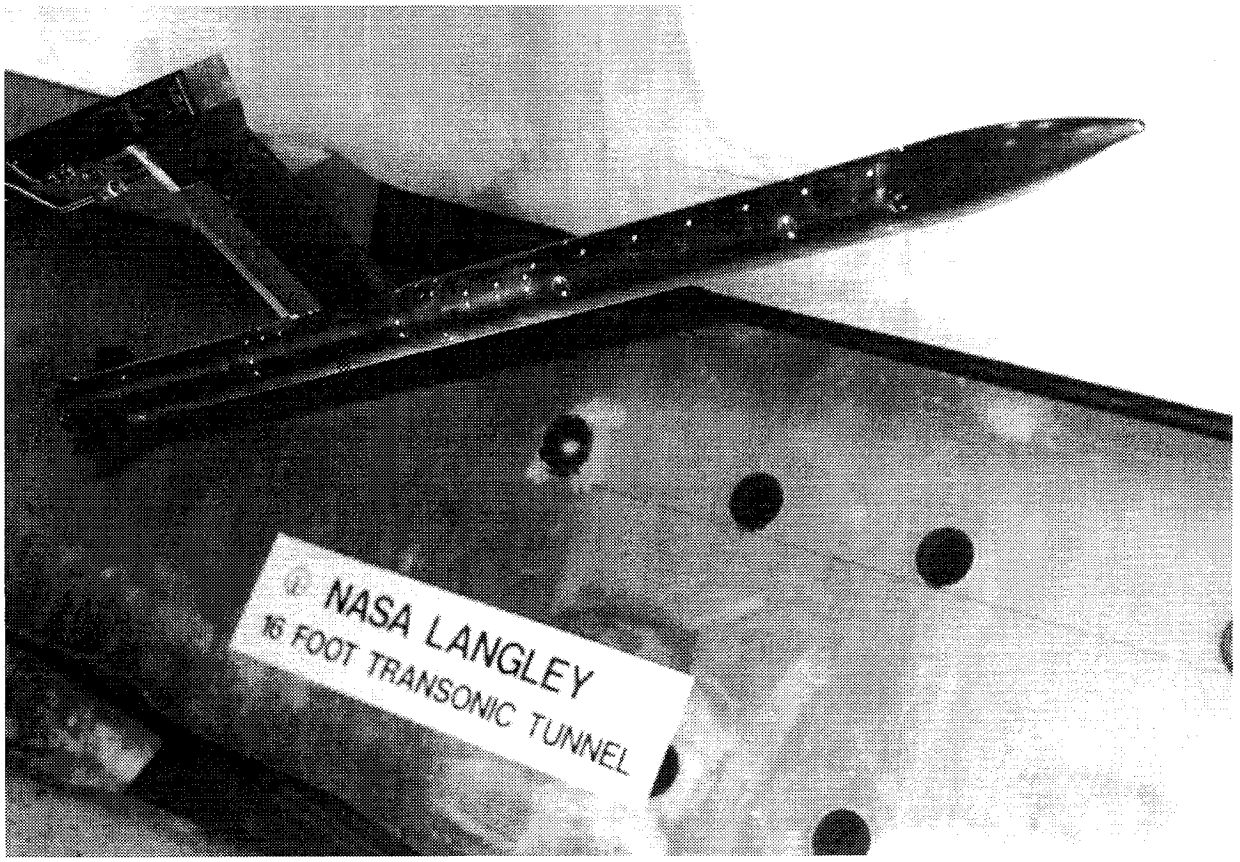

L-94-01501

Figure 49. ACT missile model installed in the Langley 16-Foot Transonic Tunnel.

resulted in jet-induced interference effects that were adverse up to 20° angle of attack and beneficial at angles greater than 20°. Operating the bottom nose jet always resulted in adverse jet-induced interference effects that at some conditions decreased pitching moment by a factor of 4. This is equivalent to about a 20-percent decrease in control effectiveness that would be provided by the jet-reaction thrust. These adverse interference effects result from a suction region on the bottom of the model that was induced by the jet.
(F. J. Capone, 757-864-3004)

Code Validation for Prediction of Hot Jet Plume Flow

The AGARD Fluid Dynamics Panel sponsored Working Group (WG) #17 for the investigation of the aerodynamics of three-dimensional (3-D) aircraft afterbodies. This group extended the work of WG #8 which reported on the aerodynamics of two-dimensional afterbodies in 1986. Three test cases proposed by ONERA (designated A.x) were chosen by the WG for the evaluation of predictive ability of basic flow physics due to their extensive flow measurement database, which included off-body flow quantity surveys. Four Langley test cases (designated B.x) were selected to represent realistic aerodynamic configurations that could involve complex attached and separated external flows interacting with simulated jet plumes. These test cases are documented in the AGARD final report.

An upwind multiblock 3-D Navier-Stokes method, PAB3D, was used to predict jet plume velocity profiles and turbulent viscous stresses for the (A.2) ONERA test case. Results of this effort were transmitted to AGARD for inclusion in the final AGARD report. The flow solutions were developed with PAB3D-V10 using a high Reynolds number formulation of the

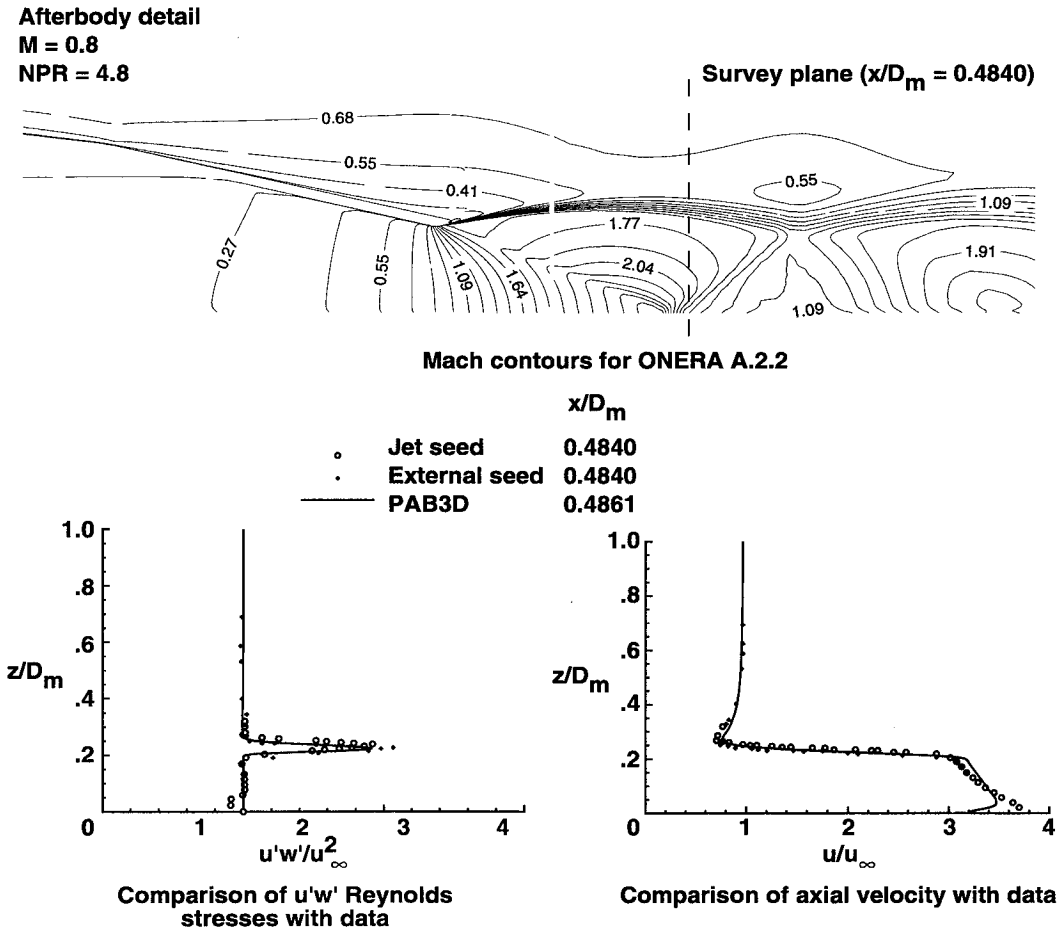

Figure 50. Calculation of hot jet plume characteristics.

standard k-ε turbulence model. The (A.2.2) case had a nozzle pressure ratio (NPR) of 4.8 jet (Total temperature = 935 K) exhausting into a free stream of Mach 0.8 flow. The computed flow field Mach contours are shown in figure 50 with the survey plane shown as a vertical dotted line. The peak Mach number at the plume centerline was approximately 2.84 due to a strong flow expansion originating at the inner lip of the nozzle trailing edge. There was excellent overall agreement between the predicted location of the shear layer and the axial velocity profile compared with the experiment. The predicted Reynolds stress, $u'w'/u_\infty^2$, is close to the experimental data as well, matching level and location of the stress peak in the shear layer. **(J. R. Carlson, 757-864-3047)**

Application of Advanced Turbulence Modeling to Shock-Separated Flows

The current investigation assesses the capability of the three-dimensional Navier-Stokes method PAB3D using algebraic Reynolds stress models to predict the shock-induced boundary-layer flow separation on a nozzle boattail. For several years, a two-equation linear k-ε turbulence model has been used to predict jet plume and nozzle afterbody propulsion interactions with good success. Typically, though, this linear turbulence model predicts a level of static pressure in the separated region of boundary-layer flow higher than the data. As a result, two explicit algebraic Reynolds stress models (ASM) have been implemented to potentially improve the predictive capability of PAB3D for complex flows.

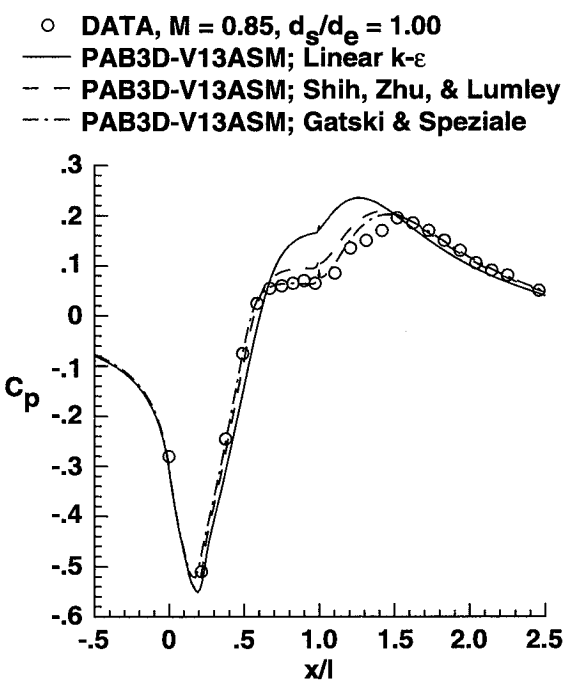

Figure 51. Comparison of predicted with experimental afterbody pressure coefficients, configuration 1, NASA TN D-7795.

In addition, flows that require anisotropic stresses to be modeled can be calculated.

Calculated surface static pressures for an axisymmetric nozzle boattail, using a linear k-ε and two ASM turbulence models, are compared with experimental data in figure 51. The linear turbulence model solution overpredicts the static pressure in the separated flow region downstream of $x/l = 0.7$. The ASM turbulence solutions predict pressures closer to the experiment as well as a slightly better predicted shock location. These results indicate the potential for improved computational fluid dynamics predictions in separated flow regions by use of an algebraic Reynolds stress turbulence model. **(J. R. Carlson, 757-864-3047)**

Experimental Investigation of Canard-Control Missile Concept Featuring Free-Spinning Tails

A wind-tunnel investigation has been conducted to evaluate the supersonic stability and control characteristics of a tactical missile concept featuring forward-mounted, cruciform canards, used for control, and cruciform tails mounted on a free-to-spin body section. The experiment was conducted in the Langley Unitary Plan Wind Tunnel as part of a cooperative agreement between NASA Langley and the Office of Naval Intelligence. The model is shown in figure 52 mounted in the tunnel.

The aerodynamic body surface fits around components of the Langley Remote Control Model system. This system was used to provide remote actuation of the control fin and model roll angles during testing, which eliminated the need to make frequent model changes. Test results were obtained at Mach numbers of 1.90, 2.36, and 2.86, angles of attack up to 23°, and roll angles up to 90°. Canard deflection angles from up to 10° were set in various combinations for pitch, yaw, and roll control. The model was tested with the tail section both locked in place and free to spin. Aerodynamic loads were measured by a six-component strain-gauge balance, and a tachometer was used to measure the spin rate of the tail section.

The test results indicate that the canards were very effective in providing control of this concept. The roll effectiveness was due primarily to the free-spinning tail section, which minimized unwanted loads on the tails resulting from the canard flow field. The spinning tails thus eliminated adverse effects from the canards while still providing adequate stability for the concept. **(J. M. Allen, 757-864-5592)**

Investigation of Cryogenic Wind-Tunnel Model Filler Materials

The National Transonic Facility (NTF) is always examining methods to improve productivity. Among the areas under review are model handling techniques. To effect a model handling improvement, the NTF funded a research and development project to find an improved filler material for filling the voids above subsurface fasteners on models. The requirements for the new candidate filler material were that it must be fast curing, hand finishable, easily applied and removed, and able to withstand the cryogenic test environment of the NTF.

As a result of the project, an ultraviolet light cured filler material modified to match the coefficient of thermal expansion to the parent model material is now a standard model filling material at the NTF. This

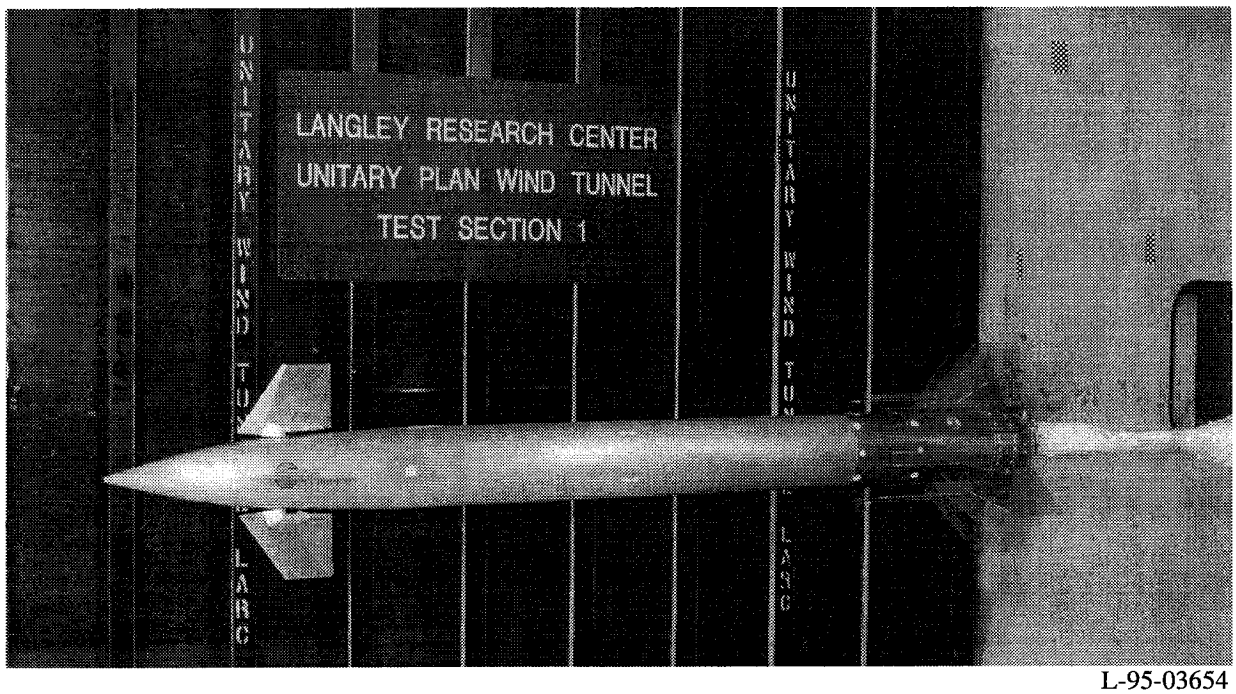

L-95-03654

Figure 52. Missile model 5 installed in the Langley Unitary Plan Wind Tunnel.

modified filler material vastly reduces the cure time from 8 hr to 15 sec. In addition, the surface finish achieved has been improved from an average of 50 rms to 11 rms. Finally, application and removal of the new filler material is simpler and faster. There have been no failures of the new filler material since application to test articles began at the NTF in May 1995. Significant cost savings have been achieved as a result of the enhanced productivity associated with the use of this modified filler material. External Langley Research Center customers have expressed interest in the use of this material.

Investigations are continuing to further the application of the modified filler material to other, less demanding facilities due to the low cost, rapid application, and cure. **(D. L. Hope, 757-864-7294)**

National Transonic Facility Productivity Assessment/Improvement Study

The National Transonic Facility (NTF) provides a one-of-a-kind test capability with the ability to achieve full-scale Reynolds number for all current and postulated near term subsonic and transonic (up to Mach 1.2) aircraft. Run times at the NTF are limited by the primary consumable, liquid nitrogen. Compromises in the test matrix and test duration are made to accommodate the liquid nitrogen constraint.

A team was assembled to consider means of reducing the NTF operating cost and increasing the NTF operational efficiency and productivity. The primary areas of interest of the team were the cost and efficiency of the test operation and the ability of the facility to support and sustain annual throughput. The largest amount of liquid nitrogen is consumed during the tunnel cooldown and recool activities and during testing. The largest amount of time is consumed during model handling activities and unscheduled down time. The most economical means of reducing the effects of the liquid nitrogen constraint are by improving the efficiency of the operations (reduce average time per data point) and/or increasing the inventory of liquid nitrogen available. The next constraint to be considered is to reduce the test duration.

Areas investigated were the tunnel cooldown and warmup, testing, model handling, and unscheduled down time. The amount of liquid nitrogen used during all cooldown processes has been previously optimized

so additional significant savings were not found. The average time per data point can be reduced by 50 percent with current state-of-the-art instruments, upgrades of computers, new or revised control algorithms, new drive control system, and revised procedures. Improvements to the current model handling system can reduce the model configuration change time by 50 percent and the model removal and installation time by 60 percent. Installation of a new model access housing for semispan models, and other improvements can reduce the semispan test program duration by 40 percent and the nitrogen required by 20 percent. Reducing the duration of the annual maintenance shutdown and reducing unscheduled down time through the installation of redundant critical systems and a centralized monitoring system can provide an additional 15 percent available operational time.

The implementation of the concepts noted above indicate that productivity can be improved by at least a factor of 2.4 for all productivity metrics (reduce cost per polar, increase polars per occupancy hour, increase annual cryogenic polars, and reduce test duration). **(H. S. Wright, 757-864-6928)**

Vertical Tail Buffeting Alleviation Using Smart Materials and Rudder

Buffet is an aeroelastic phenomenon which plagues high-performance aircraft, especially those with twin vertical tails. For aircraft of this type at high angles of attack, vortices emanating from wing/fuselage leading edge extensions burst, immersing the vertical tails in their wake. The resulting buffet loads on the vertical tails are a concern from fatigue and inspection points of view.

Buffet load alleviation through active controls is a promising solution to the buffet problem. The Actively Controlled Response Of Buffet Affected Tails (ACROBAT) program at the Langley Transonic Dynamics Tunnel (TDT) investigated the use of an actively controlled rudder, actively controlled piezoelectric devices, and other novel concepts to alleviate vertical-tail buffeting on a 1/6-scale rigid full-span model of the F/A-18 A/B aircraft with flexible tails. (See fig. 53.) The rudder and piezoelectric devices were the most promising of the actuators tested during the July and November 1995 TDT entries. Numerous control laws were tested, with many demonstrating buffeting alleviation over a large angle-of-attack range. The

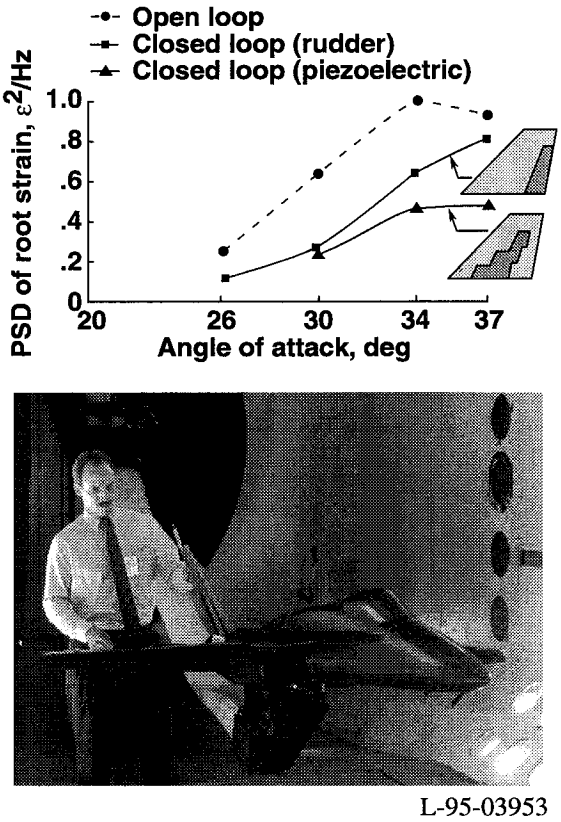

L-95-03953

Figure 53. Wind-tunnel demonstration of buffeting alleviation.

accompanying plot contains a comparison of open-loop and typical closed-loop results using the rudder and the piezoelectric devices. The peak value of the power spectral density (PSD) function of root strain at the frequency of the first vertical-tail bending mode is plotted as a function of angle of attack. At angles of attack up to about 30°, both devices were nearly equally effective in alleviating buffeting (with maximum reductions of about 60 percent). However, at higher angles of attack the piezoelectric devices had superior performance.

Building upon the success of this program are a McDonnell Douglas Aerospace program and two Wright-Patterson Air Force Base (WPAFB) programs. McDonnell Douglas wishes to extend this success to its new F-18 E/F aircraft by investigating active control of the rudder on a 15-percent F-18 E/F model. WPAFB is investigating the use of piezoelectric devices on the tail of a 4.7-percent F-15 model and on the tail of a full-scale F-18 C/D aircraft. **(R. W. Moses, 757-864-7033)**

Combustibility Tests of 1,1,1,2-Tetrafluoroethane in Simulated Compressor Cylinder

The advantages of high-molecular weight gas (heavy gas) as a wind-tunnel medium have been recognized for some time. Langley's Transonic Dynamics Tunnel (TDT) is a large scale wind tunnel that utilizes chlorofluorcarbons (CFC) refrigerant R12 as a test medium. However, this refrigerant has been linked to ozone depletion leading to a ban on its manufacture in 1995. An attractive replacement is 1,1,1,2-tetraflouroethane (refrigerant R134a). This gas has acceptable properties for wind tunnel use, such as molecular weight and speed of sound, and has no chlorine, therefore it has an ozone depletion potential (ODP) of zero. Its vapor pressure allows simplified reclamation from mixtures with air. However, it is recognized that R134a is combustible under certain conditions of temperature, pressure, and concentration.

A comprehensive study was conducted to characterize the combustibility of the gas/air mixture in a simulated compressor cylinder of the TDT reclamation system. Testing was conducted with three types of ignition sources; ASTM standard exploding wire, local high-temperature surface, and auto ignition tests. These tests were conducted over a pressure range of atmospheric to 740 psia and concentration range of 2 to 50 percent R134a. Pressure rise versus concentration for various initial pressure were determined along with the combustibility envelope for the gas/air mixtures. Also, tests of flame propagation through a compressor valve and into a length of pipe were conducted to characterize the quenching capabilities of the valve/piping system. The extensive database generated by this testing was used as a design basis for modifications to the TDT for the use of R134a heavy gas.

The database can be used to establish guidelines for the safe use and handling of R134a. This information is ideally suited to users with nontraditional or specialized applications of CFC replacement gases. The test apparatus enables the user to characterize the combustibility of a given gas for a range of temperatures, pressures, and concentrations. **(D. A. Babcock, 757-864-6916)**

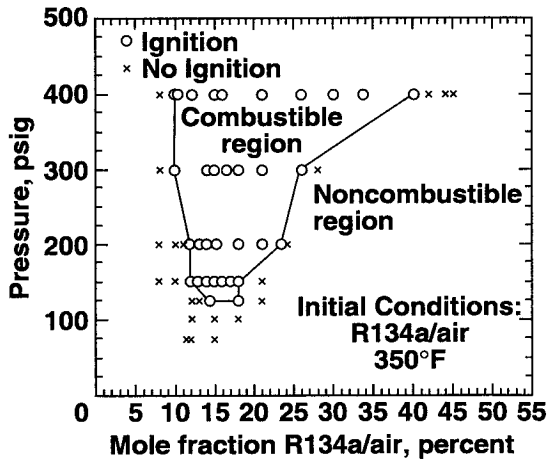

Figure 54. Pressure versus concentration exploding wire ignition.

Free-Flight Investigation of Forebody Blowing for Stability and Control

Increased emphasis on high-angle-of-attack maneuverability in recent years has required the development of novel control effectors. In addition, moving control surfaces can severely penalize configurations with respect to radar stealth requirements. Therefore, nonmoving pneumatic controls, if effective, would be a highly desirable method of control.

Wind-tunnel free-flight tests were conducted in the Langley 30- by 60-Foot Tunnel with a remotely

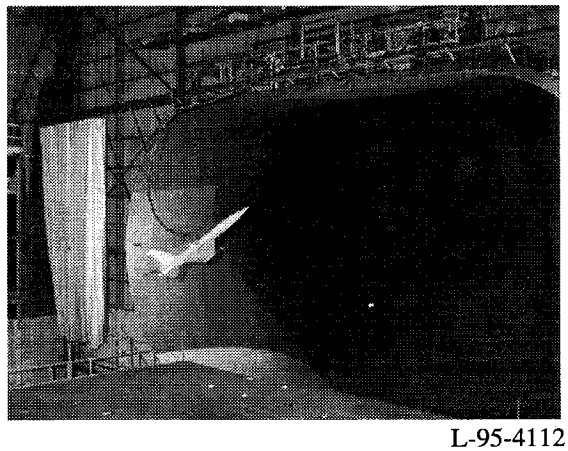

L-95-4112

Figure 55. Generic fighter model flying at 45° angle of attack using forebody pneumatic controls.

controlled, generic fighter model. The model was flown in the open test section with conventional control effectors, pitch and yaw thrust vectoring, and forebody blowing. Model airplane states, position, and control system parameters were recorded along with pilot comments for analysis. Use of forebody blowing as the only yaw control effector allowed flight to 50° angle of attack. Lag of the yawing motion response using forebody blowing was measured in flight and, although substantial, still allowed acceptable control. A photograph of the model flying at 45° angle of attack with forebody pneumatic controls is shown in figure 55.

This test represented the first demonstration of forebody blowing integrated with a flight control system for stability augmentation and control. Additionally, this test showed that it is possible to control an airplane with on/off control of the forebody blowing (instead of proportional control) which may have significant cost and complexity advantages when implemented in an actual airplane. The test also validated that the control moments measured in static tests were actually produced in the dynamic flight environment.
(J. M. Brandon, 757-864-1142)

Experimental Robust Control

This is an experimental investigation of robust tracking control for the Large Angle Magnetic Suspension Test Fixture (LAMSTF), a highly unstable system incorporating a magnetically suspended rigid body in the presence of external disturbances and uncertainties. In practice, limitations in model fidelity restrict both attainable performance and predictability. The motivation for this study is to make recent advances in multivariable robust control useful as an engineering tool. A series of experiments was conducted to study the effects of erroneous nominal and uncertainty models on the actual performance.

The LAMSTF, shown in figure 56, is operated in both a nominal and a perturbed configuration. The perturbed configuration contains an aluminum ring which provides eddy currents, a major source of dynamic model errors. The effect of eddy currents can be bounded, but is difficult to describe analytically. A series of controllers was designed and tested to maintain tracking performance both with and without the effect of dynamically induced eddy currents. To investigate the effect of using an analytical model as the nominal model, an identified model of the plant, without the externally induced eddy currents, was obtained by a closed-loop system identification technique. To investigate the influence of erroneous uncertainty models, two types of uncertainties were developed and tested. Other sources of uncertainties include linearization about equilibrium, inaccurate knowledge of spatial distribution of magnetic field, sensor nonlinearities, and calibration errors.

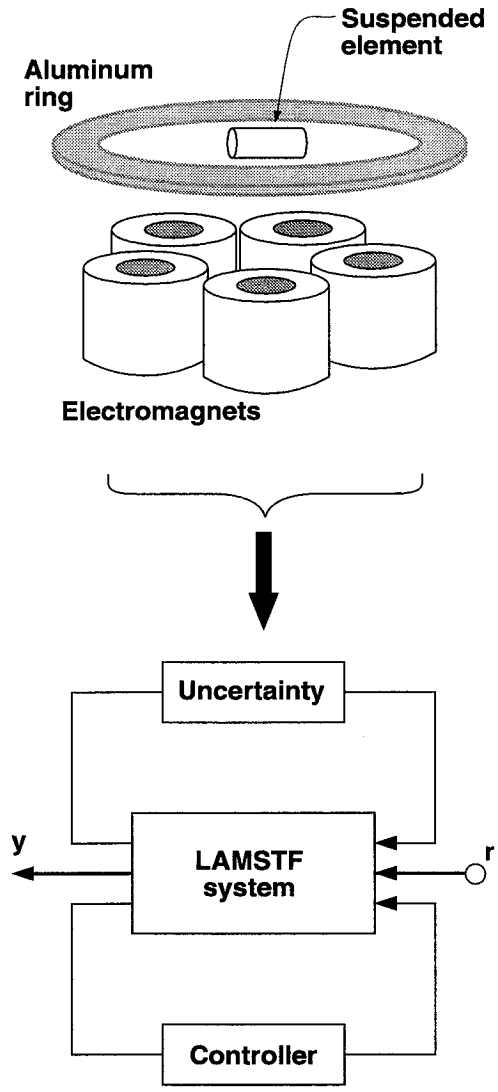

Figure 56. LAMSTF configurations.

This study shows the importance of proper uncertainty models in the design of robust control systems. It was shown that incorporating uncertainty models

which incorrectly capture the physics of the eddy currents leads to poorer performance than not designing for robustness at all. This study also demonstrates that the performance obtained via robust control techniques using only an analytical model with a physically consistent uncertainty model is comparable to the performance obtained by using an accurately identified model without robustness considerations.
(K. B. Lim, 757-864-4342)

Cranked-Arrow Wing Aerodynamics Research

Flight experiments are being conducted on an F-16XL airplane to obtain aerodynamic data and flowfield quantification of a highly-swept, cranked-arrow wing configuration for correlation with computational fluid dynamics (CFD) predictions and wind-tunnel results. In a series of flight tests, the upper-surface onflow characteristics for this wing were documented using tufts, oil flow, and liquid crystals over a variety of test conditions. The flow patterns were recorded using onboard video cameras and chase-plane still and video photography.

Figure 57 shows an example of comparative results between scientific flow visualization and CFD predictions. In this example, the video image of the left wing, as viewed by a video camera mounted at the top-left-side of the vertical tail, has been digitized for the test conditions of 13° angle of attack and 0.29 free-stream Mach number. The 2-D digitized image was mapped into 3-D space using recently developed software and then superimposed onto the same numerical surface geometry as used by the CFD. The resulting surface patterns show good agreement between the tufts and the CFD particle traces; also, good agreement is noted between the tufts and the location of the primary inboard vortex, as depicted by the stagnation pressure contours. Part of this work was done under contract with Computer Sciences Corporation.
(J. E. Lamar, 757-864-2851)

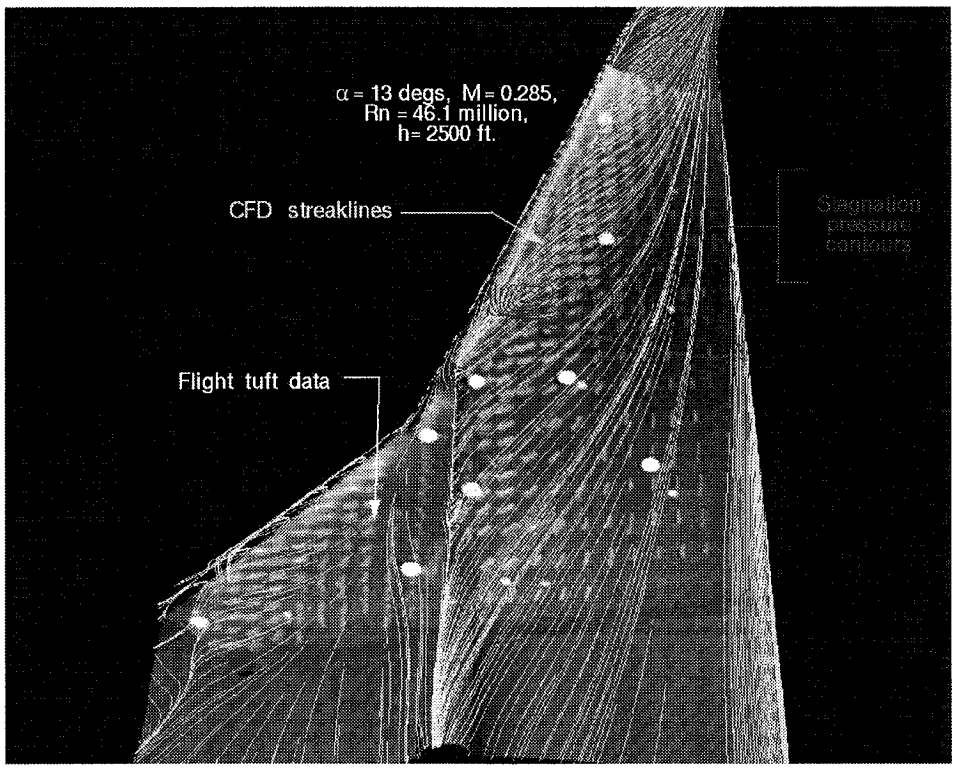

Figure 57. F-16XL flight tuft data and CFD solution.

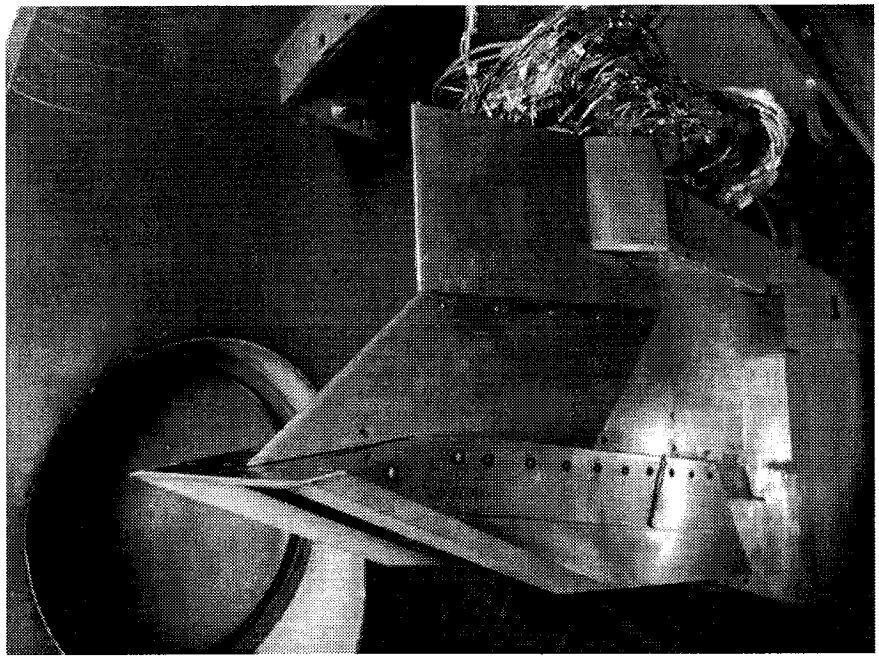

- *Develop and demonstrate technologies for air-breathing hypersonic flight.*

Mach 4 Tests of Hydrocarbon-Fueled Scramjet Engine

Hydrocarbon fuels are attractive for hypersonic missile applications because of their high density, ease of storage, and heat sink capabilities up to approximately Mach 8 (through endothermic chemical reactions related to the petroleum cracking process). Experimental studies of scramjet combustors have been conducted over the past several decades to advance technology for hydrocarbon-fueled scramjets; however, few studies exist of complete scramjet engines. The present study was conducted as part of a cooperative agreement with the Rocketdyne Division of Rockwell International who designed and fabricated a single flow path, fixed-geometry engine model to serve as a testbed for studying hydrocarbon fuels. Free-jet propulsion tests of the engine were conducted in the Langley Combustion-Heated Scramjet Test Facility (CHSTF) at a simulated Mach 4.0 flight condition. Most of the tests were conducted with gaseous ethylene as a surrogate for cracked jet-propellant fuel, and a limited number of tests were performed with gaseous hydrogen fuel for comparison.

The results indicate that flameholding with ethylene fuel was much more difficult to achieve than with hydrogen; and, hence, a pilot flame (provided by a pyrophoric gas) was required to maintain ethylene combustion at the simulated Mach 4.0 condition. However, as shown in figure 58, by piloting the ethylene and by optimizing the fuel and pilot fuel injection locations, thrust performance and engine operability were comparable to the best performance obtained with hydrogen fuel. **(C. W. Albertson, 757-864-1371)**

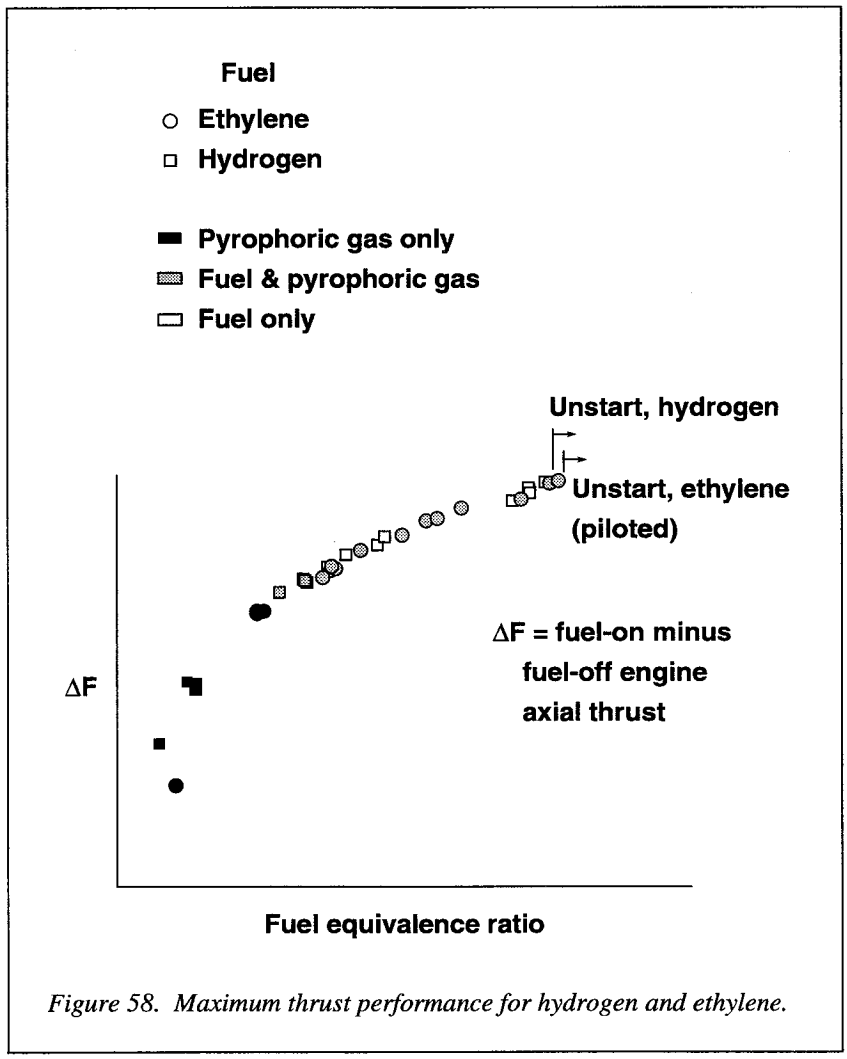

Figure 58. Maximum thrust performance for hydrogen and ethylene.

Scale Effects on Scramjet Engine Performance

Supersonic combustion ramjet (scramjet) engine wind-tunnel data for geometrically similar flowpaths at different scales were obtained and compared for the first time. Although a ground-test-generated database exists for a number of scramjet flowpath concepts in several types of ground-based propulsion test facilities, issues related to engine scale and flight condition simulation are of concern, and very little comparative data have previously been generated. During the National Aero-Space Plane (NASP) program, two geometrically similar hydrogen-fueled scramjet engines were built and tested. The subscale parametric engine (SXPE), a 12.5-percent geometrically scaled model of the NASP flight engine design, was tested in the Langley Arc-Heated Scramjet Test Facility, and the concept demonstration engine (CDE), a 30-percent geometrically scaled model of the NASP flight engine design, was tested in the Langley 8-Foot High-Temperature Tunnel. (See fig. 59.) While some data suitable for investigating scale effects were obtained in these NASP tests, the focus was primarily on demonstration of overall engine performance and operability.

In follow-on tests conducted by NASA during 1995, the effects of engine scale and flight condition simulation (pressure and test gas composition) were investigated at Mach 7 flight simulation using these engines. Preliminary data analyses indicate that for the same fuel injection schemes and levels, differences exist in heat-release profile; but when test techniques are employed to achieve similar heat-release profiles, engine operation in terms of the isolator-combustor pressure distribution is remarkably similar.
(K. E. Rock, 757-864-6265)

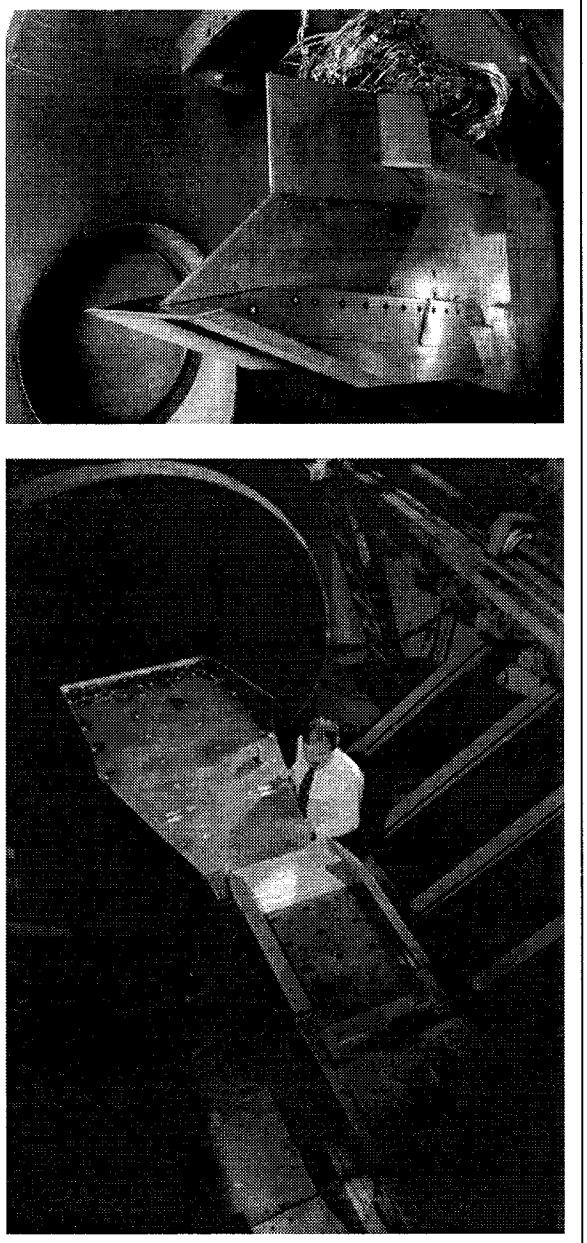

Figure 59. Subscale parametric engine mounted in the Arc-Heated Scramjet Test Facility (top) and the concept demonstration engine mounted in the Langley 8-Foot High-Temperature Tunnel (bottom) for propulsion testing.

Unsteady Pressure Behavior in Ramjet/Scramjet Inlet

Dynamic unstart information is essential in predicting thrust penalties during the unstart process, and withstanding structural loads is a major concern in the design of all supersonic/hypersonic airbreathing engine configurations. Large scale flow field fluctuations can have serious ramifications in such areas as vehicle stability and control, high instantaneous structural loading, and fatigue of the aircraft structure. The unsteadiness can also have a large effect on the uniformity of the flow entering the combustor and on the time-dependent behavior of the combustion process itself.

In cooperation with the National Research Council, Lockheed Engineering & Sciences Company, and

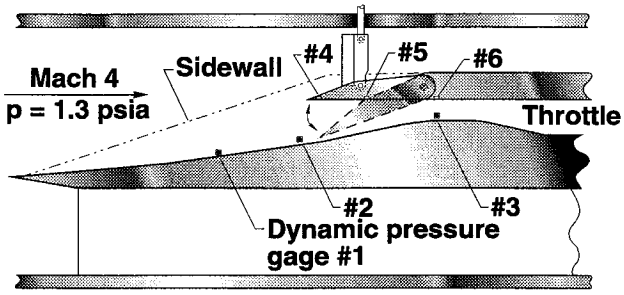

Supersonic Inlet Model

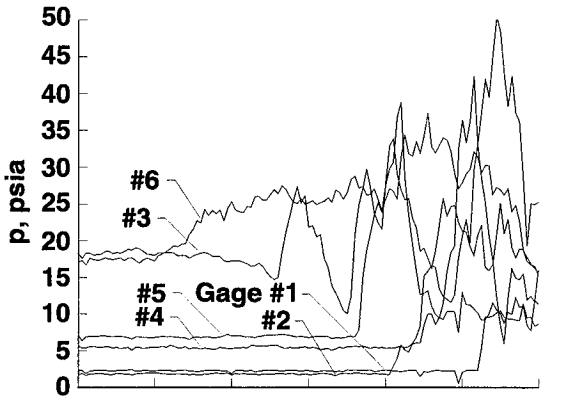

Time Accurate Unstart of a Supersonic Inlet

Figure 60. Experimental configuration and typical pressure time history recorded at 10 kHz.

Rockwell International Corporation, a series of experiments has been conducted that provide insight into the unstarting behavior of supersonic inlets. In this study, time-accurate data were acquired during over-contraction unstarts and also during unstarts due to increased back-pressure at various inlet contraction ratios. Figure 60 shows the experimental configuration and a typical pressure time history recorded at 10 kHz by the six dynamic pressure gages, as the inlet was throttled until it unstarted.

Unstarted inlet pressure fluctuations usually exhibited oscillatory behavior, or at least had deterministic characteristics as opposed to random patterns. The unstarted inlet also displayed a major redistribution of the pressure field and an increase in the level of pressure fluctuations that must be included in the structural design. Finally, dynamic pressure loads observed during the unstart process were quantified and found to be greater for high-contraction ratio inlets than for inlets of low-contraction ratio. This information is essential for the design of future ramjet/scramjet inlets.
(C. A. Trexler, 757-864-6247)

A Diode Laser Sensor System for Combustion Diagnostics

Water vapor, $H_2O(v)$, is an important species in combustion and hypersonic flow diagnostics since it is a primary combustion product. Such measurements can be used to determine performance parameters such as the extent and efficiency of combustion in propulsion and aerodynamics facilities. The $H_2O(v)$ measurements in these high-temperature hypersonic combustion conditions must be nonintrusive and possess a very fast time response.

A three-beam diode laser $H_2O(v)$ measurement system for nonintrusive combustion diagnostics has been developed by L. Wang (College of William and Mary) and successfully tested and installed at HYPULSE hypersonic combustion test facility for routine operation. The system utilizes both direct absorption (DA) and frequency modulation (FM) laser spectroscopy. A block diagram of the three-beam $H_2O(v)$ sensor as installed on the test module of the HYPULSE facility is shown in figure 61. The output beam from a distributed feedback InGaAsP diode laser (emitting around 1.39 mm) is split into three parallel beams each separated by 9 mm. With this arrangement $H_2O(v)$ number density is measured along three paths crossing the test module. Frequency modulation spectroscopy is used to achieve high-detection sensitivity with a short 0.2 msec response time. The diode laser is frequency modulated at radio frequency (RF), while the diode laser wavelength is scanned over a strong water vapor absorption line. Signals from the detector assembly are directed to the DA-FM separators where the three channels of DA signals are separated from the three channels of FM signals. The detected RF signal is then demodulated at

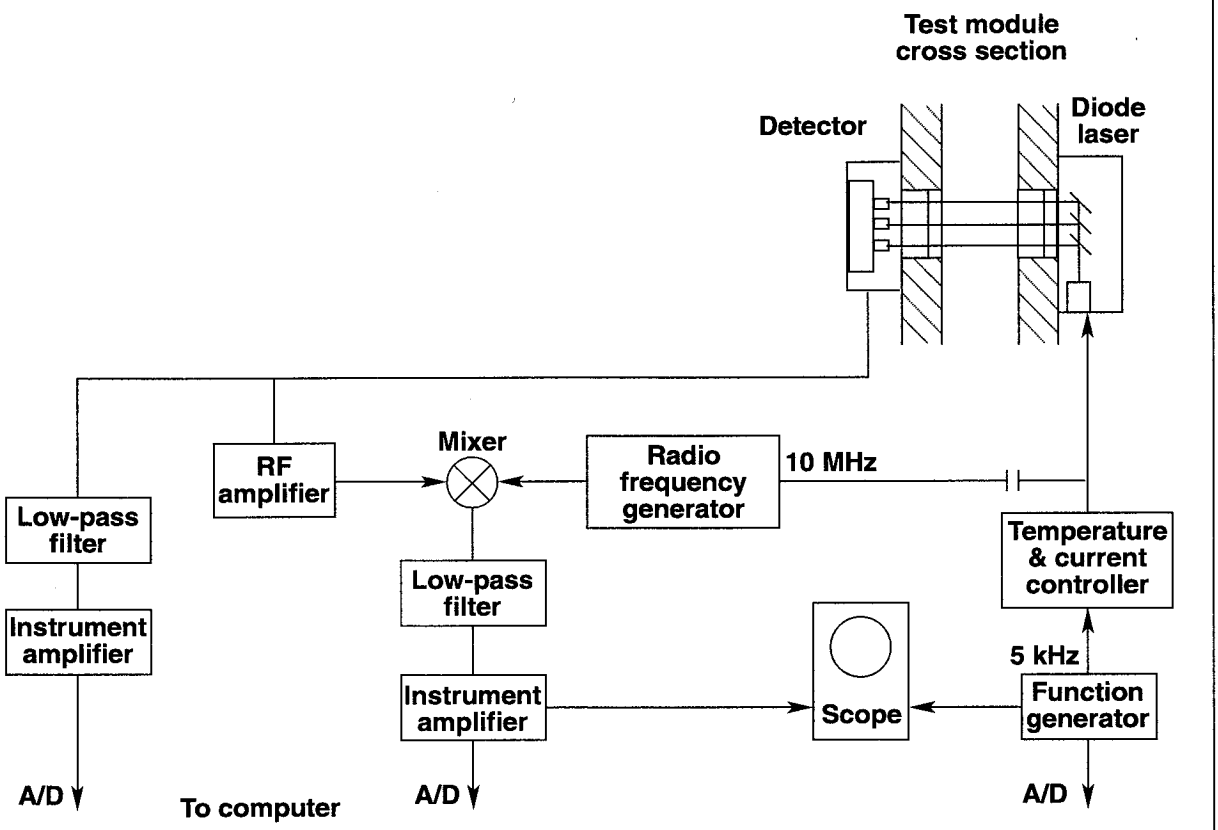

Figure 61. Block diagram of three-beam $H_2O(v)$ sensor.

the fundamental frequency of the modulation. One of the unique features of this sensor is the technique used to calibrate these FM channels. Each of the three FM signals is calibrated with its corresponding DA signal using a strong absorption line at room temperature. The calibration measurements are used to determine instrument parameters in each channel. Instrument parameters represent the instrument characteristics only and are independent of which absorption line is chosen in the calibration runs. A computer software code has been developed for data processing and analysis.

This multibeam water vapor sensor using both DA and FM laser absorption techniques has been routinely used in the HYPULSE facility for approximately 1 year. Further development of the water vapor sensor will entail further improvements in time response and measurement accuracy. The size of the system will be further reduced. It is intended that this technology will be applied to in-flight research studies, as well as ground-based combustion studies. **(G. W. Sachse, 757-864-1566)**

Design, Analysis, and Optimization of Airbreathing Hypersonic Vehicles

Hypersonic Optimization for Langley's Improved Synthesis Technology (HOLIST) is the Systems Analysis Office's (SAO) working environment for the multidisciplinary design, analysis, and optimization of airbreathing hypersonic vehicles. It is being developed by SAO in part through a contract with McDonnell Douglas. HOLIST will help to eliminate disconnects between disciplines, enable rapid multidisciplinary parametrics, allow the evaluation of design sensitivities, and will enable the optimization of the vehicle design and trajectory. Currently a parametric geometry model, Pro/ENGINEER, is being incorporated into HOLIST. This will enable the entire vehicle configuration to be represented with a number of specified design variables. HOLIST is constructed modularly such that when improvements are made in any of the discipline tools, or new tools are available, these can be easily incorporated. A user-friendly optimizer,

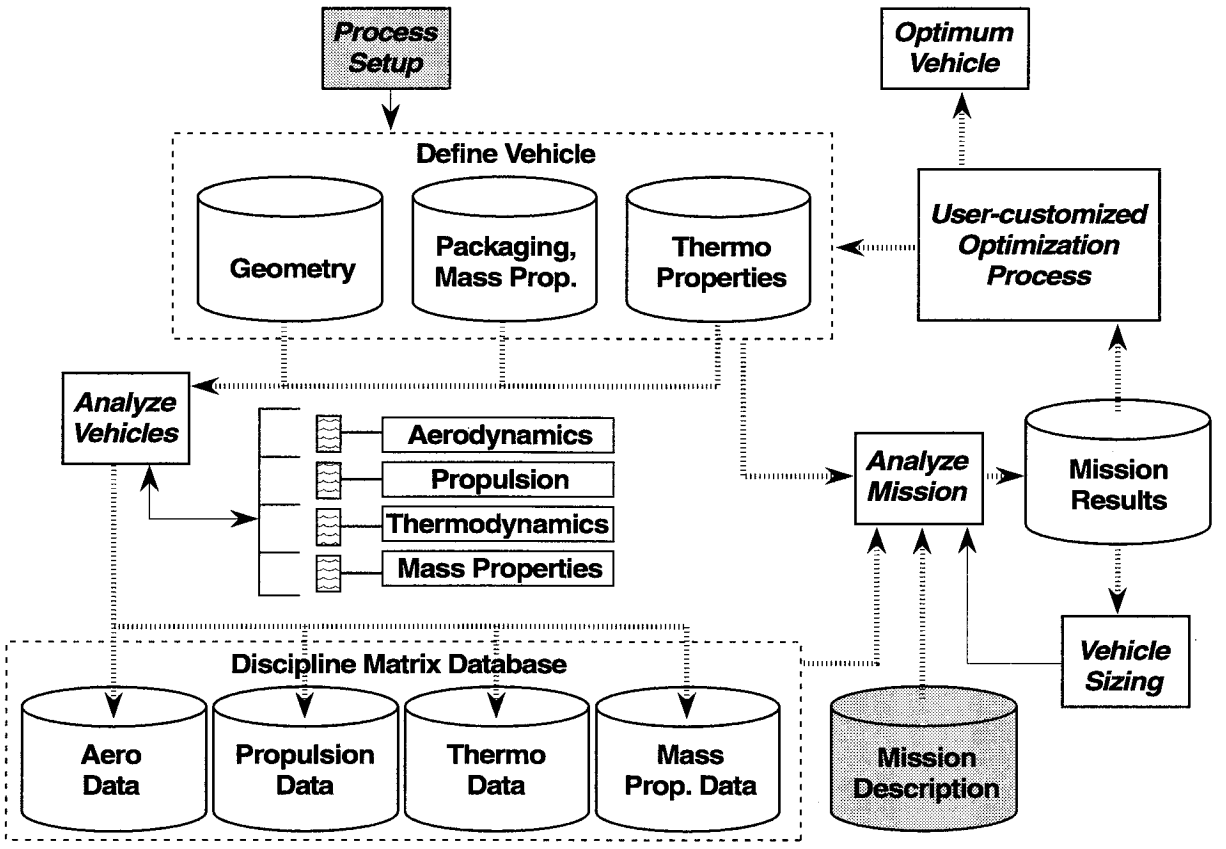

Figure 62. HOLIST design optimization.

Optdes-X, has been integrated into the environment, and the entire system is set up on workstations complete with graphical user interfaces.

A simplified flowchart illustrating how an optimization proceeds in HOLIST is shown in figure 62. In the upper left-hand corner, the process setup includes defining the design variables, objective function, constraints, and convergence criteria for a run. The baseline vehicle geometry and packaging, together with a definition of the mass and thermo properties, follow. Analysis of the configuration proceeds with aerodynamics, propulsion, etc. (Note that for simplification of the diagram several disciplines are not represented here, including structures and thermal management, for example.) The analysis can either be performed in real time, i.e. by running an analysis code, or a database can be accessed to obtain the discipline results.

Once the analyses are completed, the vehicle is flown as represented by the "Analyze Mission" box. From the mission results, the vehicle is sized. At this point, if only a single vehicle analysis were required, the process would be complete. However, if it is desired to optimize the vehicle, the optimization process begins. Finite differences are used to calculate the derivatives of the objective function with respect to each of the design variables. Thus, for the perturbation of each design variable, one pass through the loop is made. Based on the derivative information, the vehicle design for the next iteration is defined. Iterations continue until the convergence criteria and all the constraints are satisfied, yielding the optimum vehicle configuration.

Currently, the basic synthesis system of HOLIST is in operation. The capabilities include aerodynamics and propulsion analysis for Mach 6 to 25, and vehicle performance methods which can perform various mission segments such as cruise, maneuvers, descent, etc. Also included are methods for packaging, mass property definition, and vehicle sizing. **(D. H. Petley, 757-864-3759)**

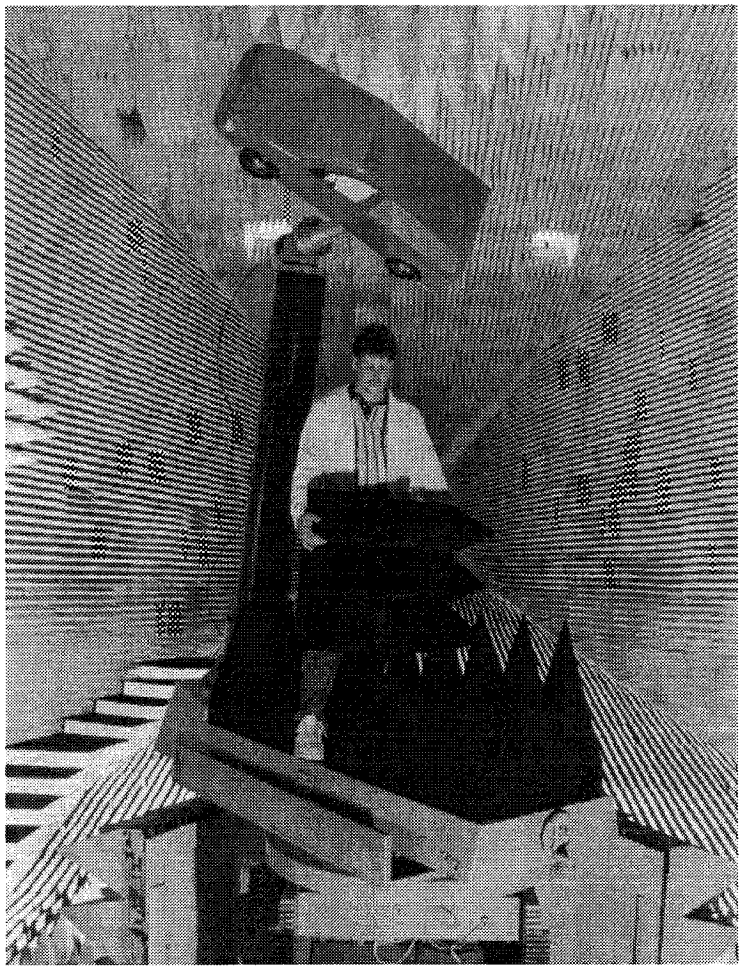

- *Develop advanced concepts, physical understanding, and theoretical, experimental, and computational tools—including high-performance computing and information technologies—to enable advanced aerospace systems.*

Tomographic Measurement of 3-D Refractive Index Field

Interferometric tomography is a technique for reconstructing three-dimensional refractive index fields from multidirectional interferometric projection data. The technique can provide means for capturing spatial distributions of physical properties of flow fields related to refractive index, including density and temperature. Before interferometric tomography can be practically used for accurate measurements with good spatial resolution in wind tunnels, the major problems of incomplete projections and noise must be solved. In order to simulate the expected experimental arrangement at a wind tunnel, a laboratory test has been conducted with a flow field produced by a thermal plume generator. The setup utilized diffuse illumination laser holographic interferometery for instantaneous flow-field recording and a phase-stepping technique for projection data extraction. Reconstructions were made from a restricted view angle of less than 40° and with incomplete projections due to blockage of the illuminating laser beam by a model to simulate wind-tunnel experiments. Figure 63 shows the reconstructed cross section of the temperature field just below a thermocouple rake used to verify temperatures at several locations. The average error in the reconstructed temperature field at the thermocouple locations was 3.5 percent. This work was done in collaboration with Professor Soyoung Cha from the University of Illinois at Chicago under a NASA grant. **(A. W. Burner, 757-864-4635)**

Numerical Study of Fundamental Shock Noise Mechanisms

The objective of this work is to develop a better understanding of the physical mechanisms responsible for noise generation in supersonic jets. Because a direct numerical simulation of the entire flow field, including acoustics, is computationally prohibitive, the approach taken here is to carefully study fundamental mechanisms responsible for sound generation in supersonic jets. The fundamental mechanism considered here is the passage of a ring vortex through a shock wave, which is a physical model of broadband shock noise generation in supersonic axisymmetric jets. The passage of a vortex ring through a normal shock wave is simulated using a high-order accurate, finite volume implementation of the essentially nonoscillatory (ENO)

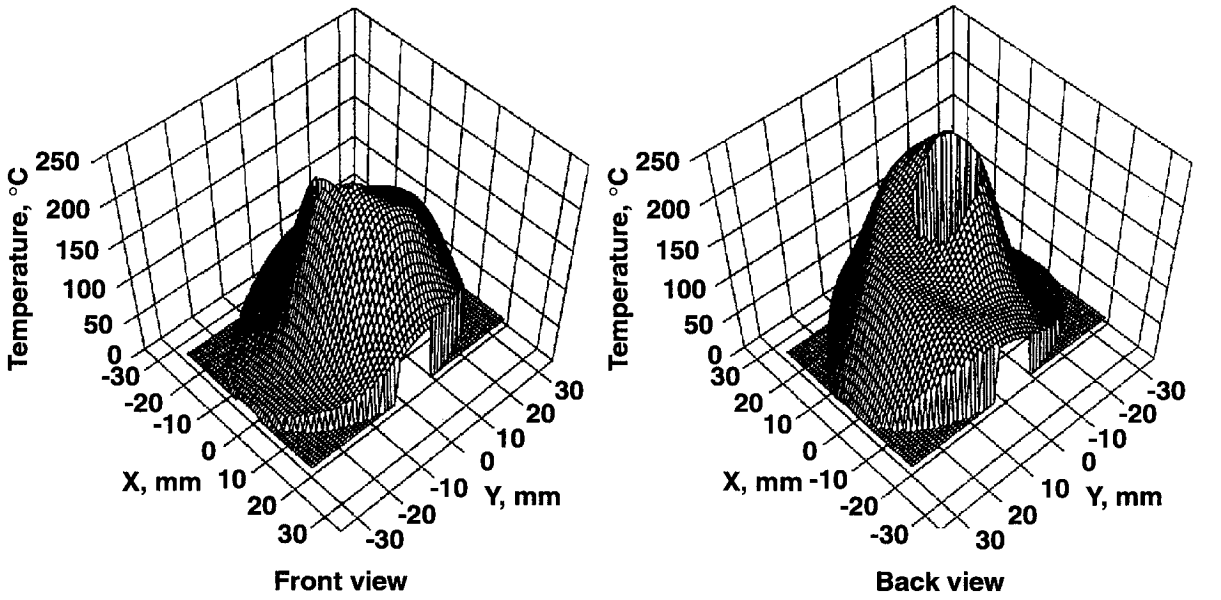

Figure 63. Reconstructed cross section of the temperature field just below the thermocouple rake.

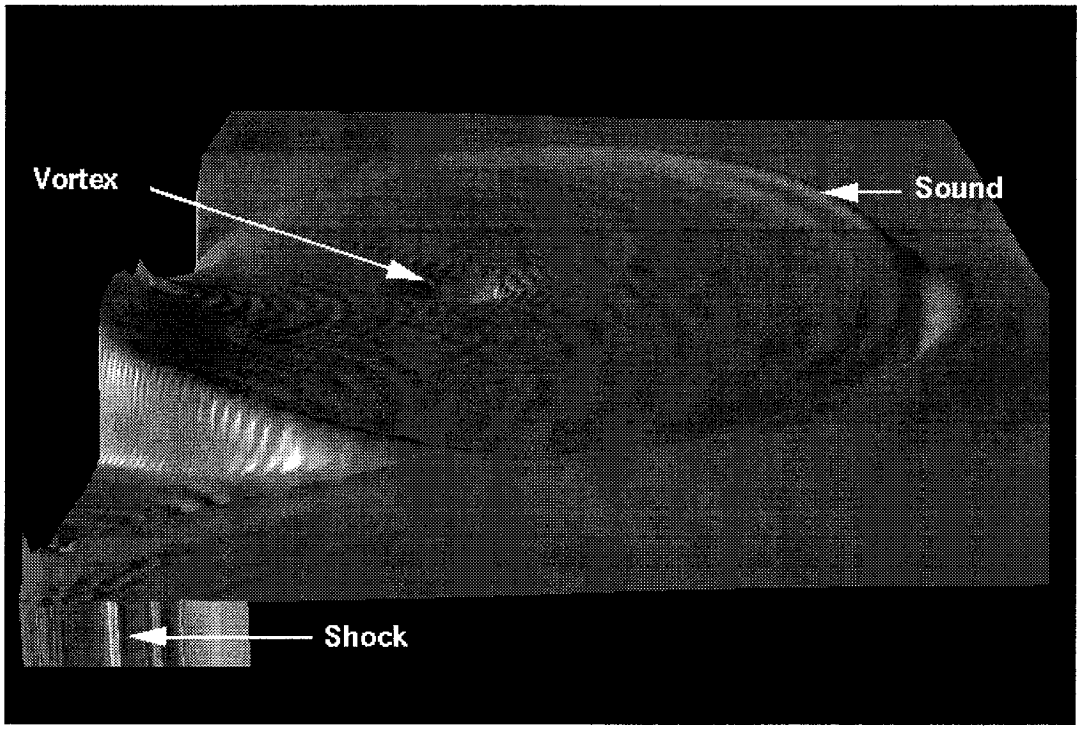

Figure 64. Sound generation by shock vortex interaction.

scheme. The governing equations are the Euler equations of gas dynamics which are solved in an axisymmetric coordinate system. The system is solved in a time-dependent fashion so that acoustic fluctuations are accurately simulated. A snapshot of the disturbance pressure field downstream of the shock is shown in figure 64. The photograph shows that a cylindrical pressure disturbance forms downstream of the shock wave after the vortex passes through the shock. Analysis shows that this disturbance is an acoustic wave which spreads cylindrically to the far field.

The numerically simulated sound pressure is found to vary as the fourth power of $\sqrt{M^2-1}$, a measure of shock strength. This numerical result is consistent with experimental measurements of shock noise in supersonic jets, and implies that significant reduction in shock noise can be accomplished by moderately reducing shock strength. **(K. R. Meadows, 757-864-3624)**

An Efficient Far-Field Quadrupole Noise Prediction

Algorithms and noise prediction codes are needed to predict transonic rotor noise generated by helicopter and tiltrotor vehicles. The quadrupole source term is an important source when the flow field around a rotor is transonic, but unlike the thickness and loading sources, the quadrupole is a volume source. Since volume integration requires orders of magnitude more computational resources than surface integration, a far-field approximation to the integration geometry is utilized in this work to effectively reduce the volume integration of the quadrupole to a surface integration. The quadrupole source strength is computed exactly.

In a new version of WOPWOP (known as WOPWOP+) the quadrupole computation is carried out in two parts: (1) a preprocessing stage which reads in the flow-field solution (from computational fluid dynamics) and computes the source strength, and (2) an

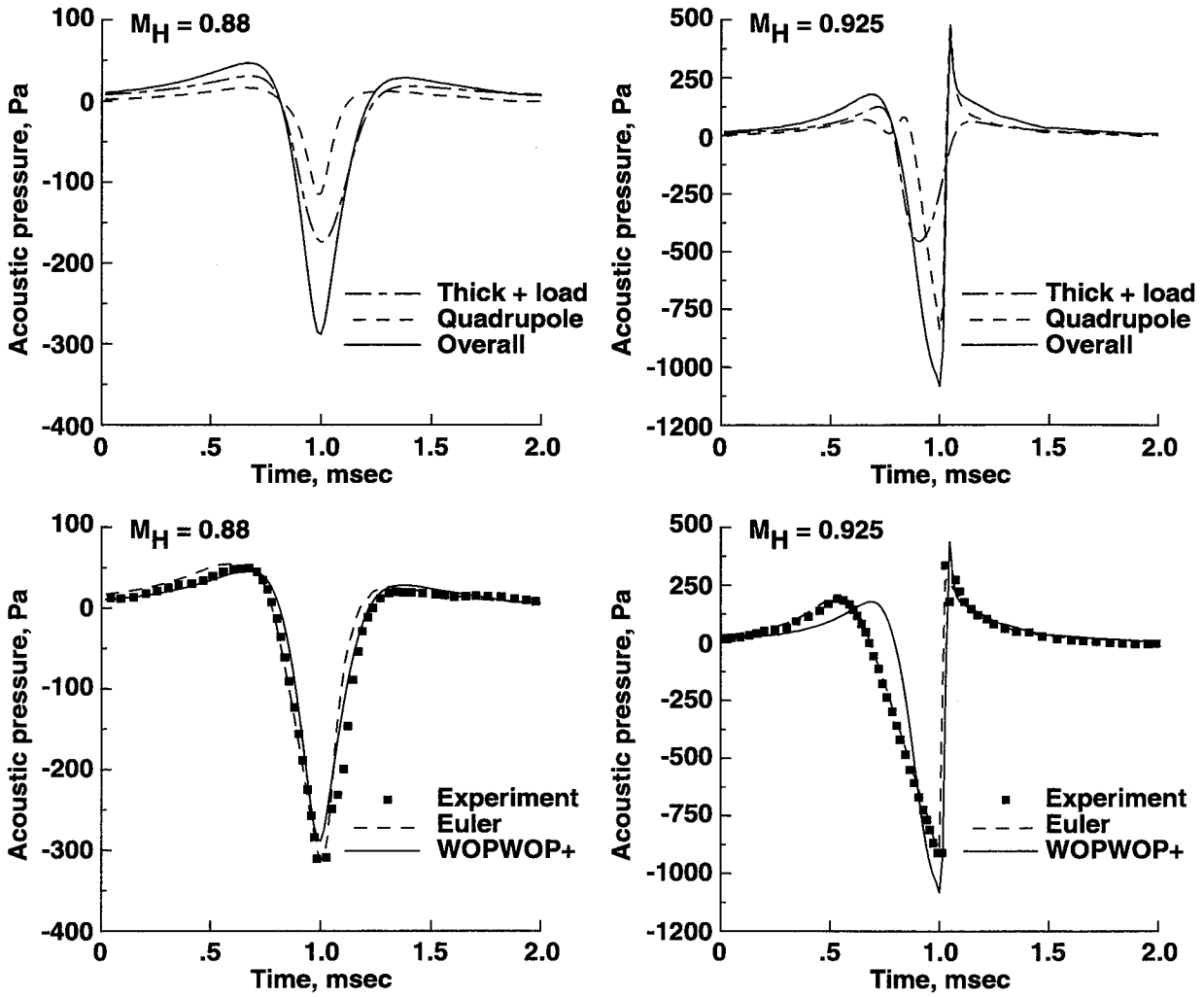

Figure 65. Predicted noise components compared with experiment and Euler calculations at two operating conditions for an untwisted, unloaded UH-1H model rotor.

acoustic calculation of the quadrupole noise. Figure 65 shows a comparison of the predicted acoustic pressure time history for an untwisted, unloaded, hovering UH-1H model rotor. The method predicts the amplitude of the signal for all of the cases and agrees very well with both experiment and a special purpose Euler calculation for hover Mach numbers, $M_H \leq 0.9$. However, it does not capture the complete waveform shape of the higher Mach number data because of the current restriction to subsonic-transonic flow integrations.

The WOPWOP+ code predicts transonic rotor noise without a large increase of computational resources over existing methods for thickness and loading effects. Direct Euler calculations are not feasible in general because the grid size and computation time for far-field observer locations would be impractical. Due to its simplicity and efficiency, this method will also be the core of a future code which will be able to integrate supersonically moving quadrupole source panels.
(K. S. Brentner, 757-864-3630)

Validation of an Unstructured Turbulent Flow Solver

This study provides a systematic assessment of the accuracy and behavior of an unstructured tetrahedral cell-centered Navier-Stokes flow solver for computing shock-induced separated flow on a wing under high Reynolds number, transonic flow conditions. The flow solver, know as USM3D, incorporates a Spalart-Allmaras one-equation turbulence model, which is coupled with a wall function. The wall function reduces the need, and hence the cost, to grid-resolve the inner portion of the turbulent boundary layer (BL) by modeling that region analytically. A series of thin-layer tetrahedral grids were generated on the ONERA M6 wing by the VGRID unstructured grid generator with sizes ranging from 324356 tetrahedral cells where the midchord (BL) is resolved by 12 tetrahedra, to 463968 cells with 30 tetrahedra resolving the BL.

Solutions were computed at an angle of attack of 5.06°, Mach number of 0.84, and Reynolds number of 11.7×10^6. The results depicted in figure 66 were computed on grids with a first-node spacing which yields a nominal y^+ of 70. The oil-flow patterns, obtained on a grid with 18 tetrahedra across the BL, reflect significant shock-induced separated flow in the outboard region of the wing. Chordwise distributions of pressure coefficient C_p are shown for two spanwise stations at 65- and 90-percent fractional semispan for 12, 18, and 30 tetrahedra across the BL. Good agreement is achieved with each case. Run times on a Cray C-90 ranged from 3 hr for the coarsest grid to 12 hr for the finer one. **(N. T. Frink, 757-864-2864)**

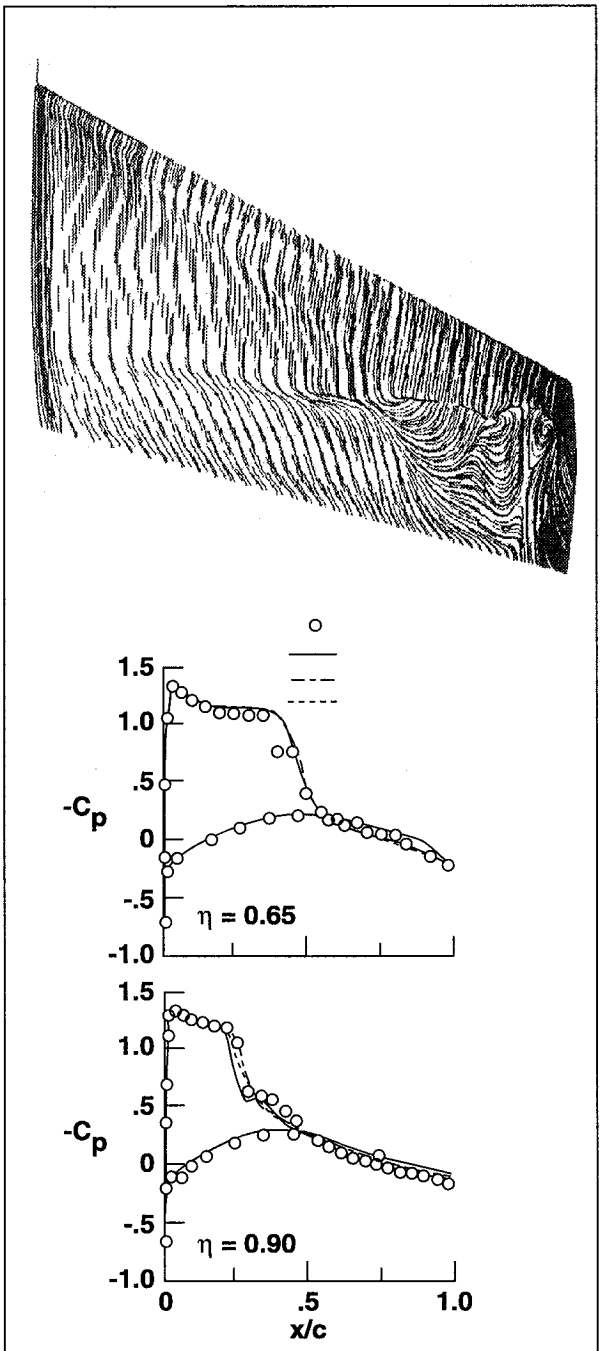

Figure 66. Surface flow patterns and effect of normal grid density on C_p distributions for ONERA M6 wing.

Generation of Unstructured Viscous Grids on Complex Configurations

An automatic method for the generation of thin-layered tetrahedral grids, suitable for viscous flow computations, has been developed and successfully demonstrated under contract with ViGYAN, Inc. The procedure, encompassed in a computer program (VGRIDns), is based on the Advancing Layers Method (ALM) for the generation of thin cells in the viscous flow regions and the Advancing Front Method (AFM) for generating regular Euler grids outside the boundary layer.

A crucial issue concerning the use of tetrahedral viscous grids has been the relatively large size of the generated grids on complex geometries. A new technique of multidirectional grid stretching has recently been developed to improve the efficiency of the grids. With such a capability, fewer points are clustered in the

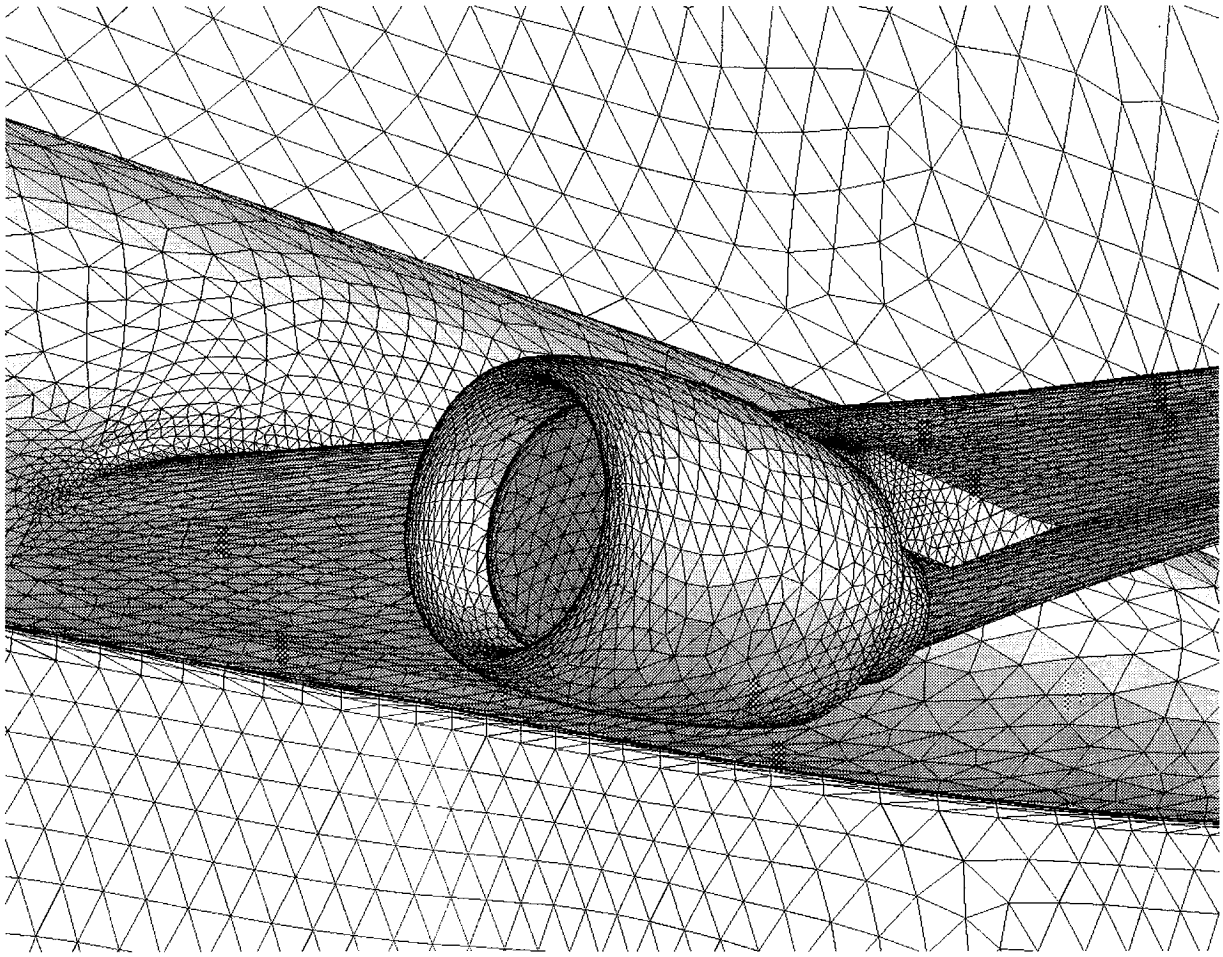

Figure 67. An unstructured viscous grid with anisotropic stretching around a subsonic transport configuration.

directions of reduced flow gradient without losing the grid resolution in other essential directions. The result is a substantial reduction in the number of grid points and cells.

To demonstrate the capability of the method, a viscous grid around a subsonic transport configuration is presented. The surface mesh (shown in fig. 67) is stretched along the fuselage, the wingspan, and around the nacelle cowl. The volume grid (not shown) is also stretched in the appropriate directions. The thin layers of viscous grid are shown on the symmetry and the engine-in flow planes. This grid contains 170258 points and 962817 tetrahedral cells. A corresponding unstretched grid, with the anisotropic stretchings deactivated, has also been generated which contains 403115 points and 2239708 cells. The example shows the effectiveness of multidirectional grid stretching in generating economical tetrahedral viscous grids. **(N. T. Frink, 757-864-2864)**

Simultaneous Aerodynamic Analysis and Design Optimization

Simultaneous Aerodynamic Analysis and Design Optimization (SAADO) is a technique that incorporates design improvement into aerodynamic analysis in order to gain computational efficiency. SAADO was developed jointly under grant with the Old Dominion University and ICASE. The present 2-D form of SAADO for a thin-layer Navier-Stokes code considers both airfoil-shape and flow-field variables as

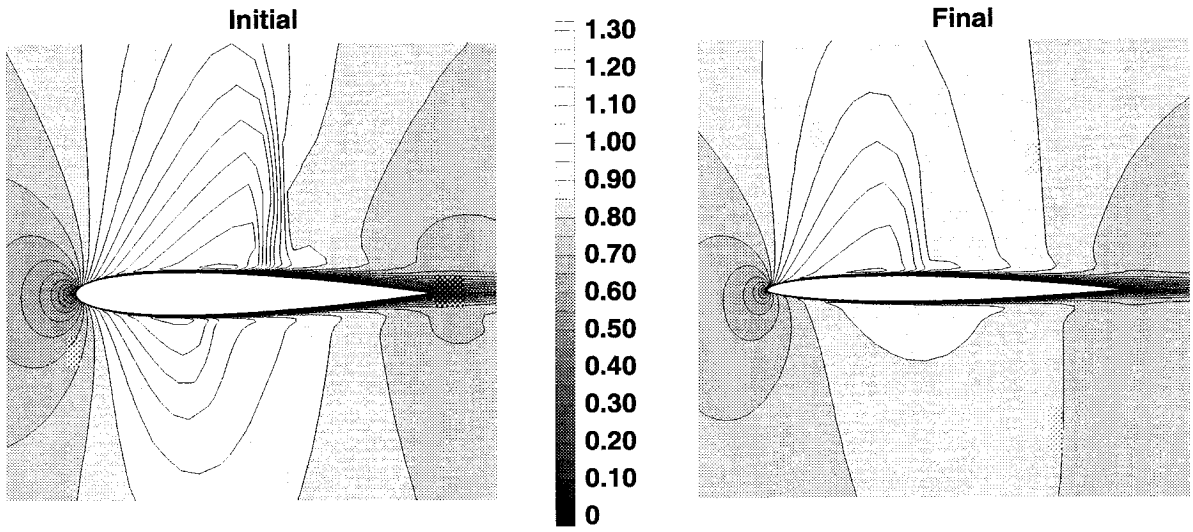

Figure 68. Airfoil shape and Mach number contour plots.

independent (design) variables and treats the flow equations as equality constraints. This large number of variables and constraints is reduced by solving a set of inexact sensitivity equations. These equations and the flow analysis are solved together in incremental iterative form. The automatic differentiation tool ADIFOR is applied to generate the required aerodynamic and grid sensitivity equations. The design optimization problem is to maximize the lift-to-drag ratio (C_l/C_d) of an airfoil in transonic turbulent flow, subject to 25 geometric constraints: 20 on surface curvature, imposed from the leading edge to 5-percent chord, and 5 on the airfoil thickness, imposed from 20- to 60-percent chord to approximate the structural wing box. Airfoil upper and lower profiles are each represented by a linear combination of 4 orthonormalized polynomials; initial values of these 8 polynomial weighting coefficients, the shape design variables, are those for the NACA 0012 airfoil.

Figure 68 shows airfoil shapes and Mach number contours for the initial and final airfoils. In 18 SAADO cycles (design variable updates), the flow analysis convergence level was reduced from 10^{-2} to 10^{-6}, producing an airfoil with about 500-percent improvement in the objective function. Two thickness constraints, those at 20- and 60-percent chord, were active. These results also show the shock wave on the lower surface of the airfoil has been eliminated while on the upper surface has been weakened considerably. The computational time required for this SAADO case is about the same as 22 flow analyses converged to 10^{-6} relative residual error on this 127×33 grid.

(P. A. Newman, 757-864-2247)

Improved Boundary Conditions for Computation of External Flows

While numerically solving a problem initially formulated on an unbounded domain, one typically truncates this domain, which necessitates setting the artificial boundary conditions (ABC's) at the computational boundary. The issue of setting the ABC's is significant in many areas of scientific computing. In computational fluid dynamics, for example, external problems represent a wide class of practical applications where the proper treatment of external boundaries has a profound impact on the overall quality and performance of numerical algorithms.

Most of the currently used techniques for setting the ABC's can basically be classified into two groups. The methods from the first group (global ABC's) usually provide for high accuracy and robustness of the numerical procedure but are relatively cumbersome and expensive. The methods from the second group (local ABC's) are, as a rule, algorithmically simple, numerically cheap, and geometrically universal; however, they usually lack accuracy in computations. In

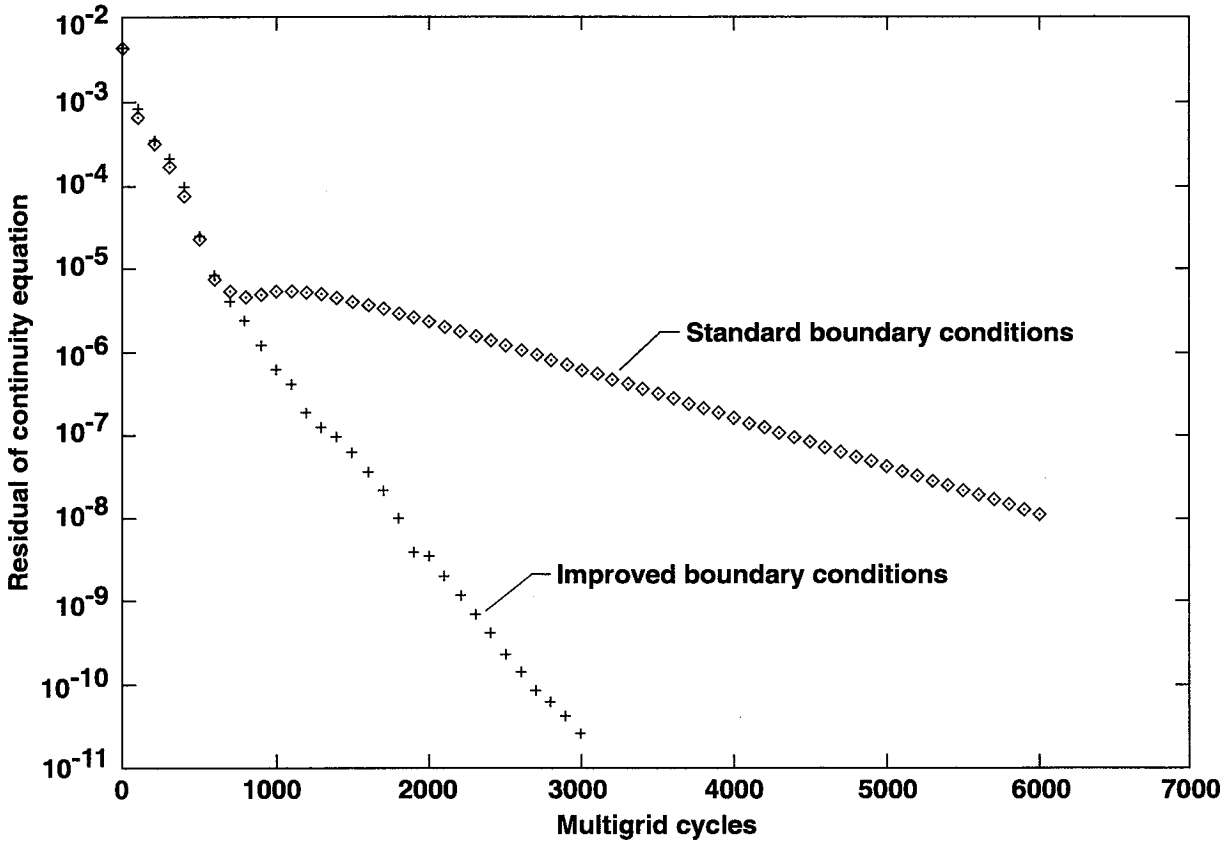

Figure 69. Convergence history—logarithm of the continuity equation residual in the maximum norm $\log \|\rho_{residual}\| L_\infty$ *versus number of cycles for the NACA 0012 airfoil;* $M_\infty = 0.63$; $\alpha = 2°$; $Re = 5000$; *grid, 256 × 64; average radius of computational domain is about 6 airfoil chords.*

this work, the new ABC's technique (*SIAM J. Numer. Anal.*, 32 (1995) pp. 1355–1389; *J. Comput. Phys.*, 116 (1995) pp. 212–225; *AIAA J.*, 34 (1996) pp. 700–706; *Appl. Numer. Math.*, 18 (1995) pp. 489–501) combines the advantages relevant to the methods of both types. The technique is based on application of the difference potentials method attributable to V. S. Ryaben'kii. This approach enables us to obtain highly accurate ABC's in the form of certain pseudodifferential boundary equations (analogous to Calderon's equations). The operators involved are analogous to the pseudodifferential boundary projections introduced by A. P. Calderon.

The improved ABC's were implemented numerically along with a multigrid solver for calculating two-dimensional steady-state external compressible viscous flows. The investigated regimes range from the low (incompressible limit) to transonic Mach numbers, and include laminar, as well as turbulent, flows. In all cases, the DPM-based ABC's clearly outperform the standard methods based on the local analysis of characteristics from the standpoints of convergence rate (as shown in fig. 69), accuracy, and robustness.

The methodology extends to three-dimensional flows, although it involves many new issues of the computational geometry type. Moreover, the methodology has been extended to the construction of ABC's for a particular class of time-dependent flows, specifically, the flows that oscillate in time (NASA TM-4714). The case of the general time-dependent problems remains a major challenge for future research. This work was conducted at NASA Langley Research Center under the auspices of the National Research Council Resident Research Associateship Program. **(R. C. Swanson, 757-864-2235)**

Simulating Shock-Induced Sound

The numerical study of aeroacoustic problems places stringent demands on the choice of a computational algorithm because it requires the ability to propagate disturbances of small amplitude and short wavelength. The demands are particularly high when shock waves are involved because the chosen algorithm must also resolve discontinuities in the solution. The extent to which a high-order-accurate shock-capturing method can be relied upon for aeroacoustics applications that involve the interaction of shocks with other waves has not been previously quantified. Figure 70 shows that the design accuracy of available shock-capturing schemes are not realized in such simulations. This work was done in cooperation with the Old Dominion University.

A variety of numerical algorithms, including a fourth-order-accurate essentially nonoscillatory (ENO) method, are used to investigate the solutions of inviscid, compressible flows with shocks in a quasi-one-dimensional nozzle flow. In all cases, the design order of accuracy is achieved in the smooth regions of a steady-state test case. However, in an unsteady test case, only first-order results are obtained downstream of a sound-shock interaction. The general application of a high-order accurate shock-capturing scheme is insufficient to guarantee a correspondingly accurate solution downstream of the shock.

If subcell resolution techniques are incorporated into the existing numerical algorithms, then a globally high-order accurate solution is obtained. Unfortunately, the subcell resolution technique is prohibitive in terms of cost and complexity, making its extension to multiple spatial dimensions unrealistic. These observations raise considerable concern in regard to the use of high-order-accurate methods in the study of unsteady flows with shocks. The challenge is to construct more efficient alternative numerical schemes which will recover design accuracy in flows with shocks for time-dependent applications such as off-design aircraft performance and noise reduction. **(M. H. Carpenter, 757-864-2318)**

Three-Dimensional Unstructured-Grid Navier-Stokes Solver

In recent years, much work has gone toward the development of both compressible and incompressible flow solvers suitable for calculating turbulent flows on unstructured grids. The strength of these algorithms has been in the wide variety of complex geometries that can be handled easily. The two-dimensional versions of

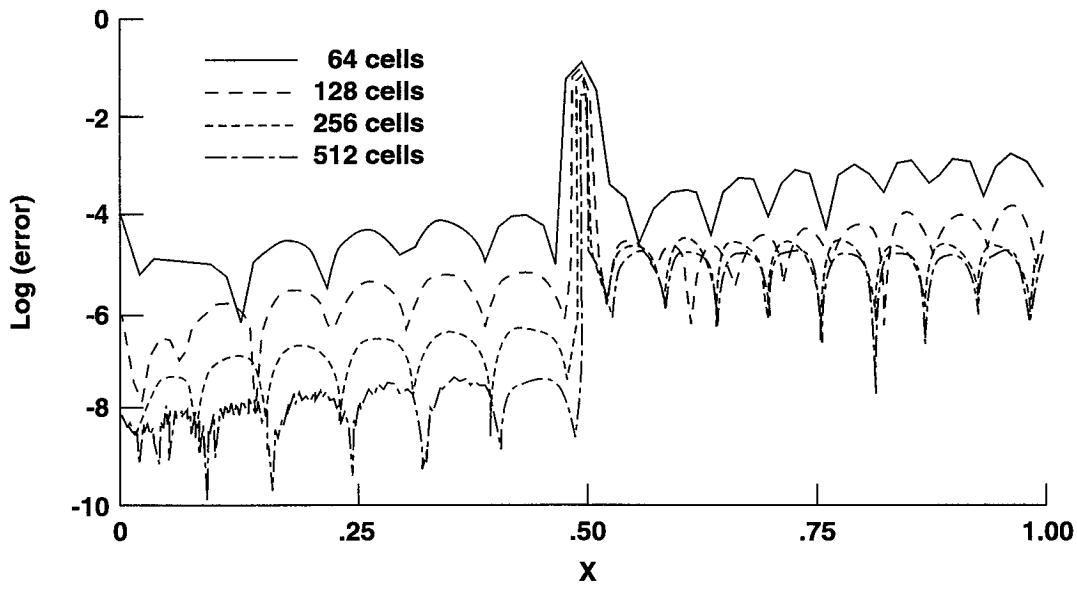

Figure 70. Pointwise error versus distance for the sound-shock interaction test case using the fourth-order ENO scheme. Design accuracy is achieved only upstream of the shock (X = 0.5).

these codes have been used extensively by a broad range of researchers in government, industry, and academia.

An efficient scheme has been developed for three-dimensional viscous flow by combining matrix solution techniques based on Krylov approximations with upwind-differenced algorithms for the convective and pressure terms of the residual equations. The three-dimensional version is now being used in several project areas to provide insight into flow physics, to provide guidance for planning experiments, and to gain valuable experience necessary for validation of the codes.

Figure 71 shows a computational simulation of a wing with a partial-span flap for a configuration tested at the NASA Ames Research Center in support of the airframe noise reduction program. The pressure contours are shown on the surface and filaments representing streamlines are shown as they traverse the wing flow field. Although the results shown below are only qualitative, quantitative results comparing the computed and experimental pressure distributions have been made, and the agreement is good (AIAA-95-1740, San Diego, California, 1995). The method is being used to provide information for the modeling, prediction, and control of sound sources of aircraft noise associated with the interaction of vortices over the flap side edge. **(W. K. Anderson, 757-864-2164)**

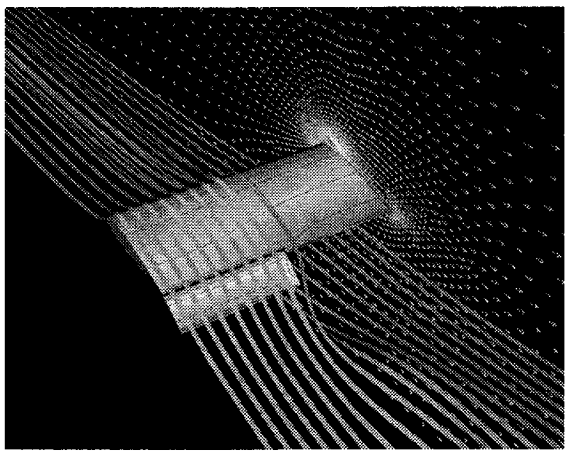

Figure 71. Three-dimensional low-speed flow past a part-span flap configuration showing pressure contours on the surface, velocity vectors in the plane of symmetry, and streamline filaments as they traverse the wing.

Implicit Method for Computation of Unsteady Flows on Unstructured Grids

For unsteady flow computations past bodies in relative motion, it is desirable to develop methods in which the time step is solely determined by the flow physics. An implicit method for the computation of unsteady flows on unstructured grids has been developed. The algorithm solves a large nonlinear system of equations at each time step by using an agglomeration multigrid procedure in which a sequence of coarse grids is generated using efficient graph-based algorithms.

The method allows for arbitrarily large time steps and is efficient in terms of computational effort and storage. Inviscid and viscous unsteady flows have been computed to validate the procedure. The present formulation allows the mass matrix, which arises with vertex-centered finite-volume schemes, to be inverted indirectly. This feature may be relaxed for further efficiency if the spatial accuracy of the scheme is second order or less.

A mesh point movement and reconnection procedure has been developed that allows the grids to evolve with the motion of bodies. The technique utilizes a spring analogy followed by a reconnection strategy to improve grid quality. A linearity-preserving, conservative interpolation has been developed to transfer information to the new grid.

As an example of flow over bodies in relative motion, the flow over a multielement airfoil system undergoing deployment is computed (AIAA Paper 95-1705-CP, San Diego, California, 1995). A steady state solution is computed at the initial flap setting of 15°. The unsteady flow resulting from a full deployment to 40° is computed in 200 time steps. The time-accurate solution is computed for another 50 time steps after the high-lift system reaches its final configuration. As the configuration changes, the grid is restructured by employing a spring analogy and reconnection algorithm. Figure 72 depicts a closeup of the grid in the flap region and the instantaneous flow solution at full deployment at a nondimensional time of 400. This work was performed under contract by the Institute for Computer Applications in Science and Engineering.
(W. K. Anderson, 757-864-2164)

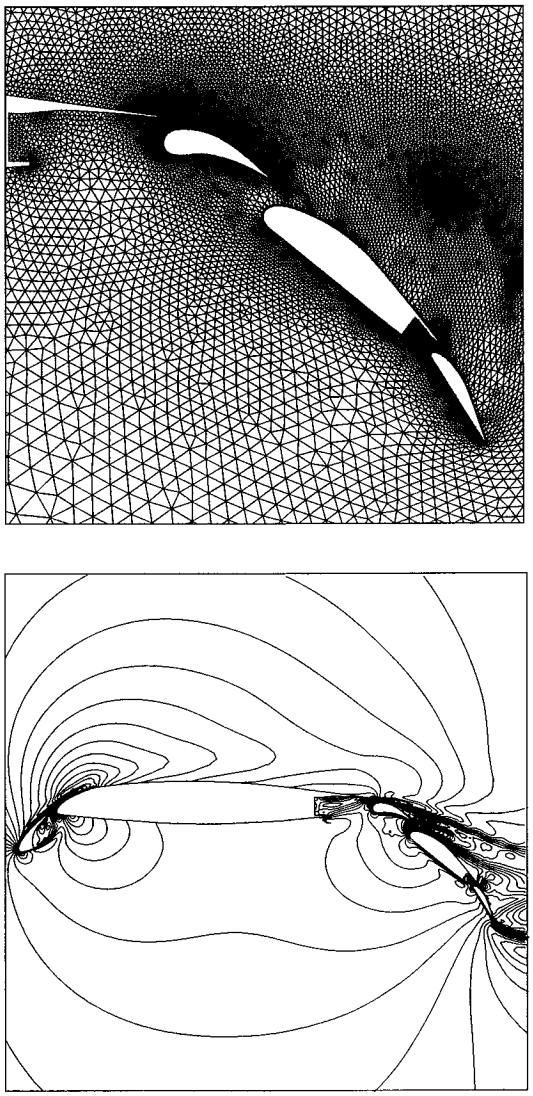

Figure 72. Closeup view of the grid at full deployment (40° flap deflection) (top) and Mach contours of the instantaneous solution at full deployment (bottom).

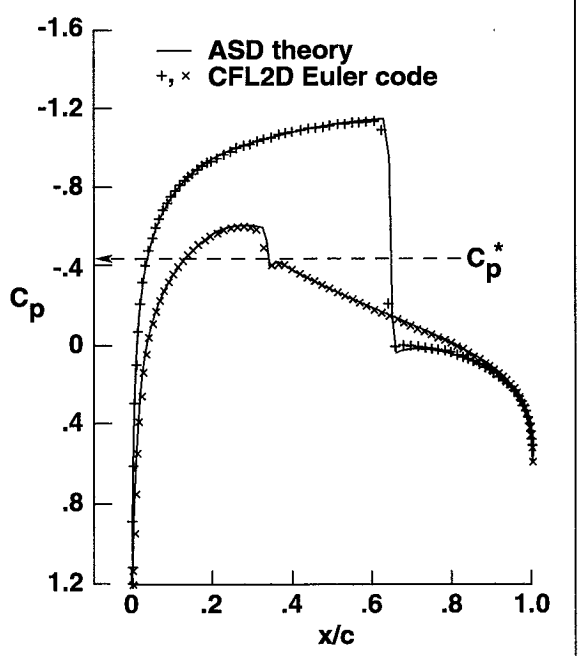

Figure 73. Comparison of NACA 0012 pressure coefficient distributions.

Advanced Small-Disturbance Theory Developed for Transonic Aerodynamic Analysis

Classical transonic small-disturbance (TSD) theory is the lowest-order mathematical approach that can model transonic aerodynamic effects such as shock waves. The TSD theory is especially attractive for unsteady aerodynamic and aeroelastic applications because of the numerous transient calculations that are required to make transonic flutter prediction. Oftentimes however, TSD calculations for practical cases are not quantitatively accurate, because the approximations that are normally used to derive the theory are overly restrictive. Therefore, an advanced small-disturbance (ASD) theory was derived to alleviate or eliminate these approximations. The ASD theory involves a modified streamwise flux in the governing equation which is exact for stagnation, free-stream, and sonic conditions. It accounts for entropy and vorticity effects by incorporating the normal shock jump relations and by modifying the streamwise velocity component for rotationality. The ASD theory further involves a higher-order mass-flux surface boundary condition which is consistent with the governing equation. Calculations were performed with the ASD approach to investigate its accuracy for a NACA 0012 airfoil at a free-stream Mach number of 0.8 and an angle of attack of 1.25°. Comparison of the resulting pressure coefficient (C_p) distributions, as a function of the fractional chord (x/c), that are shown in figure 73 indicate good agreement with results from the CFL2D Euler code.

(J. T. Batina, 757-864-2268)

Optical Angle-of-Attack Measurements

Inertial sensors are commonly used to measure angle of attack (AOA) in wind-tunnel models and are the instrument of choice when vibrations are not significant. However, inertial sensors require special handling due to their fragile nature and require wiring and space inside the model. In addition, inertial sensors cannot distinguish between the gravitational acceleration and centrifugal accelerations associated with wind-tunnel model system vibration which can result in a bias error in AOA. This potential bias error is inherent in the device and is not easily correctable without additional instrumentation and measurements. For these reasons investigations have been conducted at several facilities with a video AOA system developed at NASA Langley which is completely nonintrusive and requires no instrumentation in the model or test section.

Dynamic and static optical AOA measurements have been recently made at the 20-Inch Mach 6 CF_4 tunnel. Before testing, an accelerometer external to the model was used to establish wind-off pitch angle. The video technique was then used to determine the change in AOA of the model due to aerodynamic loading with wind on. The dynamic measurements made at the facility are useful for comparing the effects of different model injection rates. The static measurements are useful to assess sting bending under aerodynamic load. Figure 74 shows sting bending due to aerodynamic load as a function of AOA for slow and medium speed model injection rates. For comparison, wind-off data are also presented on the plot.

(A. W. Burner, 757-864-4635)

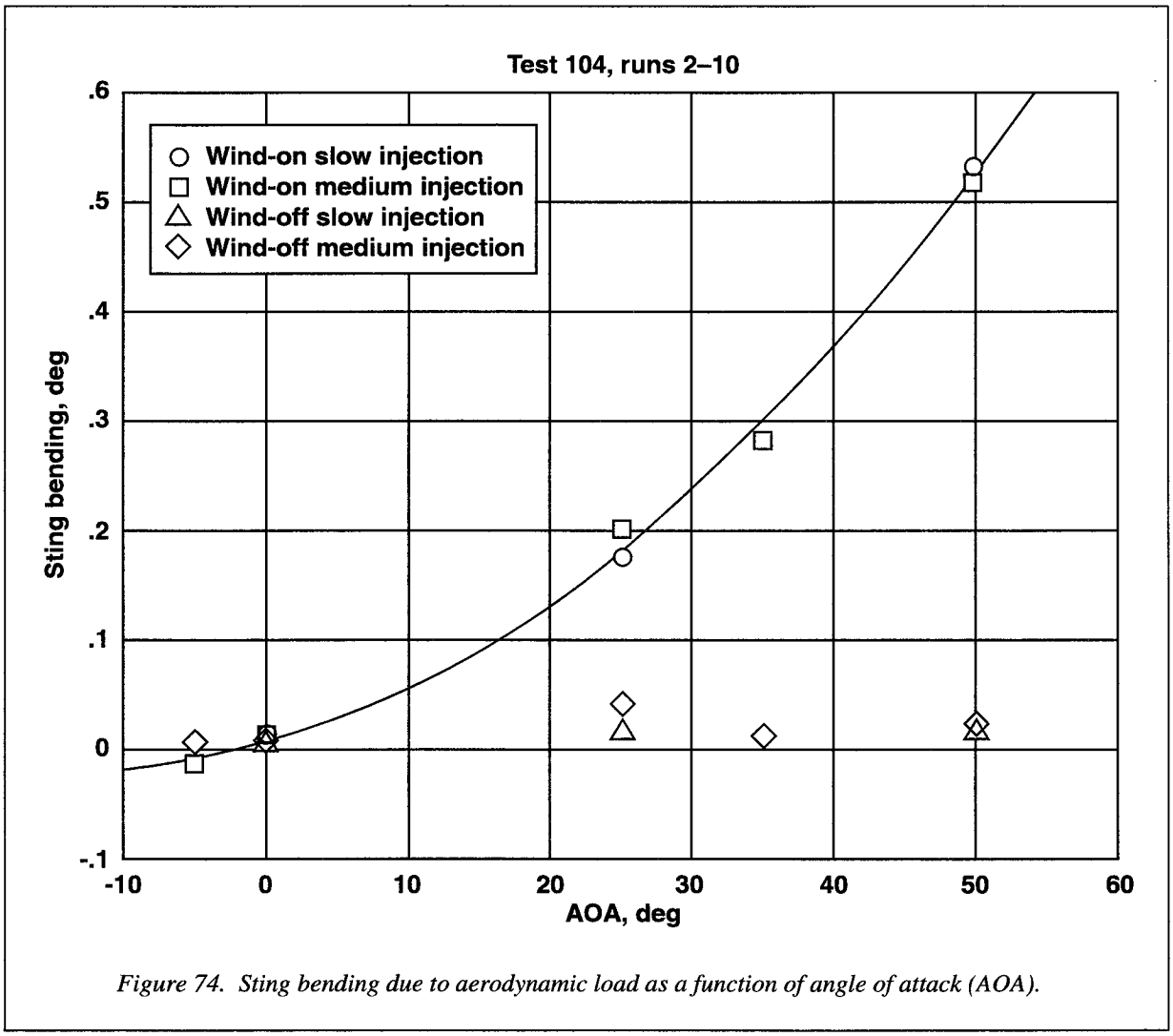

Figure 74. Sting bending due to aerodynamic load as a function of angle of attack (AOA).

Decomposing and Scheduling Multidisciplinary Design Project

Many engineering systems are large and multidisciplinary, and require a complex design cycle. Before a design cycle begins, the possible couplings among the design processes must be determined. Once this has been completed, a design cycle can be decomposed to identify its multilevel structure. Determining this scheduling is not easy, and often important couplings are overlooked. The purpose of this project is to develop a software tool to aid the design manager in making early design decisions and produce a more optimal design at less cost in less time.

The Design Manager's Aid for Intelligent Decomposition (DeMAID) was developed to aid the design manager in scheduling and decomposing large, complex, multidisciplinary design projects. DeMAID schedules the design processes, groups iterative subcycles, and displays them in a design structure matrix format. (See fig. 75.)

DeMAID was first released in 1989. Based on feedback and surveys from DeMAID customers, numerous enhancements have been added to meet their needs. Some of these enhancements include quantifying coupling strengths, identifying processes which can be performed in parallel, interfacing with existing programs, more detailed output values, and user-friendly aids such as pull-down menus. Other enhancements allow design managers to quickly examine different sequences for scheduling the design processes, optimize iterative subcycles, trace the effects of design changes, and examine possible trade-offs with respect to cost and time.

The number of DeMAID customers has grown to 23. DeMAID is being applied to a wide variety of projects, is being contemplated for use with the large airplane project at Boeing, and has been incorporated into a graduate design course at Georgia Tech. DeMAID won an honorable mention in NASA's 1995 Software of the Year Award competition.

(J. L. Rogers, 757-864-2810)

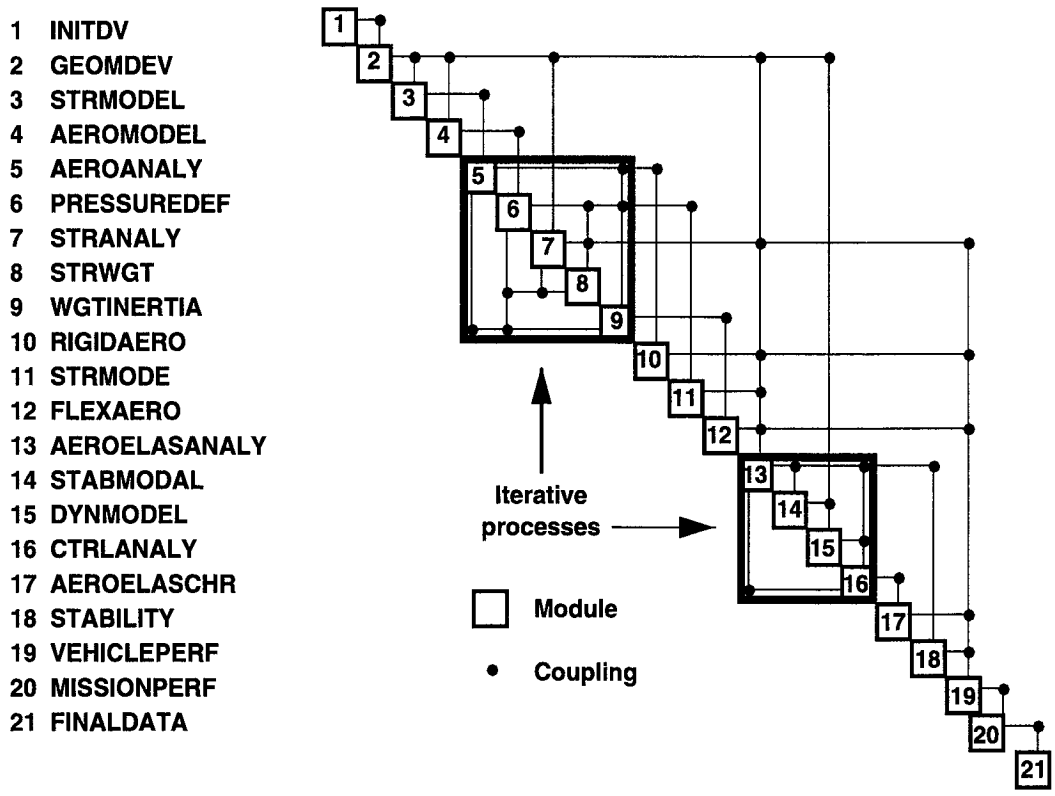

Figure 75. A design structure matrix for a conceptual design project.

Michelin Advanced Radial Aircraft Tire Mechanical Properties Measured

The objective of this program was to perform research on and define the mechanical properties of advanced radial aircraft tires under a Space Act Agreement (SAA) with Michelin Aircraft Tire Corporation. Various tire properties including relaxation length and spring characteristics are of great concern to the aerospace industry as the tire is the conduit between ground forces and the airplane structure. The proprietary Space Act Agreement required testing at the Langley Aircraft Landing Dynamics Facility (ALDF) using the research test carriage in a quasi-static mode. The extremely high tire loads requested required that concrete weights be placed on the drop carriage portion of the test carriage. A 15-ft-long built-up runway was fabricated in the carriage hangar capable of withstanding 60 tons of vertical load combined with 40 tons of side load. A "frictionless platform," which allows side loads to be induced into the test tire, was modified and installed as an integral part of the built-up runway all within the confines of the carriage hangar. Generally, three types of tests were required: yawed and unyawed relaxation length, and static lateral and fore/aft breakaway tests. Relaxation length refers to how far the tire must roll before step-changes in conditions can be fully observed. The breakaway tests define not only the friction values achieved by the tire but also the spring characteristics of the tire as well as the movement of the center of pressure in the tire footprint as shown in figure 76. Eight breakaway and 8 unyawed relaxation tests were completed, as well as 35 yawed relaxation length tests. The test matrix contained vertical load and yaw angle combinations that encompass the full range of tire conditions one would expect on the newest commercial transport aircraft or on the high-speed civil transport (HSCT). These data will be used by Michelin in the design and certification of advanced radial tires for large commercial aircraft and the HSCT.

(R. H. Daugherty, 757-864-1309)

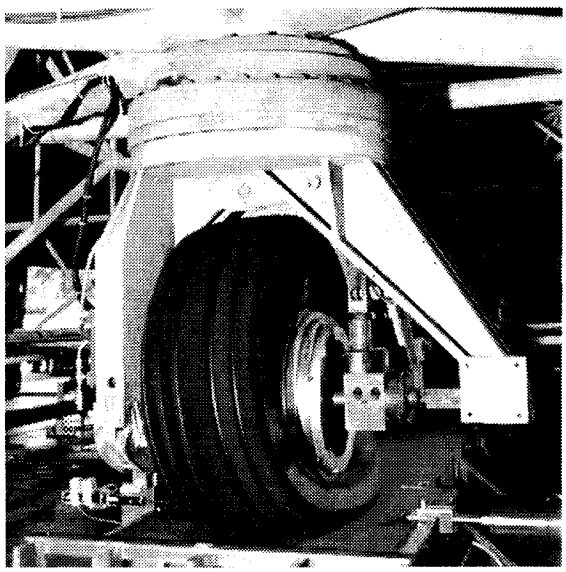

Figure 76. The advanced radial tire undergoes lateral deflection during a breakaway test.

High-Speed Civil Transport Dynamic Simulations Define Need for Vibration Suppression

The high-speed civil transport (HSCT) has been identified as a means to expand the role of the United States as the leader in aerospace well into the 21st century. However, the unique configuration of the aircraft and its operational requirements present numerous technical challenges. The HSCT has a long, narrow flexible fuselage. That, in conjunction with the relatively long distance from the forward gear to the cockpit, can result in excessive vibration levels in the cockpit and cabin. Computer simulations of the HSCT have been conducted to study the HSCT ground vibration levels during takeoff, landing, and taxiing; and to define the extent of the need for active or semiactive landing gear control systems for vibration control.

A model of the aircraft was constructed by combining the symmetric and antisymmetric fuselage modes. The landing gear was incorporated into the model as external nonlinear forces and a simulated runway profile was used as input to the simulation. Preliminary nonlinear dynamic simulations of the HSCT during taxiing operations at a speed of 30 mph on the runway have been conducted. Figure 77 shows a sketch of the aircraft with locations along the fuselage labeled 1–27 and wing locations denoted 28 and 29. Corresponding displacement amplification factors are shown, with the vertical displacement response at various locations computed and normalized with respect to the mean value of runway vertical height. These results showed unacceptable vibration levels at the cockpit location and suggest the need for vibration suppression mechanisms on the aircraft. **(M. C. Reaves, 757-864-1306)**

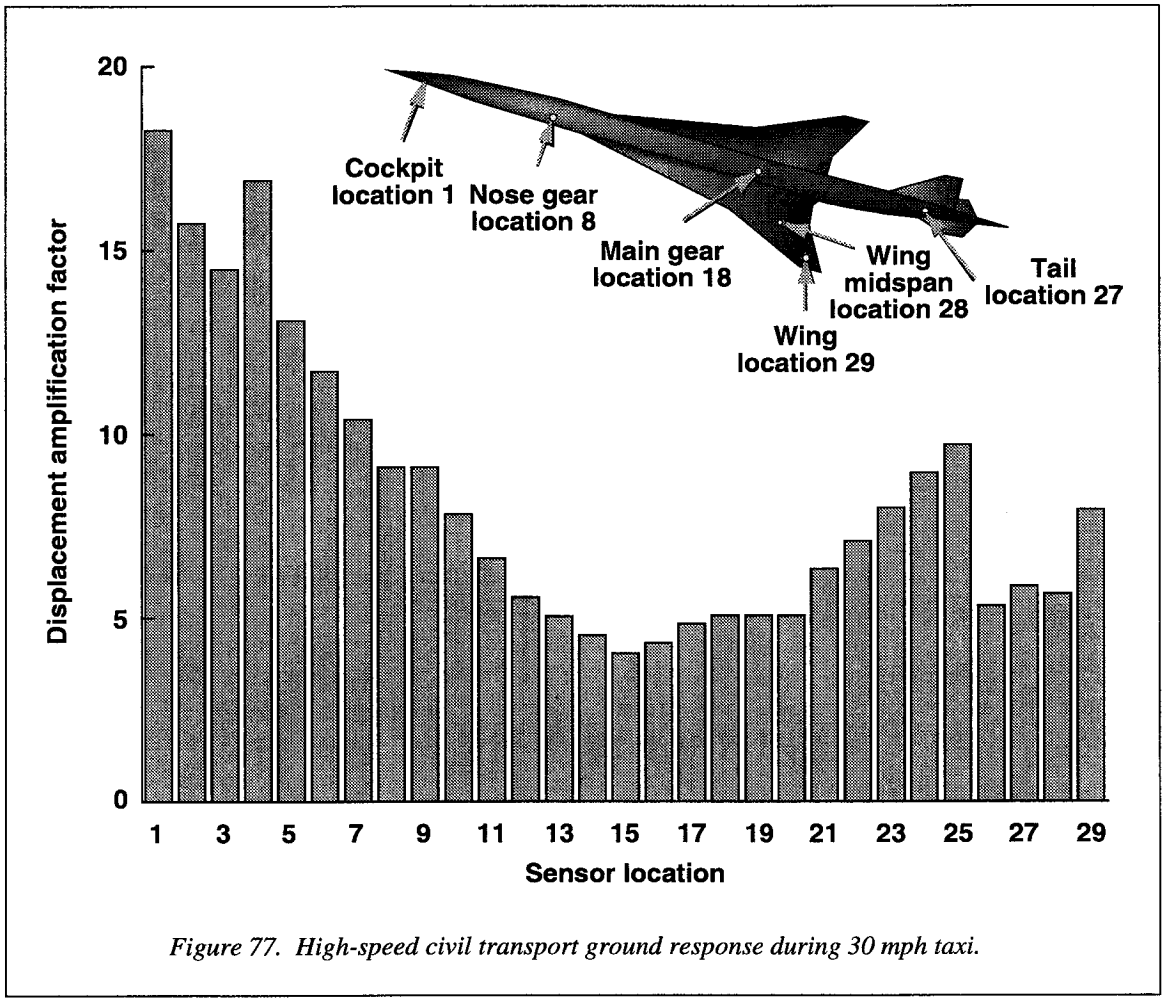

Figure 77. High-speed civil transport ground response during 30 mph taxi.

Microstructural Characterization of Semi-Interpenetrating Polymer Networks by Positron Lifetime Spectroscopy

Thermoset and thermoplastic polyimides have complementary physical/mechanical properties, whereas thermoset polyimides are brittle and generally easier to process; thermoplastic polyimides are tough but harder to process. It is expected that a combination of these two types of polyimides may help produce polymers more suitable for aerospace applications. Semi-Interpenetrating Polymer Networks (S-IPN) of selected thermoset and thermoplastic polyimides were prepared in the weight percent ratios ranging from 100:0 to 0:100. Positron lifetime measurements were made in these samples to correlate their free volume features with their physical/mechanical properties. It has been noted that the free volume goes through a minimum at 50:50 ratio, suggesting that the S-IPN samples are not

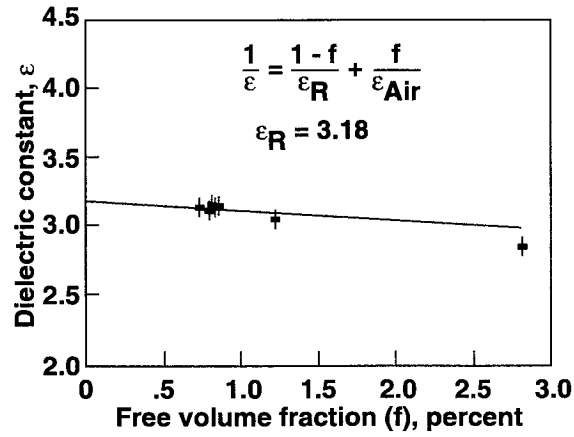

Figure 78. Dielectric constant versus free volume fraction in semi-interpenetrating polymer network samples.

merely solid solutions of the constituent polymers. The dielectric constant and the density values also exhibited nonlinear trends with the sample composition. These nonlinear features can only be explained by a combination of steric and electrostatic interactions between the constituent molecular chains. We have developed free volume models to explain this nonlinear behavior in S-IPN materials. Figure 78 shows an illustrative comparison between the experimental values of the dielectric constant and the free volume model predictions. **(J. J. Singh, 757-864-4760)**

Guidance and Control Software Project: A Software Engineering Case Study

Current software development methods and standards have been accepted primarily based on intuitive arguments or anecdotal evidence. To provide the data necessary to evaluate scientifically software processes and product quality, controlled experiments of operational software are needed. The Guidance and Control Software (GCS) project is a case study of the Requirements and Technical Concepts for Aviation RTCA/DO-178B guidelines, "Software Considerations in Airborne Systems and Equipment Certification." All civil transport airframe and equipment vendors are required to comply with these guidelines when building systems or equipment certified by the Federal Aviation Administration (FAA) for use in commercial aircraft.

In the GCS project, multiple versions of a guidance and control application, based on the terminal descent phase of the Viking Lander's mission to Mars, were developed. The DO-178B guidelines were followed during the development of two of these versions. A simulation environment was also created to evaluate operational characteristics by back-to-back testing of the software.

The GCS simulator enables multiple GCS versions to execute the same terminal descent trajectory simultaneously. The outputs are compared, as depicted in figure 79, with the assumption that no discrepancies among the outputs indicates that all versions executed that trajectory without fault. To assess performance

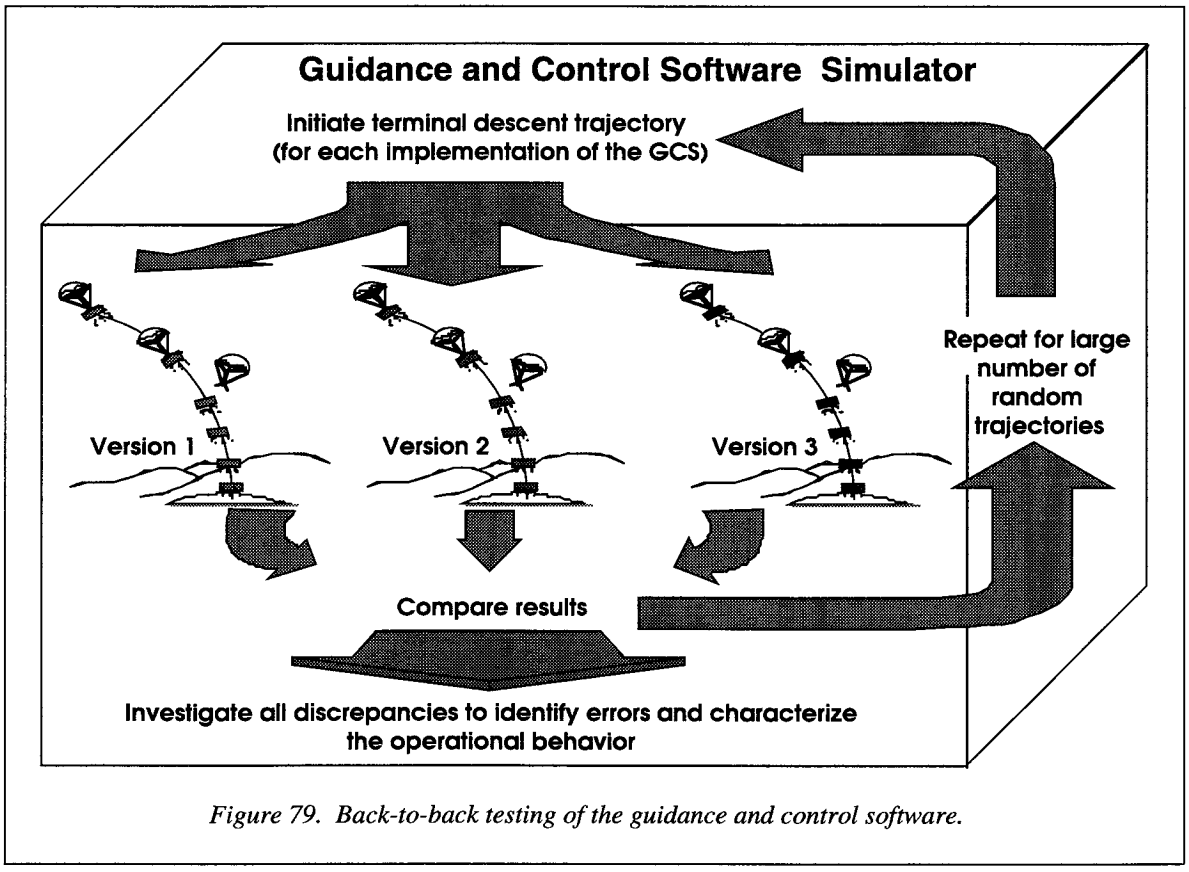

Figure 79. Back-to-back testing of the guidance and control software.

during operation, many random trajectories are run and all discrepancy data used to identify errors within each version. These data can provide insight into the effectiveness of the methods and standards used to develop those software products.

In addition to the research capability, the FAA is using the documentation and data from the GCS project to conduct software certification training for FAA Airworthiness and Certification Specialists. This training is designed to address avionics software issues arising from the application of the DO-178B guidelines. This project was funded in part by the FAA.
(K. J. Hayhurst, 757-864-6215)

Protection Shell for Enforcement of Software Safety Policies

Under a grant with the University of Virginia, a software architecture has been developed that provides a methodology for building and verifying certain aspects of the safety of large and complex software systems that are to become integral parts of safety-critical applications. The architecture provides for the enforcement of certain critical safety policies in the presence of commercial-off-the-shelf (COTS) or other software that could not otherwise assure safe operation. (See fig. 80.)

The architecture is referred to as a protection shell, and it is an analogy in the safety domain of the kernel architecture that has been used successfully to enforce security policies in security systems. The protection shell operates as an autonomous agent with a single goal of enforcing necessary safety policies. Thus, critical safety policies are enforced for the application irrespective of the actions of the remainder of the software system.

A unique feature of the approach taken in this work is that the implementation of the protection shell is synthesized from a safety policy specification. This permits considerable flexibility in the use of the shell concept because the policies enforced can be changed quickly if they are found by experience to need revision. Similarly, new policies are easily added. In addition to synthesizing the shell implementation, the tools that support this project perform analysis of the policy specification and check for a variety of potential mistakes in the specification.

A protection shell has been implemented with this approach for an experimental medical robot and integrated into the robot's software system. Extensive testing has demonstrated that the shell implements the specified policies very reliably. **(D. E. Eckhardt, Jr., 757-864-1698)**

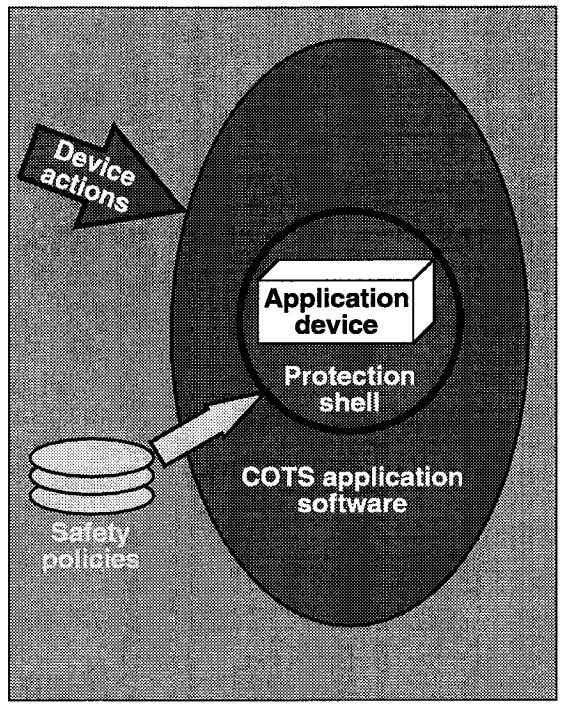

Figure 80. Software architecture for safety-critical systems.

Distributed State-Space Generation of Discrete-State Stochastic Models

The state-space exploration and generation for stochastic models is a critical step in their analysis. For large, complex models, the size of the data structures required to store the state space greatly exceeds the capability of a single workstation.

We have implemented a distributed algorithm, running on a Unix workstation network or a message-passing multiprocessor architecture, which divides the exploration work and the storage requirements over the available processors.

The distributed algorithm starts from a single initial state, and allocates states to be explored to one of the available processors according to a "partitioning

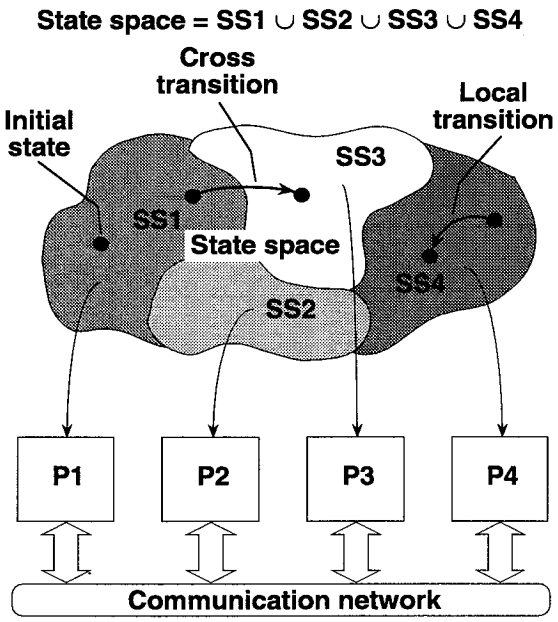

Figure 81. Distributed state-space allocation and generation divides the exploration work and data storage over multiple processors.

function." The effectiveness of this function is determined by several measures: (1) ratio of cross transitions versus local transitions between states; (2) ratio of largest versus smallest number of transitions and states (i.e., memory) allocated to any processor; and (3) overall ratio of idle time versus processing time for the processors. (See fig. 81.) For all three, smaller is better; however, their minimization might require different approaches.

This implementation defines a simple but general software interface. Thus, it is not targeted to a specific tool. With little effort, the distributed state-space exploration engine can be integrated to a large variety of tools dealing with a discrete state space. Indeed, the usefulness of state-space exploration is not limited to stochastic models. Design and verification tools are also excellent candidates for this technique.

If a numerical solution of the process is desired, it is currently performed in a centralized way; research is under way to distribute this aspect as well. This work was performed at the Institute for Computer Applications in Science and Engineering, NASA Langley Research Center, and supported in part by NASA Contract NAS1-19480. **(R. L. Jones III, 757-864-1492)**

Integrated System Analysis Using Simulation

The correctness of real-time, flight-critical systems is based on both performance and reliability requirements. However, design and analysis techniques have traditionally addressed system performance and reliability separately. In terms of improving the way such systems are studied, there is a conceivable benefit to simultaneously capturing performance and reliability aspects within the same model. This with the desire to leverage existing software and hardware capabilities has motivated research to explore the possibilities of jointly expressing reliability models and performance models in the same (commercial) simulation-based toolset. (See fig. 82.)

The approach taken was to develop a reliability analysis engine capable of being integrated with the commercial simulation-based tool BONeS Designer (Cadence Alta Group), which already supported performance analysis. Integration was accomplished by developing hooks and control structures between BONeS Designer and the reliability engine that maintained model-environment independence. This way, the reliability engine could later be integrated into another commercial tool with minimum effort. Other developed capabilities included automated optimizations to reduce size of state space that needed to be explored. Finally, the integrated performance/reliability capability was successfully proven on large complex models based on the Boeing 777 flight control system.

In addition to the Alta Group, technology transfer has taken place with Boeing Defense and Space, IBM, and AT&T. This work was performed at the Institute for Computer Applications in Science and Engineering, NASA Langley Research Center, and supported in part by NASA Contract NAS1-19480. **(R. L. Jones III, 757-864-1492)**

Parallel Discrete-Event Simulation

Discrete-event simulation is still a viable way to study the dynamic behavior of systems. Simulation is often the only way to solve system models when parametric assumptions and state-space size preclude numerical solution. However, simulation has a disadvantage in that simulation times increase drastically with increasing model complexity. One way to alleviate this problem is from the speedup gained

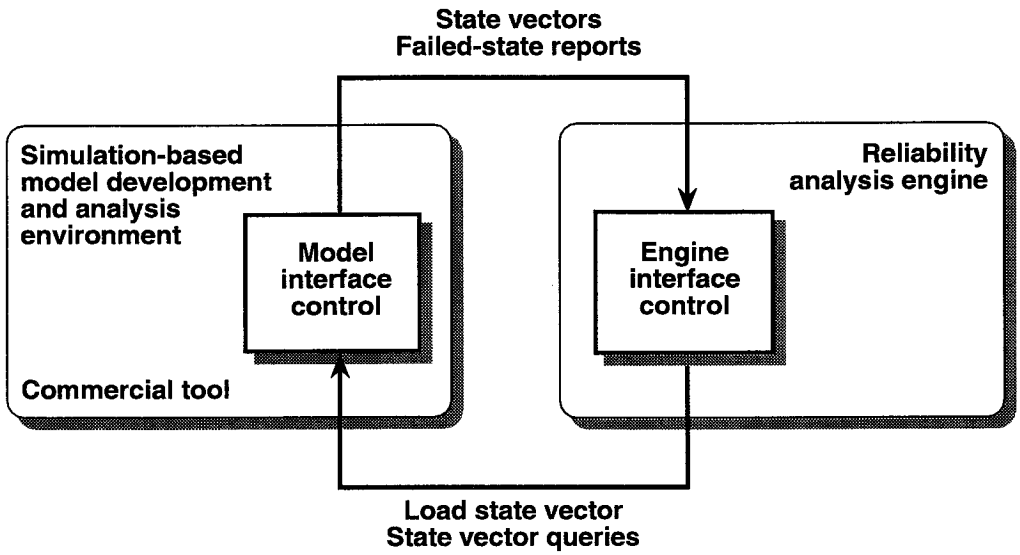

Figure 82. Integrated performance and reliability toolset for system design and analysis.

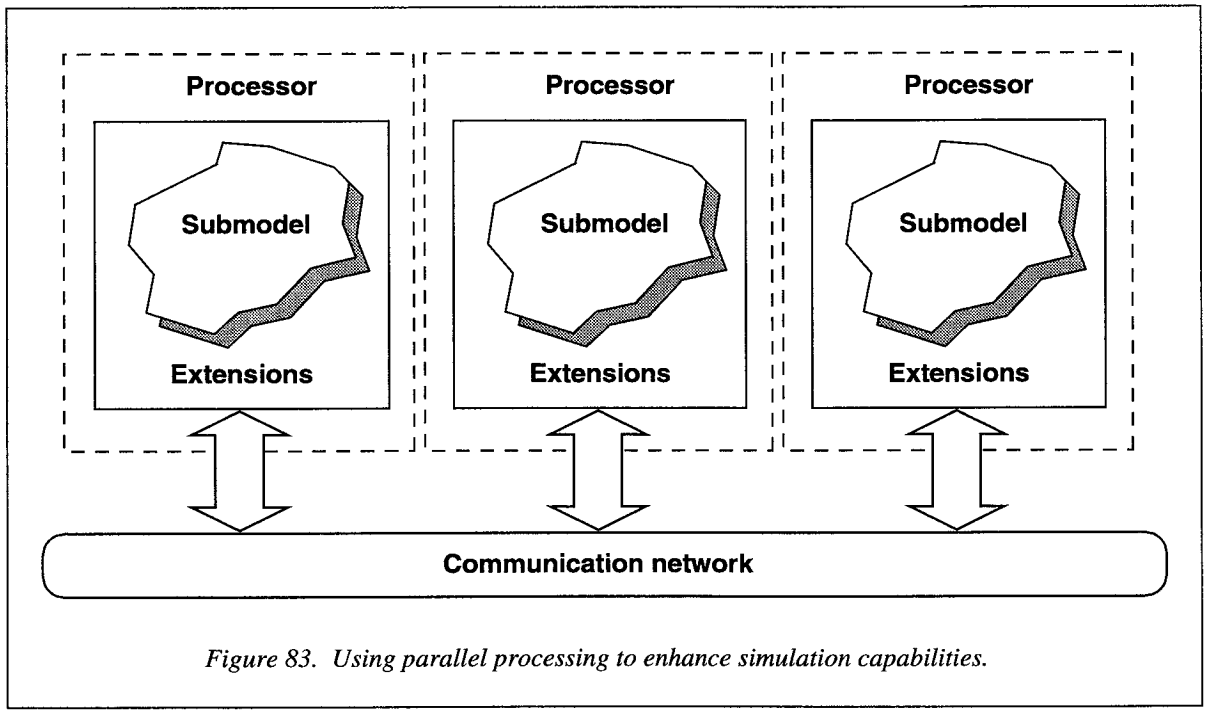

Figure 83. Using parallel processing to enhance simulation capabilities.

by extending sequential simulation to parallel architectures.

Research in this area has been motivated not only by a need for parallel-simulation capability to solve complex problems but also to do so in a way that might foster adoption by industry practitioners. Toward this goal, parallel discrete-event simulation techniques were developed with the following approach. First, the complete model is partitioned into various submodels with extensions added that define the interface between submodels. Then, the parallel simulation is developed by using a commercial tool to assign each submodel to a processor and automate the necessary communication and synchronization in a way that is transparent to the user. (See fig. 83.) Realization of the communication/synchronization mechanisms was accomplished by developing a library of simulation objects and routines. This way parallel simulation models look much like the sequential models and existing simulation models can be parallelized with minimum effort.

The feasibility of this parallel simulation approach was demonstrated successfully, achieving high speedups, on a variety of computer and communication system models. The parallel architectures ported to include an Intel Paragon and an IBM SP2. To encourage technology transfer and a growing user base, an extensions library called the Utilitarian Parallel Simulator (UPS) was written that extends parallel processing to the commercial CSIM simulation package distributed by Mesquite Software.

This work was performed at the Institute for Computer Applications in Science and Engineering, NASA Langley Research Center, and supported in part by NASA Contract NAS1-19480. **(R. L. Jones III, 757-864-1492)**

Automated Load Balancing in Parallel Discrete-Event Simulation

Discrete-event simulation can be used to examine a variety of issues such as the average aircraft delay in the National Airspace System or the performance of a parallel algorithm. Parallel discrete-event simulation (PDES) offers the potential for significant speedups over sequential simulation. In reality, high performance cannot be achieved unless the system is fine tuned to balance computation, communication, and synchronization requirements. As a result, parallel discrete-event simulation needs tools to automate the tuning process with little or no modification to the user's simulation code. (See fig. 84.)

In this work, an automated load-balancing strategy was developed for the SPEEDES simulation environment. In particular, the research investigated the increased performance that might be achieved using a

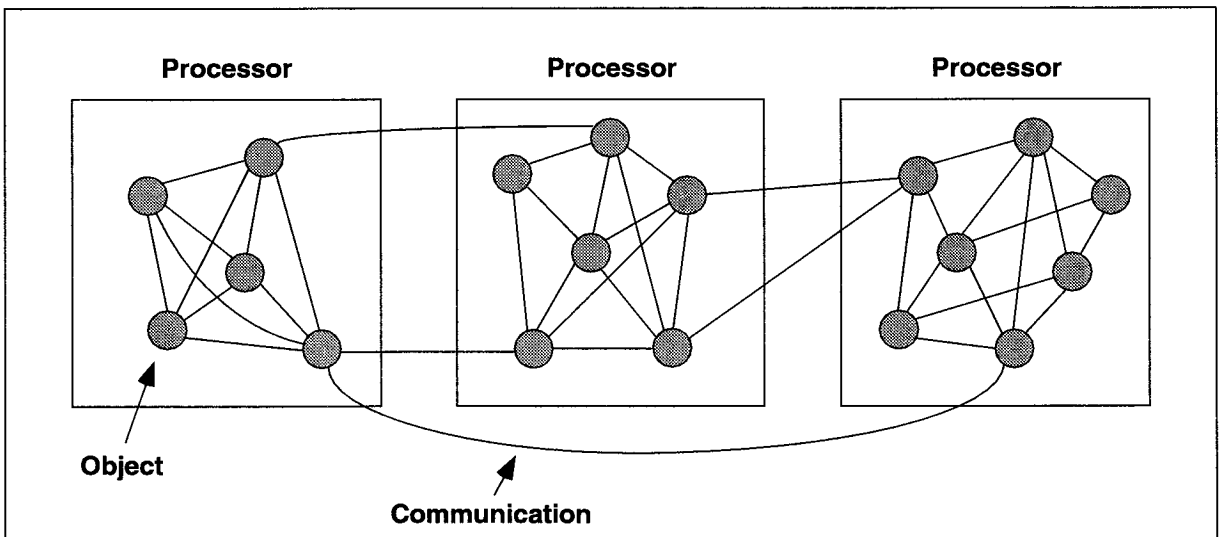

Figure 84. Balancing communication and computation requirements of discrete-event simulation objects.

load-balancing algorithm that uses run-time measurements as opposed to those that do not. Ultimately, the goal is the development of an automated remapping mechanism that will be guided by run-time measurements of a simulation workload.

The automated load-balancing mechanism in SPEEDES was designed to use one of three mapping algorithms that use run-time measurements. Using simulation models of queuing networks and the National Airspace System, the performance of the automated load-balancing system was examined on the Intel Paragon. Results from the execution of actual simulations indicate that the automated load-balancing mechanism in SPEEDES can make significant improvement in the overall execution time.

This work was performed at the Institute for Computer Applications in Science and Engineering, NASA Langley Research Center, and supported in part by NASA Contract NAS1-19480. **(R. L. Jones III, 757-864-1492)**

Predictable, High-Speed Communication for Workstation Clusters

The utility of high-speed local-area networks can be expanded by improving their usable bandwidth and performance predictability. One way is to support established software interfaces and emerging low-cost communication hardware to produce usable low-latency, high-bandwidth communication for high-performance computing, as well as predictable quality of service communication for real-time and isochronous applications. This technology will enable the migration of high-performance computing jobs from high cost, massively parallel systems to lower cost workstation clusters, in order to broaden the range of applications that can be supported on such clusters and to provide high-speed digital local-area interconnects for embedded applications with high-bandwidth requirements (radar, video, and other types of sensor data) for decision support.

A prototype high-speed messaging layer for the Myrinet called "Fast Messages" or FM, allows researchers and applications groups to achieve high performance with Myrinet hardware. This release consists of firmware that runs on the network interface card, and a software library which is linked against the user program and runs on the host processor. The FM 1.1 system running on a cluster of Sun workstations

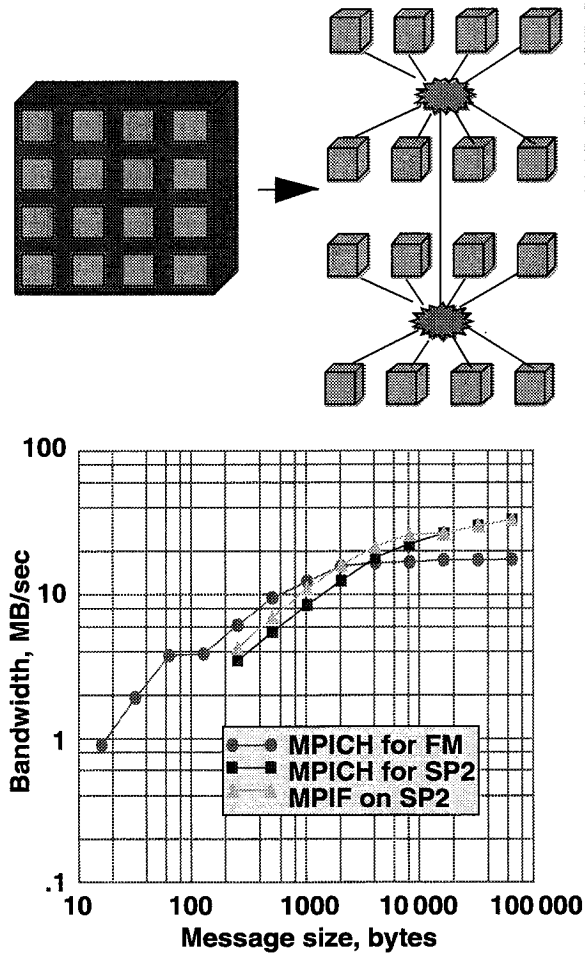

Figure 85. Supercomputer-communication performance on workstation clusters.

provides the following features: high bandwidth delivered to applications, low-latency communication, reliable delivery, and decoupled communication.

An implementation of the Message Passing Interface (MPI), a communication library standard atop FM called MPI-FM, achieves latencies (19 μsec) and bandwidths (140 MB/sec). MPI-FM is derived from the Argonne National Laboratory portable implementation of MPI called MPICH. Figure 85 compares the performance of MPI-FM to a commercial implementation of MPI from International Business Machines (IBM) on their supercomputer–the Scalable Parallel Processor or SP2. IBM's implementation is called MPIF. The figure demonstrates that our MPI-FM provides competitive

performance. For reference, the performance of MPICH on the SP2 is also included. This work was performed in the Computer Science Department at the University of Illinois Urbana-Champaign, and it was funded in part by the Illinois Computer Laboratory for Aerospace Software and Systems block grant with the Langley Research Center.

(K. A. Smith, 757-864-1699)

High-Performance Memory Systems for Advanced Multiprocessors

The objective of this research is to design multi-tera-flop, distributed multiprocessors capable of providing the enormous computing power that NASA missions will require in the next century. The challenge is how to design a sophisticated memory/network subsystem that is able to keep up with the increasing data bandwidth requirements of modern processors. This project is developing a new shared-memory multiprocessor that has sophisticated hardware and compiler support for the memory subsystem. The machine is called "Illinois Aggressive Cache Only Memory Architecture" (I-ACOMA) and is an example of an "all-cache" architecture. (See fig. 86.) The all-cache approach has the advantage that many types of cache misses can be made very cheap. In this past year, this approach has focused on four issues in the design of memory systems for these machines: (1) a new data prefetching scheme, called memory binding and group

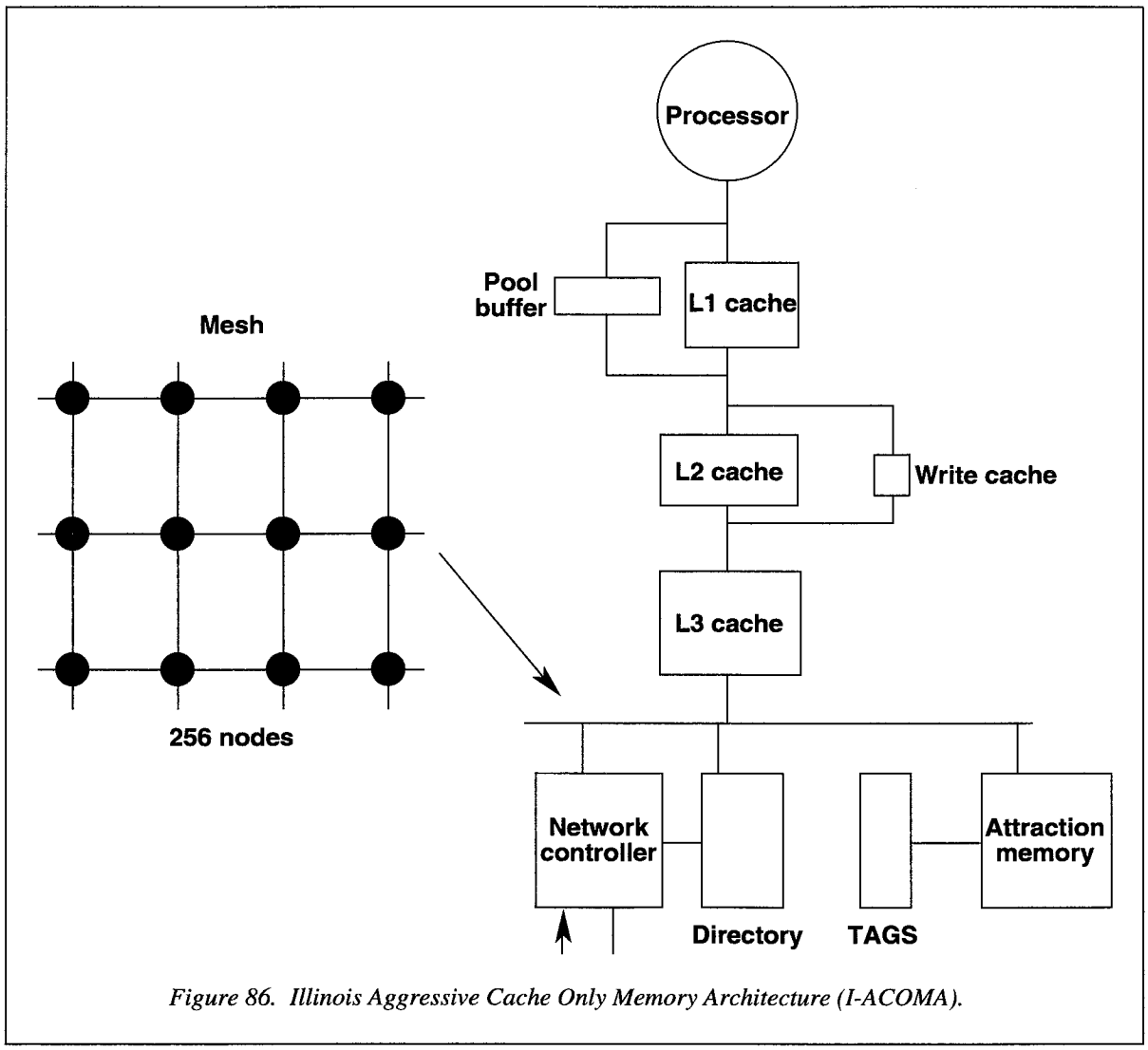

Figure 86. Illinois Aggressive Cache Only Memory Architecture (I-ACOMA).

prefetching, has been developed; (2) a new update cache coherence protocol called distance-adaptive protocol has been designed; (3) a framework for a compiler algorithm for data forwarding has been developed; and (4) the issue of optimizing the performance of the data cache for a multiprocessor operating system has been addressed. These are the types of machines that will support key applications that enhance U.S. leadership, like large database systems to increase the efficiency of the federal government, computer-based virtual testing/prototyping of nuclear weapons systems, or NASA space missions. This work was performed in the Computer Science Department at the University of Illinois Urbana-Champaign, and it was funded in part by the Illinois Computer Laboratory for Aerospace Software and Systems block grant with the Langley Research Center. **(K. A. Smith, 757-864-1699)**

Continuous Media on the World Wide Web

The architecture of the current World Wide Web (WWW) browsers and servers support full file transfer for document retrieval. Transmission Control Protocol (TCP) is used for data transfers by Web browsers and their associated Hypertext Transfer Protocol (HTTP) servers. Full file transfer and TCP are unsuitable for continuous media, such as real-time audio and video. Project Vosaic advocates a continuous media enhanced Web. (See fig. 87.) Issues of efficient network transmission of, server management of, and client side access to continuous media have been investigated. Unlike traditional file transfer, network transmission of continuous media requires timely delivery but can tolerate packet loss. A best effort, adaptive network protocol Video Datagram Protocol (VDP) based on User Datagram Protocol (UDP) is developed. It dynamically adapts to network congestion and client CPU load by adjusting sending rate while preserving video and audio integrity. Server side management focuses on flexible access and efficient reuse of continuous media. A storage model has been proposed to support hierarchical access, browse, search, and dynamic composition of video and audio. Video and audio are treated as first-class data type as text and image. A client side browser has been developed to provide easy and flexible interface for exchange and retrieval of continuous media. Current research efforts include server caching and prefetching, hypermedia presentation, and authoring on the WWW. This work was performed in the Computer

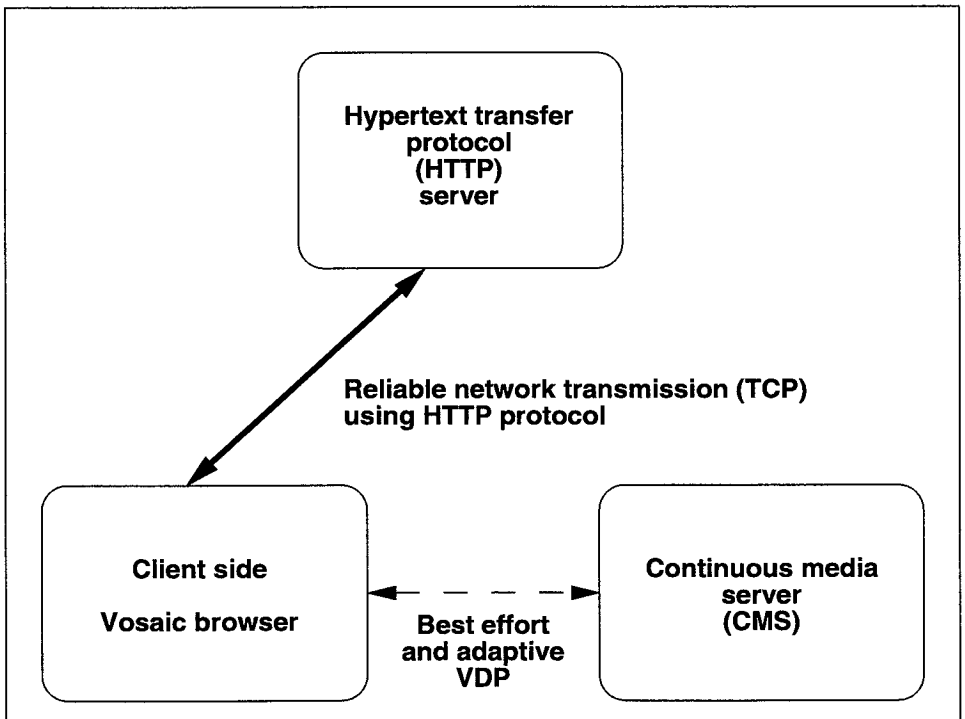

Figure 87. Architecture of Vosaic.

Science Department at the University of Illinois Urbana-Champaign, and it was funded in part by the Illinois Computer Laboratory for Aerospace Software and Systems block grant with the Langley Research Center. **(K. A. Smith, 757-864-1699)**

Cache Memory Management in Real-Time Systems

Cache memory has long been known to improve system performance. High-performance systems are particularly important in time-critical applications. These applications can be found in such industries as the aerospace industry where quick response time and dependability are essential. Real-time systems designed to run these applications are based on worst-case execution times. These times help ensure that system timing constraints are met. The determinism of worst-case execution times is significantly complicated by cache memory. To ease calculations and ensure guarantees on these times, greatly inflated worst-case times are frequently used. This leads to lower system performance and decreased system schedulability. The goal of this research is to increase the determinism of cache-based real-time systems. This will enable the calculation of worst-case execution times to more accurately reflect caching effects. One approach developed through this research to address the problem of determinism and caching is the use of preferred preemption points. (See fig. 88.) Preferred preemption points are prespecified points within a task where task switching is allowed to occur. With these known points of preemption, the cost of caching effects stemming from preemptions can be incorporated more accurately into worst-case execution times. Preferred preemption points are chosen at instances where tasks exhibit a low degree of cached state. This decreases the cost of preemptions,

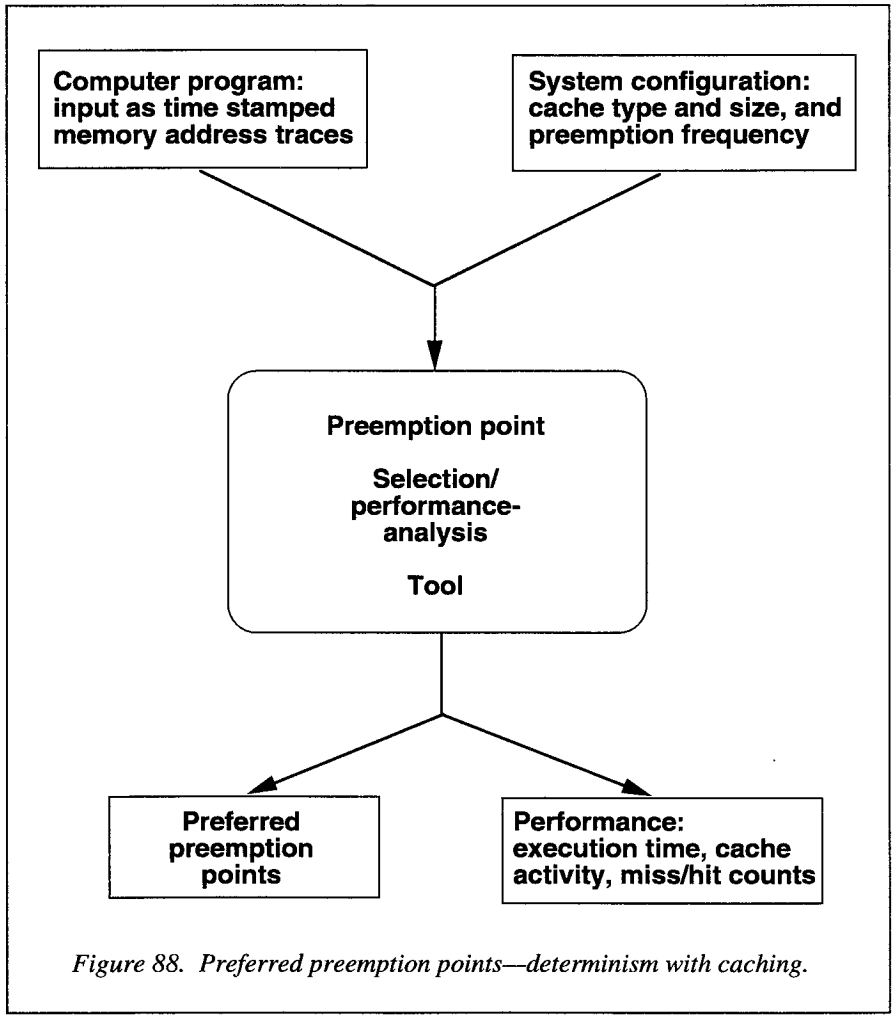

Figure 88. Preferred preemption points—determinism with caching.

increasing systems performance. An analysis tool has been developed along with the technique of preferred preemption points to determine the performance gains achievable. The tool can be provided with a set of user defined preemption points or can be set to return a set of preferred points. This work was performed in the Computer and Systems Research Laboratory at the University of Illinois Urbana-Champaign, and it was funded in part by the Illinois Computer Laboratory for Aerospace Software and Systems block grant with the Langley Research Center.

(K. A. Smith, 757-864-1699)

A Simulation-Based Environment for System Level Dependability Analysis

Future commercial systems for air, ground, and space applications will require innovative solutions to dependability problems. The classical approach of designing for performance and then addressing the dependability issues is no longer practical. Only through the use of advanced design techniques can we ensure that high-performance computing systems are produced in a timely fashion and that they meet stringent, real-time reliability and fail-safe requirements.

DEPEND is a functional, process-based simulation tool which provides an integrated design and fault injection environment for system level dependability analysis. The tool exploits the properties of the object-oriented paradigm and provides facilities to rapidly model fault-tolerant architectures and conduct extensive fault injection studies. The system behavior is described by a collection of processes that interact with one another. The user writes a control program in C++ using the objects in the DEPEND library. The library contains both elementary and complex objects.

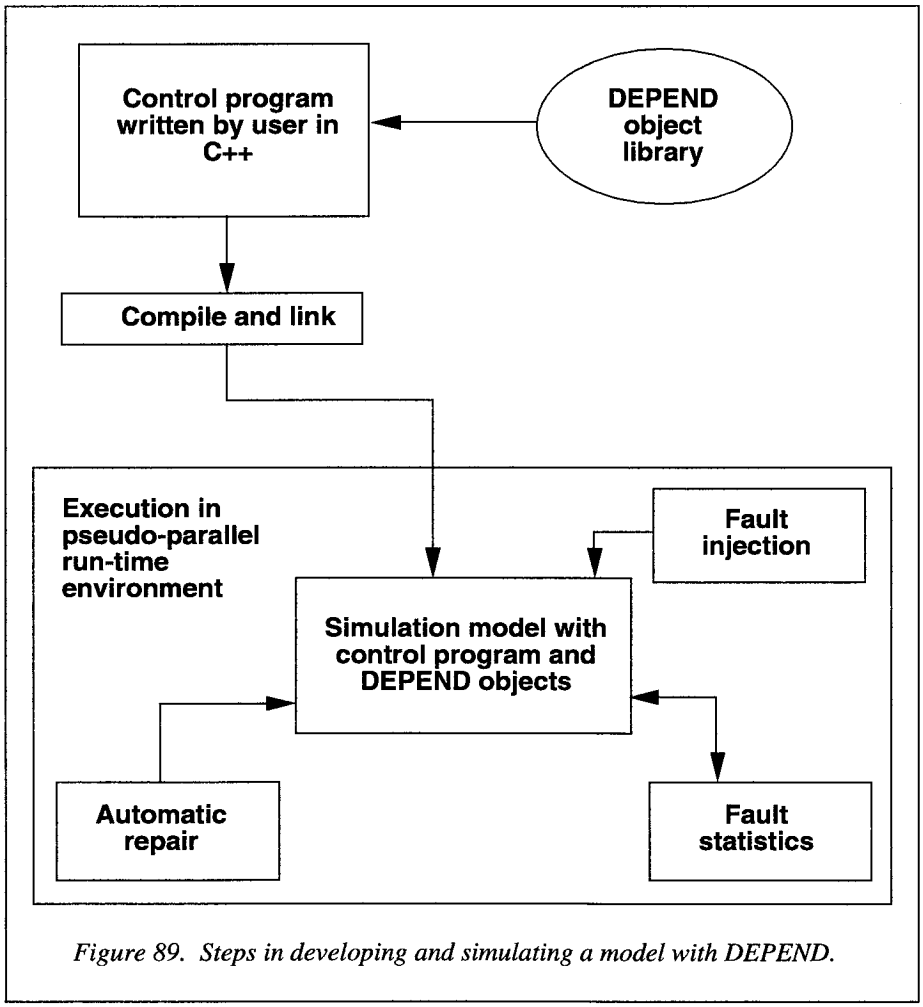

Figure 89. Steps in developing and simulating a model with DEPEND.

DEPEND was shown to be able to determine failure mechanisms, quantize the impact of faults, and evaluate fault-tolerance mechanisms and repair schemes. Results obtained using DEPEND were validated by comparing them with measurements obtained from fault injection experiments conducted on a production Tandem Integrity system. (See fig. 89.)

This work was performed in the Computer and Systems Research Laboratory at the University of Illinois at Urbana-Champaign, and it was funded in part by the Illinois Computer Laboratory for Aerospace Systems and Software block grant with NASA Langley. The University has sold a license for DEPEND to Raytheon and is in the process of licensing DEPEND to Ansaldo, Inc., and AT&T. **(K. A. Smith, 757-864-1699)**

Compilation for High-Performance Parallel Systems

The IMPACT compiler is designed with new data structures and algorithms which utilize execution profile information to perform aggressive code optimization and parallelization. The compiler generates code for the PA-RISC, SPARC, X86, and VLIW platforms. (See fig. 90.) Output code for large production programs executes about 20 percent faster than commercial compiler output codes on the existing machines. This difference is expected to increase to about 100 percent for the new wide issue microprocessors. The techniques that contribute to this performance improvement include interprocedural pointer analysis, hyperblock formation, control and data height reduction, dynamic memory address disambiguation, instruction-level parallelization, compiler-assisted data prefetch, loop blocking, software pipelining, and memory to register data migration.

The IMPACT project is currently focusing on compilation for high-performance multiprocessor systems. Parallel machine models are being developed for code optimization and parallelization. A prototype compilation system is being developed for multiprocessor systems based on the Texas Instruments C3x/C4x VLIW Digital Signal Processing (DSP) microprocessors. Existing commercial compilers have not been able to exploit more than 10 percent of the hand code performance for real DSP applications. To drastically improve program performance, new methods are under development for parallelization, granularity adjustment, data prefetching, loop blocking, and shared data register allocation. The objective is to achieve at least 50 percent of the hand code efficiency. This effort is being conducted in cooperation with ISIS Associates, Langley's industry partner specializing in developing and marketing commercial compilers in the DSP market.

In 1987, NASA became the first sponsor of the IMPACT project, followed by NSF. Since then, IMPACT has been also sponsored by many industrial partners including AMD, HP, Intel, AT&T GIS, SUN Microsystems, and ISIS. Currently, the industrial partners provide a majority of the funds required for the IMPACT project. The beta version of IMPACT has been released to the industrial partners for technology transfer and evaluation. This work was performed in the Computer and Systems Research Laboratory at the University of Illinois Urbana-Champaign, and it was funded in part by the Illinois Computer Laboratory for Aerospace Software and Systems block grant with the Langley Research Center.
(K. A. Smith, 757-864-1699)

FUNCO Functional Cohesion Measurement Tool for C Programs

Module cohesion indicates how closely related a module's internal components are to one another. A highly cohesive software module has one basic function and is indivisible—it is difficult to split a cohesive module into separate components. Cohesion is related to the ease of debugging, maintainability, and modifiability. Cohesion was originally assessed subjectively; such assessments cannot be automated. As a result, cohesion has not been effectively used as a software quality indicator. FUNCO, a new cohesion measurement tool, can objectively assess the functional cohesion of C modules. (See fig. 91.) Measurements are based on the relative number of "glue" or "adhesive" data tokens that lie on module "output data slices," a sequence of data tokens with a dependence relationship on an output. "Glue tokens" are data tokens common to more than one data slice and "superglue tokens" are common to every data slice. The adhesiveness of a data token is the number of data slices to which the data token is common. Weak functional cohesion (WFC) is the ratio of glue tokens to the total number of tokens. Strong functional cohesion (SFC) is the ratio of superglue tokens to the total number of data tokens. Adhesiveness (A) is the ratio of the amount of adhesiveness to the maximum possible adhesiveness. FUNCO was developed at Colorado State University and is now undergoing beta testing at university and commercial

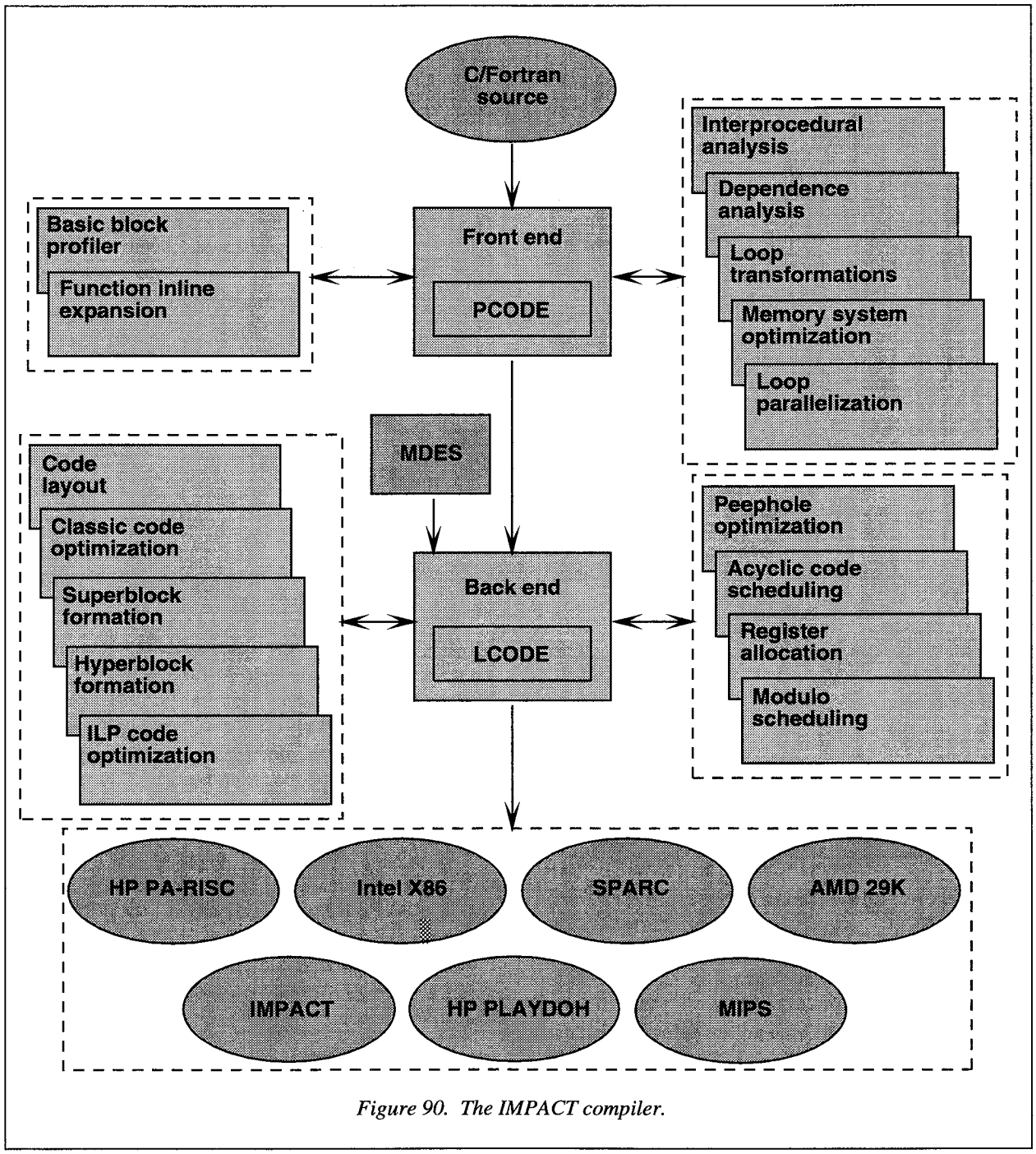

Figure 90. The IMPACT compiler.

Sum	Max.	Avg.	Statement
			void Sum_Max_Avg
1	1	1	(int arr[],
1	1	1	int n,
1		1	int *sum,
	1		int *max,
1		1	float *avg)
			{
1	1	1	int i;
2		2	*sum = 0;
	3		*max = arr[0];
5	5	5	for (i=0; i<n; ++i) {
4		4	*sum = *sum + arr[i];
	3		if (arr[i] > *max)
	3		*max = arr[i];
			}
3		3	*avg = *sum / n;
			}

Number of data tokens on each output slice

Data tokens counted in more than 1 column are glue tokens.

Those counted on all columns are superglue tokens.

Data:

Number of tokens = 29
Number of glue tokens = 19
Number of superglue tokens = 8

FUNCO measures:

WFC = 19 / 29 = 0.66
A = (11*2 + 8*3) / (29*3) = 0.53
SFC = 8 / 29 = 0.28

Figure 91. Example FUNCO calculation.

sites. This work was funded in part by a grant from NASA Langley Research Center. **(K. A. Smith, 757-864-1699)**

Computational Electromagnetic (CEM) Code Development for Advanced Aircraft Applied to Automobile Applications

The objective of the current Computational Electromagnetic (CEM) code development research is to develop novel, efficient, and accurate tools for designing antennas and predicting their performance on complex aircraft and spacecraft vehicles. A hybrid Finite Element Method (FEM), Method of Moments (MoM), and Geometrical Theory of Diffraction (GTD) code was developed to predict the performance of cavity-backed antennas on finite structures. The developed code, known as CBS3DR, accurately predicts antenna characteristics such as input impedance and radiation pattern. The application of this code was extended to civilian ground vehicles as part of the NASA technology transfer initiative. Comparisons were made between computed results from the CBS3DR codes and experimental measurements, performed in the Langley Low-Frequency Antenna Test Facility. The measurements were performed on a cavity-backed microstrip patch antenna placed on the roof of a quarter-scale automobile configuration. (See fig. 92.) The measured and computed results were in close agreement. Other computational techniques were used to accurately predict the performance of other antennas mounted on the vehicle as well. The CEM code and data will be transferred to the Ford Motor Company as part of a Memorandum of Agreement between NASA Langley and Ford Motor Company, completing the transfer of aerospace technology to civilian industry. **(F. B. Beck, 757-864-1829)**

Biocybernetic System Validates Index of Operator Engagement in Automated Task

A "closed-loop" methodology has been developed in the Human Engineering Methods Research Laboratory to support the determination of optimal "mixes" of tasks performed manually by a human and tasks

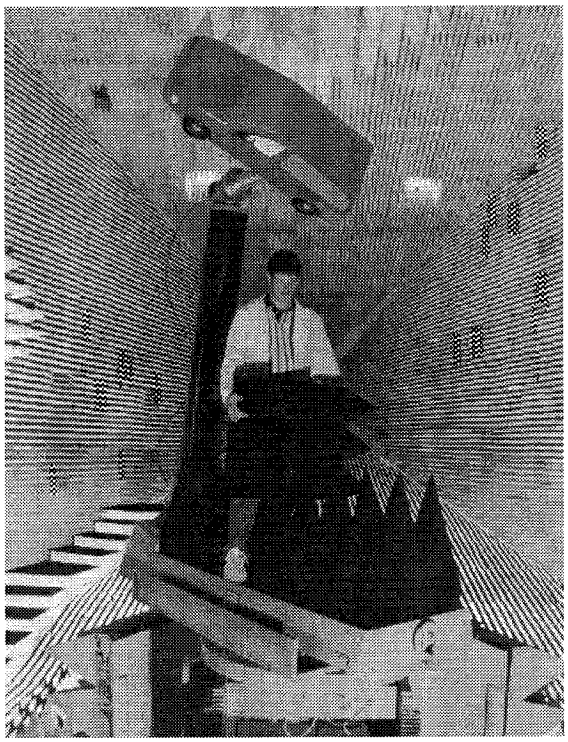

L-95-5085

Figure 92. The quarter-scale Windstar mini-van model in the Low-Frequency Antenna Test Facility for antenna radiation pattern testing.

performed automatically by a system, based upon a brain activity criterion of consistent mental engagement. In this method, an experimental subject interacts with a set of tasks while the subject's electrical brain activity is monitored. The level of automation of the task set may be varied so that all, none, or a subset of tasks require subject intervention, enabling a range of levels of demand for operator involvement in system management to be imposed. A biocybernetic loop is formed (fig. 93) by adjusting the number of manual tasks imposed on the subject, based on electroencephalographic (EEG) signals reflecting an operator's engagement in the task set. An optimal number of manual versus automated tasks is arrived at by allowing the closed-loop (negative) feedback system to attain stable operation, reflecting stable engagement, and is defined by the subset of tasks that maintain stable operation.

The ultimate objective of this effort is the development of new methodologies to assess the extent to which automated flight deck systems maintain pilot

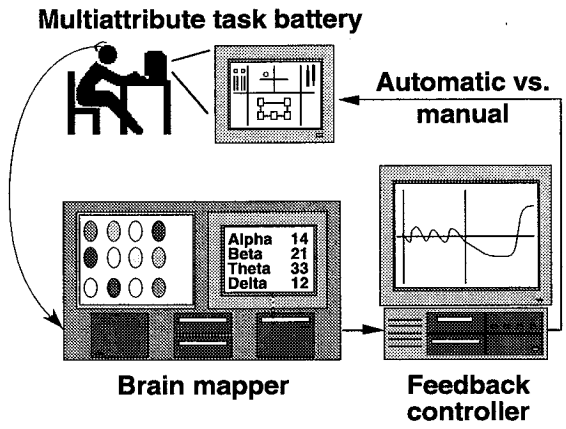

Figure 93. Biocybernetic loop for evaluating a human/automation design.

engagement. The closed-loop method provides a dynamic, interactive method of adjusting a system design to optimize the operator's engagement.
(A. T. Pope, 757-864-6642)

Aeroelastic Design Using Distributed Heterogeneous Computers

Current activity in the Framework for Interdisciplinary Design Optimization (FIDO) project is focused on providing aeroelastic analysis and efficient sensitivity analysis capability for use in MDO, based on nonlinear inviscid computational fluid dynamics (CFD) and finite-element method (FEM) structural analysis codes. The aeroelastic solutions require iteration between the CFD and FEM codes to ensure that the vehicle shape being used for the aerodynamic calculations is consistent with the structural deformations caused by the aerodynamic loads.

The FIDO system has been used to implement a tightly coupled aeroelastic analysis capability that uses a marching Euler CFD code (ISAAC) combined with an FEM structural analysis code (COMET). Both codes were available in single-processor and multiple-processor versions. COMET provides an analytic sensitivity analysis capability for structural design variables, and ADIFOR has been applied to the single-processor version of ISAAC to obtain aerodynamic sensitivity analysis. The FIDO system also includes interactions with simple propulsion and performance analysis codes.

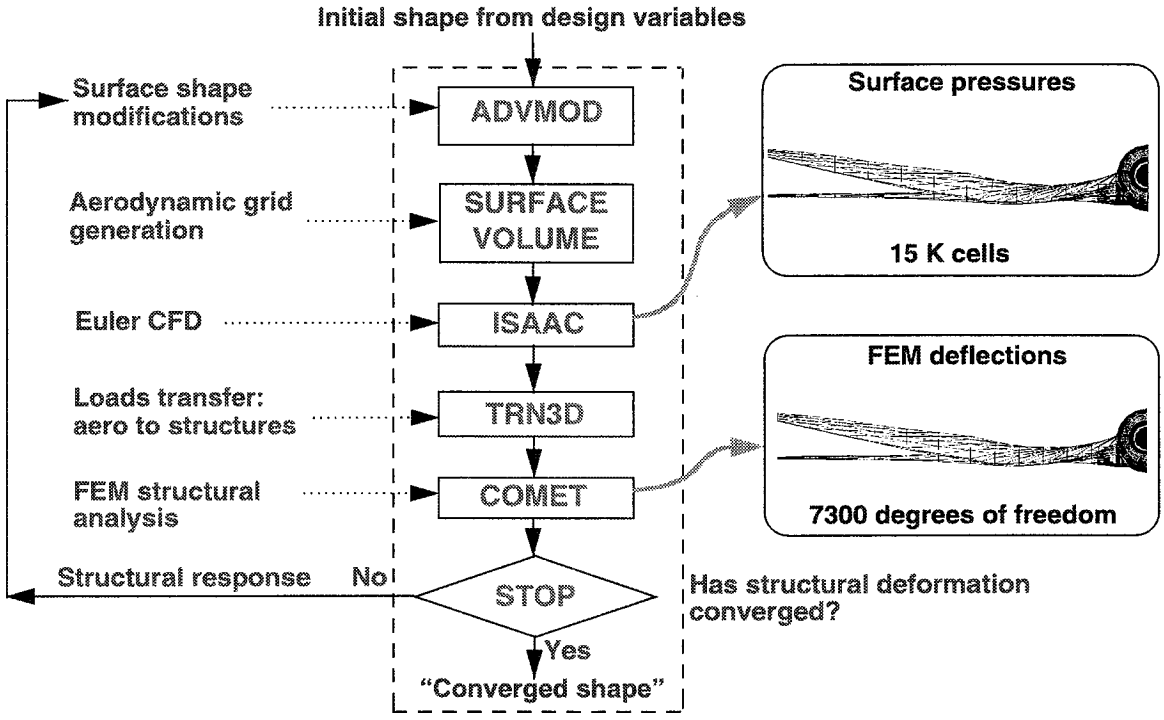

Figure 94. Key steps in the FIDO-3 aeroelastic loop.

Figure 94 schematically illustrates how the CPU-intensive aerodynamic and structural analysis codes are combined with interface routines into an aeroelastic computation loop within the FIDO system. The ADVMOD interface code is used to update the surface grid points for both the FEM grid and the aerodynamic grid based on the latest surface shape modifications. An aerodynamic volume grid suitable for the marching Euler code is then automatically generated using the updated surface coordinates. After the ISAAC code computes a new surface pressure distribution, the TRN3D code uses the shape functions from the FEM model to integrate the pressure distribution and compute the appropriate forces at the FEM node points for input into the structural analysis code. The development of these interface codes for use in the FIDO system was essential to providing an automated aeroelastic coupling capability. The aeroelastic loop typically requires about five iterations to converge the structural deformations. **(R. P. Weston, 757-864-2149)**

ADIFOR 2.0 Automatic Differentiation for Derivative-Based Multidisciplinary Design Optimization

Automatic differentiation (AD) is a powerful computational technique that provides a means to obtain exact sensitivity derivatives (SD) from existing computer programs for use in multidisciplinary design optimization. Argonne National Laboratory and the Center for Research on Parallel Computation at Rice University developed ADIFOR 2.0, a second-generation precompiler AD tool for FORTRAN 77 programs. The user identifies sets of dependent and independent variables within an existing computer code. ADIFOR 2.0 then traces the dependency path throughout the code, formulates exact derivatives via the chain rule throughout the dependency path, and generates new code to compute both the original function and the required SD matrix. ADIFOR 2.0 includes user-controlled handling of derivative singularities and transparent support for

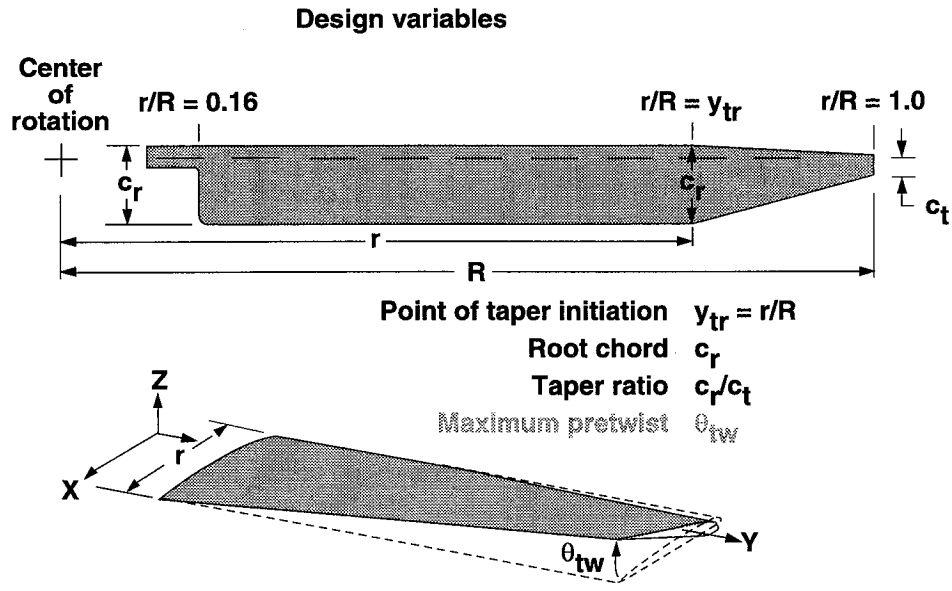

Figure 95. Select variables for helicopter blade design.

sparse derivative computations with reduced compute time and memory requirements via the SparsLinC library. The ADIFOR 2.0 tool works quickly and robustly with minimal user intervention. Many different applications in aerospace and nonaerospace fields have been demonstrated that include high-performance computing and weather modeling.

Figure 95 illustrates some of the many variables associated with helicopter blade design. Support for complex variables within ADIFOR 2.0 enabled successful applications to helicopter blade design for both hover and forward flight conditions, using the comprehensive helicopter analysis code CAMRAD-JA. The use of ADIFOR 2.0 has been more reliable in helicopter blade design than divided difference approximations. For example, the SD of required horsepower with respect to the blade pretwist angle was computed accurately by ADIFOR 2.0 for both hover and forward flight. However, the accuracy of several divided difference approximations to this SD were generally quite poor in forward flight over a range of step sizes, and different magnitudes of the step size were required for accurate approximations in hover and forward flight. **(L. L. Green, 757-864-2228)**

Coarse-Grained Parallelization of Multiblock Navier-Stokes Code

The objective of this work is to develop a general purpose multiblock Navier-Stokes flow solver that can take advantage of the combined compute power of clusters of workstations and parallel computers available in research laboratories and industry, thus making nonlinear computational fluid dynamics more widely available and affordable to researchers. A widely used multiblock Navier-Stokes code, TLNS3D-MB, developed for Cray computers, was used as a starting point for this activity. This code consists of two types of subroutines, namely driver routines and the functional routines, and only the driver routines had to be modified for parallelization. Basically, each block (or group of blocks) is assigned to a processor (or compute node). The compute node does all the calculations for the blocks assigned to it. If it needs information from a block (or blocks) that is not local to it (e.g., data at an interface), a message is sent to the appropriate processor to receive the data. Only the data required at interfaces is communicated across the network to minimize the communication cost.

Solutions for several benchmark test cases have been run on an SGI cluster consisting mainly of INDIGO2 computers and also on NASA Langley's

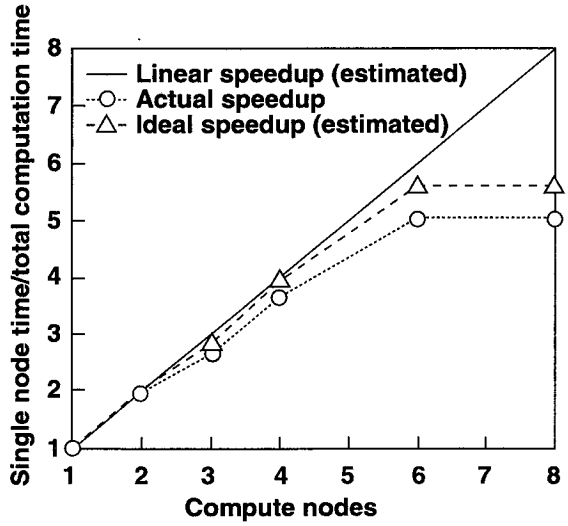

Figure 96. Speedup of computation on parallel computer for a transonic wing case as a function of the number of compute nodes.

IBM/SP2 cluster. Figure 96 shows the speedup for a transonic wing case with unequal grid blocks; the performance is close to the ideal estimated speedup for this particular multiblock grid. Near linear speedup has been achieved for up to 16 nodes on the IBM/SP2. In order to improve load balance, a special purpose utility was written to subdivide a given problem (grid and input connectivity files) into a user-specified number of blocks. This software was used to create a 24-block case for a wing/body/nacelle/pylon/tail/fin configuration which was distributed on 16 nodes, achieving a factor of 3 speedup over a single node of the Cray C-90 computer.

With the availability of this parallel version of a Navier-Stokes code, the design engineers can take advantage of the idle compute power of the workstations in their respective laboratories at off-peak hours. In addition, due to distributed memory, one can run much larger size problems that couldn't be addressed earlier due to memory limitations. This capability enables flow solutions at much lower cost and quicker run time on massively parallel computers. **(V. Vatsa, 757-864-2236)**

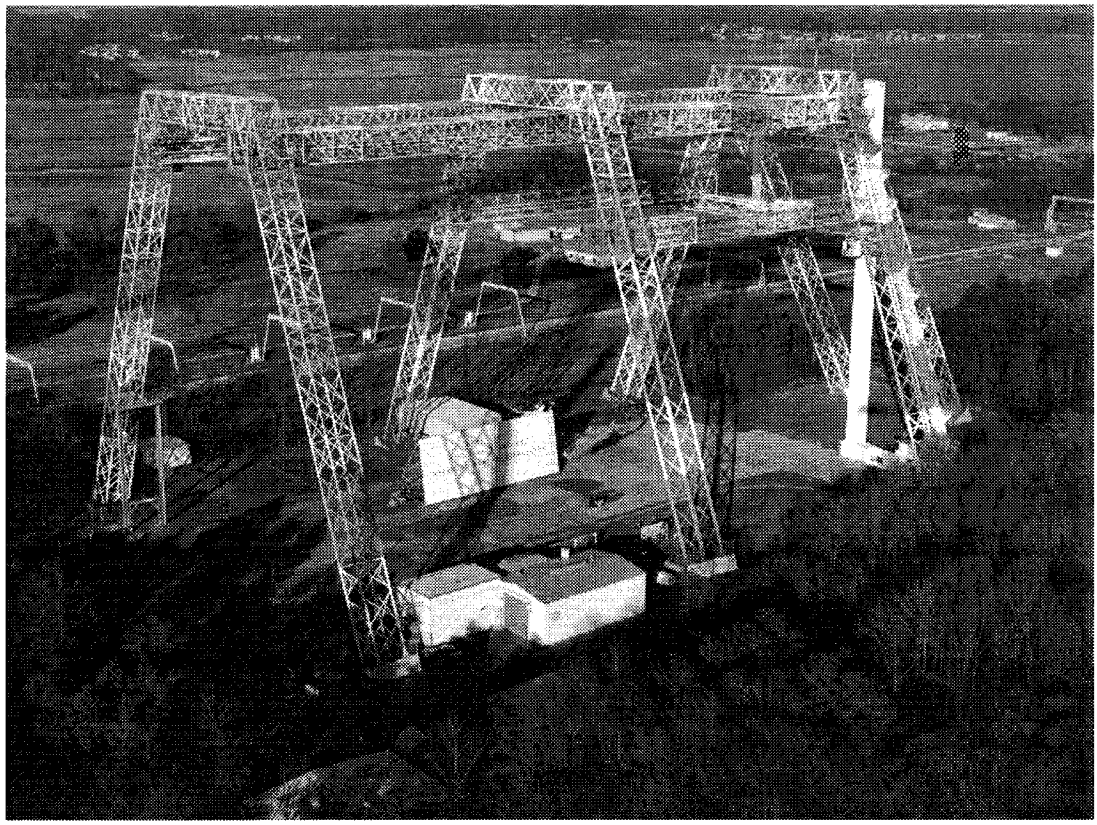

- *All NASA Langley facilities are described in detail on the NASA Langley Critical National Facilities World Wide Web Homepage, which is kept current by the Center. The URL address is http://techreports.larc.nasa.gov/LaRCfacilities.*

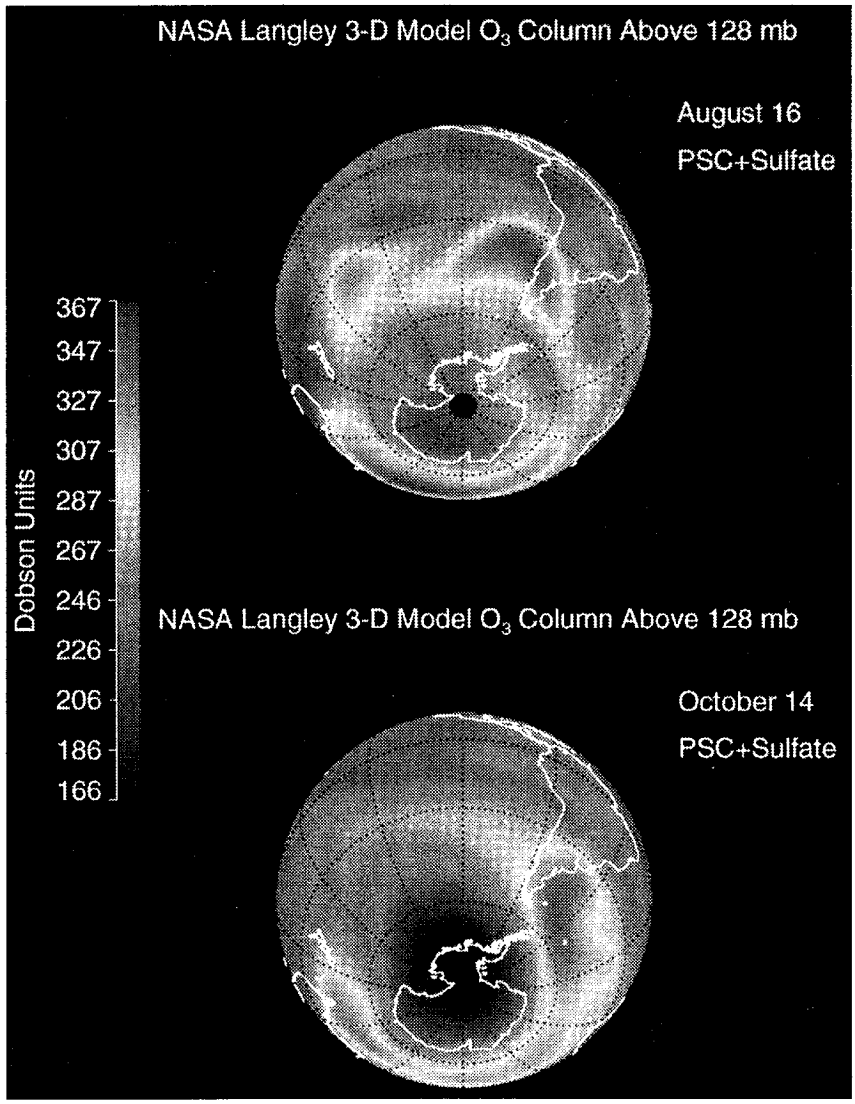

- *Expand scientific knowledge of the Earth system using NASA's unique capabilities from the vantage points of space, aircraft, and in situ platforms.*
- *Disseminate information about the Earth system.*
- *Enable the productive use of Mission to Planet Earth science and technology in the public and private sectors.*

Inhomogeneous Cloud Field Effects on Retrieving Optical Depth From Space

Clouds are a very sensitive contributor to the Earth radiation budget. Depending on their characteristics, they produce either a net warming or cooling of the atmosphere. Global monitoring of clouds from space is therefore an important element of ongoing climate studies. However, the interpretation of space-based measurements is uncertain because most models assume plane-parallel clouds, whose properties vary only in the vertical direction, while real clouds often have large amounts of horizontal inhomogeneity. The objective of this work is to assess the impact of horizontally varied cloud fields on the retrieval of optical depth τ, a key cloud physical property, from space.

The 2D Spherical Harmonic Discrete Ordinate Method radiative transport code is used to calculate the reflected radiance from subsampled slices of 45 LANDSAT remote sensing images of boundary-layer cloud fields over oceans. This is the largest real data set yet used to study inhomogeneous cloud effects. The computed radiances are used to "retrieve" the corresponding τ, which is then compared with the input or reference τ to obtain an estimate of the retrieval error. The results of this calculation are studied at the sub-sample (5.7 km) scale, a resolution characteristic of some space-based instruments. The root-mean-square (RMS) retrieval error for the samples in this study is 7 to 10 percent, though for some samples it can be a factor of two or more. Figure 97 shows the behavior of the ratio of retrieved to reference τ with cloud mean optical depth and aspect ratio for the case of overhead Sun ($\Theta_0 = 0°$). This behavior can be used to make a first correction to τ_{retr}, which significantly reduces the RMS error of the retrieval. **(L. H. Chambers, 757-864-4371)**

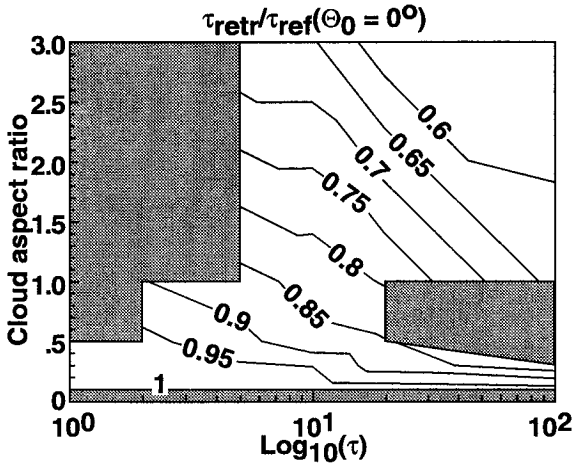

Figure 97. Ratio of retrieved to actual optical depth as a function of cloud parameters of inhomogeneous cloud fields.

Atmospheric Simulation Model for Global Change Studies

An effort has been underway at Langley Research Center to develop an atmospheric simulation model in support of NASA Upper Atmosphere Research Satellite (UARS) and Earth Observing System (EOS) programs. The overall objective of this effort is to develop a predictive model capable of studying the atmospheric response to global change and thereby contribute to a sound scientific basis for environmental policy decisions. Recent results have been obtained which represent the first demonstration of interactive coupling of radiative, chemical, and dynamical processes in an atmospheric general circulation model, including comprehensive chemistry. The model has simulated an annual cycle with circulation, thermal structure, and constituent distributions that are in good agreement with observations. The model successfully simulated the development and decay of the Antarctic ozone hole. Figure 98 shows the stratospheric ozone column (in Dobson units) on August 16 in the midst of austral winter and the subsequent development on October 14 in which the reduced ozone column over Antarctica is apparent. The ozone destruction in the model occurred as a result of denitrification and chlorine catalysis associated with heterogeneous chemical processes on polar stratospheric clouds (PSC's) and on sulfate aerosols in the lower polar stratosphere. Subsequent breakup of the ozone hole occurred with the final warming, associated with the seasonal transition in the stratosphere and rapid meridional exchange of air between the polar regions and middle latitudes.
(W. L. Grose, 757-864-5820)

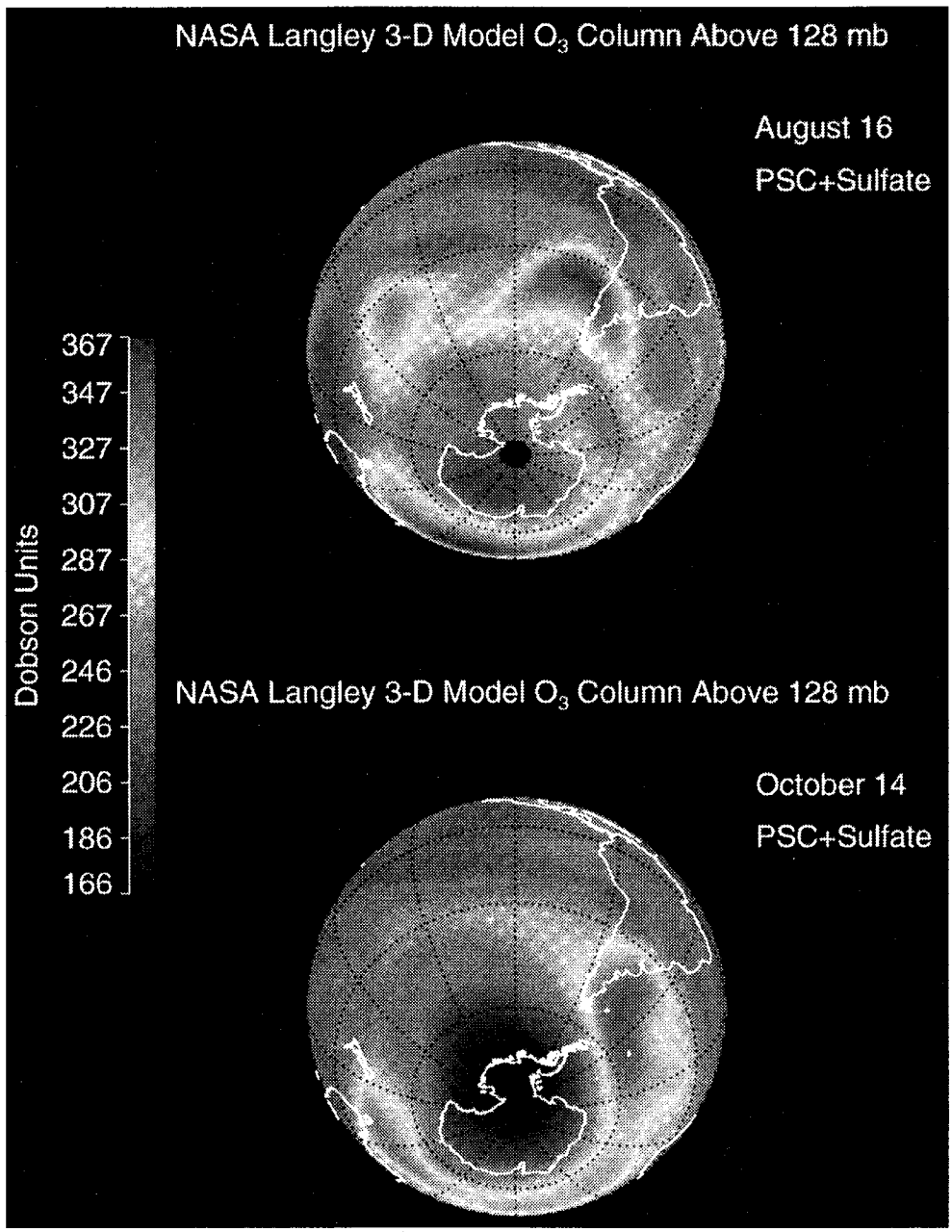

Figure 98. Orthographic projections of column ozone above 128 mb taken from a simulation with the Langley General Circulation Model/Chemical Transport Model. Top panel is for August 16; lower panel is for October 14. Units are Dobson units. (1 Dobson unit = 2.7×10^{16} molecules-cm^{-2}.)

LITE Observation of Long-Range Transport of Aerosols in Free Troposphere

The horizontal and vertical distributions of aerosols are key questions to understanding aerosol effects on the Earth's radiation budget and atmospheric chemistry. Most atmospheric aerosols are contained within the planetary boundary layer and have short atmospheric residence times (and thus only regional influences) due to wet removal processes. Aerosols that reach the free (upper) troposphere have significantly longer lifetimes and can potentially be transported over large distances. High vertical and horizontal resolution measurements of enhanced aerosol layers in the free troposphere were obtained by the Lidar In-Space Technology Experiment (LITE), a backscatter lidar which was operated for 10 days between the latitudes of 57°N and 57°S on Space Shuttle *Discovery* in September 1994. Figure 99 shows a layer of aerosol at an altitude between 5 and 10 km in the free troposphere off the east coast of Madagascar. Meteorological analysis suggests the source of this aerosol layer to be biomass fires in southeastern Africa. The smoke from these fires was lifted into the upper troposphere by synoptic-scale forcing produced by circulation around a low-pressure region, resulting in the formation of an elevated layer with an estimated optical depth of about 0.1. Other LITE observations of enhanced aerosols in the free troposphere in southern midlatitudes provide evidence that aerosols originating in southern Africa were transported by strong westerly winds to sites as far away as the eastern Pacific Ocean, a distance of more than 15000 km.
(D. M. Winker, 757-864-6747)

NASA Pacific Exploratory Mission in Northwestern Pacific Troposphere

NASA, in collaboration with NOAA and universities and government agencies in the United States, Hong Kong, Taiwan, The People's Republic of China, and Japan, has conducted the first comprehensive airborne and ground based study of the impact of human and natural emissions from the Asian continent on the chemistry of the troposphere over the northwestern Pacific Ocean. Phase A of this study, the Pacific Exploratory Mission (PEM)-West, was completed in October 1991; Phase B was completed in March 1994.

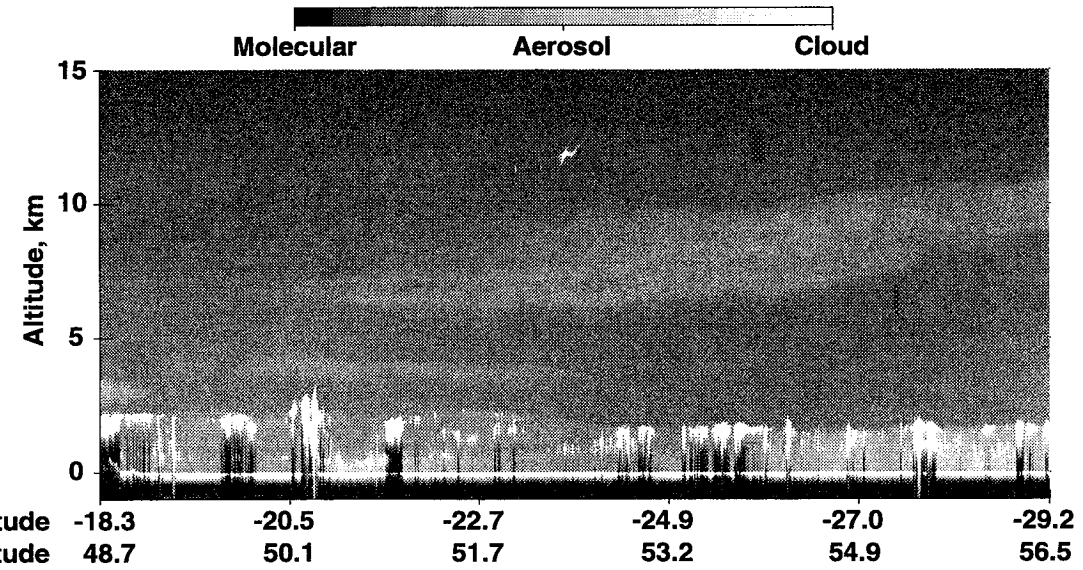

Figure 99. LITE backscatter signal from the atmosphere off the east coast of Madagascar. A deep layer of aerosol originating from the African continent is seen in the free troposphere between altitudes of 5 and 10 km.

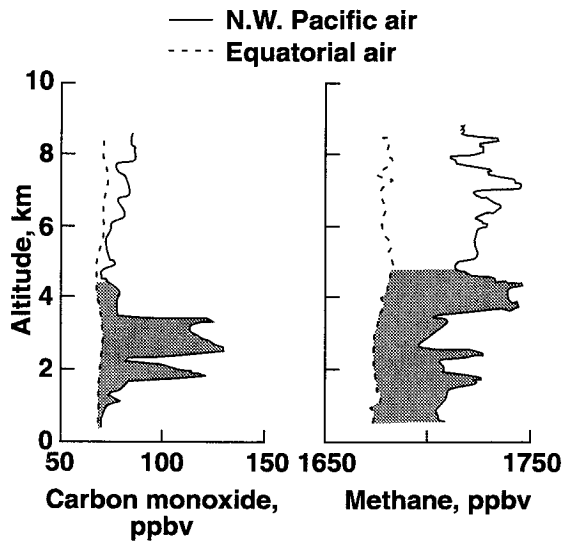

Figure 100. Fall 1991 PEM-West A aircraft measurements over the Pacific Ocean east of Asia at latitudes of the equator (equatorial air) and 30° North (N.W. Pacific air). The shaded region reflects pollution transported directly from Asia. The unshaded region includes pollution from Asia as well as global transport from Europe and North America. The N.W. Pacific air was sampled 2500 km east of Shanghai and had been over the ocean for at least 10 days.

The Pacific Ocean is, perhaps, the last remaining region of the world's lower atmosphere which is relatively free of atmospheric pollution. Therefore it is an ideal region to study carbon, nitrogen, ozone, sulfur, and aerosol chemical cycles, where the influence of the Asian and European continents is readily observed. The vertical profiles of carbon monoxide and methane shown in figure 100 serve to illustrate the extensive impact that human and biogenic emissions are having on the atmosphere over the northwest regions of the Pacific relative to the equatorial regions. More detailed discussions of the results from PEM-West A have been published in a Special Section of the January 20, 1996, *Journal of Geophysical Research (JGR) - Atmospheres.* These provide additional cases of the impact of human and natural emission on this region of the Pacific, and on the photochemical and meteorological processes that transport and process emission products into such species as ozone, oxides of nitrogen, and aerosols. The detailed measurement results from both phases of PEM-West are available from the Distributed Active Archive Center at the Langley Research Center. **(J. M. Hoell, 757-864-5826)**

Investigation of Global Tropospheric Ozone: In Situ Aircraft Measurements

As part of NASA's Global Tropospheric Experiment (GTE), in situ ozone measurements aboard aircraft have been made from 1982 to present day. Each GTE field campaign systematically addresses a specific tropospheric chemistry issue which is important to the region of study and has global implications. For example, the impact of Asian outflow on Pacific air, the influence of South American and African biomass burning on tropical Atlantic air, and the degradation of dry-season air within the Amazon have all been studied. Individual campaigns provide a snapshot picture only for the region/event of focus; figure 101 is therefore a composite of ozone histograms obtained during July to November campaigns and provides an indication of "global" trends/influences. The data are for different years and altitudes of 3 to 8 km. The impact of Asian outflow on Pacific air is highlighted by a comparison of October (hatched) and March (solid) histograms at Guam and Hong Kong. March is a period of maximum Asian outflow and histograms show enhanced ozone. Similarly, for the tropical Atlantic–summer/fall dry-season outflow from South America and Africa results in ozone enhancements (compared with interior Amazon data) at coastal sites, over the ocean between the continents and, at times, near the southern tip of Africa. The solid-shaded Amazon histogram is wet-season data (no biomass burning). The Guam, Hong Kong, and Amazon histograms illustrate that seasonal trends are sizable and comparable to global changes. Northern latitude ozone is influenced by transport of pollution from the Soviet Union, Europe, and North America and natural stratospheric exchange. **(G. L. Gregory, 757-864-5834)**

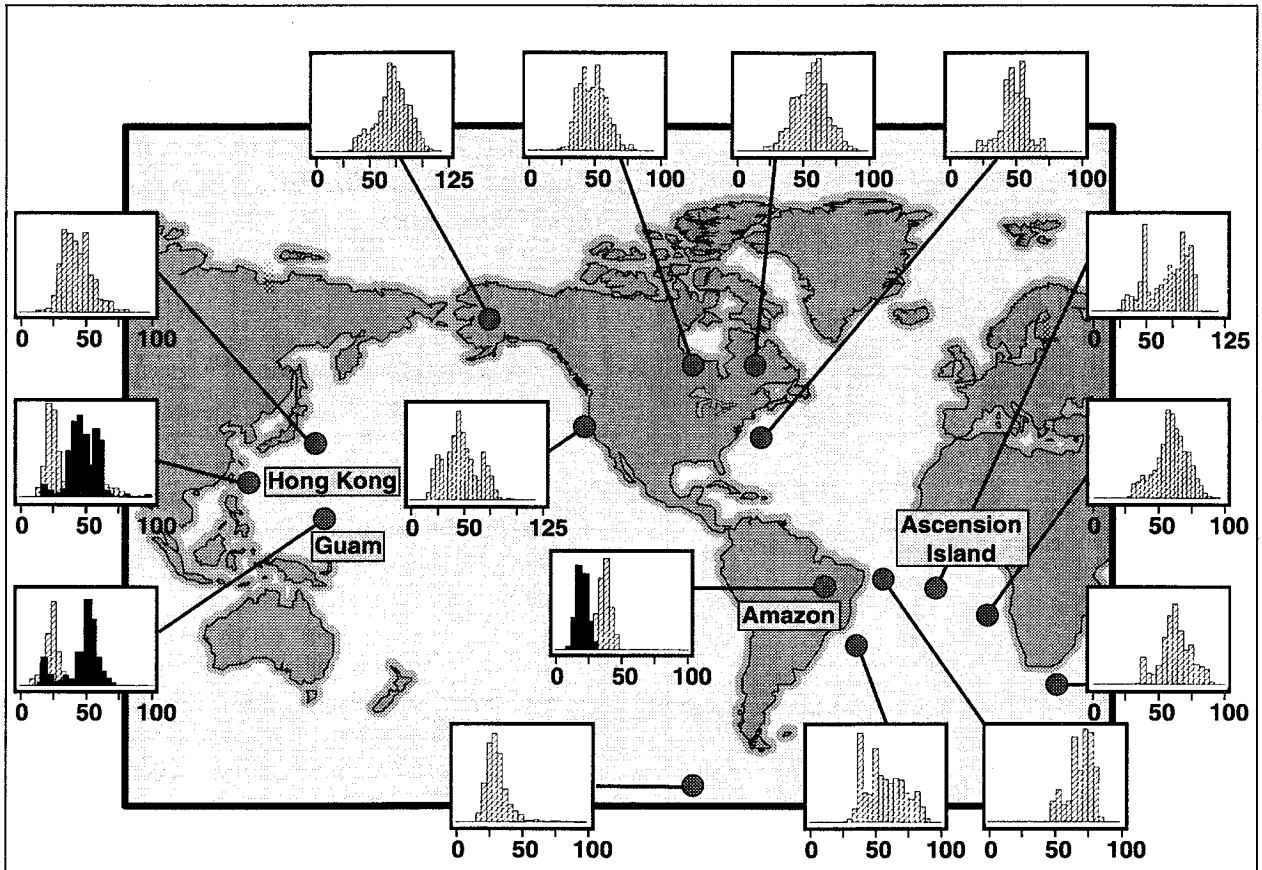

Figure 101. Tropospheric ozone data obtained from NASA aircraft measurements during July to November campaigns. Data are for different years and altitudes of 3 to 8 km above sea level. Each histogram represents ozone data (abscissa in parts-per-billion) from a GTE 4-week field campaign. Data are grouped in 4-ppbv-wide bands and the ordinate scales are proportional to the frequency of observation at each location. Hatched histograms are for the July to November campaigns. Solid histograms at Hong Kong, Guam, the Amazon, and Ascension Island are for other seasons as noted in the text.

High-Performance, Airborne Water Vapor Sensor

Water vapor plays an important role in atmospheric chemistry and radiative transfer, yet conventional sensors, principally chilled mirror hygrometers, do not meet the most demanding performance needs for airborne measurements. Existing sensors generally have slow response (seconds to minutes); may experience measurement artifacts associated with wall effects; and are insensitive at the low dew points (–60° to –90°C) that are encountered in the upper troposphere and lower stratosphere.

A new water vapor sensor based on a sensitive laser differential absorption technique has been developed and has flown during two atmospheric science campaigns (Pacific Exploratory Mission-West and the Vortex Ozone Transport Experiment) onboard the NASA DC-8 aircraft. This compact sensor consists of a window-mounted laser transceiver and a sheet of retroreflecting road sign material (50 × 50 cm) applied to the side of an outboard DC-8 engine (see fig. 102). Using small, communications diode lasers (1.4-μm wavelength) developed by AT&T Bell Labs, a differential absorption water vapor measurement is accomplished across the approximately 30-m (round-trip) external path. The inherently high performance of diode laser

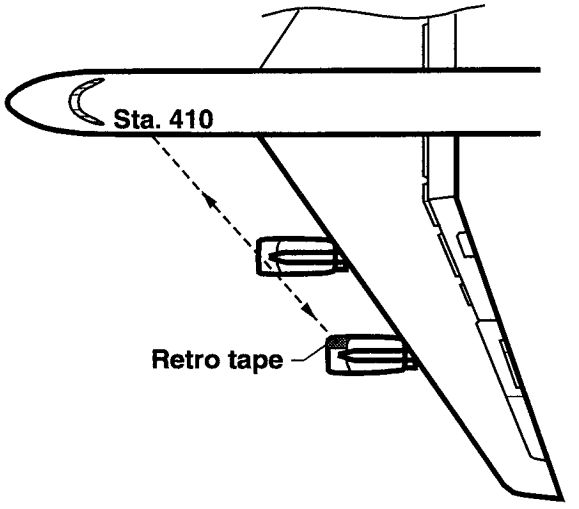

Figure 102. External path laser hygrometer.

spectroscopic techniques enables this sensor to simultaneously achieve fast response (50 msec) and high precision (a few percent) even at the lowest dew point temperatures expected within the altitude range of the DC-8 (ceiling of 41 000 ft). The external path also eliminates the potential of wall-induced instrument artifacts.

Organizations contributing to the development, evaluation, and operation of this state-of-the-art water vapor sensor include the Aerospace Electronics Systems Division of the NASA Langley Research Center, Lockheed Engineering & Sciences Company, Science and Technology Corporation, and the NASA Ames Research Center. **(G. W. Sachse, 757-864-1566)**

New Radiation Data Set for the Earth's Surface

Scientists from the Langley Research Center recently completed and distributed a satellite-derived shortwave (SW) solar and longwave (LW) thermal data set for the Earth's surface. Monthly-average values are provided for 6596 cells (280 × 280 km) over the globe. Both SW and LW results cover a longer time interval than previous data (8 years from July 1983 through June 1991) and provide the first monthly LW data set available to the global scientific community.

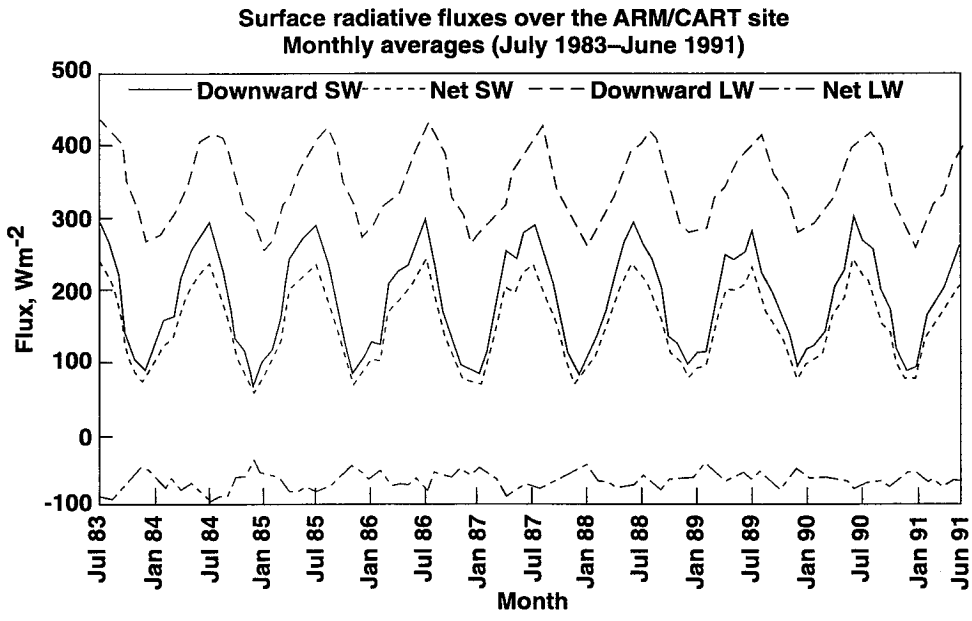

Figure 103. Eight-year time series of the monthly averages of downward and net SW and LW fluxes for the southern Great Plains ARM/CART site.

To date, 102 scientists or industrial users have obtained all or part of the data set from Langley over the internet or from a Langley-developed CD-ROM. Science uses are in support of both the U.S. Global Change Research Program and the Global Energy and Water Cycle Experiment (GEWEX) of the World Climate Research Program (WCRP). Industrial uses are related to the photovoltaic industry. Through the U. S. Department of Energy (DOE), the NASA satellite-derived data set may aid in improving the quality of life through solar-assisted electrification of remote villages in certain underdeveloped countries.

Typical results are shown in figure 103 for the southern Great Plains Atmospheric Radiation Measurement (ARM) Clouds and Radiation Testbed (CART) site in Oklahoma. The long-term satellite-derived data for downward SW and LW flux as well as net values (the amounts absorbed into the Earth's surface) are background information which can be used for testing climate models in this region of the globe. After refinement with more accurate satellite data, several Langley methods will be part of a cadre of algorithms used to produce a new 12-year GEWEX Surface Radiation Budget data product. **(C. H. Whitlock, 757-864-5675)**

The CERES/ARM/GEWEX Experiment (CAGEX) for Radiative Fluxes

Langley researchers have placed a virtual cage over a small area that is well-instrumented and have begun a long-term, collaborative effort to calculate, observe, and interpret the vertical profiles of radiative fluxes that drive the physics of climate. The CERES/ARM/GEWEX Experiment (CAGEX) is a component of the international Global Energy and Water Cycle Experiment (GEWEX) and uses measurements over the Department of Energy Atmospheric Radiation Measurement (ARM) site in Oklahoma. (See fig. 104.) CAGEX Version 1 now provides on-line access (*http://snowdog.larc.nasa.gov:8081/cagex.html*) to (1) satellite-based cloud properties and atmospheric sounding data that are sufficient for broadband radiative transfer calculations; (2) vertical profiles of radiative fluxes calculated with that data as input; and (3) validating measurements for broadband radiative fluxes and cloud properties.

Increasing concentrations of radiatively active atmospheric trace gases are expected to change the vertical profiles of shortwave (SW; solar) and longwave (LW; thermal infrared) fluxes, producing a warmer troposphere and cooler stratosphere. An observationally-based record of the full profile radiative fluxes is needed to investigate the role of radiation in hydrological and meteorological processes, to determine the forcings of aerosols and changing surface optical properties, and to validate physical models of climate. CAGEX is also used in prelaunch tests of algorithms for the retrieval of the vertical profile of SW and LW fluxes in the NASA Clouds and the Earth's Radiant Energy System (CERES) program. **(T. P. Charlock, 757-864-5687)**

Seasonal Carbon Monoxide Measurements in Free Troposphere

The Measurement of Air Pollution from Satellites (MAPS) experiment flew two missions on the Space Shuttle *Endeavour* during April 9–19, 1994, and September 30–October 11, 1994. Nearly 450 hr of carbon monoxide (CO) mixing ratios in the free troposphere were measured between 57°N and 57°S. Independent airborne measurements over North America and Australia were then compared with the 1994 MAPS data.

Figure 105 shows the data for the two 10-day flights averaged into 5° by 5° longitude areas. The sampling is nonuniform because of the presence of clouds and the shuttle track. During April, the CO mixing ratios are relatively uniformly distributed across the longitudes and the CO mixing ratios average 120 ppbv, decreasing through the tropics toward the South Pole where the CO values range between 45 to 60 ppbv. This near-global distribution is consistent with the lower rates of CO destruction during the late winter in the Northern Hemisphere, and a strong sink with evenly distributed sources in the tropics and the Southern Hemisphere. In October, the CO pattern is strikingly different with the mixing ratios north of 20°N decreased from about 120 ppbv in April to about 90 ppbv in October. The CO mixing ratios were high where the biomass burning occurred. The CO sources in the tropical regions were clearly identified as ground fires by both the astronaut crews and analyses of AVHRR data. South of 25°S, CO levels decrease to approximately 75 ppbv.

The combination of the middle tropospheric CO data from MAPS and the CO measurements made from the ground and from aircraft provide a unique seasonal depiction of the variability of CO in the lower atmosphere. These data, when combined with

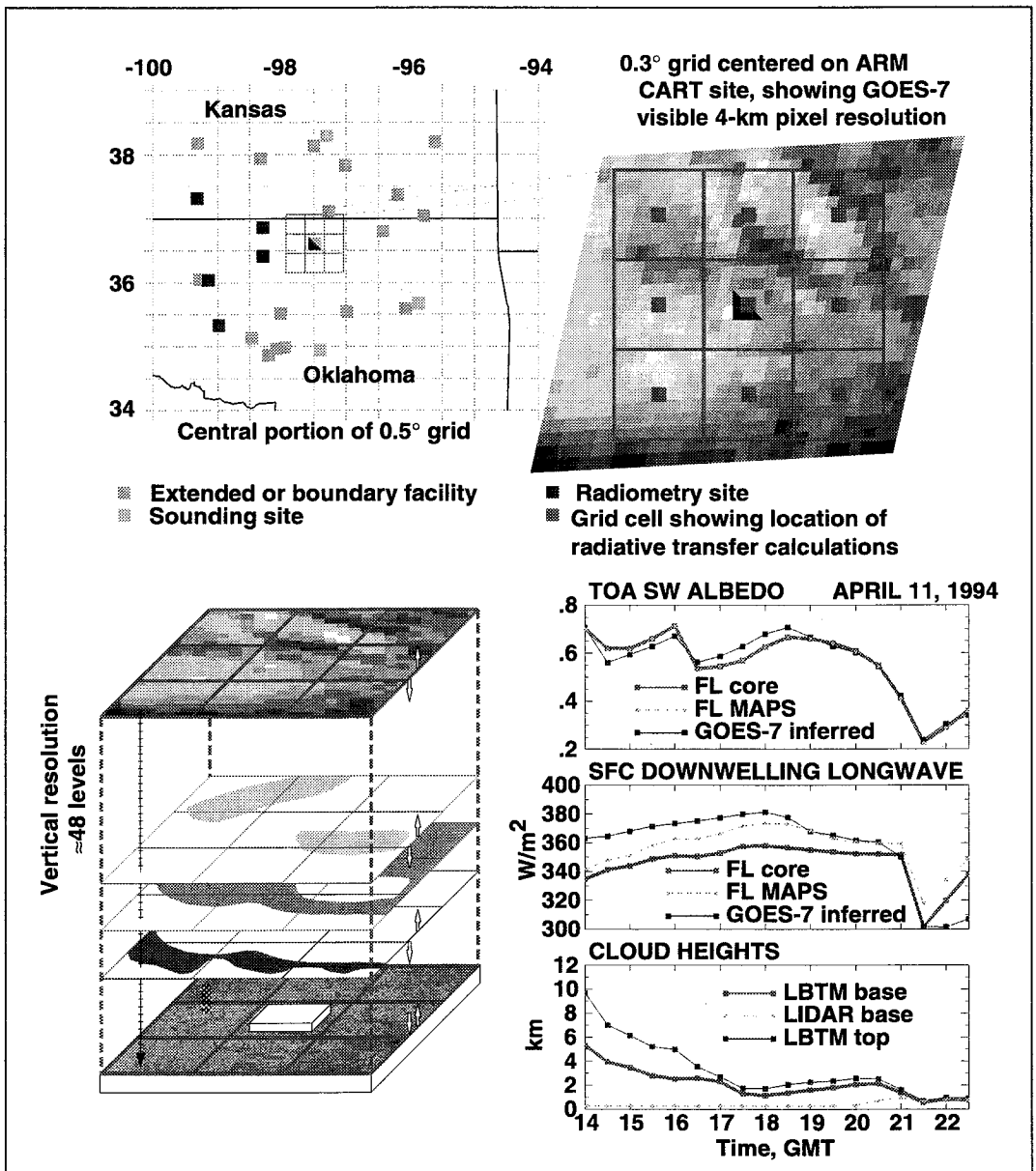

Figure 104. The CERES/ARM/GEWEX Experiment (CAGEX).

meteorological data and 3-D modeling, will significantly contribute to our understanding of the processes that control the CO distribution in the atmosphere.

The 1994 MAPS data are being archived at the Langley Distributed Active Archive Center of the Earth Observing System Data and Information System. The MAPS instrument has been reconfigured to fly on the Russian Space Station Mir during 1997. The new MAPS mission will last from 3 to 6 months.

(V. S. Connors, 757-864-5849)

Validation of LIDAR Atmospheric Sensing Experiment (LASE) Water Vapor Measurements

The Lidar Atmospheric Sensing Experiment (LASE) is an advanced laser remote sensing instrument developed at the NASA Langley Research Center (LaRC) for the measurement of atmospheric water vapor and aerosol profiles from a high-altitude ER-2 aircraft. LASE is the first fully engineered Differential

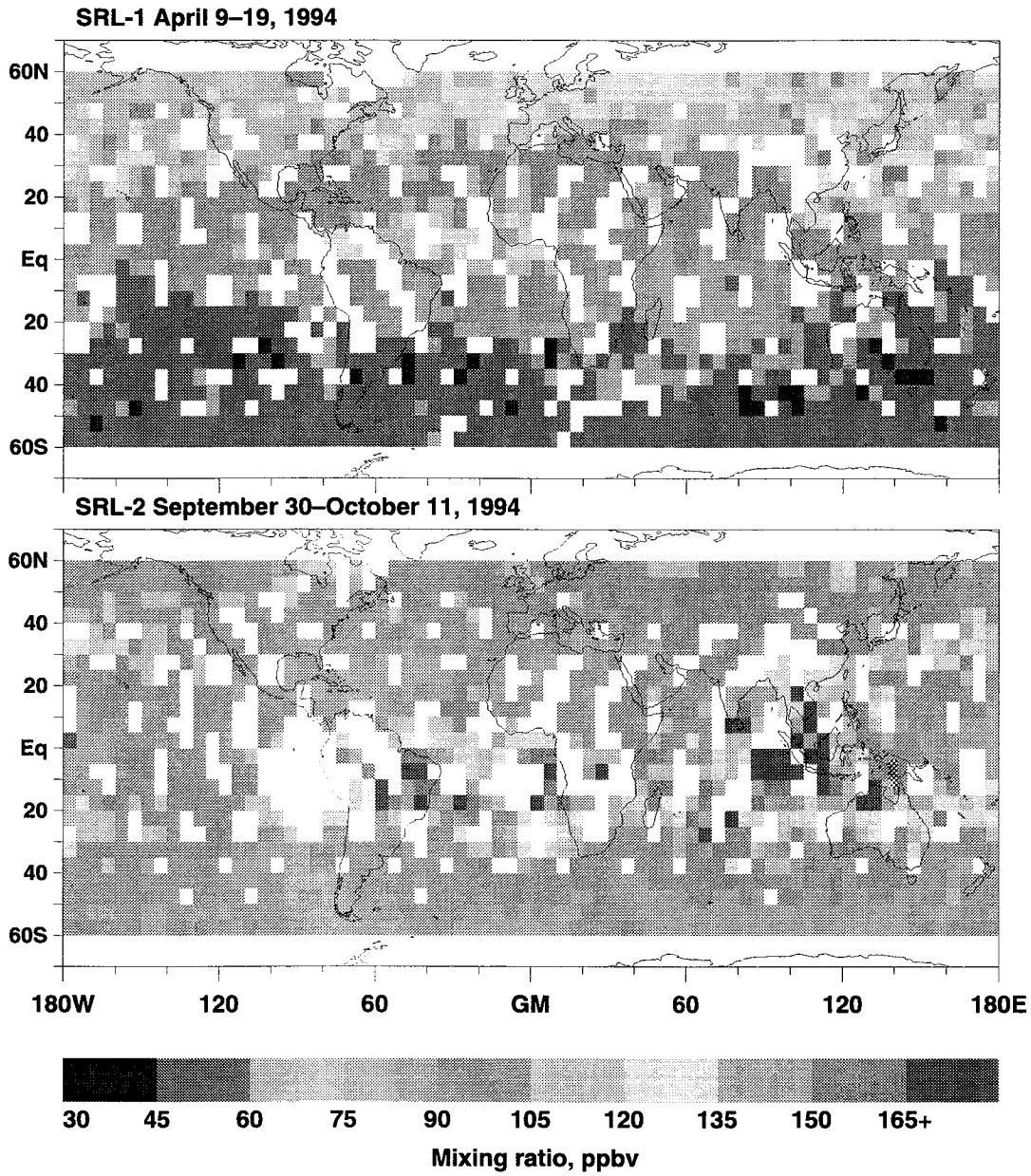

Figure 105. Measurement of air pollution from satellites.

Absorption Lidar (DIAL) system developed as a precursor to a space-based water vapor DIAL system. In September 1995, the LASE performance was evaluated during a comprehensive validation program at the NASA Wallops Flight Facility (WFF). LASE measurements of tropospheric water vapor were compared with other remote and in situ measurements of water vapor from the ground and from aircraft which underflew the ER-2. A NASA Lear Jet carried two different in situ sampling hygrometers; and a NASA C-130 was equipped with a second NASA LaRC airborne water vapor DIAL system and an in situ hygrometer for addition remote and in situ water vapor measurements. A number of radiosondes were launched, to make in situ

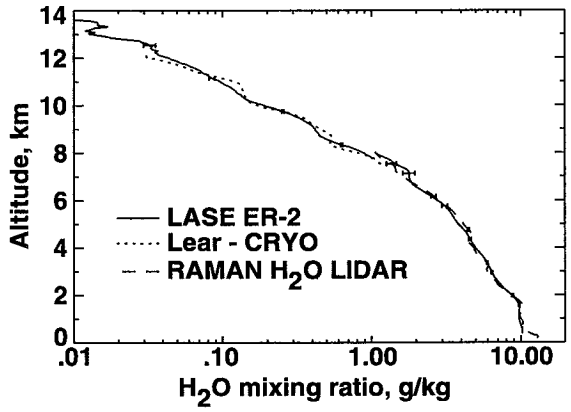

Figure 106. LASE water vapor measurements compared with in situ remote measurements.

water vapor profiles, coincident with the ER-2 flights and many of these sondes were part of a World Meteorological Organization balloon intercomparison campaign. The NASA Goddard Space Flight Center Scanning Raman lidar provided remote measurements from the ground. This LASE field experiment also studied many atmospheric processes including hurricanes, sea breeze development, and strat-trop exchange. Figure 106 shows the intercomparison of water vapor measurements from LASE with those from the airborne cryo hygrometer and the ground-based Raman lidar taken on September 12, 1995, during the LASE validation experiment. The high- and low-altitude LASE measurements were made at different times with a time separation of about 2 hr. The LASE system operated reliably and as shown in figure 106, the intercomparisons with other water vapor sensors showed excellent agreement. The completion of the development and validation of LASE has demonstrated lidar remote sensing technology applicable to space for the global measurements of lower atmospheric water vapor and aerosol profiles that affect many important global atmospheric phenomena. LASE will be used by NASA in future field programs to study a wide variety of atmospheric processes from hurricane development to cloud formation and radiation budget experiments.
(E. V. Browell, 757-864-1273)

HALOE HCl and HF Trends

The Halogen Occultation Experiment (HALOE) on the Upper Atmosphere Research Satellite (UARS) has

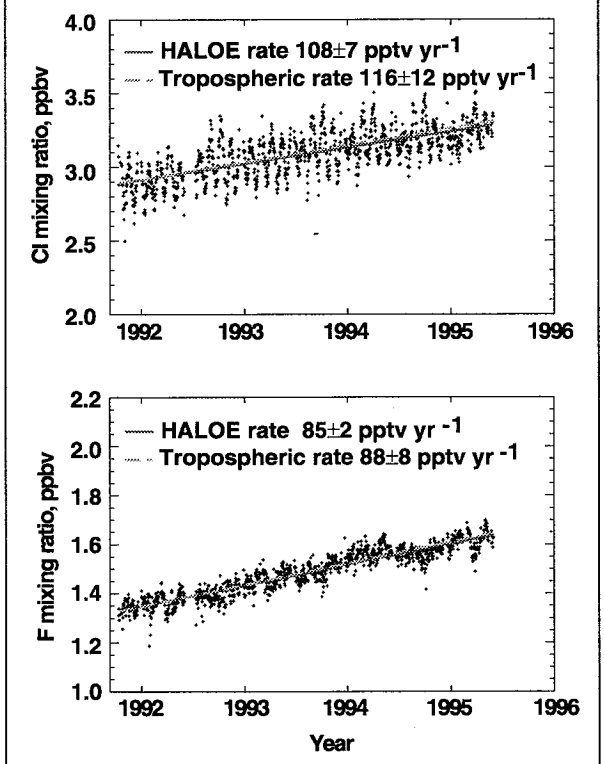

Figure 107. HALOE global average 55 km derived total Cl and F trends compared with tropospheric total Cl and F trends. The tropospheric starting value is normalized to the HALOE value at the start of the data record.

obtained key research results on the important question of the effect of continued use of chlorofluorcarbons (CFC's) on stratospheric chlorine loading. The CFC/chlorine link question has been addressed by the HALOE team using time series observations of hydrogen chloride (HCl) and hydrogen fluoride (HF) collected at 55-km altitude over a 3.6 year period and comparing these trends with trends of total chlorine and fluorine in the troposphere. Using 2-D model derived efficiency factors for conversion of HCl to total Cl and HF to total F, direct comparisons of satellite and ground based Cl and F data can be compared (fig. 107). The points in figure 107 are HALOE-derived Cl and F data, the solid lines are least-squares fits to the data, and the dashed lines represent tropospheric trends. The close agreement in trends (3 to 7 percent) clearly shows that CFC's strongly, if not completely, dominate chlorine inputs to the stratosphere. Also, total chlorine observed by HALOE at the end of the record (3.3 ppbv)

agrees with the total determined from ground based data to within 6 percent. The HALOE observed chlorine is 2.7 ppbv higher than the 0.6 ppbv it would reach if only the main natural source, CH_3Cl, is present. When these facts are considered collectively with observations showing that both Antarctic and Arctic ozone depletion is caused by elevated chlorine in the atmosphere, the inescapable conclusion is that the depletion is caused by continued use of CFC's.
(J. M. Russell III, 757-864-5691)

Middle Atmosphere Heating in Atmospheric Bands of Molecular Oxygen

The total diabatic heating in the middle atmosphere is frequently governed by numerous sources including heat generated through absorption of solar ultraviolet radiation by ozone in the Hartley band and by molecular oxygen in the Schumann-Runge band, and Schumann-Runge continuum, the Hertzberg band, and at Lyman-a wavelengths. In addition, up to seven exothermic chemical reactions may contribute to the total heating. Each of these individual heat sources may be rela-tively small, particularly in the middle mesosphere (65–80 km). However, the collective effect of a number of small terms is to create a locally significant amount of heat. A new study of the role of heating through the absorption of solar radiation by the atmospheric bands of molecular oxygen has recently been conducted. Molecular oxygen absorbs radiation in its two lowest lying electronic transitions: $O_2(^3S\text{Æ}^1D)$ at 1.27 mm (the infrared atmospheric band), and $O_2(^3S\text{Æ}^1S)$, with bands at 762 nm, 688 nm, and 629 nm, which are referred to as the A, B, and λ atmospheric bands. These bands are located in the near-infrared and visible portions of the spectrum.

The role of heating due to absorption of solar radiation in the A, B, and λ atmospheric bands of molecular oxygen was previously thought to be of importance only in the vicinity of the tropopause (10–18 km). However, this new study has found that heating in these oxygen bands is also significant in the middle mesosphere (60–80 km). The impact of the O_2 atmospheric band heating on the total heat budget is illustrated in figure 108 which shows the percentage increase in total diabatic heating (i.e., heating due to absorption of solar radiation and to exothermic chemical reactions) in the mesosphere as a result of including the O_2 atmospheric band contribution. As is shown in the figure, consideration of the O_2 atmospheric band increases the total

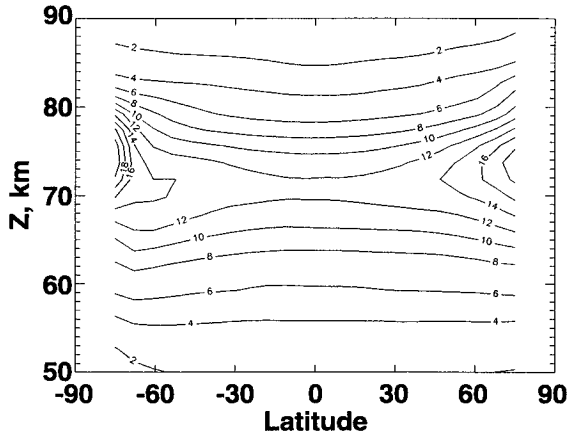

Figure 108. Percentage increase in atmospheric heating as a result of solar heating in the atmospheric bands of molecular oxygen.

diabatic heating by 5 to 15 percent between 60 and 80 km, and by 10 to 15 percent between 66 and 75 km. Heating in the O_2 atmospheric bands is therefore a significant component of the heat budget in the middle mesosphere. **(M. G. Mlynczak, 757-864-5695)**

Global Climatology of Stratospheric Aerosol Surface Area Density From SAGE II: 1984–1994

A global climatology of stratospheric aerosol surface area density has been developed using the multiwavelength aerosol extinction measurements of the Stratospheric Aerosol and Gas Experiment (SAGE) II for 1984–1994. (See fig. 109.) Stratospheric aerosols have been shown to be a key parameter in both high-latitude and mid-latitude chemical ozone destruction. The SAGE II climatology encompasses the injection and dissipation of aerosol associated with the June 1991 Mount Pinatubo eruption as well as the quasi-background (nonvolcanic) period of 1989–1991. The derived surface areas were validated by comparison with balloon-borne in situ measurements from the University of Wyoming optical particle counters. Cumulative median, 10-percentile, and 1-percentile surface area distributions for the 1984–1994 period have also been derived as a function of altitude and latitude that can be used to parameterize aerosol-driven

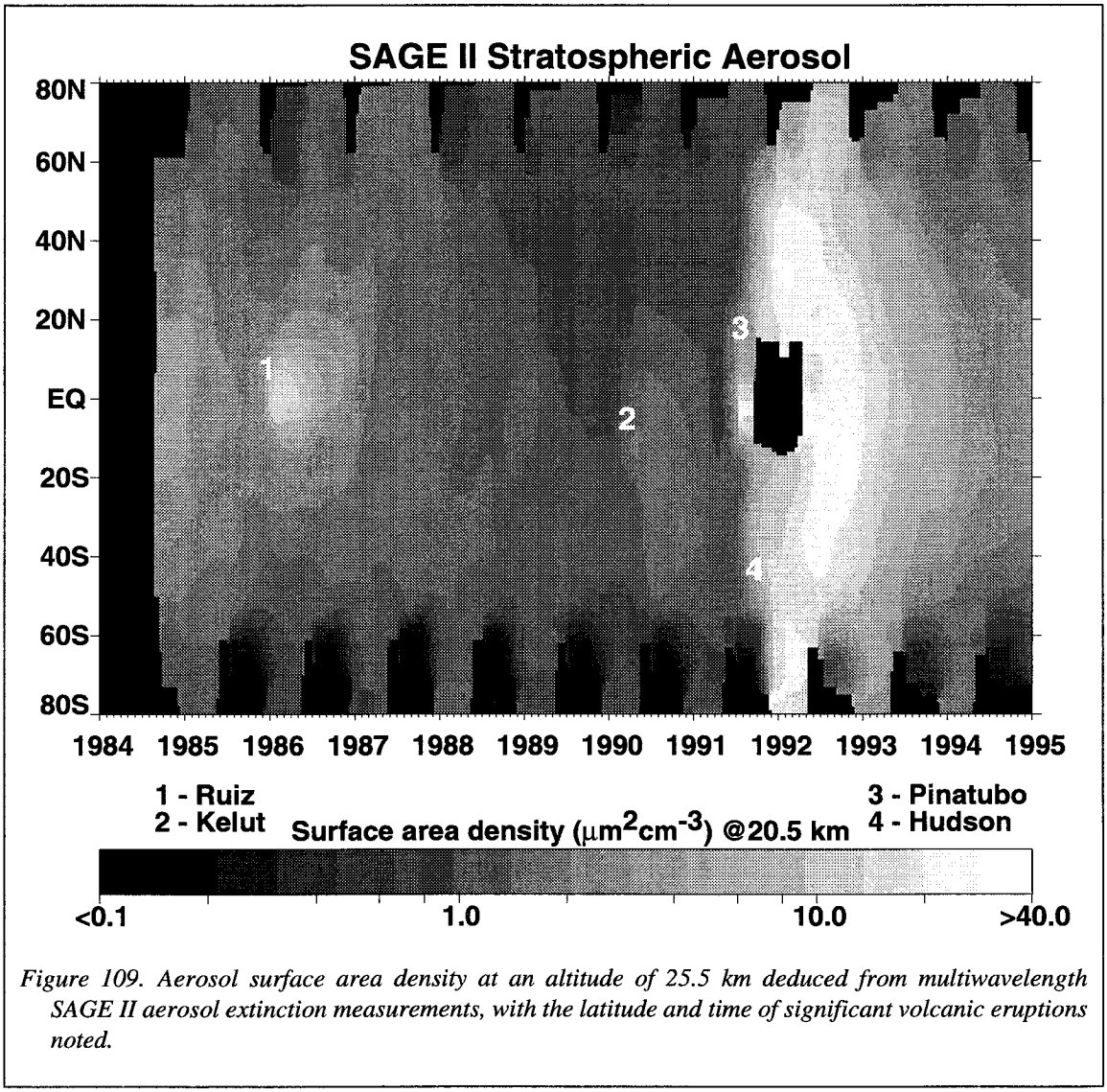

Figure 109. Aerosol surface area density at an altitude of 25.5 km deduced from multiwavelength SAGE II aerosol extinction measurements, with the latitude and time of significant volcanic eruptions noted.

heterogeneous processes in global photochemical models. A technique has also been developed for extending the SAGE II climatology using single wavelength extinction measurements by the Stratospheric Aerosol Measurement (SAM) II (1978–1994) and SAGE (1979–1981) instruments.

(L. W. Thomason, 757-864-6842)

SAGE II Studies of Upper Tropospheric Aerosols

Measurements from 1984–1991 by the spaceborne SAGE II (Stratospheric Aerosol and Gas Experiment II) sensor have been used to derive a global climatology for climatically important upper tropospheric aerosols. Other sources for data on these aerosols are quite restricted in either space or time, and they do not provide the high vertical resolution and sensitivity to small aerosol amounts offered by SAGE II. Figure 110 shows contour plots of zonally averaged aerosol extinction at a wavelength of 1.02 μm for 20° latitude bands between the equator and 60°N. Temporal and vertical resolution of the plots are 3 months and 1 km, respectively, and the white lines show the mean tropopause altitude. At low latitudes (Equator–20°N), there is relatively little influx of aerosol into the upper troposphere from either above or below, although there is some lingering descent in 1984–1985 of aerosol from the 1982 El Chichon volcanic eruption. In the 20°–40°N latitude

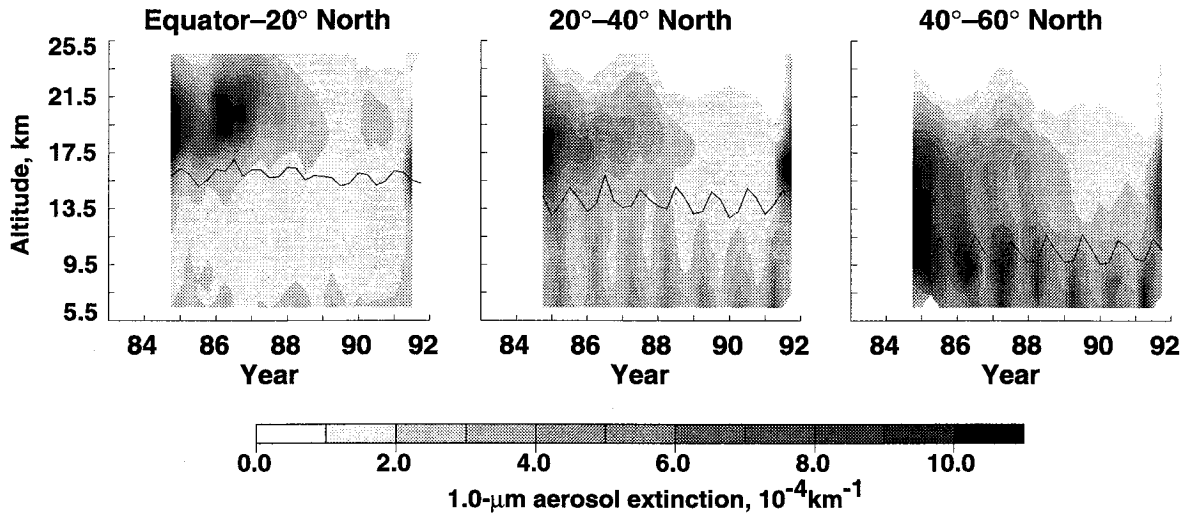

Figure 110. Zonally averaged SAGE II 1.02-μm aerosol extinction for the 6.5–24.5 km region from October 1984 through May 1991 at latitudes from the equator to 60°N.

band, descent of El Chichon aerosol into the upper troposphere extends from 1984–1986, and possibly until 1988. The 20°–40°N latitude band also shows a springtime movement of aerosol into the upper troposphere from below. These aerosols have the characteristic larger sizes of particles eroded from underlying desert regions. The 40°–60°N latitude band shows a complex pattern of both downward flux from the stratosphere and a significant upward flux from below. The aerosols moving upward are smaller than those seen at lower latitudes and appear to have been derived from anthropogenic sources. **(M. P. McCormick, 757-864-2669)**

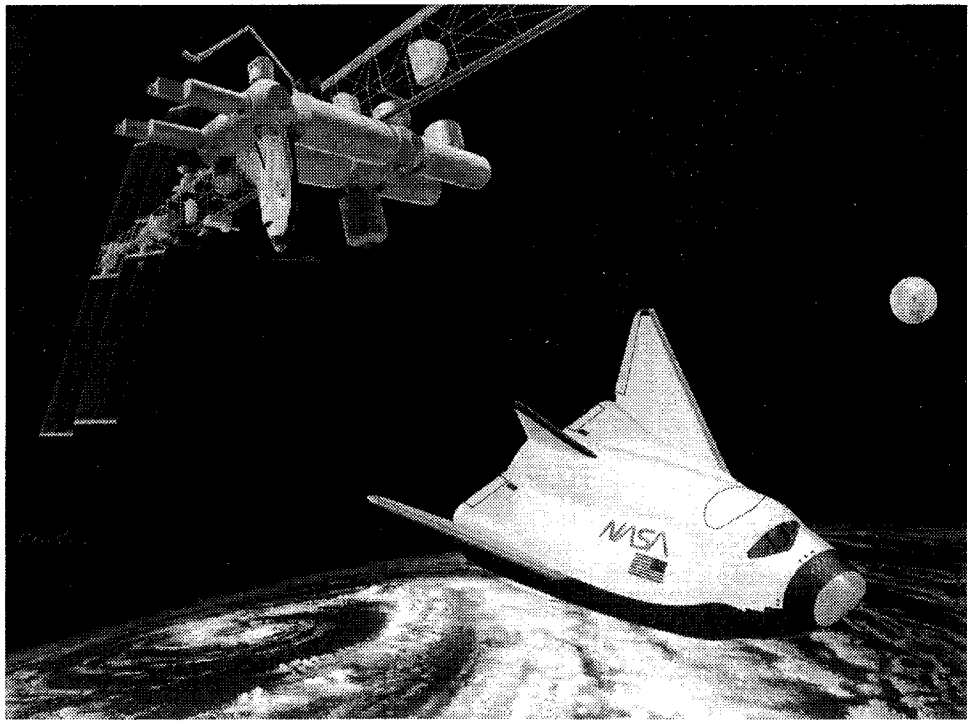

- *Increase human knowledge of nature's processes using the space environment.*
- *Explore and settle the solar system.*
- *Achieve routine space travel.*
- *Enrich life on Earth through people living and working in space.*

NUCFRG2: Nuclear Fragmentation Database Generator Software

Protective shields often are desirable or required on spacecraft to protect astronauts or electronic devices from damage by natural space radiations. These shields must be both light in weight and effective in radiation stopping power. Hence, optimum shield design requires an accurate knowledge of the transport of particulate radiation through materials and the transformation of that particulate radiation into smaller fragments within the material. This knowledge depends on solutions to complicated particle Boltzmann transport equations along with reliable atomic and nuclear databases. Hence, the ability to estimate the risk to astronauts or electronic devices depends on the quality of the nuclear database. In an analogous manner, the medical therapist using particulate radiation to kill cancer cells within the human body requires knowledge of the nuclear processes by which the ion beam interacts with and is transformed into nuclear fragments in body tissues. Therefore, the space systems engineer and the radiation therapist share common concerns regarding the adequacy of the nuclear fragmentation database.

The NUCFRG2 code is a software code that generates the nuclear fragmentation database. The code is based on experimental results from two groups involved in ion-beam therapy: Lawrence Berkeley Laboratory (LBL) and the Gesellschaft für Schwerionenforschung (GSI) facility in Darmstadt, Germany; it represents an improvement over the earlier version of the code, NUCFRG. Recently, a series of ion-beam experiments at LBL revealed an underestimation of the fragmentation production for aluminum and polyethylene targets, and GSI measurements with C, N, and O beams also revealed certain deficiencies in the then-current NUCFRG code. Explicit representation of the alpha particle knockout process has now been incorporated into NUCFRG to create the improved NUCFRG2 code. Good agreement with the GSI data is shown in figure 111. **(J. W. Wilson, 757-864-1414)**

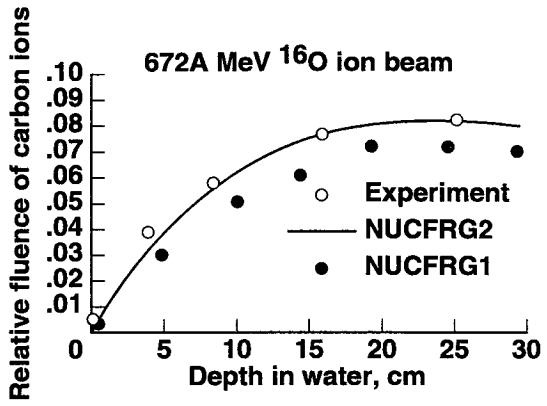

Figure 111. Secondaries produced by removal of two protons including alpha clusters for oxygen beam ion.

- *Create new scientific knowledge by exploring the Solar System and the Universe beyond and by studying the space environment and its effects on biological and physical processes.*

Archive System for Long-Duration Exposure Facility (LDEF)

The multiyear studies of the retrieved LDEF by hundreds of investigators have resulted in a large, unique, and valuable set of resources on the environments in low-Earth orbit (LEO) and the effects these environments can have on spacecraft and space operations. This set of resources includes: descriptive documentation of LDEF, the onboard experiments and the mission; data from the 57 onboard experiments and from the postretrieval studies of LDEF materials and systems by special investigation groups; approximately 15000 photographs of the effects of space exposure on typical spacecraft materials and systems; an index with abstracts for approximately 1200 LDEF-related publications; and descriptions of archived LDEF and experiment hardware that are available for study by researchers. The LDEF Archive System has been developed jointly by NASA and Boeing Aerospace Operations personnel to preserve this set of resources and to provide spacecraft designers and space environment and effects researchers a single-point access via the Internet.

The elements and organization of the LDEF Archive System are illustrated in figure 112. The system is structured from two perspectives—the type of information (e.g., photographs or hardware) or the technical discipline involved (e.g., ionizing radiation or meteoroids and man-made debris). The system is composed of both physical and electronic segments, which are maintained at a host of different locations. The electronic segments of the system are interconnected through the use of the World Wide Web (WWW) server and Mosaic client. The starting point is the system homepage, which presents descriptive information and hypertext words that the user may click on to progress to the specific parts of the system that are of interest. A user can thus browse through the system in a manner similar to paging through a book, or a user may go directly to specific pages of interest in the system by using the uniform resource locator (URL). An index of all the material in the physical archive is also maintained in an electronic segment of the archive.

Access to the LDEF Archive System on the Internet is through the NASA Langley Research Center homepage, which has the following URL: http://www.larc.nasa.gov/larc.html.

(W. H. Kinard, 757-864-3796)

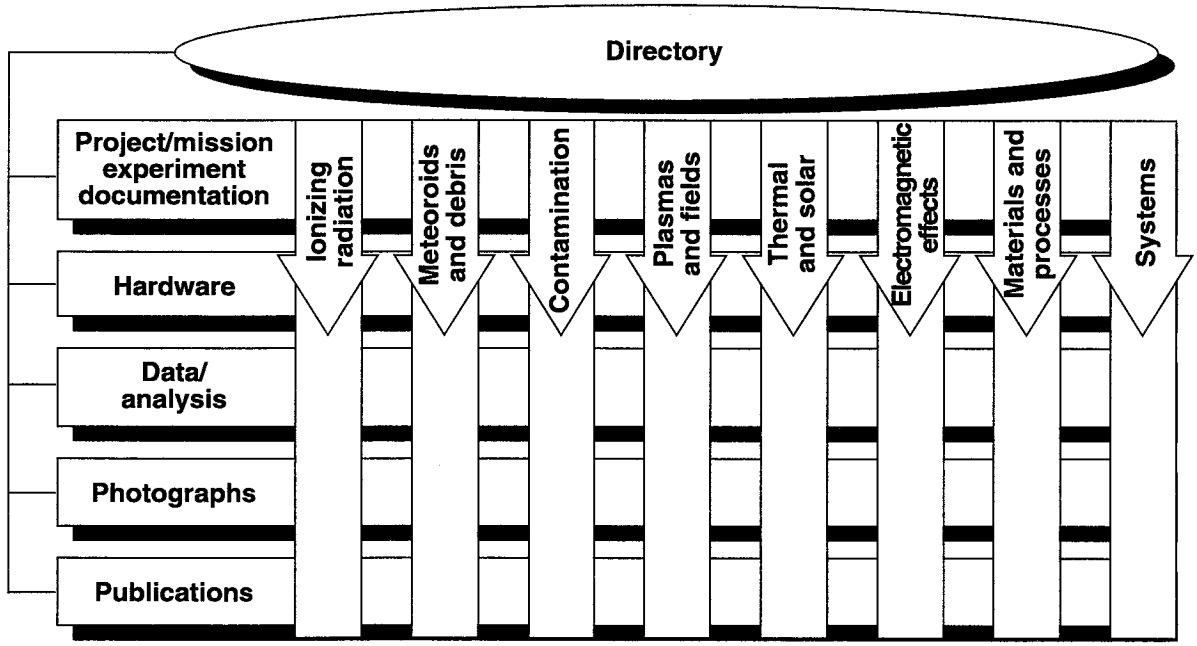

Figure 112. Elements and organization of archive system for Long-Duration Exposure Facility (LDEF).

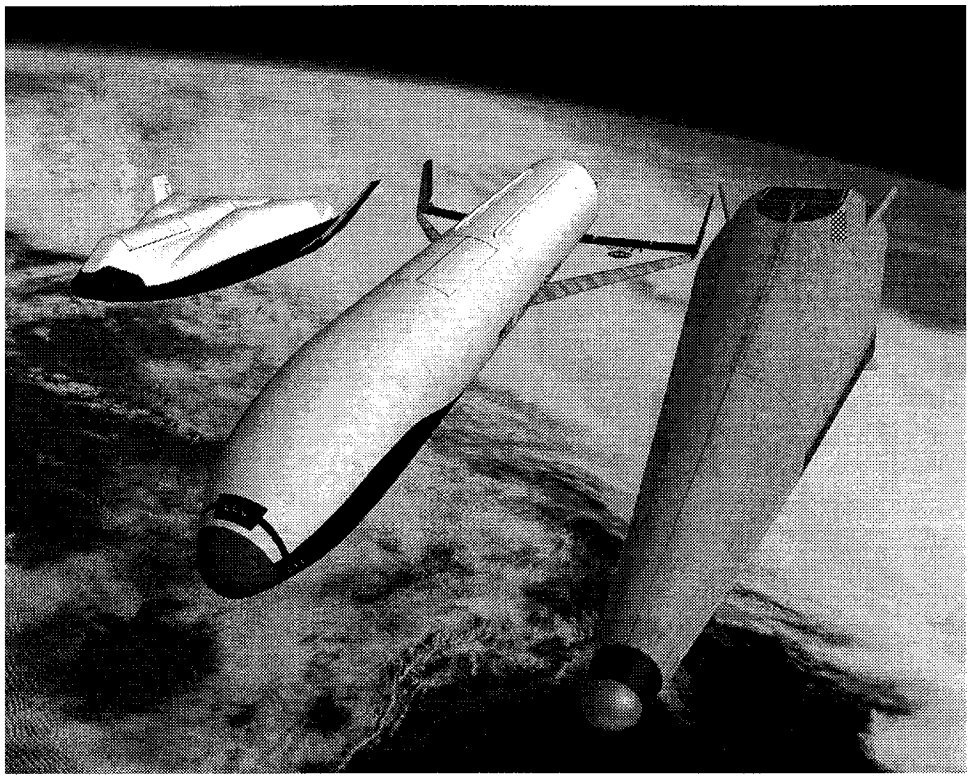

- *Reduce the cost of access to space.*
- *Provide innovative technologies to enable ambitious, future space missions.*
- *Build capability in the U.S. space industry through focused space technology efforts.*
- *Share the harvest of space endeavors with the U.S. industrial community.*

Recorder Interface Module (RIM)

The purpose of the Recorder Interface Module (RIM) is to provide an interface for data, command, control, and telemetry information between the payload instruments, and spacecraft computer and Solid State Recorder (SSR) of the "Lewis spacecraft." RIM formats data sent from the payload instruments, such as the Hyperspectral Imager (HSI), and the Linear Etalon Imaging Spectral Array (LEISA), over high speed wire interfaces to Lewis's SSR for storage. Also, RIM provides a means of sending command, control, and telemetry information from the spacecraft computer both to and from SSR using hardwire interfaces. (See fig. 113.)

In addition, RIM provides a 1553 interface from the spacecraft computer, and all payload instruments to the SSR. RIM accomplished this by the use of two Field Programmable Gate Arrays (FPGA's) and a 1553 Remote terminal chip. This work was done in support of the Small Satellite Technology Initiative (SSTI) mission, in which TRW and Langley Research Center participated in a Government/Industry cooperative partnership to develop the Data Management System on the Lewis Spacecraft. **(W. C. Wilson, 757-864-7105)**

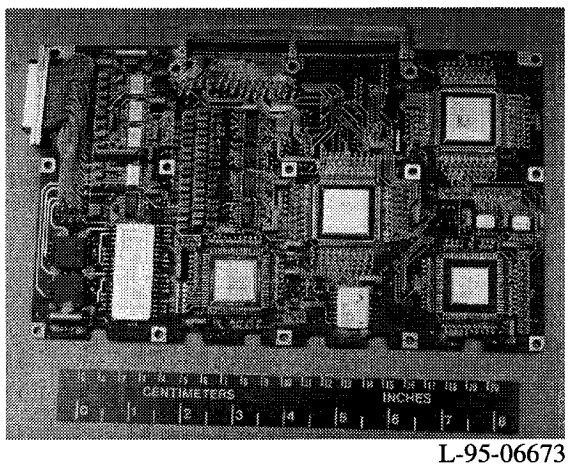

L-95-06673

Figure 113. Recorder Interface Module (RIM).

Multiwavelength Sequential Seeding Technique Used for Atmospheric Sensing

A new laser "seeding" technique has enhanced the capability of the Lidar Atmospheric Sensing Experiment (LASE) instrument to remotely measure water vapor, aerosol,s and clouds from the NASA ER-2 aircraft (65000 ft typically cruise altitude). This new approach that was demonstrated during ER-2 flights from the Wallops Flight Facility (September 1995) greatly simplifies operational aspects of LASE, increases the science impact of the data, and achieves an important step toward future space application of Differential Absorption Lidar (DIAL) systems.

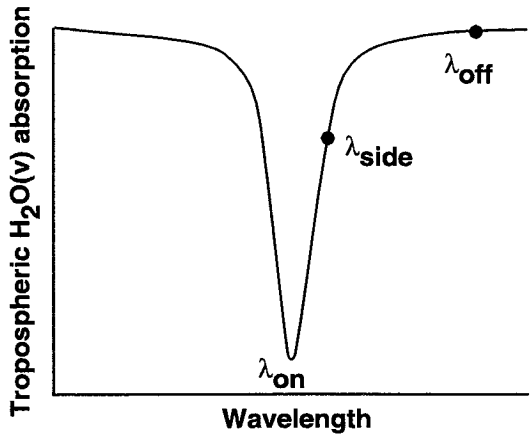

Figure 114. Multiwavelength sequential seeding method.

LASE uses a narrow linewidth (1 picometer) pulsed titanium-doped sapphire laser that is wavelength-seeded and tuned within the 813 to 819 nm water vapor ($H_2O(v)$) band by cavity injection of low power (mW) radiation from a small diode laser source. This precisely tunable diode laser seeds the pulsed laser alternately between λ_{on}, located at the center of the $H_2O(v)$ line, and λ_{off}, typically located 20 to 70 picometers away (see fig. 114). The λ_{on} and λ_{off} pulses are separated by 400 μsec and these $\lambda_{on}/\lambda_{off}$ pulse pairs are repeated every 200 msec. Because of the strong vertical gradient of atmospheric $H_2O(v)$, LASE has utilized strong lines to detect low $H_2O(v)$ concentrations at high altitudes and weak lines to detect the much higher concentration at lower altitudes. Operationally this has meant recording high-altitude $H_2O(v)$ profiles over some predetermined aircraft ground track, then retracing this ground track while recording low altitude $H_2O(v)$ data.

With the new multiwavelength sequential seeding approach (G. Sachse, L. Wang, C. Antill, S. Ismail, and E. Browell), an additional wavelength λ_{side} is used that is accurately positioned on the slope of a strong $H_2O(v)$ line (see fig. 114). In this new approach a single strong

$H_2O(v)$ line is used and the pulse pair $\lambda_{on}/\lambda_{off}$, which probes high altitude $H_2O(v)$, alternates every 200 msec with the pulse pair $\lambda_{side}/\lambda_{off}$, which probes lower altitude $H_2O(v)$. In this way, nearly simultaneous measurements of the atmosphere from sea level to 10 km is accomplished along a single ground track. This new capability substantially increases the science benefits of the LASE instrument and marks a necessary milestone prior to spaceborne application of $H_2O(v)$ DIAL systems. **(W. C. Edwards, 757-864-1555)**

Variable Geometry Truss Manipulator Arm System

The Langley Research Center is involved in a cooperative agreement, funded by the Department of Energy, with Battelle, Pacific Northwest Laboratory, and Oak Ridge National Laboratory, to develop a variable geometry truss (VGT) manipulator arm system to remove low-level radioactive hardware from nuclear facilities. (See fig. 115.) The VGT is a manipulator arm that weighs approximately 2300 lb, measures 13 ft in length, and tapers from a diameter of 46 in. at the base to a diameter of 32 in. at the tip. The three main components of the manipulator are the root VGT, a tapered static truss, and a tip VGT. The system will ultimately be mounted to RedZone Robotics's remotely operated vehicle to enable greater dexterity in the disassembly and removal of contaminated nuclear facilities.

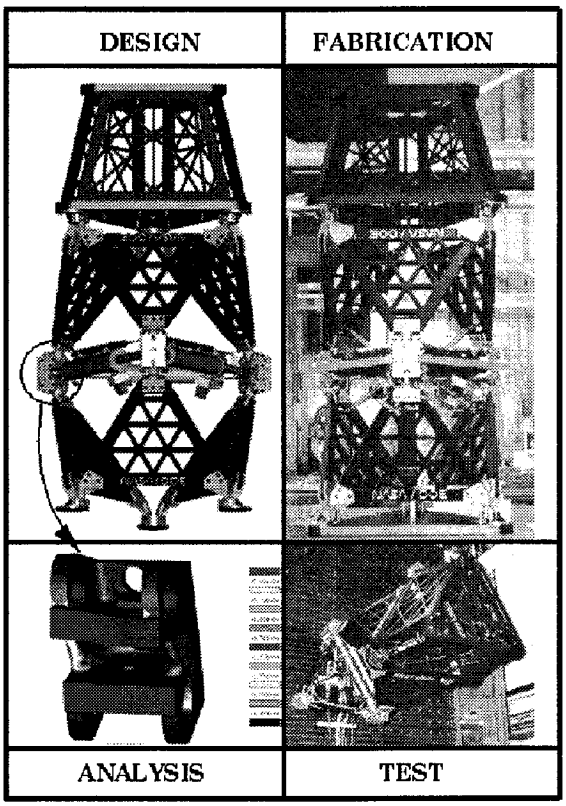

Figure 115. Variable geometry truss manipulator arm system.

The VGT is designed to support 2150 lb of load and 51000 in-lb of torque applied at the tip VGT with a safety factor of 2.5. The root and tip VGT can each rotate ±30° in either of two orthogonal planes and can each extend or contract in length. A wide range of motion, controllable through a single joystick, is made possible by this unique three degree-of-freedom design. Tight integration of design and analysis enabled the successful production of the VGT system. Detailed three-dimensional computer-aided-drafting (CAD) models were directly imported into sophisticated analysis codes to assess and reduce critical stress concentrations. Integration at the computer model level facilitated a rapid design/analysis cycle. The same CAD models were also electronically transferred to the fabrication facility for part production. The root VGT and static truss have been designed, built, tested, and shipped. **(E. L. Ahl, 757-864-7176)**

Thick Film Thermistor Elements

Thermistors (temperature sensitive resistors) are thermal sensors employed to monitor changes in temperature. These materials are semiconducting oxide ceramics which exhibit a linear decrease in electrical resistivity when exposed to a temperature increase. State-of-the-art thermistors are produced by tape casting small ceramic elements, typically 1 mm by 1 mm square, with thicknesses less than 15 μm. These elements must be individually fired at elevated temperatures to produce dense ceramic parts, leading to shrinkage variations in the resulting products. As the dimensions of the thermistors vary, the resistances also vary. These variations cause difficulties in sensor calibration, leading to the rejection of many parts.

An alternative method for producing thermistor elements utilized thick film fabrication processes to produce a multilayer device, providing the deposition of the thermistor and all electrical connections onto a single ceramic substrate. This technique greatly improves

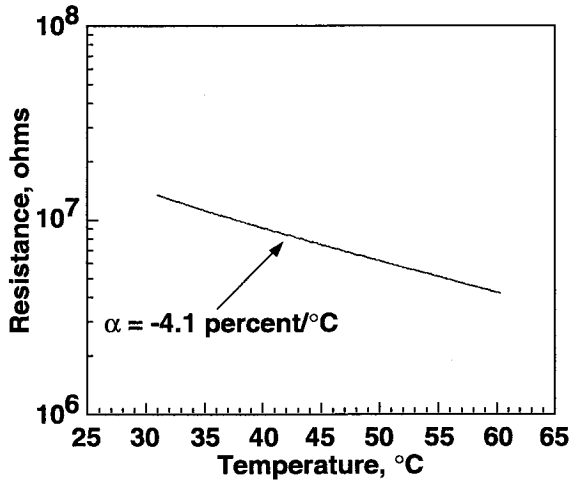

Figure 116. Resistance versus temperature data for a typical thick film thermistor element, exhibiting a 4.1 percent decrease in resistance per degree increase in temperature.

the part-to-part reproducibility by allowing rigid dimensional control of the thermistor element. Additionally, all electrical contacts and conductive paths are deposited by thick film processes onto the same substrate, thus eliminating the need for soldering wires to the fragile ceramic sensor and improving the ruggedness of the device. Finally, the production of thick film sensors allows ease of integration into hybrid circuits, which are also produced using multilayer fabrication processes.

Thick film thermistors deposited onto alumina substrates have been fabricated and tested. Figure 116 shows data for a typical thick film thermistor element. The sensor exhibited a thermistor coefficient α of –4.1 percent/°C, which is comparable to tape cast devices of the same composition. Additionally, the resistance values for thermistors produced by this process were within ±0.5 percent of each other, demonstrating process reproducibility.

(S. A. Wise, 757-864-8068)

High-Energy Diode Side-Pumped Cr:LiSAF Laser

For both aircraft and space-based missions, novel diode-pumped, solid-state lasers are projected to be the lasers of choice. One solid-state laser material,

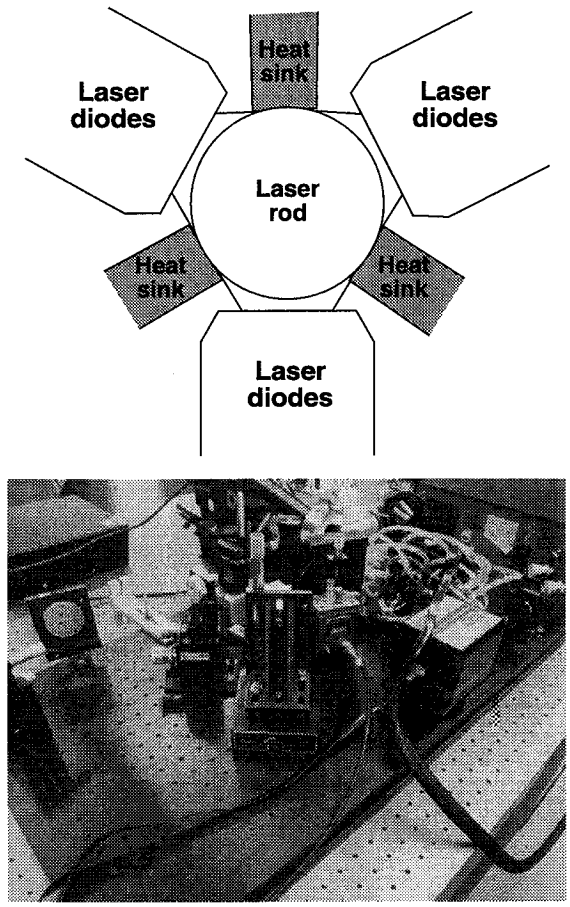

Figure 117. Side-pump configuration.

Cr:LiSAF, lases at wavelengths suitable for the measurement of water vapor and can be frequency tripled to monitor both aerosols and ozone. Recently, high-energy outputs and relatively high efficiencies have been demonstrated with flashlamp pumped Cr:LiSAF lasers. Although material quality and flashlamp heating of the material has limited the pulse repetition frequency to less than 5.0 Hz in high-power systems, the results achieved with flashlamps indicate that Cr:LiSAF-based laser systems can meet development goals.

Until recently, the low threshold, high-power visible laser diodes needed to side-pump Cr:LiSAF have not been available. However, NASA Langley has been working in conjunction with SDL, Inc., via a Small Business Innovation Research (SBIR) contract, to develop high power (360 W per array) GaInP/AlGaInP laser diodes at ≈670 nm to be used as pumping sources

for Cr:LiSAF. Flashlamps emit white light, which contains all of the wavelengths of the spectrum. Each wavelength that does not coincide with the usable region of the absorption band is converted to heat, thus introducing unwanted thermal deposits in the laser rod. Since the laser diodes emit a very narrow spectrum of light, which can coincide with the peak of the Cr:LiSAF absorption band, the majority of the emitted light can be converted to laser light, thus increasing the coupling efficiency.

Langley SBIR funding has also enabled Lightning Optical to develop the technology for the growth of higher quality (as low as 0.1 percent/cm scattering losses) LiSAF doped with various levels of Cr 3+. Laser performance was characterized utilizing a side diode-pumped scheme, in which three 680-nm laser diodes where placed at 120° increments around the laser rod (see fig. 117). The laser rod was held in place by the three heat sinks, which were water-cooled, and indium was used to provide a thermal contact between the laser rod and the heat sinks. The laser diode mounts were also water-cooled to maintain wavelength selection and to promote heat dissipation. The preliminary normal mode experiments featured a hemispherical resonator. Without any tuning elements inside the resonator, the output power obtained was 33 mJ. Since the resonator components were not optimized, the output beam was multimode. The resonator was acousto-optically Q-switched and attained pulsewidths of approximately 200 ns and a damage limited output energy of 2.5 mJ. The resonator was tuned via the use of a birefringent plate while the A-O Q-switch prism and the output coupler remained fixed. Consequently, the tuning range observed was from 780 to 900 nm.
(C. C. Johnson, 757-864-1553)

NASA Langley Demonstrates Compositional Tuning of Lasers

NASA Langley has developed new laser materials to enhance the remote sensing of water vapor. Currently, Ti:Al_2O_3 lasers operating around 0.815 μm are being used to remotely detect water vapor on the LASE mission. However, significantly stronger water vapor absorption features occur around 0.944 μm. Stronger absorption features allow the water vapor to be measured more accurately under dry conditions. The objective of the development effort is an efficient laser compatible with direct laser diode pumping which is capable of addressing these absorption features.

In collaboration with Scientific Materials of Bozeman, Montana, NASA Langley has demonstrated that Nd:YGaAlG is capable of addressing these absorption features. Scientific Materials grew these heretofore unavailable laser materials and NASA Langley performed spectroscopic and lasing experiments with these materials. By varying the Ga to Al ratio, the laser

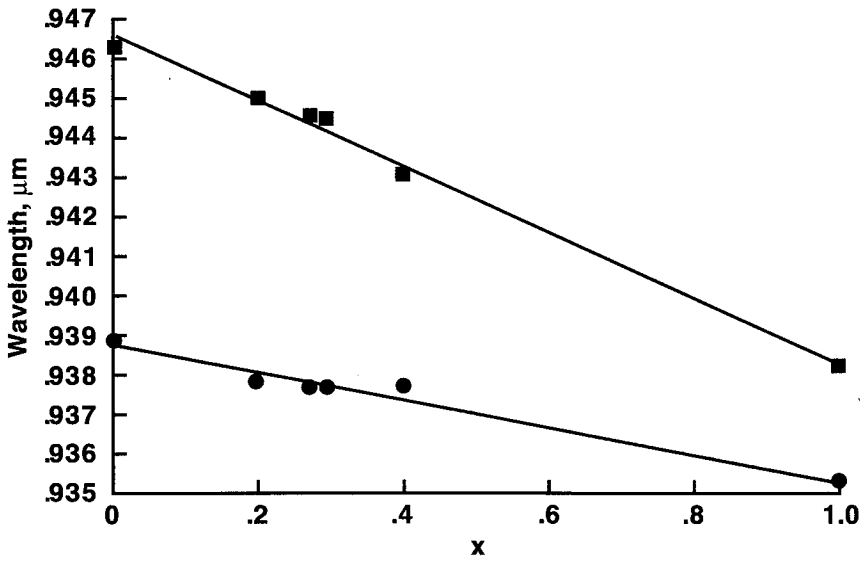

Figure 118. Emission wavelength of two Nd:YGa(x)Al(1-x)G transitions versus x.

can be tuned to the requisite wavelength. Usually compositional tuning is prohibited due to ionic valance and ionic radii considerations. However, in this case, compositional tuning was possible through a choice of laser materials based on a NASA Langley laser and spectroscopy model. The peak emission wavelength of two transitions in Nd:YGa(x)Al(1-x)G from YAG, x=0, to YGG, x=1, is shown in figure 118. As can be observed, the requisite wavelengths can be obtained.

Laser tests have demonstrated that this laser material can lase around 1.064 μm, the traditional Nd:YAG wavelength. A slope efficiency approaching 0.01 has already been achieved. Tests are proceeding with lasing around 0.944 μm. Results of this investigation have been presented in the Advanced Solid State Laser conference held in San Francisco in January 1996.
(N. P. Barnes, 757-864-1630)

NASA Langley Confirms 2.0-μm Laser Amplifier Performance

A series of models, developed at NASA Langley, to describe 2.0-μm laser amplifier performance has been confirmed with extensive experimental data. Dynamics of the 2.0-μm Ho:Tm lasers requires over 30 parameters to characterize the performance, many of which are not amenable to experimental measurements. To obviate this difficulty, NASA Langley developed a series of four models to calculate the required parameters and to predict the performance of the Ho:Tm laser amplifier. These models began with a quantum mechanical calculation of the transition probabilities and ended with a model of a quasi-four-level laser amplifier. Required input for the models consists of only published energy levels and the lattice parameters of the laser material. Given only these, the performance of a Ho:Tm laser could be predicted and optimized.

Extensive experimental results were used to confirm the predictions of the model. Data were gathered for Ho:Tm:YLF laser amplifiers with different Ho and Tm concentrations as a function of pump fluence. Different probe wavelengths and polarizations were also characterized. Results of the experiments agree quite well with the predicted performance. A sample of the results is shown in figure 119. With the experimental validation of the models, optimization of the laser performance can proceed with the high degree of confidence.

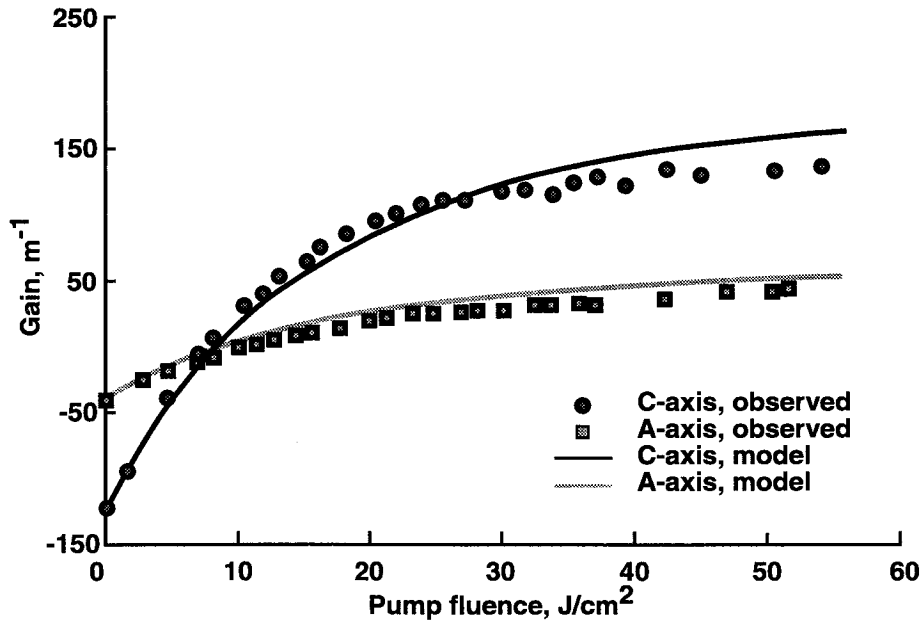

Figure 119. 2.05 μm gain in Ho:Tm:YLF.

Ho:Tm lasers are being employed to measure wind velocity for the Terminal Air Productivity Program. In addition, these lasers are prime candidates for global wind sensing instruments. A primary feature of these lasers is their nominally eyesafe wavelength. Eye safety is a primary concern for wind velocity measurements using the Doppler shift method since the laser beam is focused for more efficient heterodyne detection.

Results of the modeling effort and experimental work have been presented at the Conference on Lasers and Electro-Optics (CLEO) during 1995.
(N. P. Barnes, 757-864-1630)

Novel Method for Fabricating Adhesiveless Multilayer Flex Circuits and Cables

Electronic systems of the future for aeronautics and space applications will have to be smaller, lighter, require more efficient circuitry, and survive harsher environments. These electronic systems are increasingly becoming more complex, thus requiring denser circuitry and higher layer count (multilayer) circuits. To meet these needs, lightweight polyimide materials can be used to make one of a kind multilayer flexible printed circuits (FPC) and cables. (See fig. 120.)

Current means of fabricating multilayer FPC and cables involve bonding patterned FPC sheets together with a flexible bond ply adhesive. While adhesives are used to bond multilayer FPC and cables, they often create disadvantages such as: additional materials and processing cost, less flexible circuits, thermal mismatch between materials, greater Z-axis expansion, and an overall higher weight product. Adhesives also limit the chemical and environmental exposure of multilayer FPC and cables. Additionally, adhesives can promote wrinkling and voids in the FPC and cables leading to adhesion failure and ultimately delamination of the circuit or cable.

Most polyimide material used to fabricate FPC and cables is available only in the form of a film which necessitates the use of flexible bond ply to join the patterned films together to create multilayers. However, in the Microelectronics and Sensors Development Section, a technique for making completely adhesiveless multilayer FPC and cables has been developed by incorporating the use of a Langley developed polyimide material known as Langley Research Center-Soluble Polyimide (LaRC^{TM}-SI). LaRC^{TM}-SI's unique solubility characteristic allows it to be used as either a

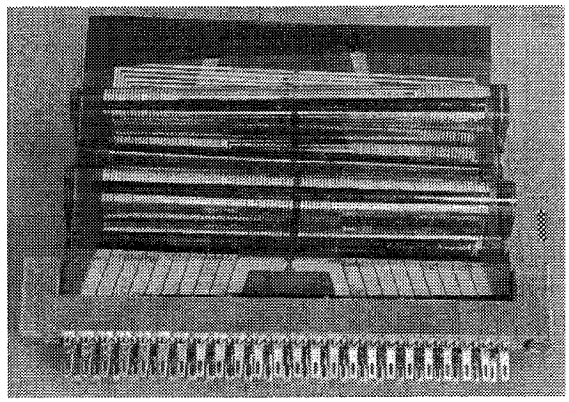

L-96-00413

Figure 120. Multilayer adhesiveless flexible cable.

solution or a film. Using LaRC^{TM}-SI in a solution form is the basis for being able to create adhesiveless multilayer FPC and cables. LaRC^{TM}-SI, in solution form, can be easily sprayed or cast directly onto a FPC or cable and when dried creates a self-bonding adhesiveless polyimide film.

Many advantages can be derived from fabricating adhesiveless multilayer FPC and cables some of which are: elimination of wrinkling and voids; lower materials and processing costs; decreased thermal mismatch between materials; higher temperature use; and thinner circuits and cables. All of these advantages result in an overall lighter end-weight product with higher performance. Utilization of LaRC^{TM}-SI to fabricate adhesiveless multilayer FPC cables can easily be incorporated into an already existing flex circuit operation and does not require the purchase of expensive processing equipment. **(N. E. Holloway, 757-864-7849)**

Enhanced Attitude Control System Experiment

The current practice in spacecraft attitude control design is based on single-input/single-output control strategy, wherein elementary and low-bandwidth controllers are designed for each of the three axes of the spacecraft separately. However, these controllers have limited performance because of their elementary nature and low bandwidth. Moreover, they are fairly hard to modify in their flight software implementation form. The enhanced attitude control system (ACS) experiment is an off-year technology demonstration experiment on NASA's small spacecraft technology initiative (SSTI) program's Lewis spacecraft to evaluate

advanced attitude control strategies. The purpose of the enhanced ACS experiment is to evaluate the feasibility of designing and implementing robust multi-input/ multi-output (MIMO) attitude control strategies for enhanced pointing performance of spacecraft to improve the quality of the measurements of the science instruments. The objectives of the experiment are:

1. To develop a MIMO ACS algorithm and flight software, and implement within the SSTI/Lewis flight onboard computer software

2. To develop MIMO attitude control designs, based on robust and modern control theory

3. To conduct attitude control experiments by implementing the MIMO control designs (instead of the baseline normal mode controller) in the normal pointing mode

4. To evaluate the performance of MIMO attitude control designs by analyzing the telemetry data

A novel and efficient algorithm, both in time and memory requirements, for the implementation of MIMO controllers has been developed. Two software implementations of the algorithms, in FORTRAN and C, have been developed and delivered to TRW, Inc., prime contractor on SSTI/Lewis spacecraft, for incorporation within the flight onboard computer software. MIMO attitude control designs for improved pointing performance have been developed for the Lewis/SSTI

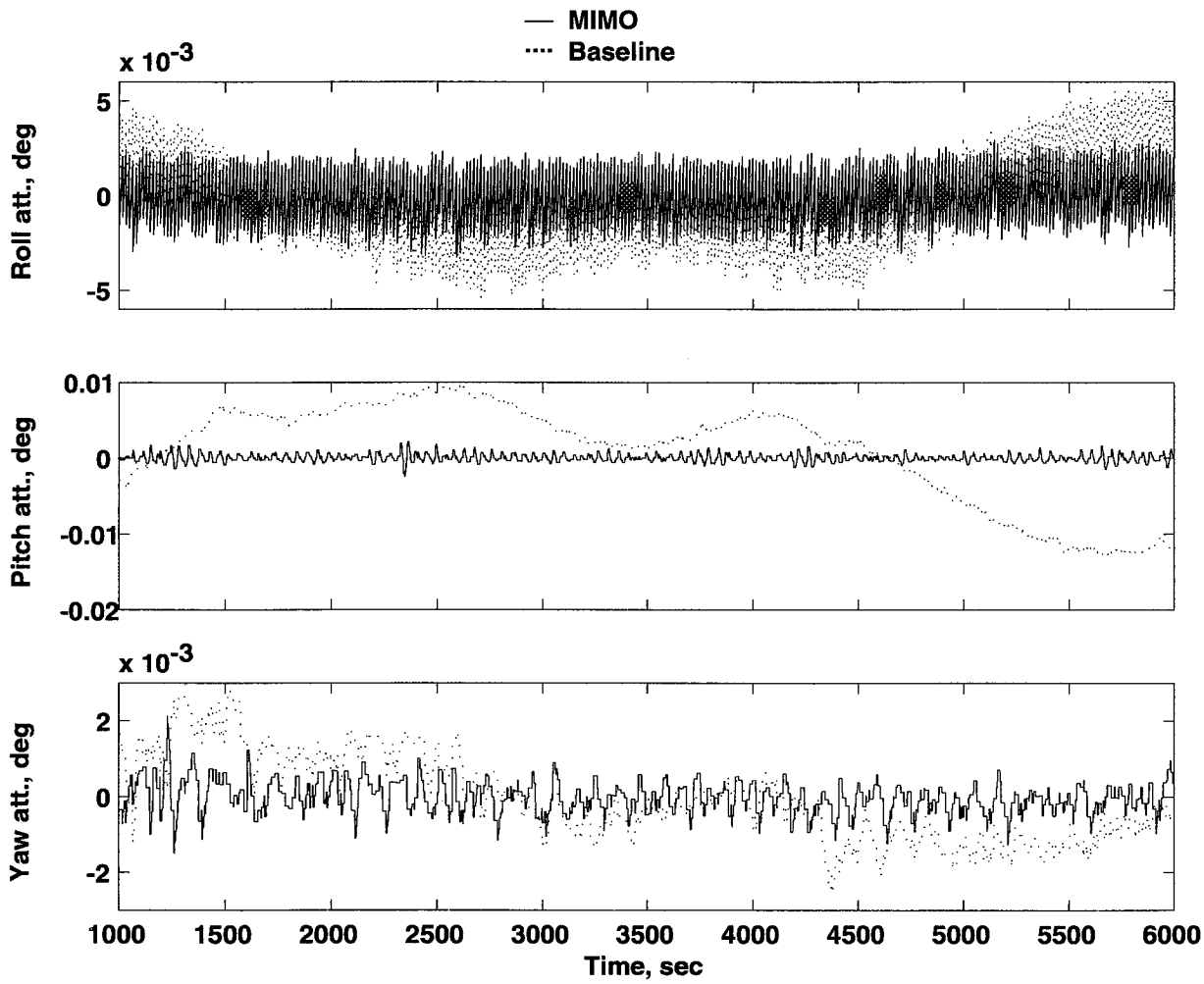

Figure 121. Response to environmental disturbance.

spacecraft and have been delivered to TRW. Simulations by LaRC and TRW (see fig. 121) have validated the MIMO algorithm and demonstrated that the MIMO controllers can improve the pointing performance of the spacecraft substantially. It should be noted that the various MIMO control designs are implemented by simply uploading the controller data sets into the MIMO routine, which also indicates the ease of modifying the controller with MIMO control. The design of MIMO controllers will continue until after July 1997, at which time the enhanced ACS experiments will commence. **(P. G. Maghami, 757-864-4039)**

Robust Control Design Framework for Substructure Models

Current technology does not allow structural testing of a large flexible structure designed for zero gravity in the $1g$ environment on the ground. If the structure is made up of smaller structures, however, they can often be tested independently in the laboratory and uncertainty models can be developed based on real test data. What is needed is a method to infer the characteristics of the assembled full structure from tests on the substructures and an understanding of the boundary conditions between the separate components. The work reported here has shown that robust control systems can be designed for the assembled structure directly from the substructure models and uncertainties, which can be based on laboratory testing.

The technique is based on combining a set of substructure robust control problems (SRCP). Figure 122 shows a general interconnected substructure where the triple, (P_i,Δ_i,k_i), denotes the nominal plant, uncertainty, and controller for ith SRCP. A block-diagonal substructure interface couples the SRCP. The dimensions of the block diagonality of interface coupling is dependent on the topology of the interconnections. The

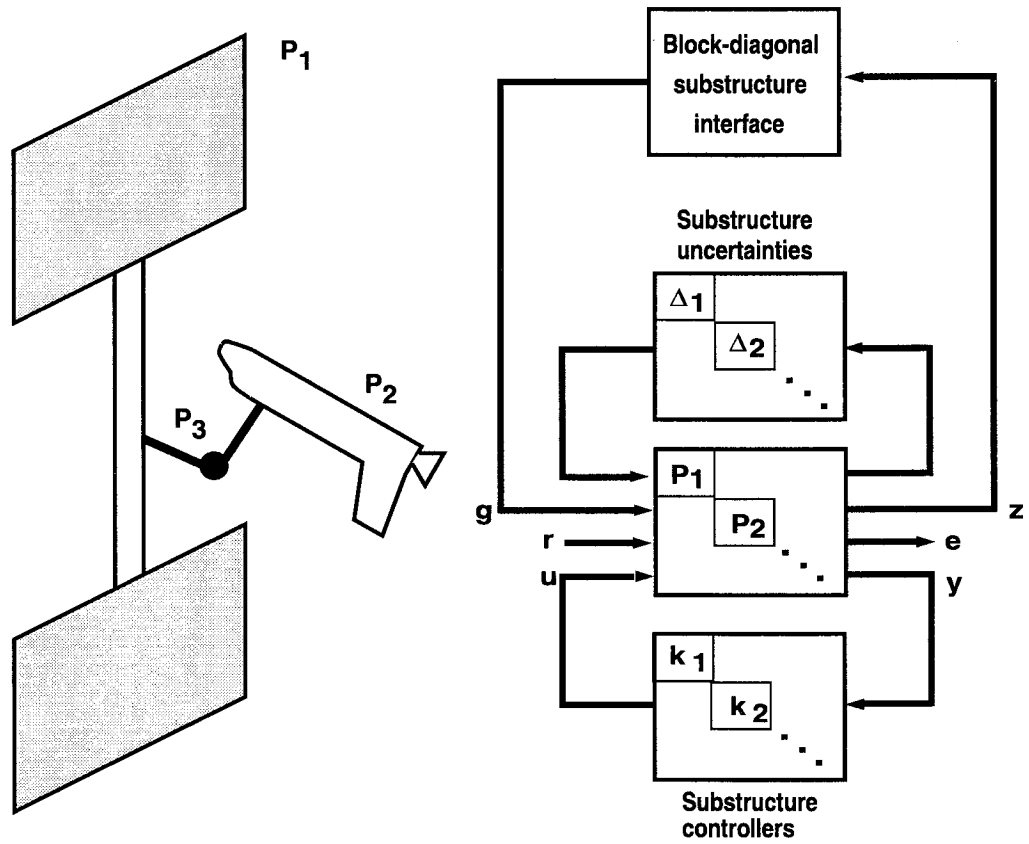

Figure 122. General coupled substructure robust control problem.

framework incorporates multivariable robust control methods to generate centralized or decentralized controllers that guarantee performance with respect to uncertainties in the interface stiffness, reduced component modes, and external disturbances. This framework takes advantage of the existing significant body of results in substructure modeling of large flexible structures and recent developments in multivariable robust control.

The new design framework developed in this study can reduce the dependence upon on-orbit system identification of the assembled structure by easier and less costly testing of substructures on the ground. This new approach also overcomes the limitation of control designs based on models of the assembled structure which cannot be experimentally validated prior to launch. **(K. B. Lim, 757-864-4342)**

Carbon-Carbon Spacecraft Radiator Panels by Rapid Densification Processing

Carbon-carbon composites comprise a special family of materials consisting of carbon fiber reinforcement within an all-carbon matrix. Although these materials afford such engineering benefits as low weight, high specific strength and modulus, zero moisture expansion, no outgassing, extremely high temperature stability (>3000°C), and other properties including high, tailorable thermal conductivity, these materials have not been widely utilized because of their long fabrication times and associated high cost. Through a contract with Lockheed Martin and their subcontractor, Textron Specialty Materials, NASA is exploring an innovative rapid densification processing method to markedly reduce fabrication time, and thereby also reduce cost.

Although a number of potential applications are being addressed under this contract, one application of particular importance is that of light-weight, highly thermally conductive panels for spacecraft radiators and for electronics thermal planes. As recently demonstrated by TRW Space & Electronics Group in an engineering trade study, spacecraft radiators employing carbon-carbon composite materials in place of conventional aluminum-based radiators can afford a greater than 55 percent weight savings, or can lead to significant cost savings by elimination of complex heat-pipes and their associated integration and testing costs.

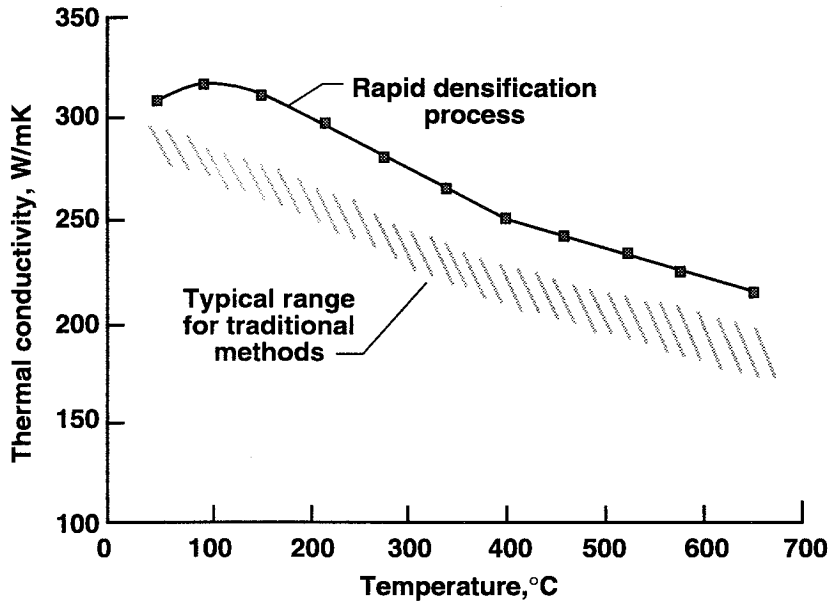

Figure 123. Thermal conductivity of carbon-carbon radiator facesheet by rapid densification process.

Figure 123 illustrates the excellent thermal properties achieved for carbon-carbon radiator facesheets fabricated by the rapid densification process in comparison with those fabricated by traditional methods. Densification time was 3 hr as opposed to several weeks for traditional methods. These results clearly demonstrate that high-quality carbon-carbon composites can be produced in a fraction of the time compared with traditional methods holding out the hope for significantly lower cost carbon-carbon composite materials. **(H. G. Maahs, 757-864-3498)**

Vibration Disturbance Rejection Demonstrated On-orbit

The Middeck Active Control Experiment (MACE) was successfully completed during Space Shuttle flight STS-67 in March 1995. Participants in the program were NASA Langley Research Center, MIT's Space Engineering Research Center, and Payload Systems, Inc. (PSI). MACE provided on-orbit validation of modern robust control theory and system identification techniques through the testing of a flexible, multi-instrument, science platform in the microgravity environment of the Space Shuttle's Middeck. The test article, shown in figure 124, was about 1.7 m long, weighed approximately 39 kg, and was instrumented with multiple actuators and sensors. The bus structure was composed of circular cross-section Lexan struts connected by aluminum nodes. At each end of the bus, a two-axes direct drive gimbal assembly was mounted. The gimbal assemblies acted as the payload at one end of the bus and as a multiaxis disturbance source at the other. During the experiment, a control strategy denoted "H-infinity design" was validated in the zero gravity (0 *G*) environment. In the H-infinity framework, robustness and performance requirements are specified using weighting functions and uncertainties. The control objective was to isolate a payload sensor from a 50 Hz bandwidth disturbance occurring on the test article. Controllers were designed with the use of finite-element models and also measurement models constructed from data by applying system identification techniques to open loop data obtained on orbit. Over 50 single-input, single-output and multi-input, multi-output, single and multiaxis H-infinity control designs were evaluated on-orbit. The experiment achieved all of the investigator's objectives. For example, up to 19 dB reduction in vibration levels and 25 Hz bandwidth of control were achieved. **(J. Woods-Vedeler, 757-864-2829)**

Reentry GPS Data Acquisition System

A Global Position System (GPS) data acquisition system was developed for the Multiple Experiment Transporter to Earth Orbit and Return (METEOR) reentry module. The GPS reentry system was designed to retrieve and store specific GPS parameters during the reentry portion of the mission in order to verify trajectory analyses and recovery locations. A complete stand-alone data package was developed employing a commercially acquired GPS receiver and antenna/preamplifier which was controllable by a small ruggedized PC/104 form-fit single board computer. Software/firmware was developed to boot-up the embedded computer, configure the GPS receiver, initiate GPS satellite acquisition, and store the acquired position data and status information in a nonvolatile memory asynchronously. (See fig. 125.) The system operated from 28 Vdc supplied by the spacecraft and contained all the required power converters and voltage regulators necessary to operate the system.

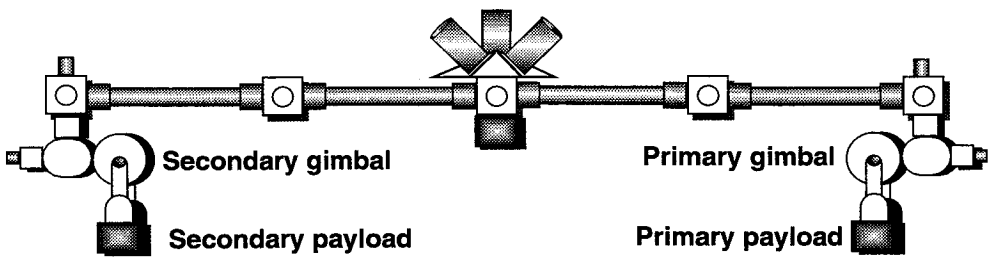

Figure 124. Middeck Active Controls Experiment (MACE) test article.

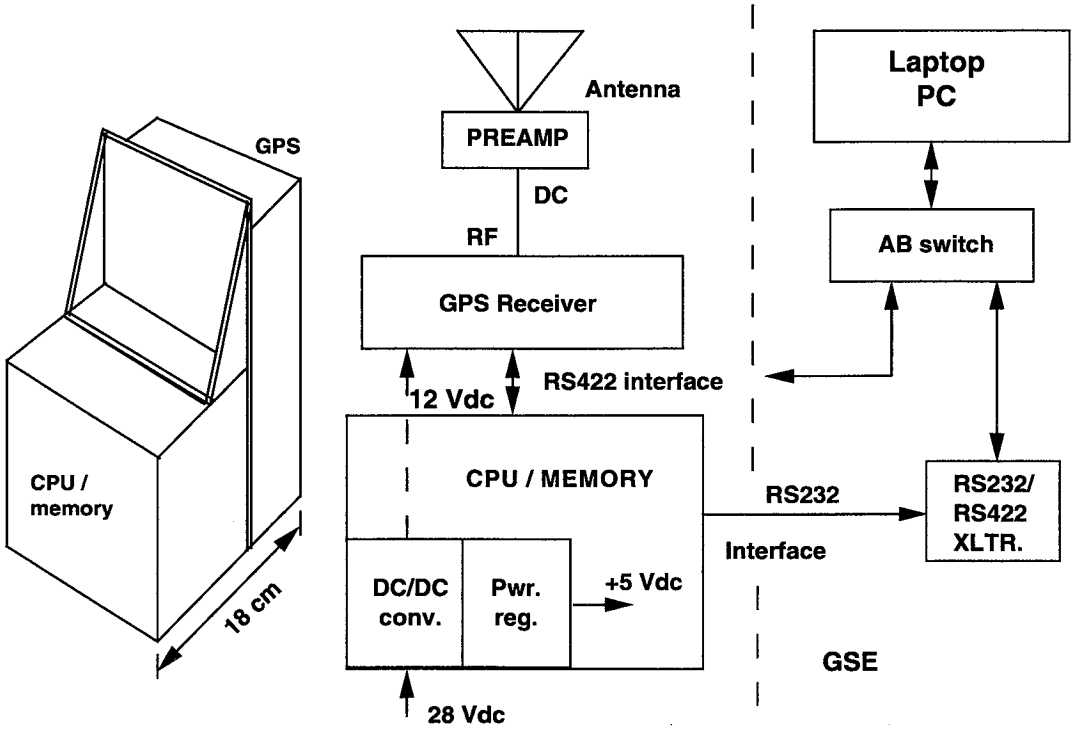

Figure 125. Reentry GPS data acquisition system.

The Reentry GPS data acquisition system is programmable and can be reconfigured to support other reentry missions as well as orbital missions. The system was designed, assembled, functionally tested, and integrated into the METEOR reentry module in about 12 weeks. The system was approximately 12 cm × 18 cm × 22 cm, weighed about 4 kg, and consumed less than 18 W of power.

The Ground Support System (GSE) consisted of a communications translator and control switch to enable the use of a laptop computer to interface with the Reentry GPS data acquisition system during laboratory integration and tests as well as to support field integration with the reentry module, prelaunch checkout, and last-minute mission parameter updates. **(N. C. Coffey, 757-864-8486)**

Aerothermodynamic Database for METEOR

In early 1995, at the request of the NASA Goddard Space Flight Center, Langley Research Center became involved in the effort for EER, Corporation, of Maryland to obtain a license to launch and recover a small satellite. In order to obtain the license EER, Corporation, had to demonstrate to the Department of Transportation (DOT) that a reentry vehicle (Multiple Experiment Transporter to Earth Orbit and Return, or METEOR), carrying a package of experimental instrumentation, would safely impact in the Atlantic Ocean off of Wallops Island, Virginia, after entering the atmosphere over the United States. The six-degree-of-freedom (6 DOF) analysis to be conducted by the Vehicle Analysis Branch (VAB) of the Space Systems and Concepts Division, to demonstrate the safe reentry, required an accurate set of aerodynamic characteristics of the entry vehicle, which previously had not been adequately defined or verified.

The Aerothermodynamics Branch (AB) of the Gas Dynamics Division undertook an extremely fast paced program to generate the required aerodynamic characteristics across the entry Mach number range using a combined computational and experimental approach. A sample computational simulation is illustrated in figure 126. In a period of less than 3 months, a wind-

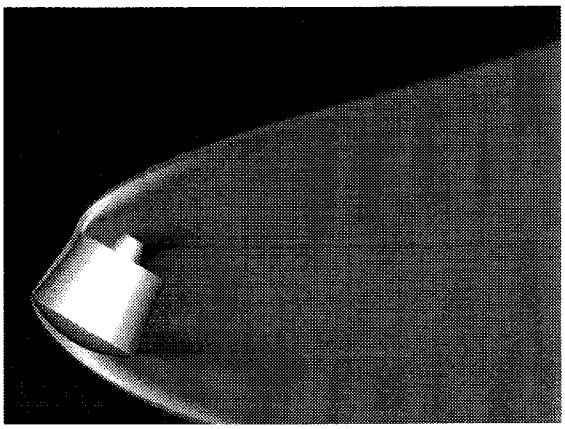

Figure 126. Pressure contours over the METEOR vehicle at Mach 25 and α = 60°. (Surface pressure and skin friction are integrated over the complete vehicle to determine aerodynamic coefficients.)

tunnel model was fabricated and tested at both Mach 6 and 10, surface and volume grids were generated, and computational results were obtained for both continuum and rarefied conditions. Direct Simulation Monte Carlo (DSMC) codes provided the rarefied flow aerodynamics for simulation of the high altitude, high Mach number, initial entry into the upper atmosphere. The Langley Aerothermodynamic Upwind Relaxation Algorithm (LAURA) code provided continuum aerodynamics and aeroheating from entry Mach numbers down to low supersonic Mach numbers, where, from a safety of impact perspective, the entry is over and there was no need to examine the subsonic/transonic characteristics of the METEOR. These computational results were complimented with experimental aerodynamics from both the 20-Inch Mach 6 and 31-Inch Mach 10 Tunnels.

This extensive aerodynamic database allowed the VAB to predict the proposed entry trajectory, and modify the timing of the deorbit burn to ensure the safe impact off the Virginia coast with sufficient confidence that the DOT issued the license for launch and recovery. **(P. A. Gnoffo, 757-864-4380)**

Multidisciplinary Optimization of Investment Strategies for Space Launch Vehicles

Efforts are underway to develop a new generation of launch vehicles that decrease the cost of space access.

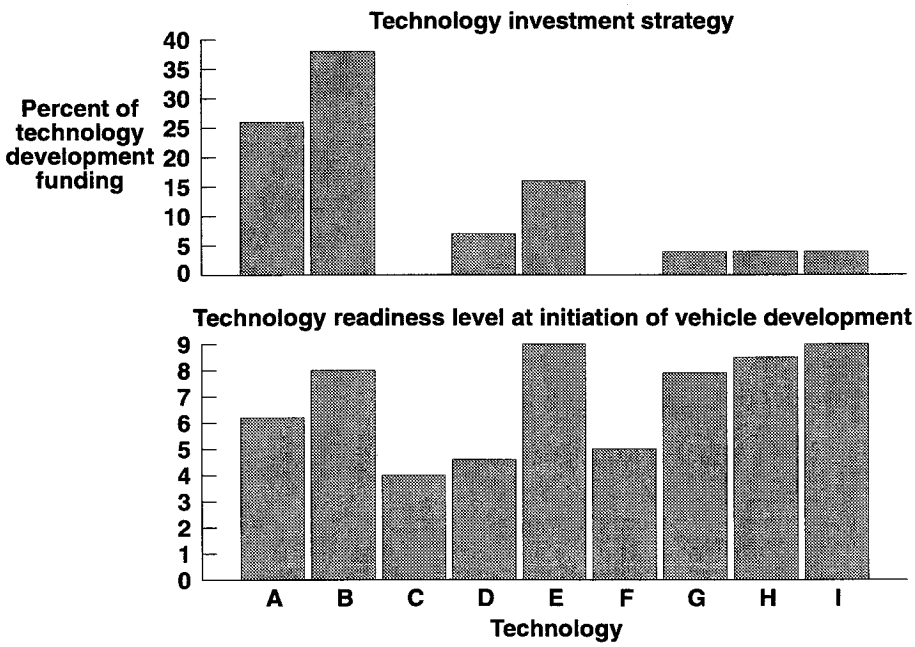

Figure 127. Optimized technology development program.

Many of these studies involve fully reusable vehicles or largely reusable elements, which, in-turn, require the maturing of numerous technologies. To date, the design efforts within NASA have been done by assuming a set of technology characteristics, designing the "optimal" vehicle with these technologies, and then determining the cost of this vehicle. In this process, costing occurs outside the design loop, i.e., cost does not influence the design process.

The use of multidisciplinary optimization (MDO) techniques allows for technology cost models to be included with the traditional disciplines of performance, weights/sizing, geometry, aerodynamics, and structures in the design loop. To demonstrate the effectiveness of using MDO, the investment strategy required to minimize the vehicle development cost of a reusable launch vehicle was determined. Figure 127 shows this optimal investment strategy for a candidate launch vehicle. The figure uses the NASA Technology Readiness Levels (0—basic principles observed, 6—model or prototype demonstrated in relevant environment, and 9—actual system "flight proven") to characterize technology maturity. Note that the optimal technology maturation strategy does not have all technologies developed to the same level. If the available funds were used to develop all technologies to level 6, the savings in vehicle development cost would be 43 percent over the strategy of no technology development. The optimal investment strategy, shown at the top of the figure, resulted in a savings of 53 percent; thus an optimal investment strategy can result in significant savings. **(A. A. Moore, 757-864-4407)**

Polymeric Precursor Oxidation Protection System

Carbon-carbon composites, the materials most widely used for high-temperature thermal protection systems on hypersonic reentry vehicles, require coatings to reduce the rate of oxidation. Two methods have traditionally been used to coat these materials: Chemical vapor deposition (CVD), where silicon carbide or silicon nitride is deposited as a coating from the gas phase; or pack conversion, where the materials are packed in containers containing powders which will react with carbon at high temperatures to form SiC coatings.

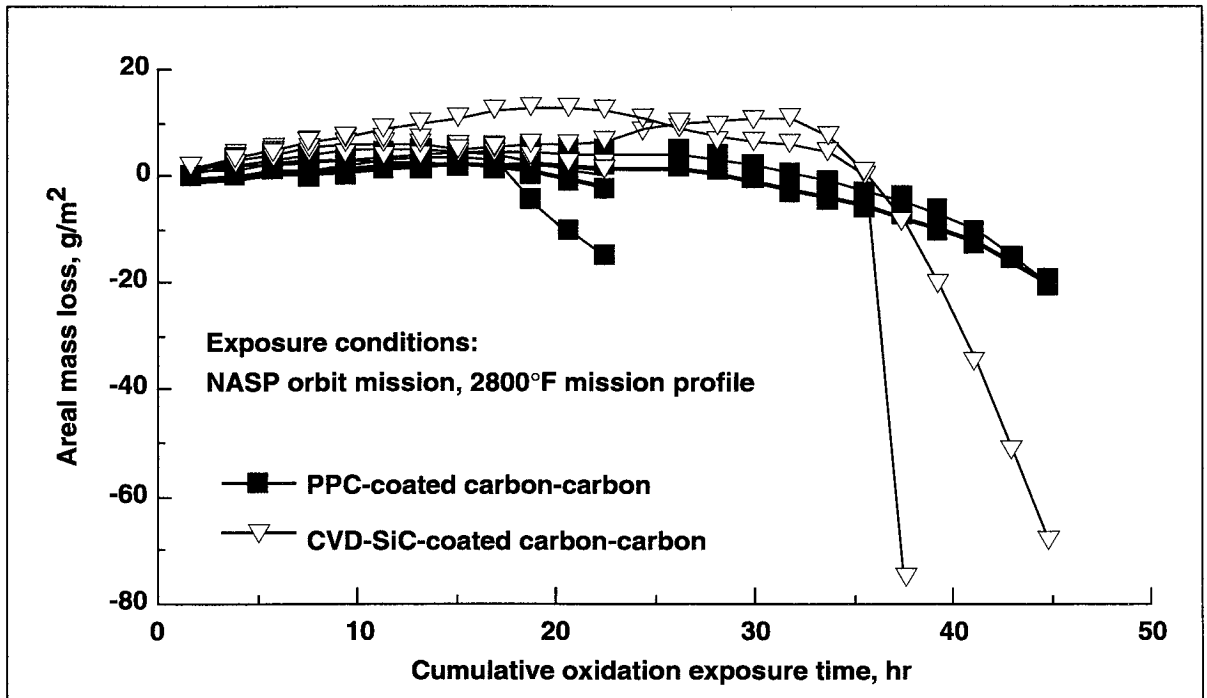

Figure 128. Polymer based coatings (PPC) on carbon-carbon composites show better or equal oxidation resistance than CVD-SiC coatings.

Within the last few years a third method has emerged in which metal-organic polymers are used to form the coating. These polymers, when heated in a suitable atmosphere (typically nitrogen, argon, or ammonia) form protective coatings of silicon-based ceramics. The advantages of this method are the ease of coating large complex parts and the degree of tailorability because the coating can be sprayed or brushed on similar to paint. The composition of the coating can be varied by altering the polymeric precursor or by adding powders. This allows the coating to be optimized for a specific environment or to be applied in a number of separate layers, each of which can contribute to the overall oxidation resistance by a different mechanism.

Figure 128 shows the results of oxidation resistance tests conducted in the Multiparameter Mission Simulation Facility in the Materials Research Laboratory. The material was tested using a time-temperature-pressure mission profile employed during the National Aero-Space Plane (NASP) program. Under subcontract to Boeing Military Airplanes, the preceramic polymer coating (PPC) was applied by Rohr Industries using a polymeric coating system formulated by Ethyl Corporation. The CVD-silicon carbide coating was applied by Chromalloy Research and Technology, Inc. The PPC-coated materials perform as well or better than the industry-standard CVD-silicon carbide coating, thus validating the viability of the polymer coating method for oxidatively protecting carbon-carbon composites. **(W. L. Vaughn, 757-864-3504)**

Higher Order Modal Methods Developed To Efficiently Solve Large Heat Transfer Problems

An advanced, higher order modal method was developed to reduce the size and computational cost of very large, complex transient thermal problems. Very large nonlinear transient thermal problems such as the thermal response of the entire Shuttle Orbiter thermal protection system (TPS) and substructure during reentry is very costly. Attempts to reduce the size of thermal problems using conventional modal methods have not been successful because the thermal response is broadband in nature and requires almost all of the mode shapes to accurately represent the response. Higher order modal methods were developed which include the forcing function and its derivative in the approximate formulation and which greatly increases the convergence of the approximate response with respect to the number of modes used. This methodology was implemented within a general-purpose finite-element code (the Computational Mechanics Testbed (COMET)). A section of a Shuttle upper wing surface was modeled and analyzed. (See fig. 129.)

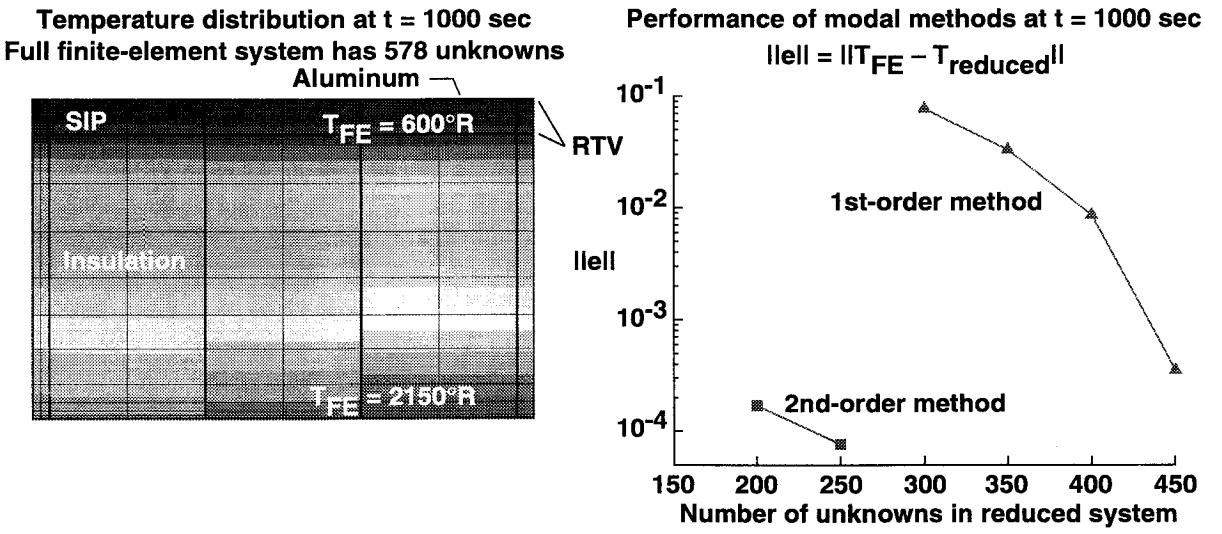

Figure 129. Modal methods reduce computational time for heat transfer analysis of shuttle wing.

Results indicate that a first-order modal method (based on the conventional modal response plus a term which includes the forcing function) can reduce problem size by approximately 50 percent and maintain errors below 10 percent. Using an even higher-order approximation, the second-order modal method can reduce the problem size by approximately 67 percent and maintain errors below 0.2 percent. These results are very encouraging and demonstrate that advanced modal methods can significantly reduce the problem size of large thermal problems while maintaining accuracy. **(K. S. Bey, 757-864-1351)**

Mechanical Property Comparison of U.S. and Russian Near-Net Shape Al-Li Extrusions

The potential cost savings and performance enhancement of using aluminum-lithium (Al-Li) alloy extrusions for cryogenic propellant tanks and dry bay structures has been recognized at both the Reusable Launch Vehicle (RLV) and Evolved Expendable Launch Vehicle programs (EELV). Both U.S. 2195 (Al-Li-Cu-Mg-Ag) and Russian 1460 (Al-Li-Cu-Sc) have been successfully extruded in cylindrical form, split and flattened into 8-ft-wide integrally stiffened panels. The mechanical properties and metallurgical structure of these panels are being investigated in laboratories within the U.S. and Russia, in a program led by NASA.

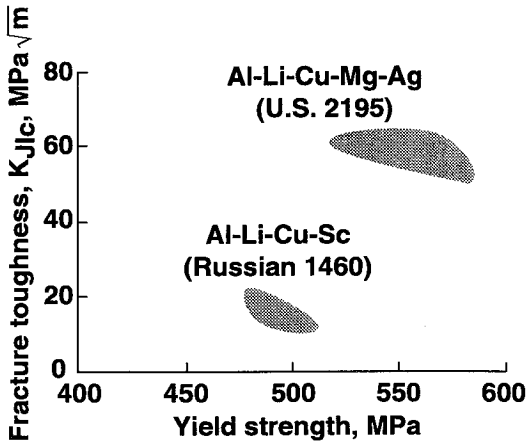

Figure 130. Room temperature fracture toughness versus yield strength of near net extruded Al-Li panels.

Fracture toughness and tensile tests have been conducted on 2195 and 1460 at NASA Langley Research Center. Two-inch-wide compact tension specimens were used to assess the materials toughness using the J-Integral technique. Figure 130 shows a plot of the room temperature fracture toughness versus yield strength for 2195 and 1460. The locus of points for each represents approximately 12 tests in which the strength-toughness combination was varied by using different age hardening heat treatments. The age hardening heat treatments consisted of aging at 300°F for 10, 15, and 24 hr for 2195 and aging at 320°F for 16, 20, and 24 hr for 1460. The data indicate that for the range of the heat treatments employed, U.S. alloy 2195 has the best strength-toughness combination and suggests that 2195 may have some advantages when compared with 1460 for certain aerospace structural applications. Work is continuing to determine the strength-toughness relationship of these alloys at cryogenic temperatures to support RLV and EELV cryotank programs. **(J. A. Wagner, 757-864-3132)**

Direct Mechanical Strain Technique for Accurately Measuring Mechanical Strain at Elevated Temperatures

An innovative test technique was developed which enables the accurate measurement of mechanical strains directly during elevated temperature testing (T > 600°F). Standard methods for measuring mechanical strain using bonded strain gages require that apparent strains (e.g., sensor induced voltages due to gage material property variation and coefficient of thermal expansion mismatch due to temperature changes) be calculated and used to correct recorded strain measurements during elevated temperature testing. This normally requires repeated thermal cycling of the specimen until the apparent strain outputs become stable and, hence, repeatable. The apparent strain curves used to correct the data are usually obtained from similar gages installed on similar material. In any event, the strain variations from gage-to-gage and the correction process (usually resulting from the differencing of two large, nearly similar strain values (total strain-apparent strain)) may result in errors.

The Direct Mechanical Strain Technique (DMST) requires the specimen to be loaded in small, rapidly applied increments followed by periods of constant load after each load increment. The mechanically

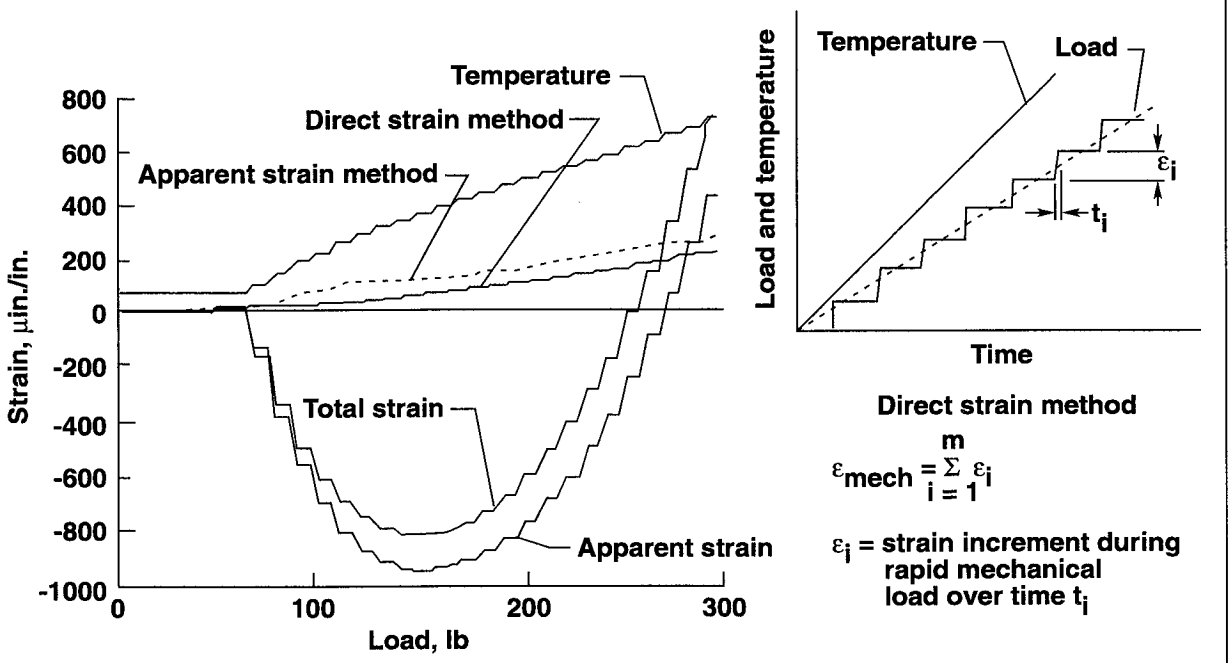

Figure 131. Direct strain method for mechanical strain measurements at elevated temperatures.

induced strains are then measured directly by summing the recorded strains measured during each rapidly applied load segment (assuming the temperature is constant during this time segment and, hence apparent strains are negligible). Tests have been conducted using a very simple rectangular Inconnel tensile specimen which was loaded in tension to 300 lb in 10 lb increments while the temperature increased linearly from room temperature to 1200°F. Mechanical strains obtained using the DMST are shown to be in good agreement with the values obtained using the apparent strain correction method over most of the load and temperature range. (See fig. 131.) In addition to increased accuracy, the proposed technique has the advantage of being able to accurately predict mechanical strain measurements during the first thermal cycle.

(J. W. Sawyer, 757-864-5432)

RLV/X-33 Aerothermodynamics

In April 1995, NASA entered into a Cooperative Agreement with three industry teams to develop a rocket powered, single stage to orbit, Reusable Launch Vehicle (RLV) for access to space. The RLV is to be preceded by the X-33 flight demonstration vehicle. Phase I of this program was for concept definition of the RLV/X-33 leading to a down-select in July 1996. Phase II of the program will be the design, construction and flight testing of the X-33 by a single NASA/industry team to demonstrate the technologies and operational procedures required for the RLV. Finally, Phase III will be the development of a viable RLV which could replace the Space Shuttle in the next century.

The Aerothermodynamics Branch (AB) of the Gas Dynamics Division worked closely as full partners with the three industry teams to provide aerothermodynamic characteristics, assessment, and optimization for three distinct vehicle concepts. The McDonnell Douglas/Boeing concept is a vertical take-off and landing vehicle while the other two concepts are vertical launch with horizontal landing vehicles. Ultimately selected by NASA was the Lockheed Martin concept, a lifting body. The Rockwell International concept is a wing/body. (See fig. 132.)

These concepts were tested at subsonic to hypersonic Mach numbers in various Langley Research Center (LaRC) and contractor facilities to provide experimental aerodynamics and aeroheating over a wide range of conditions, including real gas simulation. AB researchers working with the industry team

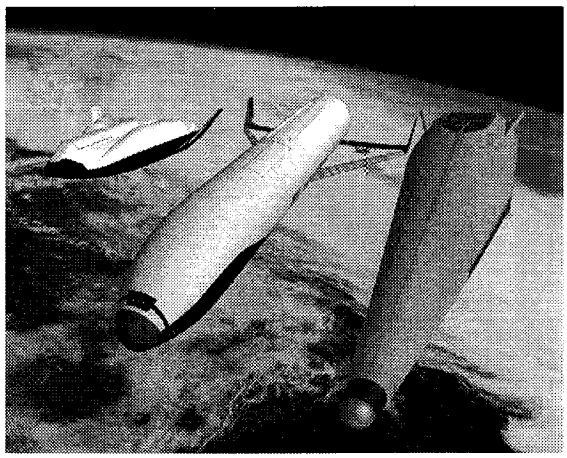

Figure 132. RLV/X-33 Phase I concepts (left to right: Lockheed Martin lifting body, Rockwell winged body, McDonnell Douglas/Boeing slender cone body).

members developed configuration changes based on the experimental results which significantly improved the aerodynamics, stability, and control of all concepts. At the same time, AB computationalists were providing high Mach number aerodynamics and aeroheating to the industry teams for the critical Thermal Protection System design. This aeroheating was backed up by the extensive experimental data set of global, surface aeroheating obtained using the Thermographic Phosphor System, developed within the AB.

This extremely fast-paced Phase I program has been fully supported by the LaRC infrastructure including a major in-house effort in model design and fabrication, and contract grid generation for computational solutions. Because of the rapid and numerous configuration changes, typical of an iterative process to improve aerothermodynamic characteristics, this Phase I program was successful because this infrastructure is in place at LaRC. **(C. G. Miller III, 757-864-5221)**

Meteoroid and Debris Impacts on Hubble Space Telescope Radiator

During the first servicing mission to the Hubble Space Telescope (HST), the original Wide Field/Planetary Camera (WF/PC I) was removed and replaced with a new camera (WF/PC II). During the subsequent post-retrieval examination of WF/PC I, it was observed that there were about 100 small spots on the 1.7-m^2 aluminum radiator where the 5-mil-thick zinc orthotitanate (ZOT) paint had been chipped away. Microscopic examination of 72 of those spots revealed that 53 were impact sites, whereas the remainder were scrapes or places where gooey particles stuck to the surface giving the appearance of chipped paint.

The number of impact sites and the extent of the damage was consistent with the impact fluxes of meteoroids and debris measured on the Long-Duration Exposure Facility (LDEF), suggesting that the orbiting debris environment had not changed noticeably from the LDEF years (1984–1990) to the WF/PC I years (1990–1993).

The effect of the ZOT paint on the shape of the damage at the smaller impact sites was, however, quite surprising. Instead of the nearly hemispherical craters seen on the LDEF plates, the damage to the WF/PC I radiator was most often an irregular field of craters, sometimes with overlapping craters and sometimes with craters separated from each other (see the sketches in figure 133). Most of the impacts are believed to have been caused by meteoroids, and the nature of the damage suggests that those meteoroids were loose aggregates that had no strength and simply fell apart upon impact with the ZOT paint.

More about this examination of the WF/PC I radiator can be found on the Internet at URL http://setas-www.larc.nasa.gov/setas/HUBBLE/WORKSHOPS/gsfc_hardware.html. SETAS is an on-line archive, for HST and other space missions, originated at NASA LaRC. **(D. H. Humes, 757-864-1484)**

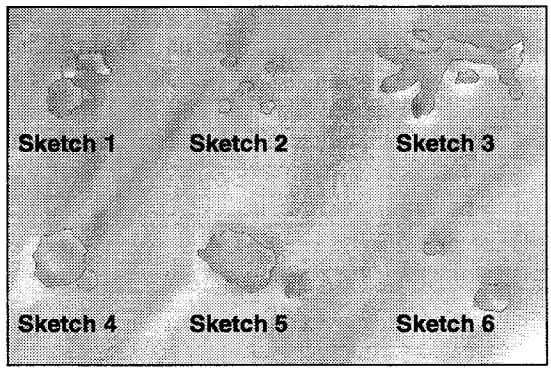

Figure 133. Crater fields seen on the Hubble Space Telescope (HST) Wide Field/Planetary Camera (WF/PC I) radiator.

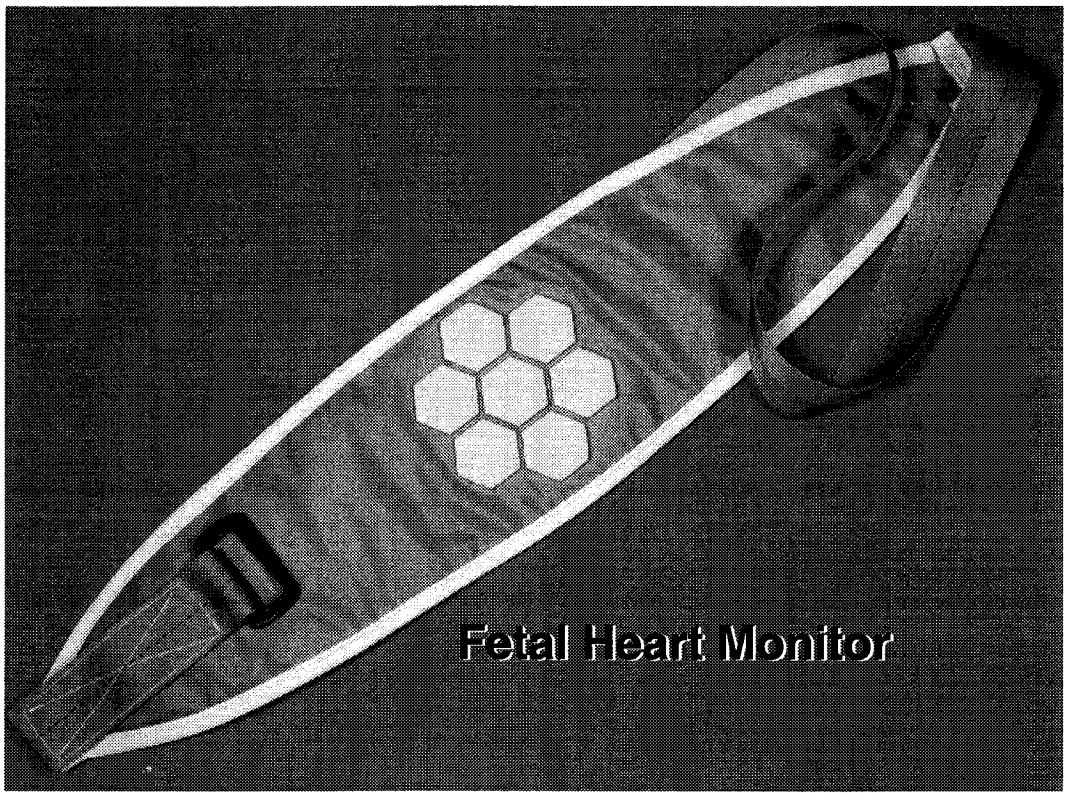

- *This section contains a brief summary of some of Langley's technology transfer activities.*

Summary of NASA Langley Activities in Technology Transfer and Commercial Development

During FY 1995, there were a number of avenues explored by Langley to disseminate information on technologies available for commercialization. One of the most visible is the Homepage located on the World Wide Web under the following URL address: **http://tag-www.larc.nasa.gov/**. This website also contains information on:

- Road Map for Initiating Business with NASA LaRC
- Technology Transfer Questions and Answers
- Commercial Opportunities Program (COOPPR)
- Commercialization Plan Preparation
- NASA's Patent Licensing Program

During the past year, Langley has successfully transferred the benefits of its technologies and expertise to the private sector. Progress has been made in several important areas especially in the outreach activities. A brief overview of major accomplishments for 1995 is provided below:

- NASA hosted a 3-day exposition called "Technology Opportunity Showcase" (TOPS) to facilitate the transfer of technology from Government research to U.S. industry profits. The technologies exhibited can be viewed on the World Wide Web under the following URL address: **http://tag-www.larc.nasa.gov/tops/tops.html**
- There were 12 licenses issued
- There were 78 patents issued
- 68 Space Act Agreements (49 nonaerospace related) were signed in support of advanced research and development efforts
- Langley received 9 Small Business Technology Transfer (STTR) Phase I Awards (totaling approximately $899,000), 8 STTR Phase II Awards (totaling approximately $4,000,000), 41 Small Business Innovation Research (SBIR) Phase I Awards (totaling approximately $2,850,000), and 20 SBIR Phase II Awards (totaling approximately $11,917,000)
- 55 copies of Langley software were transferred to U.S. nonprimary aerospace companies for nongovernmental use

In 1995, the Center received the following technology awards:

- R&D 100 Award for LaRC™-SI (a Langley-developed polyimide)

  R&D 100 Magazine sponsors an award that recognizes the top 100 most technologically significant new products of the year. LaRC™-SI won an R&D 100 award this past year. Dr. Robert G. Bryant, a chemical engineer, developed the self-bonding thermoplastic called LaRC™-SI. Three electronic technicians who helped to develop various applications of the thermoplastic shared in the award. LaRC™-SI is an amorphous thermoplastic, meaning it can be reformed at elevated temperatures and pressures. It is also recyclable. The material has an exceptional combination of properties, resulting in a wealth of applications. It can be applied in the form of spray, spin, and dip coating. Potential applications for the thermoplastic include a resin for mechanical parts such as gears, bearings, and valves and for advanced composites like carbon fiber and high-strength adhesives. It can also be used to make film and self-bonding multilayer flex circuits.

- U.S. Space Foundation Hall of Fame Award for Para-Wing/Flexible Wing

  The Space Technology Hall of Fame, a cooperative program between NASA and the Space Foundation, has three major objectives—to recognize excellence, to promote public awareness, and to foster replicating excellence in space technology. In 1948, Langley's Francis and Gertrude Rogallo developed what is known as the parawing for use on inexpensive private aircraft. This technology is a flexible, controllable, fabric airfoil designed in a V-shaped configuration. At the time, Francis was an employee of the National Advisory Committee for

Aeronautics (NACA) the precursor to NASA. With NACA approval, he obtained a flex-wing patent on the parawing in 1951. In 1958, NASA became interested in the possible use of the parawing to land space payloads. Mr. Rogallo was the project engineer and began an extensive research and development effort at NASA Langley Research Center. Many patents emerged from his work, as well as the development of a significant flexible airfoil base. The patents included both inflatable and nonflexible wings.

While NASA chose not to utilize the parawing to land spacecraft, the military was interested in its use for parachuting. In the mid-1960's, two parachute companies, Pioneer Aerospace and Irvin Industries, obtained a license from NASA and proceeded to manufacture parawings and later inflatable wings. In 1965, the Army's Golden Knight precision parachute team were the first to jump these parawings and demonstrate their unique steerability. This initial jump began what is now a $50 million annual industry known as hang gliding as well as the use of the inflatable wing by the military. Dozens of companies have been formed in the United States as well as overseas. These companies produce parawings, hang gliders, and powered gliders. These firms have also generated a second tier of supplier firms of materials, clothing, and ancillary equipment. A national association, the United States Hang Gliders Association, has been established. Hang gliding schools have been formed and several international magazines on the sport now exist. While not well known by the public, those hang gliders colorfully winging their way along beaches, sand dunes, hills, and mountains are a spinoff from NASA.

- Popular Science Award for Carbon Monoxide Catalyst

Carbon monoxide detectors warn homeowners when levels of the deadly gas rise but they don't combat the basic problem. Now a prototype catalytic system from NASA Langley Research Center converts carbon monoxide (CO) into harmless carbon dioxide (CO_2). Originally developed for lasers that run on CO_2, the device comprises a ceramic honeycomb coated with tin oxide and platinum. A home version could hit the market by 1997 at a cost of about $500. Rochester Gas and Electric Corporation has acquired the exclusive license to the NASA patents for indoor air purification, and Mantic Corporation has exclusive license for gas masks (additional information included below).

- Langley Research Center was selected by *Technology Transfer Business Magazine* in the summer 1996 issue as one of the "Top Federal R&D Labs."

A variety of NASA Langley technologies were used by the Boeing Company for the new Boeing 777, designed for medium to long-range passenger flights. The largest twin-engine jet to be manufactured, it began carrying passengers in May of 1995. Boeing announced that the 777 fleet had already captured three-quarters of the world market for aircraft in its class, further strengthening the nation's positive balance of trade. Some of the NASA Langley-developed analytical techniques and facilities used by Boeing for this aircraft included fundamental mathematical procedures for computer-generated airflow images, which enabled advanced computer-based aerodynamic analysis; wind-tunnel testing for flutter and vibration characteristics of the wing structure (for which Boeing directly reimbursed NASA) in Langley's Transonic Dynamics Tunnel; knowledge of how to reduce engine noise and other noise for passengers and terminal area residents; and strength and durability testing of tires at Langley's Aircraft Landing Dynamics Facility. NASA Langley advances were used for the aircraft's modern glass cockpit system that uses computer technology to integrate and display information on monitors in easy-to-use formats; the digital data system, an easily reconfigurable computer network that allows the aircraft's computers to communicate with each other; the "fly-by-wire" system to control wing and tail surfaces, which replaces bulkier and heavier hydraulic control systems; and increased use of lightweight aerospace composite structures, including graphite-epoxy floor beams, flaps, and the tail assembly, for increased fuel efficiency and range. The 777's aerodynamically-efficient wing evolved from many years of analytical and wind-tunnel research performed at Boeing and employs advanced wing cross-section concepts independently developed and first published as part of NASA's aeronautical research program. Other NASA Centers that contributed to fundamental research and technologies adopted for the 777 include Ames, Dryden, and Lewis.

To improve productivity of the National Transonic Facility (NTF) at Langley, a study was performed to find an improved filler material for filling the voids above subsurface fasteners on NTF wind-tunnel models. An ultraviolet-light cured filler material modified to match the thermal expansion of the parent model material is now standard filling material. The cure time for this new filler material is 15 sec compared to 8 hr for the old material, and the surface

Carolina. Clinical studies are underway with Eastern Virginia Medical School in Norfolk and Encino/Tarzana Medical Center in California. Veatronics plans to put the monitor on the market in summer 1997.

Langley developed the Self-Nulling Eddy-Current Device as an extremely sensitive detector of fatigue cracks in aluminum alloy plates. Krautkramer Branson (KKB) of Lewiston, Pennsylvania, was selected to commercialize the technology, which is called the "Crack Finder" and is marketed as a compact, hand-held probe to detect surface-braking cracks. Since large areas can be inspected quickly with unambiguous flaw detection, the market should be quite large for aging aircraft. Available since early 1995, the net sales are expected to approach $3M by the end of 1996.

A new slip casting technique for fabricating ceramics has been developed at Langley. Originally used for rapid manufacture of wind-tunnel models, the technique overcomes the expense and imprecision of conventional ceramic fabrication. Licensed to Final Touch of VA, Inc., in Richmond, Virginia, the technique will allow the company to develop and manufacture research prototypes of a wide range of consumer goods without the parting lines and surface impurities caused by separation of or from ceramic molds. An example is the fused silica ceramic mirror mount; with its much lower thermal expansion than aluminum mounts, the ceramic mirror mount allows an increase in frequency control by over an order of magnitude.

Low-temperature carbon monoxide oxidation catalysts were developed at Langley for recycling carbon monoxide and converting it back to carbon dioxide during the operation of closed cycle carbon dioxide lasers in space environments. These catalysts were developed for the high-power pulsed carbon dioxide laser in the LAWS (Laser Atmospheric Wind Sounder) satellite, which required continuous operation over a 5-year cycle without carbon dioxide replenishment. Rochester Gas and Electric Corporation of Rochester, New York, has been licensed four patents to apply the technology for inhabited spaces applications including heating, ventilating, and air-conditioning (HVAC) systems, which market studies indicate could approach a steady-state sales level of $200M per year; four patents were also licensed to STC Catalysts of Hampton, Virginia, a subsidiary of Science and Technology Corporation of Hampton, Virginia, to meet the catalyst technology requirements of space-based carbon dioxide lasers for a market that the company estimates at $20M per year; and four patents were licensed to Mantis Corporation of Salt Lake City, Utah, to commercialize the technology as personal carbon monoxide removal systems (masks) for emergency aids, with a market estimated ultimately at $40M per year.

Removal of low-level radioactive hardware from the nation's nuclear facilities is an important problem. Langley is involved in a cooperative agreement funded by the Department of Energy, with Battelle, Pacific Northwest Laboratory, and Oak Ridge National Laboratory to develop a "Variable Geometry Truss (VGT)" manipulator arm system to enable greater dexterity in the disassembly and removal of contaminated nuclear facilities by mounting the VGT onto RedZone Robotics' remotely operated vehicle. The completed VGT system was to be shipped in 1996.

REPORT DOCUMENTATION PAGE

Form Approved
OMB No. 0704-0188

1. AGENCY USE ONLY *(Leave blank)*	2. REPORT DATE	3. REPORT TYPE AND DATES COVERED
	December 1996	Technical Memorandum

4. TITLE AND SUBTITLE
Research and Technology Highlights 1995

5. FUNDING NUMBERS

6. AUTHOR(S)

7. PERFORMING ORGANIZATION NAME(S) AND ADDRESS(ES)

NASA Langley Research Center
Hampton, VA 23681-0001

8. PERFORMING ORGANIZATION REPORT NUMBER

L-17614

9. SPONSORING/MONITORING AGENCY NAME(S) AND ADDRESS(ES)

National Aeronautics and Space Administration
Washington, DC 20546-0001

10. SPONSORING/MONITORING AGENCY REPORT NUMBER

NASA TM-4765

11. SUPPLEMENTARY NOTES

12a. DISTRIBUTION/AVAILABILITY STATEMENT

Unclassified–Unlimited
Subject Category 99
Availability: NASA CASI (301) 621-0390

12b. DISTRIBUTION CODE

13. ABSTRACT *(Maximum 200 words)*

The mission of the NASA Langley Research Center is to increase the knowledge and capability of the United States in a full range of aeronautics disciplines and in selected space disciplines. This mission is accomplished by performing innovative research relevant to national needs and Agency goals, transferring technology to users in a timely manner, and providing development support to other United States Government agencies, industry, and other NASA Centers, the educational community, and the local community. This report contains highlights of the major accomplishments and applications that have been made by Langley researchers and by our university and industry colleagues during the past year. The highlights illustrate both the broad range of research and technology (R&T) activities carried out by NASA Langley Research Center and the contributions of this work toward maintaining United States leadership in aeronautics and space research. An electronic version of the report is available at URL http://techreports.larc.nasa.gov/RandT95. This electronic version allows viewing, retrieving, and printing of the highlights, searching and browsing through the sections, and access to an on-line directory of Langley researchers. For further information concerning this report, contact Dennis M. Bushnell, Senior Scientist, Mail Stop 110, NASA Langley Research Center, Hampton, Virginia 23681-0001, (757) 864-8987.

14. SUBJECT TERMS	15. NUMBER OF PAGES
Research and technology; Aeronautics; Space; Structures; Materials; Electronics; Flight systems; Technology transfer; Technology commercialization; Engineering; Aerodynamics; Wind tunnels; Facilities, Tests	147
	16. PRICE CODE A07

17. SECURITY CLASSIFICATION OF REPORT	18. SECURITY CLASSIFICATION OF THIS PAGE	19. SECURITY CLASSIFICATION OF ABSTRACT	20. LIMITATION OF ABSTRACT
Unclassified	Unclassified	Unclassified	